UNIVERSIDADE FEDERAL DA BAHIA
INSTITUTO DE GEOCIÊNCIAS
PROGRAMA DE PESQUISA E PÓS-GRADUAÇÃO EM GEOLOGIA
ÁREA DE CONCENTRAÇÃO:
PETROLOGIA, METALOGÊNESE E EXPLORAÇÃO MINERAL

TESE DE DOUTORADO

MISTURA DE MAGMAS E A FORMAÇÃO DO BATÓLITO RIO JACARÉ: EVIDÊNCIAS DE MANTO LITOSFÉRICO ENRIQUECIDO NO SISTEMA OROGÊNICO SERGIPANO, NE-BRASIL

CARLOS SANTANA SOUSA

SALVADOR
2022

MISTURA DE MAGMAS E A FORMAÇÃO DO BATÓLITO RIO JACARÉ: EVIDÊNCIAS DE MANTO LITOSFÉRICO ENRIQUECIDO NO SISTEMA OROGÊNICO SERGIPANO, NE-BRASIL

Carlos Santana Sousa

Orientador : Prof. Dr. Herbet Conceição

Coorientadora: Profa. Dra. Maria de Lourdes da Silva Rosa

Tese de Doutorado apresentada ao Programa de Pós-Graduação em Geologia do Instituto de Geociências da Universidade Federal da Bahia como requisito parcial à obtenção do Título de Doutor em Geologia, Área de Concentração: Petrologia, Metalogênese e Exploração Mineral.

SALVADOR

2022

Ficha catalográfica elaborada pela Biblioteca Universitária de Ciências e Tecnologias Prof. Omar Catunda, SIBI - UFBA.

S725 Sousa, Carlos Santana

Mistura de magmas e a formação do Batólito Rio Jacaré: evidências de manto litosférico enriquecido no Sistema Orogênico Sergipano, NE-Brasil/ Carlos Santana Sousa. – Salvador, 2022.

220 f.

Orientadora: Prof. Dr. Herbet Conceição

Tese (Doutorado) – Universidade Federal da Bahia. Instituto de Geociências, 2022.

1. Geociências. 2. Geologia. 3. Petrologia. I. Conceição, Herbet. II. Universidade Federal da Bahia. III. Título.

CDU 551

CARLOS SANTANA SOUSA

"Mistura de magmas e a formação do Batólito Rio Jacaré: evidências de manto litosférico enriquecido no Sistema Orogênico Sergipano, NE-Brasil"

Trabalho apresentado ao Programa de Pós-Graduação em Geologia da Universidade Federal da Bahia, como requisito parcial para a obtenção do Grau de Doutor em Geologia na área de concentração em Petrologia, Metalogênese e Exploração Mineral em 15/09/2022.

APROVADO PELA BANCA EXAMINADORA:

Dr. Herbet Conceição (Orientador) – (UFS)

Dr. Reinhardt Adolfo Fuck (UNB)

Dr. Adejardo Francisco da Silva Filho (UFPE)

Dr. Carlos Dinges Marques de Sá (UFS)

Dr. Rômulo Machado (USP)

Salvador – BA
2022

Senhor, fazei-me instrumento de vossa paz
Onde houver ódio, que eu leve o amor
Onde houver ofensa, que eu leve o perdão
Onde houver discórdia, que eu leve união
Onde houver dúvida, que eu leve a fé

Onde houver erro, que eu leve a verdade
Onde houver desespero, que eu leve a esperança
Onde houver tristeza, que eu leve alegria
Onde houver trevas, que eu leve a luz

Ó mestre, fazei que eu procure mais consolar que ser consolado
Compreender que ser compreendido
Amar que ser amado
Pois é dando que se recebe
É perdoando que se é perdoado
E é morrendo que se vive
Para a vida eterna

Oração de São Francisco de Assis

Dedico este trabalho aos meus amados pais,
com muito carinho.

AGRADECIMENTOS

O presente trabalho foi realizado com o apoio da Coordenação de Aperfeiçoamento de Pessoal de Nível Superior – Brasil (CAPES) – Código de financiamento 001.

Agradeço ao Programa de Pós-Graduação em Geologia da Universidade Federal da Bahia pela oportunidade de desenvolver este trabalho.

Ao Conselho Nacional de Desenvolvimento Científico e Tecnológico (CNPq) pela bolsa de doutorado.

Ao Condomínio de Laboratórios Multiusuários das Geociências da Universidade Federal de Sergipe (CLGeo-UFS), por permitir o uso de sua infraestrutura para a obtenção de análises.

Aos doutores Herbet Conceição e Maria de Lourdes da Silva Rosa, que me orientaram e foram exemplos de competência, profissionalismo e dedicação. Sou grato pelos ensinamentos e incentivos desde o início da graduação. Externo aqui, a minha imensa admiração por vocês.

Aos amigos do Laboratório de Petrologia Aplicada à Pesquisa Mineral (LAPA - UFS), em especial aos amigos Hiakan, Diego e Jailson, por todo companheirismo.

Não poderia deixar de agradecer à minha namorada Mykaelli por todo amor e apoio. Agradeço ainda a Givanda e Valter por me acolherem durante alguns meses no período de pandemia. Vocês facilitaram muito esta jornada.

Por fim, agradeço às pessoas mais importantes de minha vida, minha família. Meu pai (Antelmo), minha mãe (Jaci), minha irmã (Clara), meu irmão (Bruno) e minha cunhada (Camila). Obrigado pelo amor, carinho e apoio incondicional!

RESUMO

O Batólito Rio Jacaré (BRJ; 617 ± 4 Ma) é uma intrusão do Domínio Poço Redondo, Sistema Orogênico Sergipano. O batólito é formado por quartzo monzonitos, monzogranitos e granodioritos, dispostos nas fácies inequigranular (FI) e porfirítica (FP). Enclaves microgranulares (EM) ocorrem de forma abundante no BRJ e preservam feições de *mixing* e *mingling*. Os EM têm cores que variam de cinza claro a cinza escuro e possuem formas globulares a alongadas. Seus contatos são retos, crenulados e cúspides, ou mais raramente, difusos. Os EM são dioritos, monzodioritos, quartzo monzodioritos e monzonitos. Os EM representam o rompimento e resfriamento de magma inicialmente máfico injetado na câmara magmática félsica mais fria. A colocação desse magma máfico ocorreu em etapas diferentes da cristalização da câmara magmática do BRJ. O grau máximo de hibridização desses EM é de 57%. O magma máfico dos EM possui afinidade com a série shoshonítica e foi gerado por taxa de fusão parcial de aproximadamente 3% de fonte de manto litosférico enriquecida em elementos incompatíveis. Os cristais de plagioclásio das rochas do BRJ exibem zoneamentos composicionais, *patchy zoning*, textura *boxy cellular*, núcleos de cristais embaiados, núcleos com composição homogênea, zonas de inclusões de minerais máficos e *synneusis*. A composição do plagioclásio na FI varia de albita a andesina (An_{7-33}), na FP é albita e oligoclásio (An_{5-23}) e nos EM varia de albita a labradorita (An_{6-51}). As composições albíticas nesses cristais são limitadas às suas periferias e sugerem ação de fluidos hidrotermais, ou seja, não resultaram da cristalização do magma. As texturas identificadas nos cristais de plagioclásio permitem inferir um período de condições magmáticas estáveis, seguido por período com instabilidades marcadas por injeções de magma máfico, que modificaram as condições (temperatura, pressão e atividade de H_2O) do sistema magmático e estimularam *mixing* entre magmas durante a evolução do BRJ. As injeções do magma máfico geraram, provavelmente, correntes de convecção na câmara magmática do BRJ. Os cristais com núcleos embaiados sugerem pelo menos cinco episódios de reabsorção nesses cristais. Nas rochas do BRJ são encontrados cristais de Mg-biotita primários e reequilibrados. Os cristais primários ocorrem principalmente como inclusões em cristais de plagioclásio, enquanto os reequilibrados não ocorrem como inclusões e contêm cristais anédricos de titanita em suas clivagens. A temperatura de cristalização da Mg-biotita primária (FI: 683 a 713 °C; FP: 678 a 704 °C; EM: 685 a 745 °C) é consistente com a temperatura de cristalização de biotita em sistemas graníticos. A pressão de cristalização da Mg-biotita primária foi de 1,8 a 2,7 kbar na FI, de 1,2 a 2,2 kbar na FP e de 1,2 a 2,9 kbar nos EM. As composições dos cristais primários da FI e FP indicam que foram formados por magmas com conteúdo de H_2O entre 5 a 7%. A fO_2 (ΔNNO) durante a formação dos cristais primários variou de -16,3 a -15,0 na FI, de -15,9 a -15,4 na FP e de -15,6 a -13,9 nos EM. O reequilíbrio dos cristais estudados resultou provavelmente da exsolução de Ti, que junto com fluidos hidrotermais contendo Ca^{2+}, formou cristais anédricos de titanita em seus planos de clivagem e bordas.

Palavras-chave: *Mixing* e *Mingling*, Cristais Reequilibrados, Zoneamentos Composicionais.

ABSTRACT

The Rio Jacaré Batholith (RJB; 617 ± 4 Ma) is an intrusion of the Poço Redondo Domain, Sergipe Orogenic System. The batholith is formed of quartz monzonites, monzogranites, and granodiorites, which are arranged in inequigranular (IF) and porphyritic (PF) facies. Microgranular enclaves (ME) occur abundantly in the BRJ and preserve mixing and mingling features. MEs range in color from light gray to dark gray and have globular to elongated shapes. Their contacts are clear-cut, crenulated and cuspate, or, more rarely, diffuse. The ME are diorites, monzodiorites, quartz monzodiorites and monzonites. MEs represent the breakdown and cooling of initially mafic magma that has been injected into a cooler felsic magma chamber. The emplacement of mafic magma occurred at different stages of the crystallization of the BRJ magma chamber. The maximum degree of hybridization of these MEs is 57%. ME mafic magma has an affinity with shoshonitic series and was generated by the partial melting of approximately 3% of a lithospheric mantle source enriched in incompatible elements. The plagioclase crystals of the RJB rocks exhibit compositional zoning, patchy zoning, boxy cellular texture, embayed crystal cores, cores with homogeneous composition, inclusions zones of mafic minerals, and synneusis. The composition of plagioclase in FI varies from albite to andesine (An_{7-33}), in PF it is albite and oligoclase (An_{5-23}) and in ME it varies from albite to labradorite (An_{6-51}). The albite compositions in these crystals are limited to their periphery and suggest the action of hydrothermal fluids, that is, they did not result from magma crystallization. The textures identified in the plagioclase crystals allow to infer a period of stable magmatic conditions followed by a period with instabilities marked by mafic magma injections, which modified the conditions (temperature, pressure, and H_2O activity) of the magmatic system and stimulated mixing between magmas during the evolution of the RJB. The mafic magma injections probably generated convection currents in the RJB magma chamber. Crystals with embayed cores suggest at least five episodes of resorption in these crystals. Primary and reequilibrated Mg-biotite crystals are found in the RJB rocks. Primary crystals mainly occur as inclusions in plagioclase crystals, while reequilibrated crystals do not occur as inclusions and contain anhedral titanite crystals in their cleavages. The crystallization temperature of primary Mg-biotite (IF: 683 to 713 °C; FP: 678 to 704 °C; ME: 685 to 745 °C) is consistent with the crystallization temperature of biotite in granitic systems. The crystallization pressure of primary Mg-biotite was 1.8 to 2.7 kbar in IF, 1.2 to 2.2 kbar in PF, and 1.2 to 2.9 kbar in ME. The compositions of the primary crystals of IF and PF indicate that they were formed by magmas with H_2O content between 5 and 7%. The fO_2 (ΔNNO) during the formation of primary crystals ranged from -16.3 to -15.0 in IF, from -15.9 to -15.4 in PF, and from -15.6 to -13.9 in ME. The reequilibrating of the studied crystals probably resulted from the exsolution of Ti, which together with hydrothermal fluids containing Ca^{2+}, formed anhedral titanite crystals in their cleavage planes and edges.

Keywords: Mixing and Mingling, Reequilibrated Crystals, Compositional Zoning

SUMÁRIO

CAPÍTULO 1
INTRODUÇÃO GERAL

Cerca de 80 a 90% de todo magma fornecido à crosta se coloca internamente (e.g., Crisp, 1984; Annen et al., 2015). As rochas plutônicas, quando expostas na superfície, fornecem uma riqueza de informações sobre os mecanismos de colocação e processos de diferenciação dos magmas na crosta (e.g., Paterson et al., 2018; Glazner et al., 2018). Por isso, os granitos (*s.l.*), devido a diversidade e ocorrência, têm gerado várias questões e motivado estudos (e.g., Whalen et al., 1987; Chappell e White, 1992; Brown, 1994). Além de serem as rochas plutônicas mais abundantes na crosta continental (e.g., Campbell e Taylor, 1983; Whitney, 1988), os granitos possuem também amplo espectro de tipos petrográficos que refletem origens a partir de diversas fontes (e.g., Barbarin, 1990; Winter, 2014). Desta forma, os estudos sobre plútons graníticos contribuem para que se possa melhor compreender a evolução de sistemas orogênico e anorogênico.

Huppert e Sparks (1988) advogam que a evolução da crosta continental inferior é influenciada por injeção/*underplating* de magmas máficos mantélicos. A injeção desses magmas máficos quentes na crosta continental é frequentemente associada com a gênese de magmas félsicos por fusão parcial da crosta inferior, e subsequente interação (*mingling* e *mixing*) entre esses magmas.

A grande variação no tipo de rochas observada em intrusões pode ser produto de *mixing* e *mingling* entre magmas máfico e félsico (Hibbard, 1991). Essa interação é considerada como um dos principais mecanismos de geração de batólitos compostos (Didier e Barbarin, 1991) e essa associação é mais abundante em sistemas orogênicos (Sklyarov e Fedorovskii, 2006). A interação entre magmas crustal e mantélico em ambientes colisionais e no estágio final da colisão pode ocorrer em profundidades variando de 7 a 20 km (Sklyarov e Fedorovskii, 2006).

Evidências diretas de *mixing/mingling* entre magmas podem ser vistas em numerosos afloramentos com mesoestruturas e microestruturas magmáticas que incluem a presença de enclaves microgranulares (EM), bordas resfriadas em enclaves, zonas híbridas nos contatos entre magmas máfico e félsico, e xenocristais em ambos os tipos de magmas (Vernon, 1984; Kumar e Rino, 2006).

Os EM são os tipos mais comuns de enclaves em corpos graníticos (Barbarin e Didier, 1991) e são considerados como uma das chaves para o entendimento da gênese e evolução de rochas graníticas (Didier, 1973; Barbarin e Didier, 1991). Segundo Bonin (2004), as rochas graníticas com EM podem ser produzidas por diferenciação de magma em reservatório crustal e, enquanto ainda evoluía, sofre influxo e perturbação de novo magma vindo de regiões inferiores. Bonin (2004) argumenta que as rochas máficas (enclaves) são manto-derivadas. Por isso, é necessário identificar e entender essa interação entre magmas durante os estudos geológico, mineralógico e geoquímico de suítes magmáticas.

Os principais fatores responsáveis pela cristalização e mineralogia de uma rocha são a composição química do magma, a pressão, a temperatura, a fugacidade de oxigênio e a natureza e conteúdo de voláteis (e.g., Martin, 2007; Papoutsa e Pe-Piper, 2014; Erdmann et al., 2014). Esses fatores podem ser estimados utilizando a composição química de determinados minerais, como biotita (e.g, Dong et al., 2014). De acordo com Yazdi et al. (2019), em uma câmara magmática, o magma é afetado por vários processos físicos dinâmicos, como a presença de convecção ou injeção de magma máfico mais quente. As mudanças nas condições físico-químicas durante a cristalização do magma podem gerar texturas de desequilíbrio em minerais, principalmente em plagioclásio (Perugini et al., 2003). Portanto, a determinação da composição química e texturas de minerais desempenha papel importante em petrologia ígnea (Binele Betsi e Lentz, 2012). Assim, a definição ou avaliação desses fatores é relevante para o entendimento dos processos responsáveis pela formação de plútons.

O Sistema Orogênico Sergipano (SOS – Conceição et al., 2016) representa o resultado da colisão entre a Placa Sanfranciscana e o Superterreno Pernambuco-Alagoas durante a Orogênese Brasiliana (Davison e Santos, 1989; D’el Rey Silva, 1992; Oliveira et al., 2006, 2010). Durante essa orogênese houve a colocação de vários corpos graníticos na porção norte do SOS (e.g., Oliveira et al., 2010, 2015). A granitogênese do SOS vem sendo estudada desde a década de 70, porém de forma regional (e.g., Silva Filho et al., 1977; Santos e Souza, 1988; Gaston e Santos, 1988). O reconhecimento e a individualização dos corpos graníticos começaram a ser alvo de estudos somente a partir da década de 90 (e.g., Chaves, 1991; McReath et al., 1998). Entretanto, ainda não se conhece os processos e as fontes responsáveis pela geração de grande parte dos magmas que originaram esses corpos.

O Batólito Rio Jacaré (BRJ), objeto deste estudo, corresponde à segunda maior intrusão (167 km²) do Domínio Poço Redondo (Sousa et al., 2019), no Sistema Orogênico Sergipano (SOS – Conceição et al., 2016). O BRJ tem idade de cristalização de 617 ± 4 Ma (Sousa et al., 2019) e é formado por quartzo monzonitos, monzogranitos e granodioritos com afinidade com a série calcioalcalina de alto K. Essas rochas apresentam abundantes EM shoshoníticos com formas, contatos, tamanhos e cores variadas (Sousa et al., 2019). As rochas do BRJ possuem biotita como mineral máfico mais abundante e os cristais de plagioclásio apresentam abundantes zoneamentos composicionais e texturas variadas (e.g., zonas de inclusão de minerais máficos, *synneusis*, textura *patchy zoning*). Grande parte dos demais plútons do SOS também apresenta EM, biotita e texturas em cristais de plagioclásio (e.g., Oliveira, 2014; Conceição et al., 2016; Lima, 2016; Lisboa et al., 2019; Pereira et al., 2019; Fernandes et al., 2020;). Porém, o BRJ é o plúton que exibe a maior abundância de EM no SOS e as feições de *mixing* e *mingling* são bem preservadas entre as rochas do BRJ e seus enclaves (Sousa et al., 2019).

O BRJ é um corpo ígneo importante que apresenta características complexas e únicas no Domínio Poço Redondo (DPR), como por exemplo, ocorrência abundante de EM que preservam feições de *mixing* e *mingling,* o que não é comum nos demais corpos da região. Além disso, a afinidade shoshonítica desses enclaves (Sousa et al., 2019) torna seu estudo ainda mais importante, uma vez que a geração de magmas shoshoníticos requer condições petrogenéticas específicas tanto quanto a ambiência geodinâmica, pressão e temperatura, o que poderia ajudar na compreensão da evolução do DPR e do SOS.

Após a caracterização geológica, petrográfica, mineraloquímica e litogeoquímica do BRJ feita por Sousa et al. (2019), várias questões importantes sobre os processos que ocorreram na câmara magmática do BRJ foram levantadas. Dentre elas estão: Qual a natureza dos abundantes EM que ocorrem no BRJ? Por que possuem formas, tamanhos e cores variadas? A injeção do magma máfico dos enclaves influenciou na dinâmica dos processos da câmara magmática do BRJ? Os minerais das rochas do BRJ foram capazes de registrar os processos que ocorreram durante a evolução do BRJ?

Esses questionamentos permitiram estabelecer o principal objetivo desta pesquisa, que foi contribuir para melhor entendimento da petrogênese do BRJ. Como objetivos específicos, tem-se: (1) obter novos dados petrográficos, de química mineral e geoquímica de rocha total; (2) caracterizar o magmatismo a partir dos elementos maiores, menores e traços das rochas estudadas; (3) inferir as condições de cristalização (e.g., temperatura, pressão, fugacidade de oxigênio) utilizando dados mineraloquímicos; (4) interpretar a gênese e a evolução do magmatismo; (5) divulgar, por meio de artigos científicos, os resultados obtidos ao longo do desenvolvimento da tese.

Para que os objetivos pudessem ser alcançados, foram feitas análises das feições das rochas e EM do BRJ (e.g., relações de contatos entre EM e os granitos hospedeiros, formas de EM), bem como a inferência de seus significados. Houve também a obtenção de dados petrográficos (petrografia clássica e eletrônica), de análises químicas pontuais em minerais (elementos maiores e traços), litogeoquímicos (elementos maiores, menores e traços) e isotópicos (Rb-Sr, Sm-Nd, U-Pb e Lu-Hf).

Os dados isotópicos U-Pb em titanita, Lu-Hf em zircão (εHf(t) entre -12,05 e -14,56) e mineraloquímicos de elementos traços não puderam ser utilizados até o momento nesta pesquisa, pois não chegaram a tempo para serem tratados e interpretados. Futuramente, pretende-se incorporá-los ao estudo.

O BRJ, objeto deste estudo, localiza-se na região norte do Estado de Sergipe (Figura 1), a sul de Poço Redondo. O batólito dista 180 km da capital do estado, Aracaju. A área objeto deste estudo é delimitada pelas coordenadas em UTM: 624.000/8.916.000 e 664.000/8.896.000.

A elaboração desta tese foi realizada com base no regimento do Programa de Pós-Graduação em Geologia da Universidade Federal da Bahia, sendo adotada a Resolução 01/2015 que determina a confecção da tese sob a forma de artigos. Durante a confecção da tese foram redigidos três artigos sobre a geologia do Batólito Rio Jacaré.

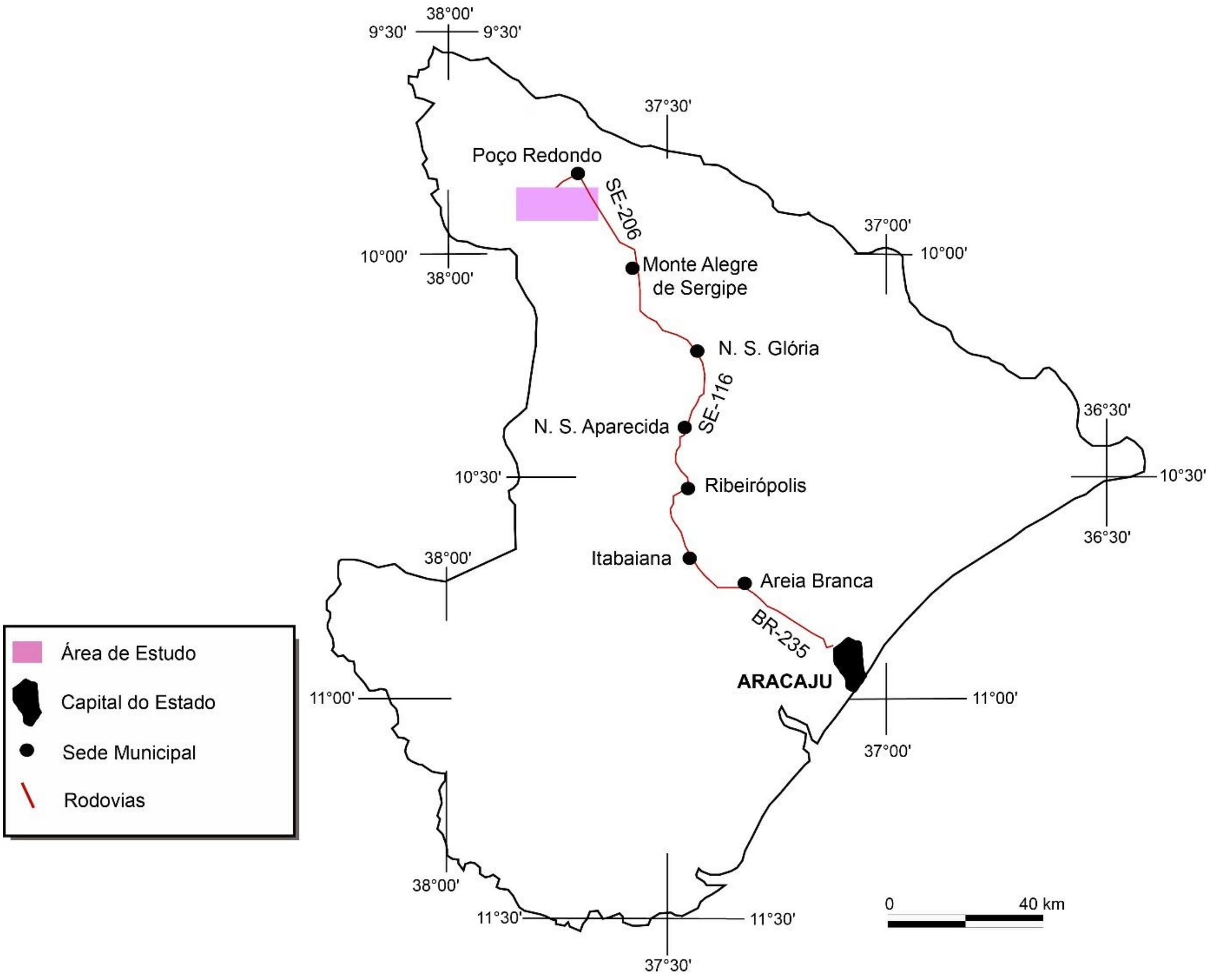

Figura 1. Mapa de localização e acesso, nos limites geográficos do Estado de Sergipe, da área de estudo.

O primeiro artigo, "Injections of enriched lithospheric mantle magmas explain the formation of microgranular enclaves in the Rio Jacaré Batholith, Borborema Province, Brazil", foi submetido ao Brazilian Journal of Geology (*Qualis* A3) e aceito em julho de 2022. Este trabalho representou o exame de qualificação, defendido em 2021.1. Nele caracterizou-se a geologia, petrografia e geoquímica dos enclaves microgranulares no BRJ. Os enclaves microgranulares são abundantes e possuem composições, formas e cores variadas, resultantes da atuação dos processos de *mingling* e *mixing.* O magma dos enclaves foi gerado a partir de taxa de 3% de fusão parcial do manto litosférico enriquecido. Logo após, esse magma foi injetado em estágios diferentes da cristalização da câmara magmática do BRJ.

O segundo artigo, intitulado "Magmatic processes recorded in plagioclase crystals of the Rio Jacaré Batholith, Sergipano Orogenic System, Northeast Brazil", foi submetido ao Journal of South American Earth Sciences (*Qualis* A3) e aceito em julho de 2022. Esse trabalho relata e discute os resultados de estudo sistemático em cristais de plagioclásio nas rochas do Batolito Rio Jacaré e nos enclaves microgranulares associados. Os cristais de plagioclásio estudados exibem variações composicionais de oligoclásio a labradorita (An_{11-51}), e várias texturas, como *patchy zoning*, textura *boxy cellular*, núcleos de cristais embaiados, zonas de inclusão de minerais máficos e *synneusis*. A identificação das texturas dos cristais foi feita a partir de petrografia clássica. A determinação das variações composicionais e a melhor visualização da geometria das texturas foi feita utilizando os detectores de elétrons retroespalhados, secundários e espectrômetro de energia dispersiva instalados em microscópio eletrônico de varredura. As feições encontradas nos cristais estudados sugerem modificações nas condições físico-químicas (temperatura, pressão e atividade de H_2O) do sistema magmático BRJ durante sua evolução. Essas modificações foram ocasionadas por injeções de magma máfico, que provocaram *mixing*, *mingling* e correntes de convecção na câmara magmática do BRJ. Superfícies de reabsorção podem ser identificadas em núcleos dos cristais de plagioclásio e sugerem pelo menos cinco momentos sucessivos de reabsorção nesses cristais durante a evolução do BRJ.

O terceiro artigo, nomeado "Mineral chemistry of the Rio Jacaré Batholith biotite, Poço Redondo Domain, Sergipano Orogenic System: petrogenetic implications", foi submetido ao Brazilian Journal of Geology (*Qualis* A3) em março de 2022. A motivação para este artigo surgiu quando se percebeu a presença de cristais de biotita magmáticos e magmáticos reequilibrados nas rochas das fácies inequigranular, porfirítica e enclaves microgranulares do Batolito Rio Jacaré. Com base no estudo sistemático de texturas e composições químicas desses cristais, percebeu-se que os cristais primários/magmáticos geralmente ocorrem como inclusões em plagioclásio e os magmáticos reequilibrados contêm, em suas clivagens, cristais anédricos de titanita. Os cristais estudados correspondem a Mg-biotita e suas condições de cristalização inferidas (e.g., temperatura de 678 a 745 °C e pressão de 1,2 a 2,9 kbar) são consistentes com cristalização da biotita em sistemas graníticos. A identificação de processos magmáticos (e.g., vários pulsos de magma máfico durante a evolução do BRJ) pôde ser feita ao se correlacionar a variação de temperatura com a variação de *f*O2 de cristais em diferentes amostras de enclaves microgranulares.

Referências

Annen, C., Blundy, B. D., Leuthold, J., Sparks, R. S. J. (2015). Construction and evolution of igneous bodies: towards an integrated perspective of crustal magmatism. Lithos, 230, 206-221. Doi: 10.1016/j.lithos.2015.05.008

Barbarin, B. (1990). Granitoids: main petrogenetic classifications in relation to origin and tectonic setting. Geological Journal, 25, 227-238.

Barbarin, B., Didier, J. (1991). Macroscopic features of mafic microgranular enclaves. In: J. Didier, B. Barbarin, Enclaves in granite petrology, development in petrology (pp. 263-275). Amsterdam: Elsevier.

Bineli Betsi, T., Lentz, D. R. (2013). Chemical composition of rock-forming minerals in granitoids associated with Au-Bi-Cu, Cu-Mo, and Au-Ag mineralization at the Freegold Mountain, Yukon, Canada: magmatic and hydrothermal fluid chemistry and petrogenetic implications. International Geology Review, 55 (6), 657-691. Doi: 10.1080/00206814.2012.731767.

Bonin, B. (2004). Do coeval mafic and felsic magmas in post-colisional to within-plate regimes necessary imply two contrasting, mantle and crustal, sources? A review. Lithos, 78, 1-24.

Brown, M. (1994). The generation, segregation, ascent and emplacement of granite magma: the migmatite-to-crustally-derivered granite connection in thickened orogens. Earth-Science Reviews, 36, 83-130.

Campbell, I.H., Taylor, S. R. (1983). No water, no granites – no oceans, no continents. Geophysical Research Letters, 10 (11), 1061-1064.

Chappell, B. W., White, J. R. (1992). I- and S-type granites in the Lachlan Fold Belt. Transation of Royal Society Edinburg: Earth Sciences, 83 (1-2), 1-26.

Conceição, J. A., Rosa, M. L. S., Conceição, H. (2016). Sienogranitos leucocráticos do Domínio Macururé, Sistema Orogênico Sergipano, Nordeste do Brasil: Stock Glória Sul. Brazilian Journal of Geology, 46 (1), 63-77.

Chaves, J. M. (1991). Maciços Cel. João Sá e Glória: petrologia e geoquímica de granitoides do Domínio Macururé, Faixa Sergipana (NE do Brasil). Dissertação. Universidade Federal da Bahia. Salvador, 134 p.

Crisp, J. A. 1984. Rates of magma emplacement and volcanic output. Journal of Volcanology and Geothermal Research, 20, 177-211. Doi: 10.1016/0377-0273(84)90039-8

Davison, I., Santos, R. A. (1989). Tectonic Evolution of the Sergipano Fold Belt, NE-Brazil, during the Brasiliano Orogeny. Precambrian Research, 45, 319-342.

D'el Rey Silva, L. J. H. (1992). Tectonic Evolution of the Southern Part of the Sergipano Fold Belt, Northeastern Brazil. Tese de Doutorado, University of London.

Didier, J. (1973). Granites and their enclaves. Elsevier: Amsterdam, 393 p.

Didier, J., Barbarin, B. (1991). Enclaves and granites petrology. Elsevier: Amsterdam, 625p.

Dong, Q., Du, Y., Pang, Z., Miao, W., Tu, W. (2014). Composition of biotite within the Wushan granodiorite, Jiangxi Province, China: petrogenetic and metallogenetic implications. Earth Sciences Research Journal, 18(1), 39-44. Doi: 10.15446/esrj.v18n1.40830

Erdmann, S., Martel, C., Pichavant, M., Kusgnir, A. (2014). Amphibole as an archivist of magmatic crystallization conditions: problems, potential, and implications for inferring magma storage prior to the paroxysmal 2010 eruption of Mount Merapi, Indonesia. Contributions Mineralogy Petrology, 167, 1-23. Doi: 10.1007/s00410-014-1016-4

Fernandes, D. M., Lisboa, V. A. C., Rosa, M. L. S., Conceição, H. (2020). Petrologia e idade do Stock Fazenda Lagoas, Domínio Macururé, Sistema Orogênico Sergipano, NE-Brasil. Geologia USP. Série Científica, 20(1), 39-60. doi: 10.11606/issn.2316-9095.v20-160040

Gaston, G. O., Santos, R. A. (1988). Geoquímica de alguns granitoides do Sistema de Dobramentos Sergipana. XXXV Congresso Brasileiro de Geologia. Belém: Sociedade Brasileira de Geologia, 1037-1052.

Hibbard, M. J. (1991). Textural anatomy of twelve magma-mixed granitoid systems. In: Didier, J., Barbarin, B. (eds). Enclaves and granite petrology, developments in petrology. Elsevier: Amsterdam, 431-444.

Huppert, H. E., Sparks, R. S. J. (1988). The generation of granitic magmas by intrusion of basalt into continental crust. Journal of Petrology, 29(3), 599-624.

Glazner, A. F., Coleman, D. S., Mills, R. D. (2018). The volcanic-plutonic connection. In Physical geology of shallow magmatic systems, (eds C Breitkreuz, S Rocchi), pp. 61-82. Berlin, Germany: Springer.

Kumar, S., Rino, V. (2006). Mineralogy and geochemistry of microgranular enclaves in Palaeoproterozoic Malanjkhand granitoids, Central India: evidence of magma mixing, mingling, and chemical equilibration. Contributions to Mineralogy and Petrology, 152, 591-609.

Lima, D., 2016. Caracterização petrológica e geoquímica do Pluton Curituba, Domínio Poço Redondo-Marancó, Cinturão Sergipano. Dissertação de Mestrado. Universidade Federal de Pernambuco.

Lisboa, V. A. C., Conceição, H., Rosa, M. L. S., Fernandes, D. M. (2019). The onset of post-collisional magmatism in the Macururé Domain, Sergipano Orogenic System: The Glória Norte Stock. Journal of South American Earth Sciences, 89, 173-188. doi: 10.1016/j.jsames.2018.11.005

Martin, R. F. (2007). Amphiboles in the igneous environment. Reviews in Mineralogy and Geochemistry, 67(1), 323-358. Doi: 10.2138/rmg.2007.67.9

McReath, I., Lafon, J. M., Davison, I., Chaves, J. M., Conceição, H. (1998). Brasiliano-age granitoids in the Sergipana Fold Belt, NE Brazil: the Coronel João Sá Plúton. Journal of South American Earth Sciences, 11(1), 51-66. Doi: 10.1016/S0895-9811(97)00036-9

Papoutsa, A., Pe-Piper, G. (2014). Geochemical variation of amphiboles in A-type granites as an indicator of complex magmatic systems: Wentworth pluton, Nova Scotia, Canada. Chemical Geology, 384, 120-134.

Paterson S. R., Ardill K., Vernon R., Žák J. (2018). A review of mesoscopic magmatic structures and their potential for evaluating the hypersolidus evolution of intrusive complexes. Journal of Structural Geology, 125, 134-147. doi: 10.1016/j.jsg.2018.04.022

Pereira, F. S., Rosa, M. L. S., Conceição, H. (2019). Condições de colocação do magmatismo máfico do Domínio Macururé, Sistema Orogênico Sergipano: Maciço Capela. Geologia USP. Série Científica, 19, 3-29. doi: 10.11606/issn.2316-9095.v19-151464

Perugini, D., Busa, T., Poli, G., Nazzareni, S. (2003). The role of chaotic dynamics and flow fields in the development textures in volcanic rocks. Journal of Petrology, 44, 733-756.

Oliveira, A. C. (2014). Petrogênese do Stock Granítico Monte Alegre, noroeste do Domínio Macururé, Faixa Sergipana. Dissertação de Mestrado. Universidade Federal de sergipe.

Oliveira, E. P., Bueno, J. F., McNaughton, N. J., Silva Filho, A. F., Nascimento, R. S., Donatti-Filho, J. P. (2015). Age, composition, and source of continental arc- and syn-collision granites of the Neoproterozoic Sergipano Belt, Southern Borborema Province, Brazil. Journal of South American Earth Sciences, 58, 257-280.

Oliveira, E. P., Toteu, S. F., Araújo, M. N. C., Carvalho, M. J., Nascimento, R. S., Bueno, J. F., McNahghton, N., Basilici, G. (2006). Geologic correlation between the Neoproteroxoic Sergipano belt (NE Brazil) and the Yaoundé belt (Cameron, Africa). Journal of African Earth Sciences, 44, 470-478. doi:10.1016/j.jafrearsci.2005.11.014

Oliveira, E. P., Windley, B. F., Araújo, M. N. (2010). The Neoproterozoic Sergipano orogenic belt, NE Brazil: A complete plate tectonic cycle in western Gondwana. Precambrian Research, 181, 64-84.

Santos, R. A., Souza, J. D. (1988). Programa Levantamentos Geológicos Básicos do Brasil – Piranhas Folha SC.24-X-C-VI – Estados de Sergipe, Alagoas e Bahia. Brasília, 154 p.

Silva Filho, M. A., Bonfim, L. F. C., Santos, R. A., Leal, R. A., Santana, A. C., Braz Filho, P. A. (1977). Geologia da Geossiclinal Sergipana e do seu embasamento, Alagoas, Sergipe e Bahia, Projeto Baixo São Francisco/Vaza Barris. DNPM/CPRM, 131 p.

Sousa, C. S., Soares, H. S., Rosa, M. L. S., Conceição, H. (2019). Petrologia e Geocronologia do Batólito Rio Jacaré, Domínio Poço Redondo, Sistema Orogênico Sergipano, NE do Brasil. Geologia USP. Série Científica, 19(2), 171-194. doi:10.11606/issn.2316-9095.v19-152494

Sklyarov, E. V., Fedorovskii, V. S. (2006). Magma mingling: tectonic and geodynamic implications. Geotectonics, 40(2), 120-134.

Vernon, R. H. (1984). Microgranitoid enclaves in granites – globules of hybrid magma quenched in a plutonic environment. Nature, 309, 438-439.

Whalen, J. B., Currie, K. L., Chappell, B. W. (1987). A-types granites: geochemical characteristics, discrimination and petrogenesis. Contribution to Mineralogy and Petrology, 95(4), 407-419.

Whitney, J. A. (1988). The origin of granite: the role and source of water in the evolution of granitic magmas. Geological Society of American Bulletin, 100 (12), 1886-1897.

Winter, J. D. (2014). Principles of igneous and metamorphic petrology. Harlow: Pearson, 738 p.

Yazdi, A., Ardalan, A. A., Emani, M. H., Dabiri, R., Foudazi, M. (2019). Magmatic interactions as recorded in plagioclase phenocrysts of quartenary volcanics in SE Bam (SE Iran). Iranian Journal of Earth Sciences, 11(3), 215-225.

CAPÍTULO 2
INJECTIONS OF ENRICHED LITHOSPHERIC MANTLE MAGMAS EXPLAIN THE FORMATION OF MICROGRANULAR ENCLAVES IN THE RIO JACARÉ BATHOLITH, BORBOREMA PROVINCE, BRAZIL

Carlos Santana Sousa[1,2], Hiakan Santos Soares[1,2], Maria de Lourdes da Silva Rosa[2,3], Herbet Conceição[1,2,3]

[1] Programa de Pós-graduação em Geologia, Instituto de Geociências, Universidade Federal da Bahia (UFBA), Rua Barão de Jeremoabo, s/n, Federação, 40170-209, Salvador, Bahia, Brazil

[2] Laboratório de Petrologia Aplicada à Pesquisa Mineral (LAPA), Universidade Federal de Sergipe (UFS), Avenida Marechal Rondon, s/n, Jardim Rosa Elze, 49100-000, São Cristóvão, Sergipe, Brazil

[3] Programa de Pós-graduação em Geociências e Análise de Bacias (PGAB), Universidade Federal de Sergipe, Avenida Marechal Rondon, s/n, Jardim Rosa Elze, 49100-000, São Cristóvão, Sergipe, Brazil

karlcss@ufba.br (C.S. Sousa); hiakanss@ufba.br (H.S. Soares); lrosa@academico.ufs.br (M.L.S. Rosa) & herbet@academico.ufs.br (H. Conceição)

Abstract

The Rio Jacaré Batholith (RJB; 617 ± 4 Ma) is inserted in the Poço Redondo Domain, Sergipano Orogenic System. This batholith is formed by monzodiorite, quartz monzodiorite, monzonite and quartz monzonite, and has abundant microgranular enclaves (MEs). The MEs have colors that vary from black to light gray and have globular to slightly elongated shapes. Their contacts are clear-cut, crenulated and cuspate, or, more rarely, diffuse. MEs correspond to diorites, monzodiorites, quartz monzodiorites and monzonites; and the textures present in these rocks indicate the mixing of magmas (e.g., compositional zoning in plagioclase, inclusion zones in plagioclase phenocrysts, poikilitic alkali feldspar, acicular apatite, ocellar quartz). Through the calculations of the linear correlations of major elements, it is observed that the smallest fraction of mafic magma involved in the mixing was 0.43. MEs represent the breakdown and cooling of a mafic magma that has been injected into a cooler felsic magmatic chamber. The emplacement of this mafic magma occurred during different stages of crystallization of the magmatic chamber of the RJB. MEs are magnesian and metaluminous, and they have an affinity with shoshonitic series. The Ba/Nb (>23), Ba/La (>15) and Nb/La (0.22–0.69) ratios are characteristic of magmas generated from the partial melting of an enriched lithospheric mantle source. Batch melting modeling suggests that source melting rates of less than 3% are necessary to generate magmas similar to those of the RJB MEs.

Keywords: Sergipano Orogenic System; Mixing; Mingling; Shoshonitic Magmatism.

1. INTRODUCTION

According to Elburg (1996), there are four types of enclaves formed by different processes: (i) restite is solid residue resulting from magma generation (e.g., Chen et al., 1990); (ii) xenoliths are fragments of country rock (e.g., Hall, 1991); (iii) enclaves can be formed through the segregation of early mafic minerals (e.g., Dodge and Kistler, 1990); and (iv) microgranular enclaves are cooled droplets of mafic magmas that intruded host granitic magmas (e.g., Didier, 1973; Clemens et al., 2017; Siuda and Bagiński, 2019).

Microgranular enclaves (MEs) are the most common types of inclusions in granitic bodies (Barbarin and Didier, 1991) and are considered to be one of the keys to understanding the genesis and evolution of granites (Didier, 1973; Barbarin and Didier, 1991; Sarjoughian et al., 2017).

Some authors consider the presence of MEs with cooled edges and xenocrysts in granites as evidence of the coexistence of magmas with different viscosities (e.g., Vernon, 1984; Kumar and Rino, 2006; Siuda and Bagiński, 2019). The rocks formed have characteristic textures (e.g., rapakivi texture, ocellar quartz, inclusion zones in phenocrysts, compositional zoning in plagioclase, biotite blades) that indicate the actions of mingling between magmas (Hibbard, 1991). Geochemical data can also preserve evidence of mixing; the mixing can cause, for example, the predominance of intermediate compositions, resulting from the mixture of basic and acid magmas, and linear trends in Harker-type diagrams (e.g., Nardi and Lima, 2000; Reubi and Blundy, 2009; Ruprecht et al., 2012; Kumar et al., 2017).

In the Sergipano Orogenic System (SOS; Conceição et al., 2016), there is evidence of voluminous Neoproterozoic plutonism that has been the target of several studies over the last few decades (e.g., Santos and Souza, 1988; Davison and Santos, 1989; Santos et al., 2001; Bueno et al., 2009; Oliveira, 2014; Oliveira et al., 2015; Conceição et al., 2016; Fontes et al., 2018; Lisboa et al., 2019; Pinho Neto et al., 2019; Santos et al., 2019; Sousa et al., 2019; Fernandes et al., 2020). Many of these studies identified the presence of MEs in these intrusions; however geological, petrographic and geochemical data from MEs in the SOS are still scarce.

This study presents and discusses the geological, petrographic and geochemical data of the microgranular enclaves of the Rio Jacaré Batholith (RJB), which is an important intrusion in the Poço Redondo Domain, located in the northern sector of the SOS.

2. REGIONAL CONTEXT

The SOS (Figure 1A) is inserted in the southern portion of the Borborema Province (Almeida et al., 1977). This orogen is interpreted to be the result of the collision between the Sanfranciscana plate, to the south, and the Pernambuco-Alagoas Domain, to the northeast, during the Brasiliano Orogeny (D'el Rey Silva, 1992; Oliveira et al., 2006, 2010). The seven geological domains of the SOS are limited by shear zones (Davison and Santos, 1989; Silva Filho and Torres, 2002): Estância, Vaza-Barris, Macururé, Marancó, Poço Redondo, Canindé and Rio Coruripe. The Macururé, Marancó, Poço Redondo and Canindé domains are characterized by abundant presence of granites.

The RJB occurs in the Poço Redondo Domain (PRD; Figure 1B), which, according to Santos et al. (2001), represents the deepest crustal exposure of the SOS. This domain is formed by the Poço Redondo Migmatitic Complex (Santos and Souza, 1988) and by Neoproterozoic granites (Carvalho, 2005; Pinho Neto et al., 2019; Sousa et al., 2019). The PRD is limited to the north by the Canindé Domain and the Macururé Shear Zone (Figure 1A) and to the south by the Marancó Domain and the Poço Redondo Shear Zone.

2.1 Microgranular enclaves in the Sergipano Orogenic System

In the SOS, MEs have been described in several intrusions (Table 1). These enclaves, according to several authors (e.g., Gentil, 2013; Silva, 2014; Lima, 2016; Lisboa et al., 2019; Pereira et al., 2019; Santos et al., 2019; Fernandes et al., 2020), show globular and elliptical shapes. Their sizes range from centimetric to metric.

In the granites of the Macururé and Poço Redondo domains (e.g., Oliveira, 2014; Silva, 2014; Sousa et al., 2019; Lisboa et al., 2019; Fernandes et al., 2020), multiple enclaves, some with chilled margins, are described. These enclaves are randomly distributed in the intrusions or gathered in syn-plutonic dikes. In several of these enclaves, alkaline feldspar xenocrystals attributed to the host granites occur. These features provide evidences for mixing between mafic and felsic magmas during the evolution of these intrusions (e.g., Lisboa et al., 2019; Sousa et al., 2019).

The MEs of the Ediacaran bodies in the SOS have compositions ranging from diorite, quartz diorite, monzodiorite, quartz monzodiorite, monzonite, syenite and alkali-feldspar syenite to alkali-feldspar-quartz syenite (Figure 2A). The mafic minerals in these rocks are hornblende, biotite, diopside and titanite, as accessory minerals magmatic epidote, apatite, opaque minerals and zircon are found. These rocks have silica contents varying from 44 to 63%, pointing to distinct degrees of evolution (Figure 2B), and they have an affinity with shoshonitic series (Figure 2C).

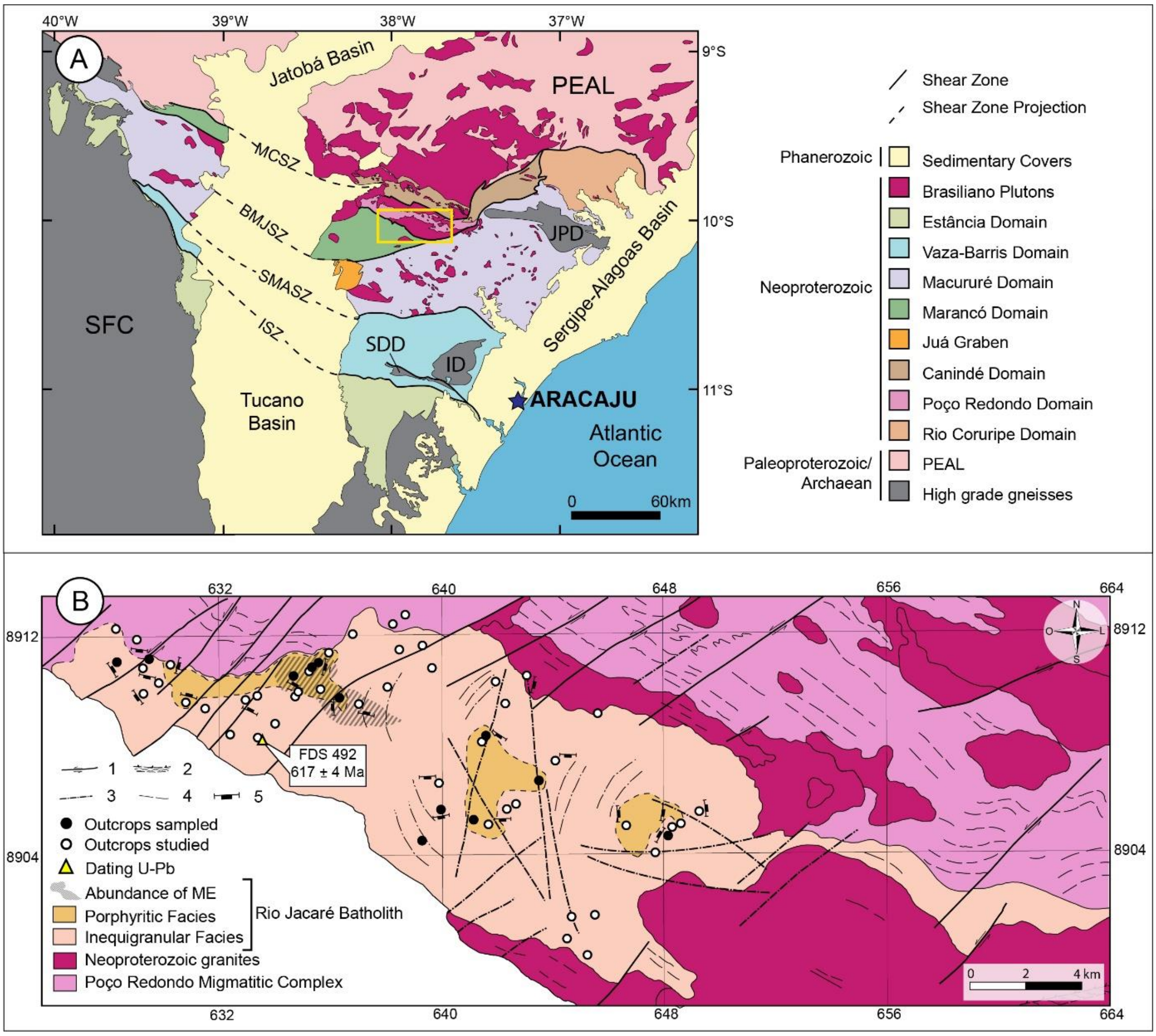

Figure 1. Geological schemes that contextualize the regional and local geology of the Rio Jacaré Batholith. (A) Sergipano Orogenic System (Oliveira et al., 2006, after Pinho Neto et al., 2019); (B) Rio Jacaré Batholith (Sousa et al., 2019). São Francisco Craton (SFC); Pernambuco-Alagoas Massif (PEAL). Shear zones: Macururé (MCSZ); Belo Monte Jeremoabo (MBJSZ); São Miguel do Aleixo (SMASZ); Itaporanga (ISZ). Domes: Itabaiana (ID); Simão Dias (SDD); Jirau do Ponciano (JPD). 1 – Fault; 2 – Shear zone; 3 – Fracture; 4 – Lineament; 5 – Magmatic foliation.

Table 1. Characteristics of the microgranular enclaves bearing host plutons in the Macururé and Poço Redondo domains of the Sergipano Orogenic System.

Pluton	Location	Rocks	Geochemistry affinity	Crystallization age (U-Pb$_{SHRIMP}$)	Reference
Curituba Batholith	Poço Redondo Domain	Monzogranite, syenogranite, monzonite and syenite	Shoshonitic	624 ± 16 Ma	Gentil (2013); Lima (2016)
Capela Stock	Macururé Domain	Diorite, hornblende, gabbro and granite	Shoshonitic	631 ± 3 Ma	Pereira et al. (2019)
Glória Sul Stock	Macururé Domain	Syenogranite	High K calc-Alkaline	626 ± 7 Ma	Conceição et al. (2016); Rosa et al. (2017)
Fazenda Lagoas Stock	Macururé Domain	Granodiorite, granite and quartz monzonite	Shoshonitic	623 ± 4 Ma	Fernandes et al. (2020)
Monte Alegre Stock	Macururé Domain	Monzonite and granite	High K calc-alkaline	621 ± 5 Ma	Oliveira (2014); Rosa et al. (2017)
Lagoa do Roçado Stock	Macururé Domain	Granodiorite	High K calc-alkaline	618 ± 4 Ma	Silva (2014)
Propriá Stock	Macururé Domain	Monzonite and Granite	High K calc-alkaline	615 ± 6 Ma	Santos et al. (2019)
Glória Norte Stock	Macururé Domain	Quartz monzonite and monzogranite	Shoshonitic	588 ± 5 Ma	Lisboa et al. (2019)

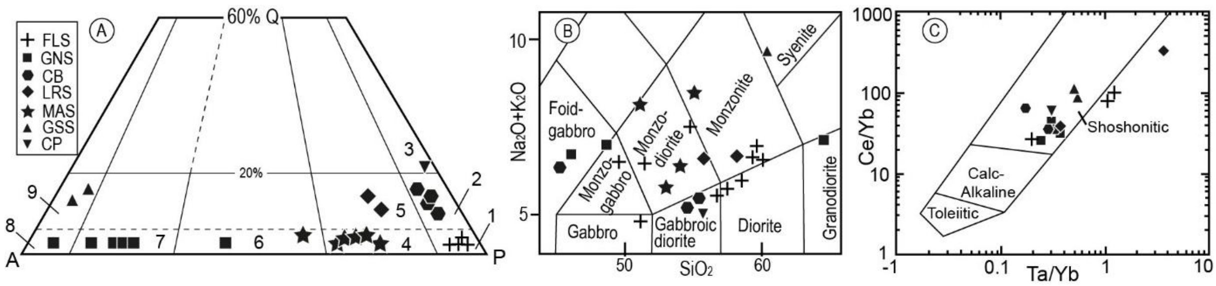

Figure 2. Modal and chemical diagrams applied to the enclaves of different bodies of the geological domains of the SOS. (A) Streckeisen's (1976) QAP triangular diagram. Q: quartz, A: alkali feldspar + albite with <5% anorthite, P: plagioclase (anorthite > 5%). 1: Diorite; 2: quartz diorite; 3: tonalite; 4: monzodiorite; 5: quartz monzodiorite; 6: monzonite; 7: syenite; 8: alkali-feldspar syenite; 9: alkali-feldspar-quartz syenite. (B) TAS diagram with fields proposed by Middlemost (1985). (C) Ta/Yb versus Ce/Yb diagram with fields defined by Pearce (1982). GNS – Glória Norte Stock (Lisboa et al., 2019); CB – Curituba Batholith (Gentil, 2013); LRS – Lagoa do Roçado Stock (Silva, 2014); MAS – Monte Alegre Stock (Oliveira, 2014); GSS – Glória Sul Stock (Conceição et al., 2016); CP – Capela Pluton (Pereira et al., 2019); FLS – Fazenda Lagoas Stock (Fernandes et al., 2020).

2.2 Rio Jacaré Batholith

The RJB (167 km²) has a U-Pb$_{SHRIMP}$ zircon crystallization age of 617 ± 4 Ma (Sousa et al., 2019). It is intrusive to the Poço Redondo Migmatitic Complex and Sítios Novos Batholith (Sousa et al., 2019). This batholith is composed of monzodiorite, quartz monzodiorite, monzonite and quartz monzonite, which occur in two petrographic facies, inequigranular and porphyritic (Figure 1); they always present abundant microgranular enclaves.

The Inequigranular Facies (Figure 3A) is predominant in the RJB and consists of gray rocks with a medium to fine inequigranular texture. Eventually these rocks have magmatic foliation and the elongated enclaves appear parallel or subparallel to the foliation of the rocks that host them. The Porphyritic Facies (Figure 3B) differs from the previous facies due to the presence of alkali feldspar phenocrysts to macrocrystals, with sizes ranging from 1 to 5 cm. The rocks of this facies are composed of plagioclase (An_{11-33}), microcline (Or_{75-98}), quartz, biotite ($0.3 < Fe/(Fe + Mg) < 0.6$), Mg-hornblende, titanite, magmatic epidote, F-apatite, magnetite, ilmenite and zircon.

The RJB rocks are magnesian and metaluminous, and have a high-K calc-alkaline affinity and geochemical signature consistent with a post-collisional environment (Brito, 1996; Sousa et al., 2019).

According to Oliveira et al. (2015), the RJB was probably formed by a mixture of mantle-derived and crustal magmas. These authors support this hypothesis based on $(^{87}Sr/^{86}Sr)_i$ ratios ranging from 0.70656 to 0.70789, with $\varepsilon_{Nd(617\ Ma)}$ between -1.15 and -2.55 and T_{DM} ranging from 1.2 to 1.3 Ga.

3. MATERIALS AND METHODS

The studied samples correspond to microgranular enclaves, with colors ranging from light gray to dark gray. These rocks show no evidence of alteration and have magmatic textures. In this study, only samples from the central parts of the enclaves were collected in an attempt to avoid possible interactions between the periphery and the host magma. After grinding, the feldspar xenocrysts present in some enclaves were manually removed in order to obtain chemical data that corresponded as close as possible to the composition of the original magma that originated these rocks.

In this study, rocks were named using IUGS recommendations (Le Maître et al., 1989), and the modal data were obtained from the modified CIPW standard norm for hornblende-bearing rocks.

The geochemical analysis of major elements was obtained from pressed pellets using a Shimadzu XRF-1800 X-ray fluorescence spectrometer at the Condominium of Multiuser Laboratories of Geosciences of the Federal University of Sergipe. The pellets were made by mixing the samples with boric acid, which was sprayed onto the samples, with a ratio of samples to boric acid of 3:1. Then, the sample / boric acid mixtures were pressed in a hydraulic press with a pressure of 60 kN for 30 seconds. The degree of confidence of the analysis was evaluated through a comparison with certified reference materials (e.g., AVG-1, DTS-1, QLO-1). The loss on ignition was determined by calcinating the samples at a constant temperature of 1000 ºC in a muffle furnace for 2 hours.

The trace elements analysis was performed at the ALS commercial laboratory, Brazil, using ICP-MS and an analytical package for petrological purposes (ME-MS81D).

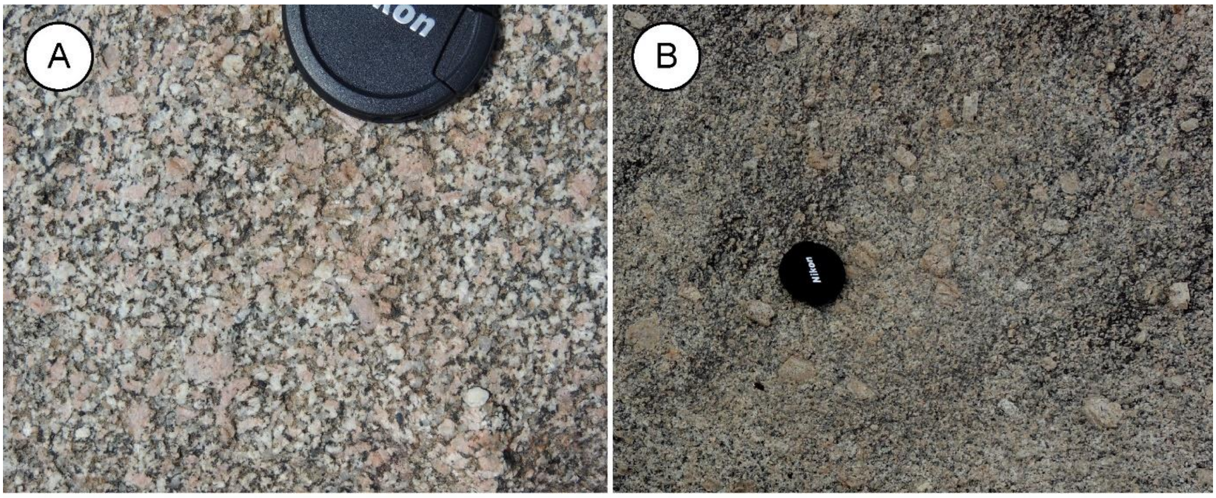

Figure 3. RJB rocks in the field. (A) Inequigranular Facies and (B) Porphyritic Facies. Note the centimetric sizes of the alkali feldspar crystals and the finer grain of the matrix. Pinkish minerals with rectangular sections correspond to alkali feldspar crystals, white minerals correspond to plagioclase and black minerals correspond to biotite and hornblende. The diameter of the black circle is 7 cm.

4. MICROGRANULAR ENCLAVES OF THE RIO JACARÉ BATHOLITH

4.1 Geology

The RJB MEs are fine-grained and show sizes from 2 cm to 2 m, black to light gray colors, globular to elliptical shapes and, clear-cut, crenulated, and diffuse types of contacts.

In the eastern portion of the RJB, the MEs have smaller sizes, round shapes (Figure 4A) and black color, and they are isolated. In the western region, the MEs are more abundant, have larger sizes and occur more frequently in syn-plutonic dikes (Figure 4B–D). These dikes are subvertical and have widths ranging from 1.5 m to 6 m; their lengths are greater than 10 m. In the western sector, there is a greater variety of enclave shapes exhibiting rounded to elongated features. They tend to present varying shades of gray.

Globular to elongated MEs with clear-cut contacts (Figure 4E) predominate throughout the RJB. The elongated types are oriented parallel to the batholith´s magmatic foliation. In the western region, the MEs are also clear-cut but with more complex contacts (Figure 4F), including crenulated (Figure 4G), lobate, sinuous and cuspate. The MEs with crenulated contacts are typically 15 cm long, while the MEs with other types of contacts are larger.

Some MEs have a grain size that decreases from the nucleus to the border (Figure 4E). Alkali feldspar and quartz xenocrysts in the MEs are recurrent features and can be identified by their grain size, which is similar to that of the host granite and larger than the grain size of the MEs (Figure 4H). In some cases, multiple MEs are observed in the center of the RJB (Figure 4I); these enclaves are gray and contain smaller, black enclaves. These black enclaves occur both within the gray enclaves and in the host granite.

Figure 4. Field images showing different structures of the various types of MEs identified in the RJB. (A) MEs with globular to elongated shapes and clear-cut straight contacts. (B, C and D) Set of elongated enclaves with different sizes interpreted as syn-plutonic dikes. Note the feature in the left corner of image D suggesting that the enclave's magma was undergoing rupture as it generated microgranular enclaves. (E) ME with clear-cut contacts, showing a grain size increase from the edges to the center. Note the darker edges. (F) ME with crenulated to lobate margins. (G) Round ME with a crenulated contact in its left portion. (H) Alkali feldspar xenocrysts in ME. It is possible to observe crystals penetrating the enclave edges. (I) Multiple MEs in the RJB. Note the black enclaves inside the larger gray enclave.

4.2 Petrography

The RJB MEs have dioritic, monzodioritic, quartz monzodioritic and monzonitic compositions (Figure 5). These rocks are composed essentially of plagioclase (An_{11-51}), microcline, quartz, hornblende and biotite. The accessory minerals are titanite, epidote, allanite, F-apatite, magnetite, ilmenite and zircon. MEs have a massif structure with fine-grained, porphyritic and hypidiomorphic textures (Figure 6A). In the porphyritic rocks, there are plagioclase phenocrysts and microcline and ocellar quartz xenocrysts (Figure 6B and C). All the textures observed in these rocks are igneous and show no evidence of solid-state deformation or recrystallization.

Plagioclase occurs as phenocrysts (1.7–5.8 mm) and in the matrix (0.1–1.4 mm). These crystals are subhedral and show albite and albite-Carlsbad twinning and frequent compositional zoning. The zoning is parallel to the crystal faces and by the presence of opaque, biotite and hornblende mineral inclusions (Figure 6D). In some crystals, zoning develops from rounded plagioclase nuclei, suggesting dissolution (Figure 6E). Patchy, boxy, cellular and stepwise textures can occasionally occur, indicating complex evolution during crystallization. Sometimes, saussuritization is observed in the grain nuclei of some crystals. A myrmekitic texture is occasionally present.

Perthitic microcline is anhedral, poikilitic and occurs in the matrix (0.1–1.5 mm) and as xenocrysts (1.7–11.7 mm). It often shows albite-pericline twinning, but occasionally remnants of Carlsbad twinning are found. Quartz presents a weak undulose extinction. It occurs in the matrix (0.1–1.3 mm) and sometimes as xenocrysts (1.5–4.3 mm) in the ocellar texture (Figure 6B and C), which shows zones of biotite and hornblende inclusion at the edges.

Brown biotite is subhedral and has brown to yellow pleochroism. It is frequently associated with hornblende crystals in mafic aggregates. Titanite crystals and anhedral opaque minerals occur as inclusions in grain margins and in cleavage planes. Green hornblende is subhedral to euhedral and presents pleochroism in shades of green. It commonly occurs in clusters along with biotite, titanite and opaque minerals.

Epidote is subhedral or anhedral. Anhedral crystals are usually observed in the contacts with biotite, hornblende and plagioclase. The subhedral crystals are considered to be magmatic, showing dissolution features. They can also occur as rims around allanite crystals. Rarely, vermicular quartz inclusions are observed in epidote. Allanite occurs sporadically. Subhedral titanite occurs as inclusions in most minerals and locally forms clusters. Apatite is euhedral and acicular (Figure 6F), and, as individual elongated grains, it may be found often included in various minerals (e.g., in plagioclase and biotite); it may be a product of early crystallization. Zircon is euhedral (~0.1 mm) and occurs as inclusion. Anhedral opaque minerals (magnetite and ilmenite) no larger than 0.4 mm are associated with biotite, hornblende and titanite crystals.

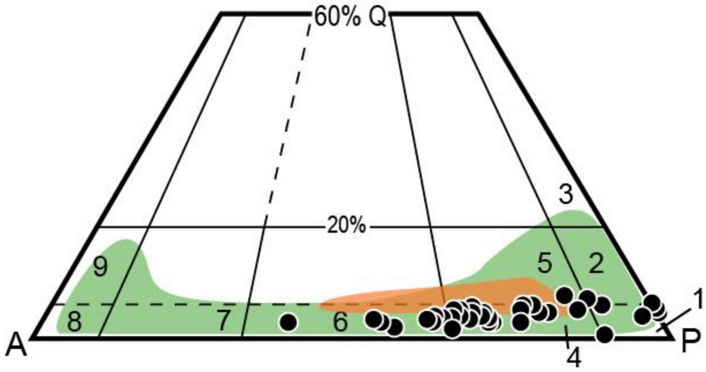

Figure 5. Classification of the RJB MEs using the QAP diagram (Streckeisen, 1976). Q: quartz, A: alkali feldspar + albite with <5% anorthite, P: plagioclase (anorthite > 5%). 1: Diorite; 2: quartz diorite; 3: tonalite; 4: monzodiorite; 5: quartz monzodiorite; 6: monzonite; 7: syenite; 8: alkali-feldspar syenite; 9: alkali-feldspar-quartz syenite. The orange area represents the composition of the RJB rocks. The green area represents the compositions of the other SOS MEs.

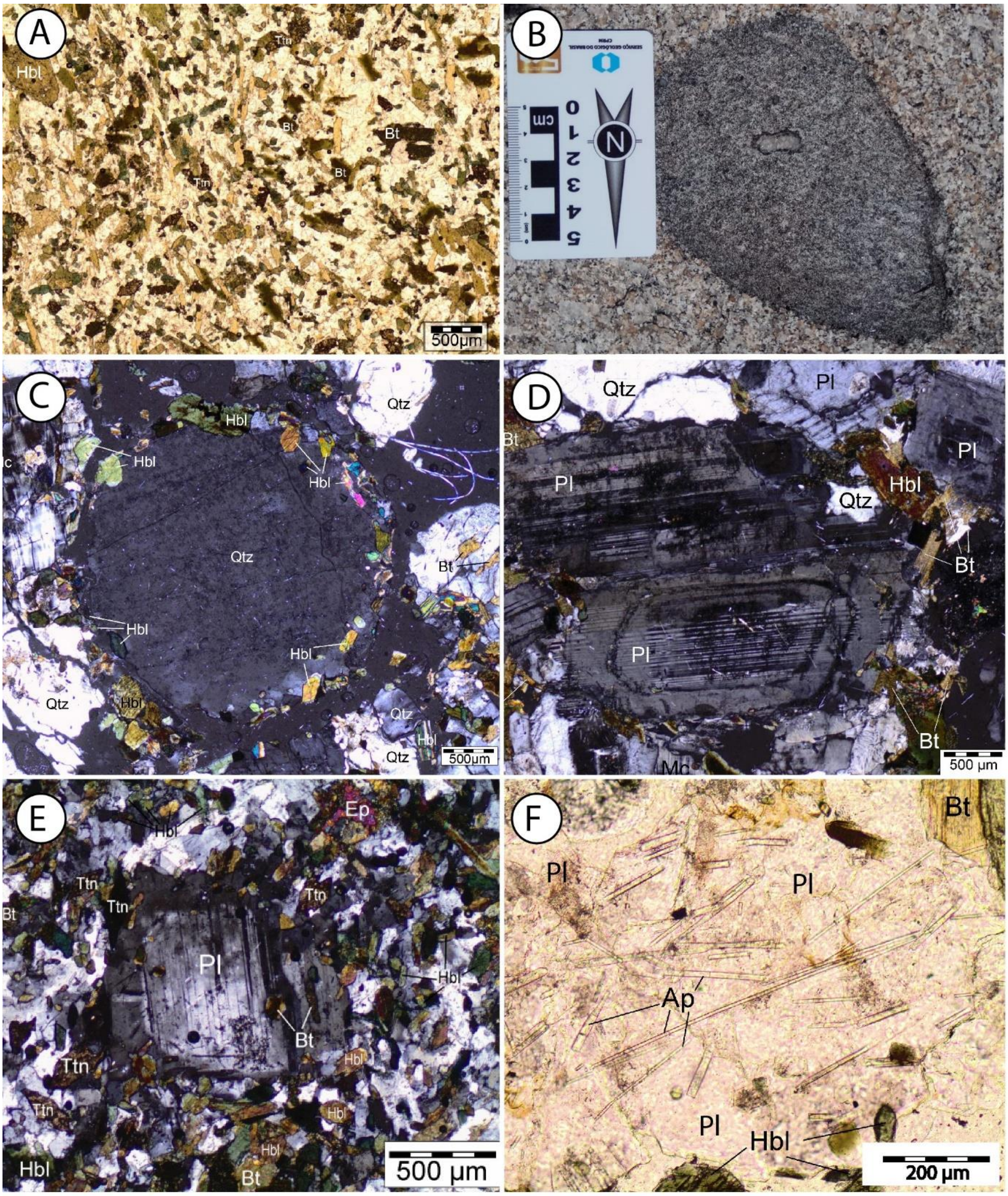

Figure 6. RJB ME textures. (A) General view of the microgranular enclave texture (parallel nicols). (B) Macroscopic image of ME showing the quartz ocellar texture (note black minerals at the edges of the crystal). (C) Quartz with ocellar texture. Note hornblende inclusions only at the edges of the crystal. (D) Compositional zoning and inclusion zone in plagioclase. Note that the compositional zoning and the inclusion zone are parallel to each other. (E) Plagioclase showing a nucleus with rounded faces and compositional zoning at the edges. (F) Acicular apatite crystals. [Qtz] quartz; [Hbl] hornblende; [Bt] biotite; [Pl] plagioclase; [Ttn] titanite; [Ep] epidote; [Ap] apatite.

4.3 Geochemistry

The chemical data of representative samples of the RJB MEs is shown in Tables 2 and 3.

In the Na_2O + K_2O versus SiO_2 diagram, MEs are placed in the monzogabbro, monzodiorite, monzonite and quartz monzonite fields (Figure 7A). Most samples show SiO_2 contents of 53 to 61 wt%, except for sample SOS-850B, which is 48% SiO_2. The MgO (2.5–7.17%), K_2O (2.05–7.54%), Fe_2O_3 (5.5–12.21%), CaO (3.5–8.21%) and Na_2O (2.1– 4.63%) contents of the MEs also show wide variation. The Al_2O_3 content varies little (13.61–16.69%). The total amount of alkalis (Na_2O + K_2O) in the studied rocks ranges from 5.87–9.64%, and the K_2O/Na_2O ratio ranges from 0.46–3.59.

The RJB MEs are metaluminous (Figure 7B) and they belong to the magnesian suite (Figure 7C). The K_2O-SiO_2, K_2O-Na_2O and Ce/Yb-Ta/Yb relationships indicate a shoshonitic affinity (Figure 8A–C). There is an increase in K_2O in a group of samples with SiO_2 contents between 58 to 61%, splitting the population into two groups: one is positioned in the calc-alkaline field and the other in the shoshonitic field (Figure 8A). This K_2O variation may be due to an increase in the volume of alkali feldspar. The patterns rare earth elements (Figure 9) show enrichment in light rare earth elements (LREEs) rather than in heavy rare earth elements (HREEs). The $[La/Yb]_N$ and $[La/Sm]_N$ ratios range from 9.08–33.26 and 2.04–4.77, respectively. Negative Eu anomalies are present with Eu/Eu* ranging from 0.48–0.88. It is observed that the samples are distributed into three groups of spectra (Figure 9): 1—the sample SOS 850B (48.09 % SiO_2), which has a higher sum of ETR; 2—a set of samples with weak negative Eu anomalies (0.68–0.88); 3—samples SOS 844B and SOS 867B, which show the most negative Eu anomalies (0.48–0.65).

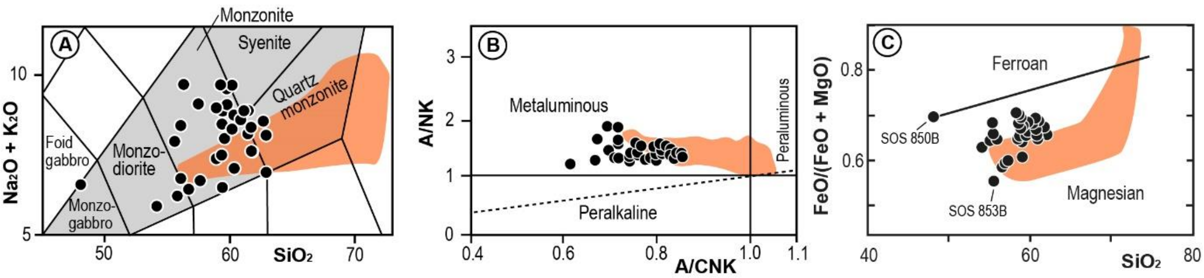

Figure 7. Chemical classification diagram applied to the RJB MEs. (A) Na_2O + K_2O versus SiO_2 diagram with fields defined by Middlemost (1985). (B) Aluminium saturation A/CNK (Al_2O_3/(CaO + Na_2O + K_2O)) versus A/NK (Al_2O_3/(Na_2O + K_2O)) diagram of Maniar and Picolli (1989). (C) FeOt/(FeOt + MgO) versus SiO_2 diagram (Frost et al., 2001). The orange area corresponds to the RJB rocks, and the gray area, in diagram A, represents the field of medium alkalinity rocks.

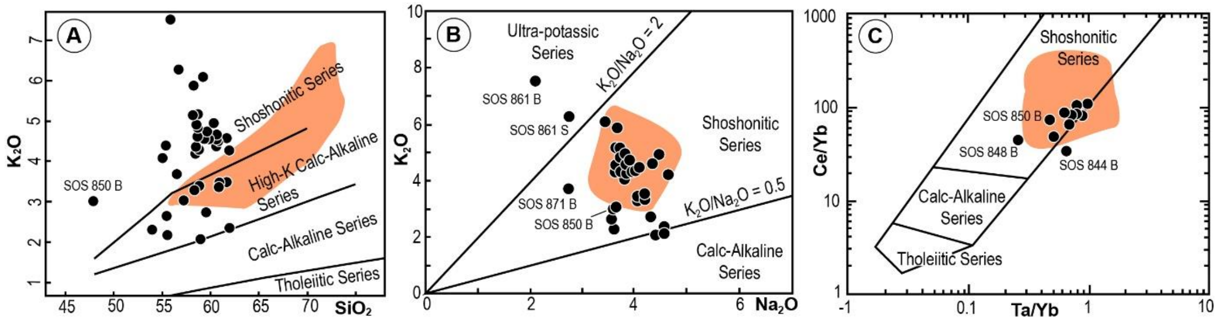

Figure 8. Geochemical diagrams for magmatic affinity inference. (A) K_2O versus SiO_2 diagram of Peccerillo and Taylor (1976). (B) K_2O versus Na_2O diagram of Turner et al. (1996), characterizing the nature of the ME magma. (C) Ta/Yb versus Ce/Yb, with fields defined by Pearce (1982). The orange area corresponds to the RJB compositions.

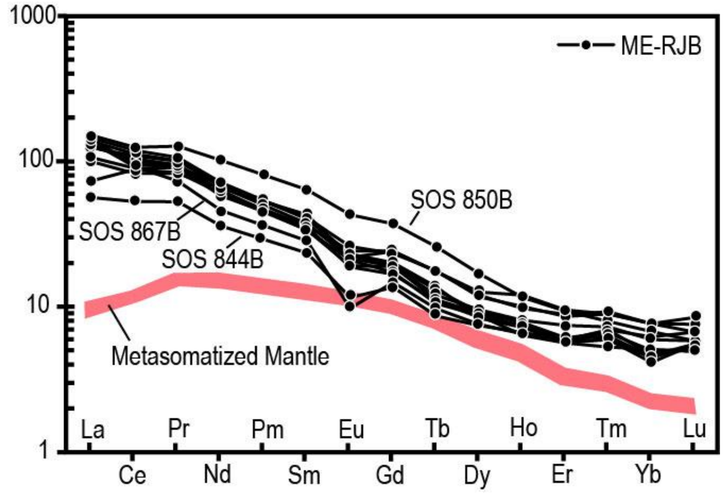

Figure 9. Chondrite-normalized (Nakamura, 1974) REE diagram for the RJB MEs. Composition of the metasomatized mantle of Kaczmarek et al. (2016). ME-RJB = microgranular enclaves of the Rio Jacaré Batholith.

Table 2. Chemical analysis of major and minor elements and normative compositions (CIPW standard with hornblende) of the RJB MEs. LOI: Loss on ignition.

%	SOS 850B	SOS 876B	SOS 867B	SOS 860E	SOS 853B	SOS 849B	SOS 861B	SOS 871B	SOS 861S	SOS 844B	SOS 861M	SOS 853D	SOS 861L	SOS 853I	SOS 861O	SOS 853C	SOS 853G	SOS 861Q	SOS 861P	SOS 860D
SiO_2	48.09	53.99	55.04	55.39	55.52	55.55	55.88	56.56	56.86	57.23	58.19	58.33	58.34	58.49	58.62	58.63	58.65	58.72	58.72	58.74
TiO_2	1.92	1.29	0.82	0.88	0.56	1.34	0.54	0.61	0.65	0.83	0.72	1.04	0.69	1.35	0.69	0.89	0.92	0.70	0.71	0.73
Al_2O_3	16.69	15.23	15.08	15.49	14.04	15.13	13.83	13.61	14.19	14.35	15.01	15.16	15.50	16.51	15.22	15.82	16.13	14.85	15.08	15.15
Fe_2O_3	12.22	9.74	8.61	8.56	8.80	8.99	8.16	9.55	7.00	8.59	6.97	7.27	6.14	5.50	6.92	5.80	5.98	6.77	6.78	6.67
MnO	0.14	0.12	0.12	0.10	0.14	0.14	0.15	0.13	0.13	0.18	0.10	0.11	0.08	0.08	0.09	0.07	0.06	0.10	0.10	0.08
MgO	5.22	5.82	4.80	5.05	7.17	4.77	4.50	6.84	4.89	5.83	2.96	4.02	2.64	2.59	3.35	2.53	2.71	3.08	3.06	3.56
CaO	8.22	7.06	6.04	5.30	6.71	6.17	5.97	5.78	5.50	5.37	5.22	5.25	4.70	3.96	4.76	3.93	3.73	4.99	4.95	4.69
Na_2O	3.59	3.60	3.79	3.93	3.55	4.57	2.10	2.73	2.74	3.63	3.69	4.05	3.65	4.64	4.03	4.46	4.34	3.65	3.74	3.84
K_2O	2.99	2.28	4.07	4.38	2.63	2.15	7.54	3.69	6.27	3.03	5.14	3.27	5.88	4.20	4.34	4.92	4.60	5.16	4.85	4.26
P_2O_5	1.08	0.55	0.70	0.85	0.33	0.37	0.67	0.25	0.72	0.36	0.74	0.62	0.79	1.16	0.67	1.14	1.03	0.71	0.71	0.66
LOI	0.31	0.77	0.72	0.87	0.86	0.62	0.66	0.93	0.76	0.48	0.71	0.59	0.88	0.84	0.60	0.63	0.83	0.88	0.93	0.73
Total	100.46	100.45	99.79	99.81	100.32	99.80	100.00	100.69	99.71	99.88	99.45	99.70	99.29	99.32	99.29	98.80	98.97	99.62	99.62	99.3
Q	4.05	13.52	9.32	8.76	14.15	11.54	8.04	17.69	10.36	16.27	10.53	14.60	8.84	10.27	12.11	9.40	10.91	11.47	11.97	13.24
Or	5.64	0.09	12.97	16.59		1.72	34.22	6.05	25.77	4.46	23.53	10.05	28.65	18.86	17.92	23.23	20.98	23.40	21.59	16.95
Ab	30.38	30.44	32.08	33.27	30.07	38.67	17.77	23.10	23.19	30.74	31.24	34.26	30.92	39.25	34.13	37.74	36.68	30.89	31.61	32.50
An	20.60	18.66	12.12	11.68	14.58	14.42	6.04	13.99	7.91	13.90	9.22	13.54	8.55	11.82	10.60	8.61	10.95	8.90	10.06	11.51
Wo	5.47	5.32	5.53	3.76	6.43	5.75	8.02	5.46	6.11	4.35	4.93	3.54	4.01	0.12	3.61	1.43	0.33	4.68	4.11	3.66
Il	0.30	0.26	0.25	0.21	0.30	0.30	0.32	0.29	0.28	0.39	0.21	0.24	0.18	0.18	0.20	0.14	0.13	0.20	0.20	0.18
Hm	12.22	9.74	8.61	8.56	8.80	8.99	8.15	9.55	7.00	8.59	6.97	7.27	6.14	5.50	6.92	5.80	5.97	6.77	6.78	6.67
Ap	2.56	1.31	1.66	2.02	0.78	0.87	1.59	0.59	1.71	0.84	1.76	1.47	1.87	2.74	1.58	2.69	2.44	1.69	1.68	1.56
Bi	17.22	19.22	15.86	13.36	22.33	15.75	14.85	22.59	16.16	19.25	9.77	13.26	8.71	8.56	11.05	8.35	8.93	10.18	10.09	11.77
Hbl					1.63															
Sum	98.45	98.57	98.42	98.22	99.08	98.02	99.01	99.31	98.49	98.80	98.17	98.24	97.86	97.29	98.14	97.42	97.34	98.19	98.12	98.04

%	SOS 860B	SOS 860C	SOS 853M	SOS 861R	SOS 861E	SOS 853N	SOS 861J	SOS 861N	SOS 861I	SOS 861F	SOS 861T	SOS 861G	SOS 853J	SOS 853E	SOS 861D	SOS 848B	SOS 860F	SOS 861C	SOS 853F
SiO_2	58.79	58.89	58.93	59.16	59.33	59.58	59.64	59.80	60.39	60.62	60.62	60.65	60.89	60.91	60.97	61.70	61.72	61.98	61.98
TiO_2	1.08	0.63	0.56	0.68	0.75	0.69	0.68	0.74	0.65	0.65	0.68	0.68	0.70	0.78	0.62	0.83	0.58	0.58	0.52
Al_2O_3	15.26	14.73	14.49	15.14	15.00	15.32	15.18	15.39	14.99	14.92	14.91	15.08	14.85	15.14	15.03	15.38	14.97	14.87	14.94
Fe_2O_3	6.92	7.11	7.81	5.90	6.73	6.94	6.53	6.36	6.11	6.30	6.03	6.31	6.27	5.80	6.31	6.16	5.67	5.87	6.11
MnO	0.11	0.10	0.13	0.08	0.09	0.08	0.09	0.09	0.08	0.09	0.07	0.08	0.09	0.08	0.08	0.08	0.07	0.09	0.09
MgO	3.88	4.05	5.09	2.80	3.60	3.61	3.05	3.15	2.86	3.30	2.74	3.19	3.46	2.68	3.37	3.08	2.80	3.07	3.22
CaO	4.91	4.84	5.37	4.53	4.35	4.94	4.10	3.91	4.10	4.16	4.08	3.73	4.30	3.59	4.23	4.69	3.70	3.69	4.52
Na_2O	4.06	3.61	4.39	3.43	3.65	4.30	3.90	3.80	3.81	3.72	4.10	3.65	4.20	4.11	4.06	4.19	3.86	3.75	4.55
K_2O	3.38	4.30	2.05	6.09	4.54	2.72	4.73	4.56	4.94	4.36	4.65	4.54	3.34	4.48	3.45	3.48	4.57	4.26	2.33
P_2O_5	0.71	0.62	0.33	0.66	0.66	0.50	0.71	0.71	0.65	0.53	0.70	0.69	0.58	0.89	0.52	0.56	0.55	0.44	0.40
LOI	0.82	0.50	0.65	0.92	0.73	0.49	0.67	0.70	0.69	0.75	0.76	0.77	0.58	0.74	0.83	0.45	0.61	0.57	0.75
Total	99.90	99.38	99.80	99.38	99.43	99.18	99.28	99.21	99.26	99.40	99.33	99.38	99.25	99.19	99.47	100.59	99.12	99.17	99.41
Q	15.12	14.68	17.30	10.29	14.60	16.44	13.29	14.59	13.86	16.17	13.76	16.59	17.36	15.18	17.65	17.01	16.42	18.11	19.43
Or	11.03	16.11	0.42	29.55	18.55	7.73	20.95	19.71	22.59	18.18	21.18	19.47	11.78	20.28	12.62	13.47	20.59	18.09	6.38
Ab	34.31	30.56	37.12	28.99	30.88	36.40	33.02	32.14	32.27	31.48	34.67	30.87	35.50	34.80	34.33	35.44	32.66	31.77	38.47
An	13.47	11.27	13.76	7.93	11.12	14.48	9.94	11.46	9.21	11.12	8.54	11.36	11.83	9.63	12.59	12.89	10.01	11.15	13.48
Wo	2.61	3.62	4.47	4.26	2.56	2.84	2.42	1.37	2.87	2.53	2.99	1.09	2.38	1.00	2.08	2.80	1.98	1.78	2.63
Il	0.23	0.21	0.27	0.17	0.19	0.18	0.19	0.19	0.18	0.19	0.16	0.17	0.18	0.16	0.18	0.16	0.16	0.20	0.19
Hm	6.92	7.11	7.81	5.90	6.73	6.94	6.53	6.36	6.11	6.30	6.03	6.31	6.26	5.80	6.31	6.16	5.67	5.87	6.11
Ap	1.68	1.47	0.79	1.57	1.56	1.17	1.67	1.68	1.53	1.25	1.65	1.64	1.36	2.10	1.23	1.32	1.30	1.04	0.95
Bi	12.80	13.36	16.80	9.24	11.89	11.93	10.06	10.40	9.44	10.91	9.03	10.53	11.43	8.84	11.14	10.17	9.23	10.13	10.62
Sum	98.16	98.39	98.76	97.91	98.09	98.13	98.08	97.9	98.06	98.14	98.02	98.06	98.09	97.80	98.14	99.43	98.04	98.15	98.26

Table 3. Representative chemical analysis of trace elements of RJB MEs.

	SOS 850B	SOS 876B	SOS 867B	SOS 849B	SOS 844B	SOS 861M	SOS 853D	SOS 861P	SOS 861E	SOS 861T	SOS 848B	SOS 861C
Ba	1162	626	770	564	300	819	655	819	947	896	817	862
Rb	208.4	98.8	158.0	120.0	174.0	234.0	132.5	233.0	233.0	243.0	115.5	213.0
Sr	969	683	540	678	316	463	585	450	491	489	561	521
Zr	271	230	237	228	177	240	196	242	250	242	264	212
Nb	15.35	10.70	9.80	8.74	13.00	11.00	12.36	11.40	10.50	11.30	9.60	11.00
La	50.4	34.5	45.1	33.2	18.8	45.9	35.4	48.2	41.5	42.0	43.5	46.9
Ce	109.3	76.9	80.4	72.3	46.3	98.2	78.4	104.0	95.4	90.9	88.8	84.1
Pr	14.41	9.48	8.28	9.35	5.97	11.45	10.28	12.05	11.35	10.7	10.25	10.2
Nd	64.8	38.6	29.3	41.7	22.9	42.5	44.2	45.6	44.9	40.2	37.0	37.9
Sm	13.1	7.39	5.82	8.80	4.80	7.66	8.40	8.29	8.25	6.90	7.24	6.93
Eu	3.34	2.16	1.32	1.70	1.35	1.29	2.02	1.36	1.39	1.28	1.32	1.69
Gd	10.37	6.74	4.10	6.70	3.79	5.30	6.49	5.60	5.37	4.80	4.67	5.27
Tb	1.23	0.83	0.46	0.83	0.41	0.53	0.84	0.65	0.62	0.50	0.52	0.57
Dy	5.85	4.37	2.62	4.15	2.57	3.14	4.05	2.89	3.17	3.02	2.93	3.3
Ho	0.82	0.85	0.46	0.69	0.47	0.51	0.71	0.51	0.55	0.45	0.53	0.57
Er	2.12	2.16	1.32	2.01	1.35	1.29	1.95	1.36	1.39	1.28	1.32	1.69
Tm	0.24	0.27	0.18	0.28	0.21	0.18	0.27	0.19	0.20	0.16	0.21	0.22
Yb	1.50	1.70	0.99	1.70	1.38	0.92	1.70	1.01	1.11	1.13	1.03	1.32
Lu	0.20	0.29	0.19	0.23	0.23	0.19	0.26	0.18	0.17	0.17	0.19	0.20
Y	24.23	20.30	11.20	19.84	13.20	13.30	21.30	13.40	13.40	12.70	13.00	14.80
Cs	25.00	5.82	7.30	10.36	13.15	13.40	6.71	15.15	17.00	18.65	4.74	14.15
Ta	0.71	0.90	0.70	0.44	0.90	0.90	0.92	0.80	0.70	1.00	0.80	0.90
Hf	7.96	5.80	6.10	6.55	5.50	6.00	5.88	6.40	6.20	6.00	6.70	5.60
Ga	31.9	23.7	23.6	27.1	29.7	24.8	27.1	25	24	25.3	24.2	25.1
Sn	8.4	4.0	6.0	4.1	9.0	5.0	1.1	5.0	4.0	4.0	4.0	4.0
Th	8.40	5.66	9.86	4.60	5.81	10.80	8.80	11.25	9.59	9.84	13.10	10.80
V	227	172	137	133	118	113	110	120	123	102	125	98
W	4.9	276.0	274.0	<0.1	4.0	720.0	<0.1	693.0	529.0	542.0	7.0	428.0
Eu/Eu*	0.88	0.82	0.48	0.68	0.65	0.81	0.84	0.81	0.81	0.87	0.77	0.76
$(La/Yb)_N$	22.40	9.61	30.37	13.02	9.08	33.26	13.88	31.82	24.92	24.78	28.16	23.69
$(La/Sm)_N$	2.37	2.04	4.77	2.32	2.41	3.69	2.59	3.58	3.09	3.74	3.70	4.16

5. DISCUSSION

The MEs found in the RJB are easily observed in the field due to their abundance, high frequency in outcrops and dark color and because they are fine-grained, differing from the light-colored rocks that dominate this batholith. According to Kumar et al. (2004), enclaves with grain size finer than the host granites and lacking cumulate texture are not the residuum of a fractional crystallization that might have generated the host. According to Torkian and Furman (2015), the presence of MEs with fine-grained margins, microgranular or/and porphyritic textures, plagioclase crystals showing disequilibrium textures and compositional variation indicates that these enclaves are products of magmatic mingling. These features are found in the RJB MEs and suggest that they were formed from magma and do not represent cumulates or restites. Therefore, the nature of these enclaves must reflect magmatic processes, such as the mixing of magmas and fractional crystallization.

5.1 Evidence for mixing and mingling processes

5.1.1 Mixing

The RJB MEs show a large variation in their SiO_2 content (48–61%), but intermediate compositions predominate. According to Reubi and Blundy (2009) and Ruprecht et al. (2012), the generation of rocks with intermediate compositions results, in most cases, from the coexistence and mixing of contrasting magmas. According to Janousek et al. (2004), the compositional variation of MEs can be considered the mixing of a mantle-derived mafic magma with crustal magmas. Some authors (e.g., Barbarin and Didier, 1991; Shukla and Mohan, 2019) consider some features that are also found in the RJB MEs (e.g., variation in the color of the MEs, presence of multiple MEs, diffuse contacts) a reflection of different degrees of homogenization and the role of mixing between the parental mafic magma and the felsic host.

The mixing of two magmas only occurs when their viscosities are similar (Fernandez and Barbarin, 1991; Weidendorfer et al., 2014). According to Winter (2014), the catazone is a region in the crust where rocks experience high temperatures and the viscosity difference between different materials is relatively low. According to Sousa et al. (2019), the RJB rocks, the host rocks of the studied MEs, were crystallized at a depth of 25 km with Mg-hornblende crystallization temperature of 826 ºC. Probably, these emplacement conditions of the RJB allowed its magma and the ME magma to have similar viscosities, favoring mixing processes to occur.

Mixing between magmas can often be inferred by identifying linear trends in binary diagrams. The samples studied in the CaO/SiO_2 versus FeO_t/SiO_2 diagram show an alignment that suggests that mixing between magmas has occurred (Figure 10A). This trend is consistent with two mixing components: a mafic magma (enclaves) and felsic magma (host granite).

The variation in the SiO_2 content of the RJB MEs suggests that the compositions represent different degrees of hybridization. Therefore, the relative contributions of the mafic and felsic magmas were estimated using the linear correlation of major elements with the mixing algorithm of Fourcade and Allègre (1981). According to these authors, if mixing occurs, this process will affect each chemical element of the magmas, so that it will satisfy the following relation: $C^i_i - C^i_f = m(C^i_m - C^i_f)$, where C^i_i is the concentration of element *i* in the hybrid magma, C^i_f is the concentration in the felsic magma, C^i_m is the concentration in the mafic magma and *m* is the fraction of the mafic magma in the mixture.

Using the Fourcade and Allègre (1981) algorithm, the samples SOS 850B (48% SiO_2) and SOS 854 (72.6% SiO_2, obtained from Sousa et al., 2019) were considered as representatives of the mafic and felsic magmas, respectively. To represent the hybrid magma, microgranular enclave SOS 816C, which has a relatively high SiO_2 content (61.9%), was used, because it is the ME with the highest degree of hybridization (high SiO_2 and low V). A good linear correlation was obtained with the analyzed rocks, with $R^2 = 0.991$ (Figure 10B). The angular coefficient obtained represents the fraction of the mafic magma involved in the mixing; for the SOS 816C sample, it is 43%.

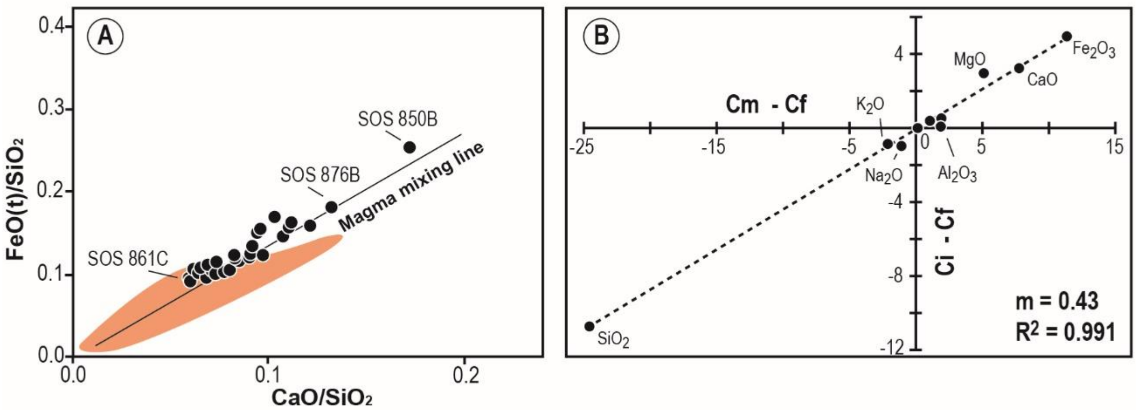

Figure 10. Geochemical diagrams used to simulate the mixture of mafic and felsic magmas. (A) CaO/SiO_2 versus FeO_t/SiO_2 diagram of Berzina et al. (2014) and (B) test diagram of the mixing of larger elements of Fourcade and Allègre (1981), which indicate the role of the mixing of the ME and RJB magmas. The orange area corresponds to the RJB compositions. Cf = element concentration in felsic magma, Cm = element concentration in mafic magma, Ci = element concentration in hybrid magma, m = fraction of mafic magma in the mixture, R^2 = correlation coefficient.

5.1.2 Mingling

According to Perugini and Poli (2012), the evolution of the rheological contrast between magmas can be rebuilt from the study of magmatic enclaves. The various forms of MEs can be controlled by the differences in the viscosities/rheologies of the magmas, and the more complex the forms, the greater these differences will be (Fernandez and Barbarin, 1991; Perugini and Poli, 2011). According to Petford (2003), several studies estimate that, regardless of composition, the transition from Newtonian to non-Newtonian behavior for magmas occurs when the magma is between 30 and 50% crystallized. Fernandez and Barbarin (1991) acknowledge that the injection of mafic magma at different stages of felsic magma crystallization can generate varied structures: (i) when the felsic host magma has a Newtonian behavior (up to 30% crystallized), active convection induces the dispersion of mafic magma droplets, generating globular MEs; (ii) when felsic magma has a visco-plastic behavior (30 to ~50% crystallized), the ME shapes can be deformed; (iii) when the felsic magma is 70–90% crystallized, early fractures can be formed and allow the mafic magma to be injected, which will result in syn-plutonic dikes. The formation of these syn-plutonic dikes can occur in two ways, depending on their thickness. When the mafic magma is injected as thin dikes, it quickly reaches a thermal balance by cooling down and becoming rigid. During the subsequent movements of the host magma, the dikes are broken, resulting in a syn-plutonic dike composed of MEs with angular contacts. When the mafic dike is thicker, its cooling is slower and it can overheat the host magma at the contacts, which will undergo limited partial melting. Local convection, caused by the increase in the thermal gradient, will induce the dispersion of the mafic magma as bubbles of various sizes, transforming the mafic dike into a corridor of microgranular enclaves (syn-plutonic dike).

In the RJB, MEs with globular, elongated shapes and well-defined contacts (crenulated, cuspate, lobate and sinuous) are found, in addition to syn-plutonic dikes composed of various enclaves of different shapes and sizes. These features indicate that mafic magmas were injected during two different crystallization stages in the RJB magmatic chamber. According to the model of Fernandez and Barbarin (1991), MEs with globular shapes were formed when mafic magma was injected into the felsic magmatic chamber of the RJB, with up to 30% crystallized, and disaggregated by convective movements; this also agrees with interpretations of other authors about the genesis of globular MEs (e.g., Vernon et al., 1988; Castro et al., 1991; Liu et al., 2013; Shukla and Mohan, 2019). Since microgranular enclaves with such features are well distributed throughout the RJB, we believe that the input of mafic magma in this stage was important. It is believed that the RJB MEs with crenulated, cuspate, lobate and sinuous contacts were formed when the felsic magmatic chamber had a degree of crystallization greater than 30%, as a greater difference of viscosity is necessary to generate these more complex forms (e.g., Perugini and Poli, 2011). The input of mafic magma was probably more restricted at this stage, as enclaves with these types of contacts in the RJB only occur in the western region of the batholith.

The syn-plutonic dikes observed in the RJB indicate the occurrence of mafic magma pulses in the late stages of crystallization, when 70–90% of the felsic magmatic chamber was crystallized, and that the presence of this mafic magma increased the local temperature, provoking the partial melting of the felsic magma. It is suggested that the contribution of mafic magma in the late stages of the crystallization of the RJB was restricted, as the syn-plutonic dikes are limited to the western region. The RJB's multiple ME types also suggest the occurrence of more than one mafic magmatic pulse during the evolution and formation of this batholith.

Some textures found in the RJB MEs also indicate that these enclaves probably represent the breakdown of the mafic magma that was injected and cooled in a cooler felsic magmatic chamber: (1) zones of inclusion in plagioclase and ocellar quartz crystals (Hibbard, 1991); (2) a boxy cellular plagioclase texture (Hibbard, 1991); and (3) acicular apatite (Wyllie et al., 1962; Hibbard, 1991). According to Torkian and Furman (2015), these textures and the crenulated and cuspate contacts between the MEs and the host rocks can be attributed to the mingling/mixing of magmas.

Feldspar and quartz xenocrystals in the ME can be observed in the field. The presence of xenocrystals in these enclaves indicates that the phenocrysts of the host magma surpassed the ME edges and were trapped inside (Barbarin and Didier, 1991; Perugini et al., 2003). This indicates that the mafic and felsic magmas interacted with each other and had different rheologies, allowing the exchange of crystals between them in a mingling process (e.g., Perugini et al., 2003; Yang et al., 2015).

Therefore, it is suggested that the studied rocks are a product of partial chemical equilibrium between mafic and felsic magmas, representing a mingling/mixing process.

5.2 Magma of the microgranular enclaves

MEs in granites have been interpreted (e.g., Bonin, 2004; Janousek et al., 2004; Chen et al., 2007) as mantle-derived mafic magmas that underwent mixing/mingling after being injected into a deep crustal felsic magmatic chamber. The chemical compositions of the MEs studied reveal their affinity with the magnesian series and indicates that this mafic magma was hydrated and crystallized in an oxidizing environment, as suggested by Frost and Lindsley (1991) for rocks in this series. High fO_2 can also be inferred from the presence of titanite, quartz, magnetite and hornblende (e.g., Wones, 1989). Furthermore, most of the RJB MEs have high K_2O, with $K_2O/Na_2O > 1$, which is characteristic of shoshonitic rocks (Figure 8A–C). K_2O is high regardless of the rocks' SiO_2 content, and according to Turner et al. (1996), rocks with these characteristics probably reflect a potassium phase not only during fractionation, but also at the source.

According to Furman and Graham (1999), an increase in the Rb/Sr ratio in relation to the primitive mantle may suggest that phlogopite was the hydrated mineral present at the source, while high Ba/Rb ratios suggest the presence of amphibole. The Rb/Sr ratios of the RJB MEs range from 0.14 to 0.55 and the primitive mantle has a ratio of 0.03 (Sun and McDonough, 1989), suggesting mingling and also indicating that the phlogopite in the source participated in the partial melt responsible for the magmas that generated the studied MEs (Figure 11).

Shoshonitic magmas have as their main source the subcontinental lithospheric mantle or the asthenospheric mantle, which are both previously enriched in incompatible elements by subduction (e.g., Aldanmaz et al., 2000). The studied MEs show depletion in Ti, Nb and Ta (Figure 12) and high Th/Yb ratios, which are typical signatures of magmas generated in an orogenic environment and represent contributions from the subducted plate (e.g., Ringwood, 1990; Foley and Wheller, 1990; Pearce, 2008). RJB MEs have higher Th/Yb ratios than mantle evolution curves defined for MORBs and OIBs, which suggest subduction-induced source metasomatism (Figure 13). The Hf, Th, Zr, Ce and Nb content of the studied rocks indicates that this magma formed in a post-collisional orogenic environment (Figure 14A and B).

High LILE and high Ba/Nb (>13) and Ba/La (>8) ratios are suggestive of enriched mantle sources (Ryan et al., 1996; Kepezhinskas et al., 2016). Such ratios in the RJB MEs are above 23 and 15, respectively, so they are compatible with enriched mantle source. In addition, the low values of the Nb/La ratios (0.22–0.69) are consistent with a lithospheric mantle source (Figure 15).

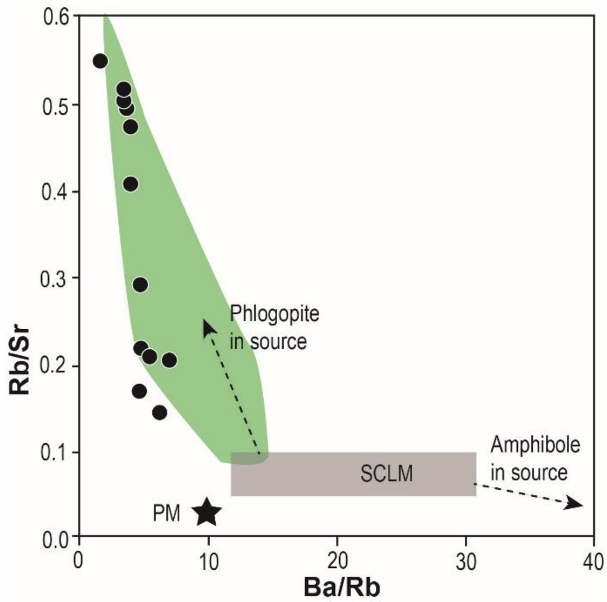

Figure 11. Ba/Rb versus Rb/Sr diagram after Furman and Graham (1999), suggesting the presence of phlogopite in the mantle source of the RJB MEs. [SCLM] Subcontinental lithospheric mantle; [PM] primitive mantle (Sun and McDonough, 1989). The green area represents the compositions of the other SOS MEs.

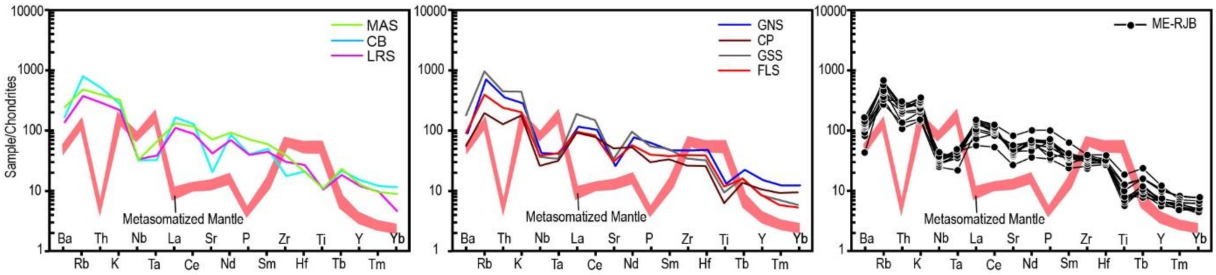

Figure 12. Chondrite multi-elemental diagrams for the RJB MEs (Thompson, 1982). Composition of the metasomatized mantle from Kaczmarek et al. (2016). The colored lines correspond to the average compositions from enclaves of the Glória Norte Stock [GNS; Lisboa et al., 2019]; Curituba Batholith [CB; Gentil, 2013]; Lagoa do Roçado Stock [LRS; Silva, 2014]; Monte Alegre Stock [MAS; Oliveira, 2014]; Glória Sul Stock [GSS; Conceição et al., 2016]; Capela Pluton [CP; Pereira et al., 2019]; and Fazenda Lagoas Stock [FLS; Fernandes et al., 2020].

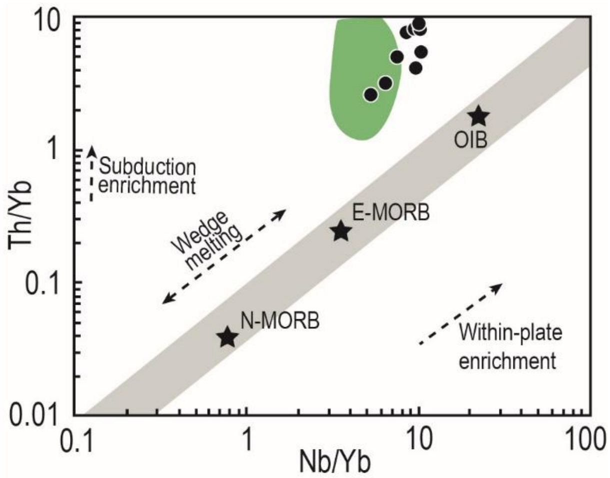

Figure 13. Nb/Yb versus Th/Yb diagram (Pearce, 2008) applied to the RJB MEs. The green area represents the compositions of other SOS MEs.

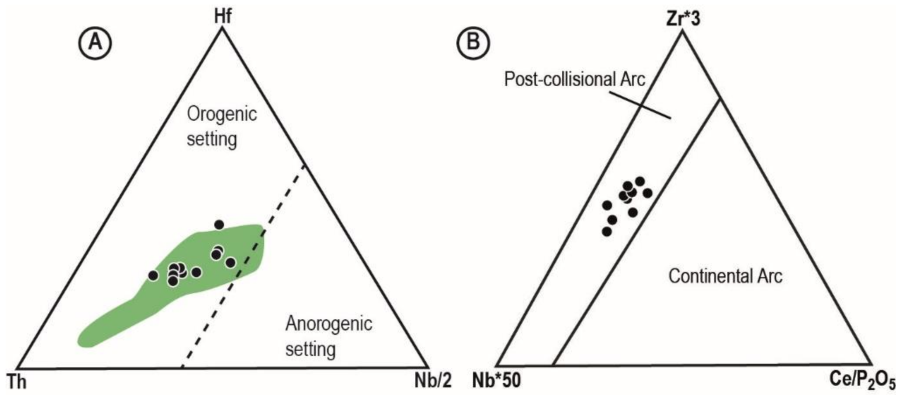

*Figure 14. (A) Hf-Th-Nb/2 diagram (Krmíček et al., 2011) and (B) Nb*50 – Zr*3 – Ce/P_2O_5 diagram (Müller et al., 1992) applied to the RJB MEs, showing the post-collisional orogenic affinity. The green area represents the compositions of other SOS MEs.*

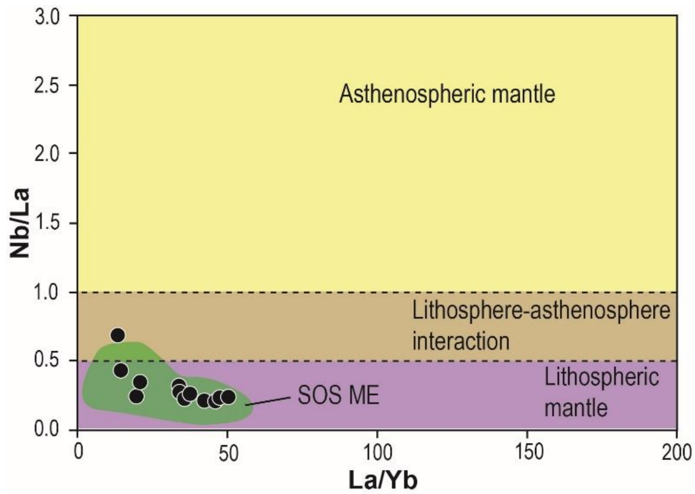

Figure 15. La/Yb versus Nb/La diagram (Smith et al., 1999) applied to the RJB MEs.

Sample SOS 850B is considered to be the most primitive of the RJB MEs, without evidence of cumulatic texture, low SiO_2 content (48%), moderate MgO (5.2%) and high CaO (8.2%) and V (227 ppm). It is also the only sample that presents normative olivine. Although the MgO content of this sample is not the highest among the MEs, its composition is similar to the compositions described for shoshonitic basalts (Morrison, 1980) or trachybasalts of the Roman Province (Müller and Groves, 2019). When calculating the partial melting of metasomatized mantle by using the mantle composition (which consists of clinopyroxene (43%), amphibole (34%), phlogopite (22%) and spinel (1%)) of Kaczmarek et al. (2016), employing the batch melting model, the result points to a partial melting rate of less than 3% to generate magmas with compositions similar to that of sample SOS 850B (Table 4 and Figure 16). According to Conceição and Green (2004), low melting rates are necessary for the formation of shoshonitic magmas; this is consistent with the values obtained in this work.

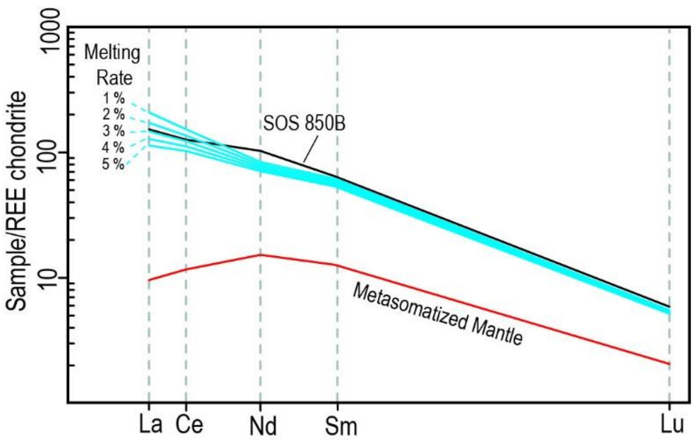

Figure 16. Chondrite multi-elemental diagram (Nakamura, 1974) of the partial melting of metasomatized mantle (Kaczmarek et al., 2016). The blue lines were obtained from the batch melting calculation. The partition coefficients used in the calculation from Foley et al. (1996), Zack et al. (1997), Grégoire et al. (2000) and Elkins et al. (2008).

Table 4. Values obtained from the calculation of the partial melting of metasomatized mantle (MM; Kaczmarek et al., 2016) using the batch melting method. Partition coefficients in the calculations from Foley et al. (1996), Zack et al. (1997), Grégoire et al. (2000) and Elkins et al. (2008). [PM] Partial melting rate.

	PM 1 %	PM 2 %	PM 3%	PM 4 %	PM 5 %	MM	SOS 850B
La	68.75	56.87	48.49	42.26	37.45	3.17	50.4
Ce	132.17	117.79	106.23	96.74	88.80	10.1	109.3
Nd	52.77	50.49	48.39	46.46	44.68	9.62	64.8
Sm	12.56	12.09	11.65	11.24	10.86	2.58	13.1
Lu	0.19	0.18	0.18	0.17	0.17	0.07	0.2

Sousa et al. (2019) found normal zoning in plagioclase crystals of the RJB MEs. This type of zoning may suggest that these MEs, in addition to resulting from the mixing of magmas, also result from the fractionation of minerals during their magmatic evolution. The occurrence of pronounced valleys in Ba and Sr and the negative Eu anomalies in multi-elementary diagrams (Figure 12) may indicate the fractionation of plagioclase. The predominance of P peaks (Figure

12) may suggest the chemical diffusion of P from the host magma to the enclave magma, leading to the crystallization of apatite (Nardi and Lima, 2000). The decrease in the P_2O_5 and (La + Ce) content with the evolution of the ME magma supports the assumption that the fractional crystallization of apatite was an active process (Figure 17). The Ti valleys in multi-elementary diagrams, in addition to representing a signature of the magmatic source, also suggest the fractioning of titanite and opaque minerals. By observing the behavior of compatible elements in some minerals (Sr and CaO in plagioclase, Sr and (FeO*+MgO) in amphibole, P_2O_5 and (La + Ce) in apatite and V and TiO_2 in titanite) and the degree of ME magma evolution, it was observed that there is a decrease in these chemical elements with the evolution of the ME magmas (Figure 17). This reinforces the hypothesis that the fractional crystallization of these minerals may have also contributed to the compositional variation of the MEs studied.

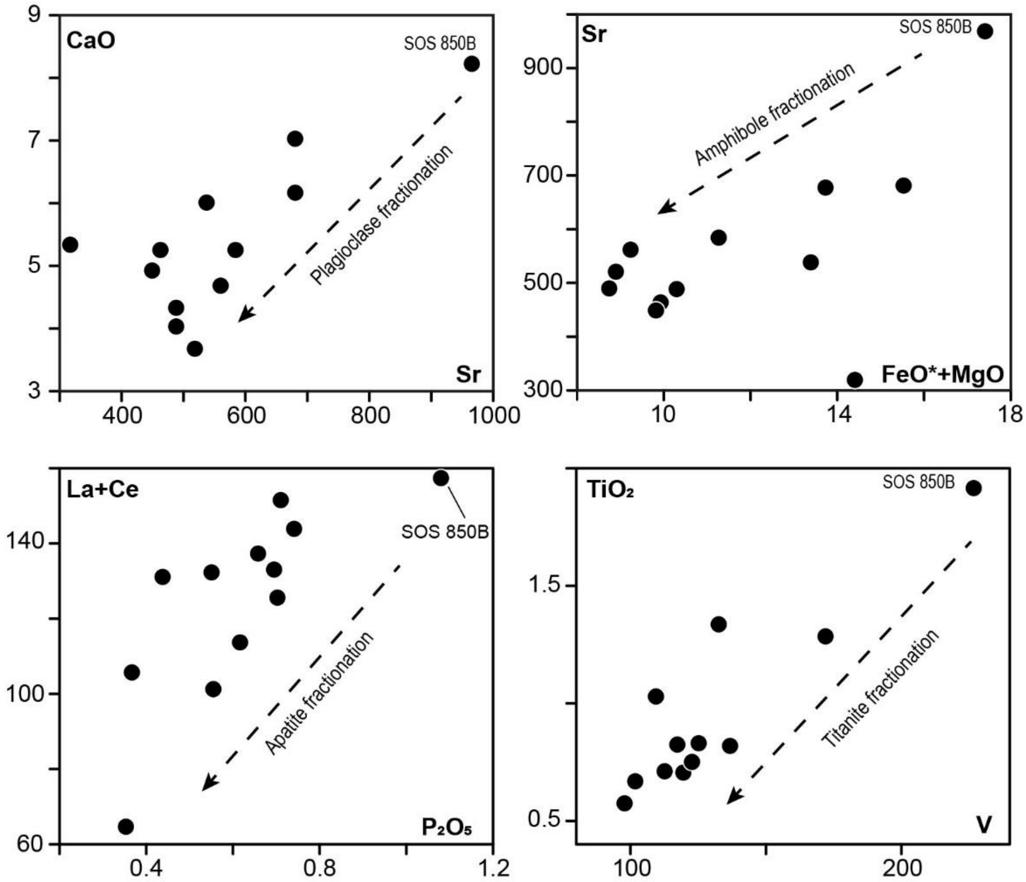

Figure 17. Binary Sr versus CaO, (FeO + MgO) versus Sr, P_2O_5 versus (La + Ce) and V versus TiO_2 diagrams applied to the RJB MEs, showing vectors that correspond to the fractionation of plagioclase, amphibole, apatite and titanite.*

5.3 Inference about the nature of mafic magmas in the Sergipano Orogenic System

In the SOS, MEs are found mainly in intrusions of the Macururé and Poço Redondo domains, such as in the Glória Norte Stock (Lisboa et al., 2019), Curituba Batholith (Gentil, 2013; Lima, 2016), Lagoa do Roçado Stock (Silva, 2014), Monte Alegre Stock (Oliveira, 2014), Glória Sul Stock (Conceição et al., 2016), Fazenda Lagoas Stock (Fernandes et al., 2020), Rio

Jacaré Batholith (Sousa et al., 2019) and Capela Stock (Pereira et al., 2019). Many of these plutons are more than 10 km apart and have ages varying from 631 Ma to 588 Ma.

The geochemical data of the studied samples were compared with those ME of other plutons of the SOS. The geochemistry indicated that all these MEs are metaluminous and magnesian, and they have shoshonitic affinity. The abundances of trace elements and REEs in the MEs are also similar, and this is reflected by similar incompatible elements patterns (Figure 12).

Despite their different ages, the MEs from the Macururé and Poço Redondo plutons have similar characteristics, which suggests that the mafic magma responsible for the formation of these MEs had a similar source to the magma of the RJB MEs: the lithospheric mantle enriched in incompatible elements. This type of source was also attributed to K-diorites from the Borborema Province by Hollanda et al. (2003) and is confirmed when comparing the variation of the $(^{87}Sr/^{86}Sr)_i$ ratios (between 0.7059 and 0.71202) and of ε_{Nd} (from -9.3 to -20.1). It is likely that the source of the RJB MEs is the same as the source described by Hollanda et al. (2003) for the potassic mafic magmas of the Borborema Province.

6. CONCLUSIONS

The origin of the RJB MEs can be summarized in four steps (Figure 18):

- Step 1—A 3% rate of partial melting of the lithospheric mantle, previously enriched in incompatible elements by subduction, originating the shoshonitic mafic magma responsible for the generation of the microgranular enclaves of the RJB.
- Step 2—The injection of this mafic magma when the RJB magmatic chamber had crystallization rates ranging from 0–30% allowed mixing between these magmas, the disaggregation of the mafic magma by convection currents and the subsequent formation of MEs with globular shapes throughout the RJB.
- Step 3—New injections of shoshonitic mafic magma, which occurred when the RJB magmatic chamber was more than 30% crystallized, generating MEs with complex shapes and crenulated, sinuous and cuspate contacts in the western region of the batholith.
- Step 4—The late injection of mafic magma in the western region of the RJB magmatic chamber (which was 70–90% crystallized) resulted in the formation of syn-plutonic dikes.

The chemical data of the studied MEs suggest that the mixing between the ME mafic magma and the RJB felsic magma was important, and also that the smallest fraction of mafic magma involved in this process was 43%. Mixing was responsible for the generation of MEs with various colors (black to gray) and contributed to the compositional variation of these rocks, which have diorite, monzodiorite, quartz monzodiorite and monzonite compositions. Furthermore, the fractionation of plagioclase, hornblende, titanite and apatite may have also contributed to the compositional variation of the RJB MEs.

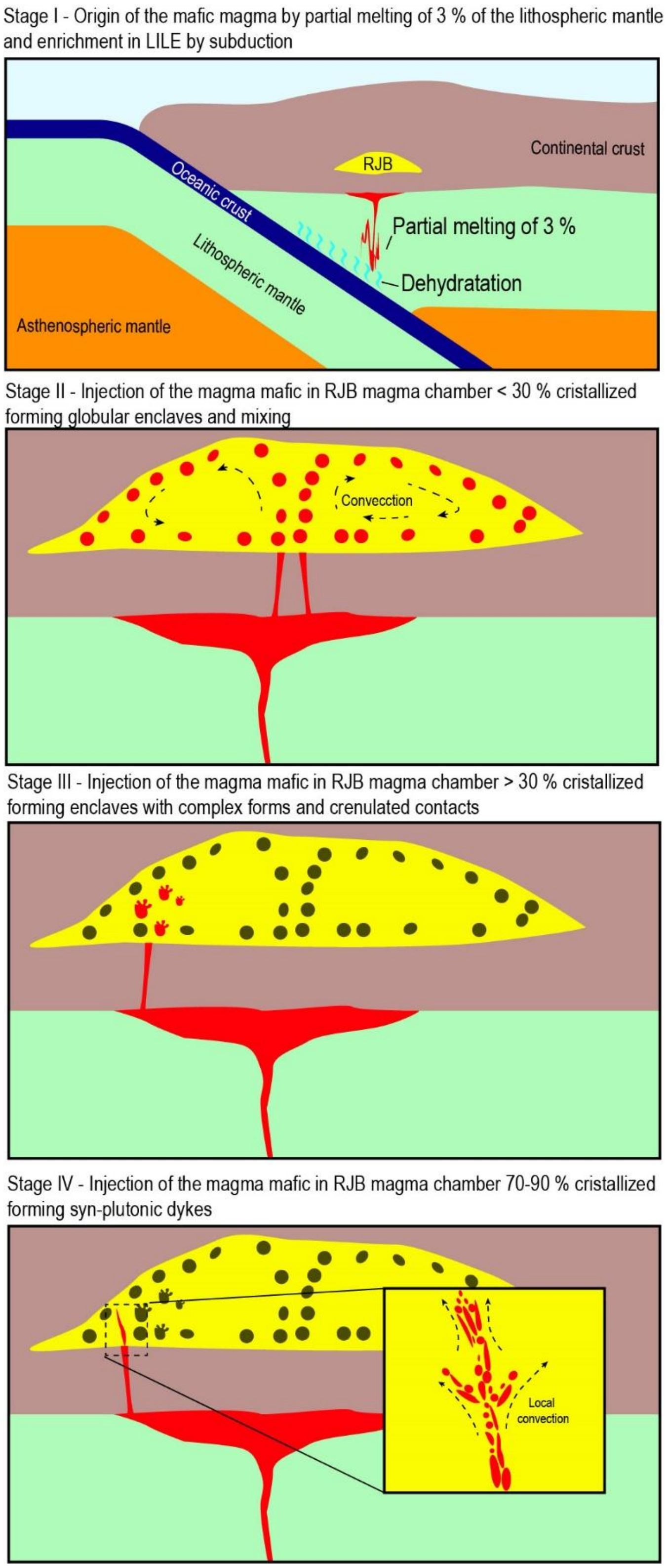

Figure 18. Schematic model of the different steps of the formation of MEs in the RJB. Mafic magma (red color); microgranular enclaves (black color).

7. ACKNOWLEDGMENTS

This work was carried out with the support of the Coordenação de Aperfeiçoamento de Pessoal de Nível Superior – Brasil (CAPES) – Financing Code 001. The authors Carlos Santana Sousa and Hiakan Santos Soares thank CNPq for their PhD scholarships, whose processes are 163770/2018-2 and 169765/2018-0, respectively. This work is part of the above mentioned first author's PhD thesis at the Geology Postgraduate Program at the Federal University of Bahia (UFBA - Universidade Federal da Bahia). The authors are grateful for the support of the Laboratory of Petrology Applied to Mineral Research at the Federal University of Sergipe (LAPA - UFS) (UFS- Universidade Federal de Sergipe) in the development of the research.

8. BIBLIOGRAPHY

Aldanmaz, E., Pearce, J. A., Thirlwall, M. F., Mitchell, J. G. 2000. Petrogenetic evolution of late Cenozoic, post-collision volcanism in western Anatolia, Turkey. *Journal of Volcanology and Geothermal Research*, **102**, 67-95. doi: 10.1016/S0377-0273(00)00182-7

Almeida, F. F. M., Hasuí, Y., Brito Neves, B. B., Fuck, R. A. 1977. Províncias estruturais brasileiras. In: Simpósio de Geologia do Nordeste. Campina Grande, 363-391.

Barbarin, B., Didier, J., 1991. Macroscopic features of mafic microgranular enclaves. In: J. Didier, J. and Barbarin, B. (Eds.), Enclaves in Granite Petrology (Development in Petrology), Amsterdam, Elsevier, p. 253-262.

Berzina, A. P., Berzina, A. N., Gimon, V. O. 2014. Geochemical and Sr–Pb–Nd isotopic characteristics of the Shakhtama porphyry Mo–Cu system (Eastern Transbaikalia, Russia). *Journal of Asian Earth Sciences*, **79**, 655-665. doi: 10.1016/j.jseaes.2013.07.028

Bonin, B. 2004. Do coeval mafic and felsic magmas in post-collisional to within-plate regimes necessarily imply two contrasting, mantle and crustal, sources? A review. *Lithos,* **78**, 1-24. doi: 10.1016/j.lithos.2004.04.042

Brito, M. F. (1996). *Geologia, geoquímica e petrologia do Complexo Granítico Sítios Novos, Sistema de Dobramentos Sergipano*. MS Dissertation, Universidade Federal de Pernambuco, Recife.

Bueno, J. F., Oliveira, E. P., McNaughton, N. J., Laux, J. H. 2009. U-Pb dating of granites in the Neoproterozoic Sergipano Belt, NE-Brazil: Implications for the timing and duration of continental collision and extrusion tectonics in the Borborema Province. *Gondwana Research*, **15**(1), 86-97. doi: 10.1016/j.gr.2008.06.003

Carvalho, M. J. (2005). *Evolução Tectônica do Domínio Marancó-Poço Redondo: Registro das Orogêneses Cariris Velhos e Brasiliana na Faixa Sergipana, NE do Brasil*. PhD Thesis, Universidade de Campinas, Campinas, 202 p.

Castro, A., Moreno-Ventas, I., De La Rosa, J. D. 1991. H-type (hybrid) granitoids: a proposed revision of the granite-type classification and nomenclature. *Earth-Science Reviews*, **31**(3-4), 237-253. doi: 10.1016/0012-8252(91)90020-G

Chen, B., Zhai, M. G., Tian, W. 2007. Origin of the Mesozoic Magmatism in the North China Craton: Constraints from Petrological and Geochemical Data. *Geological Society*, **280**, 131-151. doi: 10.1144/SP280.6

Chen, Y. D., Price, R. C., White, A. J. R., Chappell, B. W. 1990. Mafic inclusions from the Glenbog and Blue Gum Granite Suites, southeastern Australia. *Journal of Geophysical Research*, **97**(B11), 17757-17785. doi: 10.1029/jb095ib11p17757

Clemens, J. D., Elburg, M. A., Harris, C. 2017. Origins of igneous microgranular enclaves in granites: the example of Central Victoria, Australia. *Contributions to Mineralogy and Petrology*, **172**(88). doi: 10.1007/s00410-017-1409-2

Conceição, J. A., Rosa, M. L. S., Conceição, H. 2016. Sienogranitos leucocráticos do Domínio Macururé, sistema Orogênicos Sergipano, nordeste do Brasil: stock Glória Sul. Brazilian *Journal of Geology*, **46**, 63-77. doi: 10.1590/2317-4889201620150044

Conceição, R. V., Green, D. H. 2004. Derivation of potassic (shoshonitic) magmas by decompression melting of phlogopite+pargasite lherzolite. *Lithos*, **72**(3-4), 209-229.

Davison , I., Santos, R. A. 1989. Tectonic evolution of the Sergipano fold belt, NE Brazil, during the Brasiliano Orogeny. *Precambrian Research*, **45**, 319-342. doi: 10.1016/0301-9268(89)90068-5

D'el Rey Silva, L. J. (1992). *Tectonic Evolution of the Southern Part of the Sergipano Fold Belt, Northeastern Brazil*. PhD Thesis, University of London, London, 288 p.

Didier, J., 1973. *Granites and their enclaves.* Amsterdam, Elsevier, 393 p.

Dodge, F. C. W., Kistler, R. W. 1990. Some additional observations on inclusions in the granitic rocks of the Sierra Nevada. *Journal of Geophysical Research*, **95**(B11), 17841-17848. doi: 10.1029/JB095iB11p17841

Elburg, M. A. 1996. Evidence of isotopic equilibration between microgranitoid enclaves and host granodiorite, Warburton Granodiorite, Lachlan Fold Belt, Australia. *Lithos*, **38**, 1-22. doi: 10.1016/0024-4937(96)00003-5

Elkins, L. J., Gaetani, G. A., Sims, K. W. W. 2008. Partitioning of U and Th during garnet pyroxenite partial melting: Constraints on the source of alkaline ocean island basalts. *Earth and Planetary Science Letters*, **265**, 270-286. doi:10.1016/j.epsl.2007.10.034

Fernandes, D. M., Lisboa, V. A. C., Rosa, M. L. S., Conceição, H. 2020. Petrologia e idade do *Stock* Fazenda Lagoas, Domínio Macururé, Sistema Orogênico Sergipano, NE-Brasil. *Geologia USP. Série Científica*, 20(1), 39-60. doi: 10.11606/issn.2316-9095.v20-160040

Fernandez, A. N., Barbarin, B., 1991. Relative rheology of coeval mafic and felsic magmas: nature of resulting interaction processes and shape and mineral fabrics of mafic micro-granular enclaves. In: Didier, J., Barbarin, B. (Eds.) Enclaves and granite petrology (developments in petrology). Amsterdam, Elsevier, p. 263-275.

Foley, S. F., Wheller, G. E. 1990. Parallels in the origin of the geochemical signatures of island arc volcanics and continental potassic igneous rocks: The role of residual titanates. *Chemical Geology*, **85**(1-2), 1-18. doi: 10.1016/0009-2541(90)90120-V

Foley, S. F., Jackson, S. E., Fryer, B. J., Greenouch, J. D., Jenner, G. A. 1996. Trace element partition coefficients for clinopyroxene and phlogopite in an alkaline lamprophyre from Newfoundland by LAM-ICP-MS. *Geochimica et Cosmochimica Acta*, **60**(4), 629-638. doi:10.1016/0016-7037(95)00422-x

Fontes, M. P., Conceição, H., Rosa, M. L. S., Lisboa, V. A. C. 2018. Minettes do Stock Monzonítico Glória Norte: evidência de magmatismo ultrapotássico pós-orogênico, com assinatura de subducção, no Sistema Orogênico Sergipano. *Geologia USP. Série Científica*, **18**(1), 51-66. doi: 10.11606/issn.2316-9095.v18-133599

Fourcade, S., Allegre, C. J. 1981. Trace elements behavior in granite genesis: a case study the calc-alkaline plutonic association from the Querigut Complex (Pyrénées, France). *Contributions to Mineralogy and Petrology*, **76** (2), 177-195. doi: 10.1007/bf00371958

Frost, B. R., Barnes, C. G., Collins, W. J., Arculus, R. J., Ellis, D. J., Frost, C. D. 2001. A Geochemical Classification for Granitic Rocks. *Journal of Petrology*, **42**(11), 2033–2048. doi: 10.1093/petrology/42.11.2033

Frost, B. R., Lindslay, B. H. 1991. The occurrence of Fe-Ti oxides in igneous rocks. Oxide minerals: petrogenetic and magnetic significance. *Mineralogical Society of America. Ver. Mineral*, **25**, 433-486.

Furman, T., Graham, D. 1999. Erosion of lithospheric mantle beneath the East African Rift system: geochemical evidence from the Kivu volcanic province. *Lithos*, **48**(1-4), 237-262. doi: 10.1016/S0024-4937(99)00031-6

Gentil, T., 2013. *Petrologia e Geoquímica do Batólito Shoshonítico Serra do Brejo no Domínio Poço Redondo, Faixa Sergipana (Sul da Província Borborema)*. MS Dissertation, Universidade Federal de Sergipe.

Grégoire, M., Moine, B. N., O'Reilly, S. Y., Cottin, J. Y., Giret, A. 2000. Trace Element Residence and Partitioning in Mantle Xenoliths Metasomatized by Highly Alkaline, Silicate- and Carbonate-rich Melts (Kerguelen Islands, Indian Ocean). *Journal of Petrology*, **41**(4), 477-509. doi: 10.1093/petrology/41.4.477

Hall, A. 1991. *Igneous Petrology*. Harlow: Longman Scientific & Technical.

Hibbard, M. J. 1991. Textural anatomy of twelve magma-mixed granitoid systems. In: Didier, J. and Barbarin, B. (Eds.), Enclaves and granite petrology (developments in petrology). Amsterdam, Elsevier, 431-444.

Hollanda, M. H. B. M., Pimentel, M. M., Jardim de Sá, E. F. 2003. Paleoproterozoic subduction-related metasomatic signatures in the lithospheric mantle beneath NE Brazil: inferences from trace element and Sr-Nd-Pb isotopic compositions of Neoproterozoic high-K igneous rocks. *Journal of South American Earth Sciences*, **15**, 885-900. doi: 10.1016/S0895-9811(03)00014-2

Janoušek, V., Braithwaite, C. J. R., Bowes, D. R., Gerdes, A. 2004. Magma-mixing in the genesis of Hercynian calc-alkaline granitoids: an integrated petrographic and geochemical study of the Sázava intrusion, Central Bohemian Pluton, Czech Republic. *Lithos*, **78**, 67-99. doi: 10.1016/j.lithos.2004.04.046

Kaczmarek, M. A., Bodinier, J. L., Bosch, D., Tommasi, A., Dautria, J. M., Kechid, S. A. 2016. Metasomatized mantle xenoliths as a record of lithospheric mantle evolution of the nothern edge of the Ahaggar Swell, in Teria (Algeria). *Journal of Petrology*, **57**(2), 345-382. doi:10.1093/petrology/egw009

Kepezhinskas, P. K., Eriksen, G. M. D., Kepezhinskas, N. P. 2016. Geochemistry of Ultramafic to Mafic Rocks in the Norwegian Lapland: Inferences on Mantle Sources and Implications for Diamond Exploration. *Earth Science Research*, **5**(2), 148-187. doi: 10.5539/esr.v5n2p148

Krmíček, L., Cempírek, J., Havlín, A., Přichystal, A., Houzar, S., Krmíčhová, M., Gadas, P. 2011. Mineralogy and petrogenesis of a Ba–Ti–Zr-rich peralkaline dyke from Šebkovice (Czech Republic): Recognition of the most lamproitic Variscan intrusion. *Lithos*, **121**(1-4), 74-86. doi:10.1016/j.lithos.2010.10.005

Kumar, S., Bora, S., Sharma, U. K., Yi, K., Kim, N. 2017. Early Cretaceous subvolcanic calc-alkaline granitoid magmatism in the Nubra-Shyok valley of the Shyok Suture Zone, Ladakh Himalaya, India: Evidence from geochemistry and U–Pb SHRIMP zircon geochronology. *Lithos*, **277**, 33-50. doi:https: 10.1016/j.lithos.2016.11.019

Kumar, S., Rino, V. 2006. Mineralogy and geochemistry of microgranular enclaves in Palaeoproterozoic Malanjkhand granitoids, central India: evidence of magma mixing, mingling, and chemical equilibration. *Contributions to Mineralogy and Petrology*, **152**, 591-609. doi: 10.1007/s00410-006-0122-3

Kumar, S., Rino, V., Pal, A. B. 2004. Field evidence of magma mixing from microgranular enclaves hosted in Palaeoproterozoic Malanjkhand granitoids, central India. *Gondwana Research*, **7**(2), 539-548. doi: 10.1016/S1342-937X(05)70804-2

Le Maître, R. W., Bateman, P., Dudek, A., Keller, J., Lameyre, M., Le Bas, M. J., Sabine, P. A., Shimid, R., Sørensen, H., Streckeisen, A. Wolley, R., Zanettin, B. 1989. *A Classification of Igneous Rocks and Glossary of Terms*. Oxford: Blackwell Scientific Publications.

Lima, D., 2016. *Caracterização petrológica e geoquímica do Pluton Curituba, Domínio Poço Redondo-Marancó, Cinturão Sergipano.* MS Dissertation, Universidade Federal de Pernambuco.

Lisboa, V. A. C., Conceição, H., Rosa, M. L. S., Fernandes, D. M. 2019. The onset of post-collisional magmatism in the Macururé Domain, Sergipano Orogenic System: The Glória Norte Stock. *Journal of South American Earth Sciences*, **89**, 173-188. doi: 10.1016/j.jsames.2018.11.005

Liu, L., Qiu, J. S., Li, Z. 2013. Origin of mafic microgranular enclaves (MMEs) and their host quartz monzonites from the Muchen pluton in Zhejiang Province, Southeast China: Implications for magma mixing and crust–mantle interaction. *Lithos*, **160-161**, 145-163. doi: 10.1016/j.lithos.2012.12.005

Maniar, P. D., Picolli, P. M. 1989. Tectonic discrimination of granitoids. *Geological Society American*, **101**(5), 635-643. doi:10.1130/0016-7606(1989)101<0635:TDOG>2.3.CO;2

Middelmost, E. A. K. 1985. *Magmas and magmatic rocks: an introduction to igneous petrology.* London and New York: Longman.

Müller, D., Groves, D. I. 2019. *Potassic igneous rocks and associated gold-copper mineralization*. Springer International Publishing. doi: 10.1007/978-3-319-92979-8

Müller, D., Rock, N. M. S., Groves, D. I. 1992. Geochemical discrimination between shoshonitic and potassic volcanic rocks from different tectonic settings: a pilot study. *Mineralogy and Petrology*, **46**, 259-289. doi: 10.1007/BF01173568

Morrison, G. W. 1980. Characteristics and tectonic setting of the shoshonite rock association. *Lithos*, **13**(1), 97-108. doi: 10.1016/0024-4937(80)90067-5

Nakamura, N. 1974. Determination of REE, Ba, Fe, Mg, Na and K in carbonaceous and ordinary chondrites. *Geochemica et Cosmochimica Acta*, **38**(5), 757-775. doi: 10.1016/0016-7037(74)90149-5

Nardi, L. V. S., Lima, E. F. 2000. Hybridisation of mafic microgranular enclaves in the Lavras Granite Complex, southern Brazil. *Journal of South American Earth Sciences*, **13**, 67-78. doi: 10.1016/S0895-9811(00)00006-7

Oliveira, A.C., 2014. *Petrogênese do Stock Granítico Monte Alegre, noroeste do Domínio Macururé, Faixa Sergipana.* MS Dissertation, Universidade Federal de sergipe.

Oliveira, E. P., Bueno, J. F., McNaughton, N. J., Silva Filho, A. F., Nascimento, R. S., Donatti-Filho, J. P. 2015. Age, composition, and source of continental arc- and syn-collision granites of the neoproterozoic Sergipano belt, southern Borborema province, Brazil. *Journal of South American Earth Science*, **58**, 257-280. doi: 10.1016/j.jsames.2014.08.003

Oliveira, E. P., Toteu, S. F., Araújo, M. N. C., Carvalho, M. J., Nascimento, R. S., Bueno, J. F., McNahghton, N., Basilici, G. 2006. Geologic correlation between the Neoproteroxoic Sergipano belt (NE Brazil) and the Yaoundé belt (Cameron, Africa). *Journal of African Earth Sciences*, **44**, 470-478. doi:10.1016/j.jafrearsci.2005.11.014

Oliveira, E. P., Windley, B. F., Araújo, M. N. C. 2010. The Neoproterozoic Sergipano orogenic belt, NE Brazil: a complete plate tectonic cycle in western Gondwana. *Precambrian Research*, **181**, 64-84. doi: 10.1016/j.precamres.2010.05.014

Pearce, J. A., 1982. Trace element characteristics of lavas from destructive plate boundaries. In: Thorpe, R.S. (Eds.) Andesites: orogenic andesites and related rocks. New York, Wiley, p. 525-548.

Pearce, J. A. 2008. Geochemical fingerprinting of oceanic basalts with applications to ophiolite classification and the search for Archean oceanic crust. *Lithos*, **100**(1-4), 14-48. doi: 10.1016/j.lithos.2007.06.016

Peccerillo, A., Taylor, S. R. 1976. Geochemistry of Eocene calc-alkaline volcanic rocks form the Kastamonu area. *Contributions to Mineralogy and Petrology*, **58**, 63-81. doi: 10.1007/BF00384745

Pereira, F. S., Rosa, M. L. S., Conceição, H. 2019. Condições de colocação do magmatismo máfico do Domínio Macururé, Sistema Orogênico Sergipano: Maciço Capela. *Geologia USP. Série Científica*, **19**, 3-29. doi: 10.11606/issn.2316-9095.v19-151464

Perugini, D., Poli, G. 2011. Intrusion of mafic magmas into felsic magma chambers: new insights from natural outcrops and fluid-mechanics experiments. *Italian Journal of Geosciences*, **130**(1), 3-15. doi: 10.3301/IJG.2010.22

Perugini, D., Poli, G. 2012. The mixing of magmas in plutonic and volcanic environments: analogies and differences. *Lithos*, **153**, 261-277. doi: 10.1016/j.lithos.2012.02.002

Perugini, D., Poli, G., Christofides, G., Eleftheriadis, G. 2003. Magma mixing in the Sithonia plutonic complex, Greece: evidence from mafic microgranular enclaves. *Mineralogy and Petrology*, **78**(3-4), 173-200. doi: 10.1007/s00710-002-0225-0

Petford, N. 2003. Rheology of granitic magmas during ascent and emplacement. *Annual Review of Earth and Planetary Sciences*, **31**, 399-427. doi: 10.1146/annurev.earth.31.100901.141352

Pinho Neto, M. A., Rosa, M. L. S., Conceição, H. 2019. Petrologia do Batólito Sítios Novos, Sistema Orogênico Sergipano, Província Borborema, NE do Brasil. *Geologia USP*. *Série Científica*, **19**(2), 135-150. doi:10.11606/issn.2316-9095.v19-152469

Reubi, O., Blundy, J. 2009. A dearth of intermediate melts at subduction zone volcanoes and the petrogenesis of arc andesites. *Nature*, **461**, 1269-1273. doi: 10.1038/nature08510

Ringwood, A. E. 1990. Slab-mantle interaction - Petrogenesis of intraplate magmas and structure of the upper mantle. *Chemical Geology*, **82**, 187-207. doi: 10.1016/0009-2541(90)90081-H

Rosa, M. L. S., Conceição, J. A., Lisboa, V. A., Silva, C. C., Pereira, F. S., Conceição, H. 2017. U-Pb Zircon Ages in Granites (940 to 583 Ma) in the Sergipano Orogenic System, NE Brazil. *Goldschmidt 2017* (pp. 3403-3403). Paris: Holanda: European Association of Geochemistr.

Ruprecht, P., Bergantz, G. W., Cooper, K. M., Hildreth, W. 2012. The crustal magma storage system of Volcán Quizapu, Chile, and the effects of magma mixing on magma diversity. *Journal of Petrology*, **53**(4), 801-840. doi: 10.1093/petrology/egs002

Ryan, J. G., Morris, J., Bebout, G., Leeman, B. 1996. Describing chemical fluxes in subduction zones: insights from “depth profiling” studies of arc and forearc rocks. In: Bebout, G.E., Scholl, D.W., Kirby, S.H. and Platt, J.P., *Subduction top to bottom* (pp. 263-268). Washingtin DC: American Geophysical Union.

Santos, I. S., Conceição, H., Rosa, M. L. S., Marinho, M. M. 2019. Magmatismos shoshonítico e cálcio-alcalino de alto potássio pós-orogênico (615 Ma) na porção leste do Domínio Macururé, Sistema Orogênico Sergipano: Stocks Propriá, Amparo do São Francisco e Fazenda Alvorada. *Geologia USP. Série Científica*, **19**(1), 99-116. doi:10.11606/issn.2316-9095.v19-141362

Santos, R.A., Martins, A.A., Neves, J.P., Leal, R.A., 2001. Programa Levantamentos Geológicos Básicos do Brasil - PLGB. Geologia e recursos minerais do Estado de Sergipe.

Escala 1:250.000. Texto Explicativo do Mapa Geológico do Estado de Sergipe. Brasília: CPRM/DIEDIG/DEPAT, CODISE.

Santos, R.A., Souza, J.D., 1988. Programa Levantamentos Geológicos Básicos do Brasil. Carta Geológica Piranhas. Escala 1:100.000. Brasília: DNPM/CPRM.

Sarjoughian, F., Lentz, D., Kananian, A., Ao, S., Xiao, W. 2017. Geochemical and isotopic constraints on the role of juvenile crust and magma mixing in the UDMA magmatism, Iran: evidence from mafic microgranular enclaves and cogenetic granitoids in the Zafarghand igneous complex. *International Journal of Earth Sciences*, **107**(3), 1127-1151. doi: 10.1007/s00531-017-1548-8

Shukla, S., Mohan, M. R. 2019. Magma mixing in Neoarchean granite from Nalgonda region, Eastern Dharwar Craton, India: Morphological, mineralogical and geochemical evidences. *Journal of Earth System Science*, **128**(3). doi: 10.1007/s12040-019-1095-8

Silva, C.C., 2014. *Petrologia e geocronologia do Stock Granodiorítico Lagoa do Roçado, Domínio Macururé, Faixa Sergipana-SE.* MS Dissertation, Universidade Federal de Sergipe.

Silva Filho, M. A., Torres, H. H. 2002. A new interpretation on the Sergipano Belt domains. *An. Acad. Bras. Cienc. Anais*, **74**(3), 556-557. doi: 10.1590/S0001-37652002000300049

Siuda, J. D., Bagiński, B. 2019. Magma mingling textures in granitic rocks of the eastern part of the Strzegom-Sobótka Massif (Polish Sudetes). *Acta Geologica Polonica*, **69**(1), 143-160. doi: 10.24425/agp.2019.126437

Smith, E. I., Sánchez, A., Walker, J. D., Wang, K. 1999. Geochemistry of Mafic Magmas in the Hurricane Volcanic Field, Utah: Implications for Small- and Large-Scale Chemical Variability of the Lithospheric Mantle. *The Journal of Geology*, **107**, 433-448. doi: 10.1086/314355

Sousa, C. S., Soares, H. S., Rosa, M. L. S., Conceição, H. 2019. Petrologia e Geocronologia do Batólito Rio Jacaré, Domínio Poço Redondo, Sistema Orogênico Sergipano, NE do Brasil. *Geologia USP. Série Científica*, **19**(2), 171-194. doi:10.11606/issn.2316-9095.v19-152494

Streckeisen, A. 1976. To each plutonic rock its proper name. *Earth Science Reviews*, **12**(1), 121-133. doi: 10.1016/0012-8252(76)90052-0

Sun, S. S., McDonough, W. F. 1989. Chemical and isotopic systematics of oceanic basalts: implications for mantle composition and processes. *Geological Society, London, Special Publications*, **42**(1), 313-345. doi: 10.1144/gsl.sp.1989.042.01.19

Thompson, R. N. 1982. Magmatism of the British Tertiary Volcanic Province. *Scottish Journal of Geology*, **18**, 50-107. doi: 10.1144/sjg18010049

Torkian, A., Furman, T. 2015. The significance of mafic microgranular enclaves in the petrogenesis of the Qorveh Granitoid Complex, northern Sanandaj-Sirjan Zone, Iran. Neues Jahrbuch Für Mineralogie – Abhandlungen. *Journal of Mineralogy and Geochemistry*, **192**(2), 117-133. doi:10.1127/njma/2015/0275

Turner, S., Arnaud, N., Liu, J., Rogers, N., Hawkesworth, C., Harris, N., Kelley, S., Van Calsteren, P., Deng, W. 1996. Post-collision, Shoshonitic Volcanism on the Tibetan Plateau: Implications for Convective Thinning of the Lithosphere and the Source of Ocean Island Basalts. *Journal of Petrology*, **37**(1), 45-71. doi:10.1093/petrology/37.1.45

Vernon, R. H. 1984. Microgranitoid enclaves in granites—globules of hybrid magma quenched in a plutonic environment. *Nature*, **309**, 438-439. doi: 10.1038/309438a0

Vernon, R. H., Etheridge, M. A., Wall, V. J. 1988. Shape and microstructure of microgranitoid enclaves: indicators of magma mingling and flow. *Lithos*, **22**(1), 1-11. doi: 10.1016/0024-4937(88)90024-2

Weidendorfer, D., Mattson, H. B., Ulmer, P. 2014. Dynamics of Magma Mixing in Partially Crystallized Magma Chambers: Textural and Petrological Constraints From the Basal Complex of the Austurhorn Intrusion (SE Iceland). *Journal of Petrology*, **55**(9), 1865-1903. doi: 10.1093/petrology/egu044

Winter, J.D., 2014. *Principles of Igneous and Metamorphic Petrology* (2° ed.). Edinburgh: Pearson New International Edition.

Wones, D. R. 1989. Significance of the assemblage titanite + magnetite + quartz in granitic rocks. *American Mineralogist*, **74** (7-8), 744-749.

Wyllie, P. J., Cox, K. G., Biggar, G. M. 1962. The Habit of Apatite in Synthetic Systems and Igneous Rocks. *Journal of Petrology*, **3**(2), 238-243. doi: 10.1093/petrology/3.2.238

Yang, H., Ge, W., Zhao, G., Dong, Y., Xu, W., Ji, Z., Yu, J. 2015. Late Triassic intrusive complex in the Jidong region, Jiamusi–Khanka Block, NE China: Geochemistry, zircon U–Pb ages, Lu–Hf isotopes, and implications for magma mingling and mixing. *Lithos*, **224-225**, 143-159. doi: 10.1016/j.lithos.2015.03.001

Zack, T., Foley, S. F., Jenner, G. A. 1997. A consistent partition coefficient set for clinopyroxene, amphibole and garnet from laser ablation microprobe analysis of garnet pyroxenites from Kakanui, New Zealand. *Neues Jahrbuch fur Mineralogie, Abhirchen*, **172**(1), 23-41. doi: 10.1127/njma/172/1997/23

CAPÍTULO 3

MAGMATIC PROCESSES RECORDED IN PLAGIOCLASE CRYSTALS OF THE RIO JACARÉ BATHOLITH, SERGIPANO OROGENIC SYSTEM, NORTHEAST BRAZIL

Magmatic processes recorded in plagioclase crystals of the Rio Jacaré Batholith, Sergipano Orogenic System, Northeast Brazil

Carlos Santana Sousa [a, b, *], Herbet Conceição [a, b, c], Hiakan Santos Soares [a, b], Diego Melo Fernandes [a, b], Maria de Lourdes da Silva Rosa [b, c]

[a] *Programa de Pós-Graduação em Geologia, Universidade Federal da Bahia, Rua Barão de Jeremoabo, s/n - Ondina, Salvador, BA, 40170-290, Brazil*
[b] *Laboratório de Petrologia Aplicada à Pesquisa Mineral, Universidade Federal de Sergipe, Avenida Marechal Rondon, s/n, Jardim Rosa Elze, 49100-000, São Cristóvão, Sergipe, Brazil*
[c] *Programa de Pós-Graduação em Geociências e Análise de Bacias, Universidade Federal de Sergipe, Avenida Marechal Rondon s/n - Rosa Elze, São Cristóvão, SE, 49100-000, Brazil*

ARTICLE INFO

Keywords:
Compositional zonings
Magma mixing
Crystal resorption

ABSTRACT

Plagioclase crystallization is common in magmatic systems and are textures can provide valuable information about the physicochemical conditions present during magmatic evolution. This work presents a systematic study of textures and compositional variation in plagioclase crystals in the granites and microgranular enclaves of the Rio Jacaré Batholith (RJB) aiming to infer the magmatic processes that were recorded in these crystals. Plagioclase of the inequigranular facies has composition ranging from albite to andesine (An_{7-33}), while in the porphyritic facies it is albite and oligoclase (An_{5-23}). In microgranular enclaves plagioclase composition ranges from albite to labradorite (An_{6-51}). In addition to the presence of chemical zoning in plagioclase of the RJB rocks, patchy zoning, boxy cellular texture, crystal cores showing embayed or homogeneous composition as well as inclusion zones of mafic and synneusis minerals also occur. The textures identified in the RJB rocks allowed us to infer that during the evolution of the RJB magma, there was a period of stable conditions followed by a period with injections of mafic magmas, which modified the conditions (temperature, pressure, and H_2O activity) of this magmatic system and stimulated mixing between magmas. The mafic magma injections are most likely to have generated convection currents in the magmatic chamber of the RJB. In addition to this process, it is also necessary to consider the decompression of magma, caused by its rapid rise. This complex evolution of the Rio Jacaré magmatic system was registered in the textures and compositions of the plagioclase crystals and suggests at least five successive moments of resorption in these crystals.

1. Introduction

Orogenic environments are places where mantle mafic magmas have access to the continental crust and can mix with felsic crustal magmas (Donaldson et al., 2003). When the interaction between these magmas results in a homogeneous mixture, a hybrid magma of intermediate composition is formed and this process is called mixing (Fernandez and Barbarin, 1991; Sklyarov and Fedorovskii, 2006). When the interaction between magmas results in heterogeneous mixture, mafic magma bubbles (microgranular enclaves) are formed in the felsic magma and this process is called mingling (Poli and Tommasini, 1991; Fernandez and Barbarin, 1991; Sklyarov and Fedorovskii, 2006). According to Vernon (1984), Hibbard (1991) and Kumar and Rino (2006), evidence of mixing and mingling processes between magmas have been registered and interpreted in outcrops (mesostructures), in hand samples and thin sections (textures).

Feldspar crystals in igneous rock have often been the subject of several studies (e.g. Vance, 1962, 1965; Hibbard, 1981; Anderson, 1984; Nelson and Montana, 1992; Anderson and Eklund, 1994; L'Heureux and Fowler, 1994; Hattori and Sato, 1996; Castro, 2001; Karsli et al., 2004; Bennett et al., 2019; Gogoi and Saikia, 2019), as they are common minerals in these rocks and can exhibit varied and frequent textures that are not easily found in other minerals. Many of these studies (e.g. Hibbard, 1981; Hattori and Sato, 1996; Kuşcu and Floyd, 2001;

* Laboratório de Petrologia Aplicada à Pesquisa Mineral, Universidade Federal de Sergipe, Avenida Marechal Rondon, s/n, Jardim Rosa Elze, 49100-000, São Cristóvão, Sergipe, Brazil.

E-mail addresses: karlcss@ufba.br (C.S. Sousa), herbet@academico.ufs.br (H. Conceição), hiakanss@ufba.br (H.S. Soares), dmfernandes@ufba.br (D.M. Fernandes), lrosa@academico.ufs.br (M.d.L.d.S. Rosa).

https://doi.org/10.1016/j.jsames.2022.103942
Received 30 November 2021; Received in revised form 1 April 2022; Accepted 19 July 2022
0895-9811/

Perugini et al., 2003; Humphreys et al., 2006) consider the formation of several textures and compositional zoning in feldspar as a reflection of physicochemical instability resulting from varying factors: temperature and pressure change, magma flow in the magmatic chamber caused by convection currents and also due to variation of H_2O activity during crystallization and transport of the magma.

From the identification of textures (e.g. rapakivi, sieve, patchy, boxy cellular) and compositional zoning present in feldspar, several authors suggest that it is possible to identify and infer the presence of magmatic processes during rock formation, such as: mixing and mingling (Hibbard, 1981, 1991; Nelson and Montana, 1992; L'Heureux and Fowler, 1994; Hattori and Sato, 1996; Holten et al., 2000; Grogan and Reavy, 2002; Karsli et al., 2004; Tepper and Kuehner, 2004), assimilation (Castro, 2001), degassing (Holten et al., 2000) or decompression (Vance, 1962, 1965; Anderson, 1984; Kuşcu and Floyd, 2001).

Several textures and compositional zoning in plagioclase are found in granites, granodiorites and diorites of the Rio Jacaré Batholith (RJB), which is the second largest intrusion of the Poço Redondo Domain (Fig. 1), with an area of 167 km² (Sousa et al., 2019). It is the main representative of the Queimada Grande Intrusive Suite (Teixeira, 2014) in the Sergipano Orogenic System (SOS, Conceição et al., 2016).

A study of petrography, mineral chemistry and whole rock geochemistry was carried out on the RJB rocks by Sousa et al. (2019), but the meaning of all textures and zoning patterns of plagioclase crystals has not been detailed. Therefore, it is not yet known which magmatic processes were responsible for generating this variety of textures and zoning in the RJB plagioclase. The identification of textures and systematic studies of the compositional variations of plagioclase crystals can reveal which magmatic processes occurred during their formation.

In this work, plagioclase crystals of the RJB were investigated and used as petrogenetic markers and their textures and compositional variations were used to infer the sequence of magmatic processes involved during the crystallization of this batholith.

2. Feldspar textures

According to Hibbard (1981), physicochemical disequilibrium during magma crystallization is responsible for the development of textures in minerals. Karsli et al. (2004) consider that textures and compositional zoning in feldspars provide important information on the evolution conditions of magmatic systems.

Some textures are presented in the literature as being produced by certain magmatic processes. For instance, sieve texture is an indication of rapid decompression in magmatic systems (Kuşcu and Floyd, 2001); rapakivi and antirapakivi textures, inclusion zones in feldspar, small lath-shaped plagioclase, spike zones, spongy cellular and boxy cellular zones in plagioclase suggest the presence of mixing process between magmas (Hibbard, 1981; Hibbard, 1991; Nelson and Montana, 1992; L'Heureux and Fowler, 1994; Hattori and Sato, 1996; Holten et al., 2000; Grogan and Reavy, 2002; Karsli et al., 2004).

Oscillatory zoning in plagioclase has been explained by several hypotheses. Some authors consider this kind of zoning as a reflection of changes in temperature (e.g. Hattori and Sato, 1996; Lange et al., 2009; Bennett et al., 2019), pressure (e.g. Ustunisik et al., 2014; Bennett et al., 2019), changes in water activity (e.g. Lange et al., 2009; Cao et al., 2019), degassing (e.g. Cao et al., 2019) and the presence of repetitive injections of mafic magmas into a magmatic chamber of intermediate or felsic nature (e.g. Cao et al., 2014).

The synneusis texture (Vance, 1969; Gogoi and Saikia, 2019) is interpreted as being formed by the assemblage of plagioclase crystals in aggregates that can form phenocrysts.

3. Materials and methods

In this work, 37 polished thin sections were analyzed with an Opton (TNP - 09NT) petrographic microscope under transmitted and reflected light. In this study, the textures present in the plagioclase crystals of the inequigranular, porphyritic facies and the RJB enclaves were identified.

After petrographic study, the polished thin sections were metallized with gold (metallization film thickness of 8–10 nm) to be investigated by a scanning electron microscope (SEM) using backscattered electron detector (BSE), secondary electrons, cathodoluminescence and energy dispersive spectrometer detectors (EDS). These detectors allowed better visualization of textures and compositional variation in plagioclase crystals. These equipments are installed on a TESCAN scanning electron microscope, Veja-3 LMU model, in the Laboratory of Microanalysis of the Condominium of Multiuser Laboratories of Geosciences (CLGeo), Federal University of Sergipe (UFS).

A total of 1065 (supplementary material) spot chemical compositions in feldspar were obtained with EDS (SDD- Silicon Drift Detectors) from Oxford Instruments®, X-Act model, with a resolution of 128 eV. The following analytical parameters were used for chemical analysis: voltage of 20 kV, current of 15–17 nA, diameter of the electron beam between 0.28 and 0.40 μm, 15 mm distance. and counting time of 60 s. The spectral lines used for the quantification of elements, the internal EDS standards and the associated uncertainties (3σ) were: SiKα (quartz, ± 4), AlKα (corundum, ± 2), FeKα (metallic iron, ± 4), CaKα (wollastonite, ± 2), NaKα (albite, ± 2), KKα (sanidine, ± 2) e BaLα (BAF_2, ±2).

The EDS was calibrated using copper energy and the reliability and reproductivity evaluation of the feldspar data were carried out with analyzes of international standards, mineral mount model, with composi-

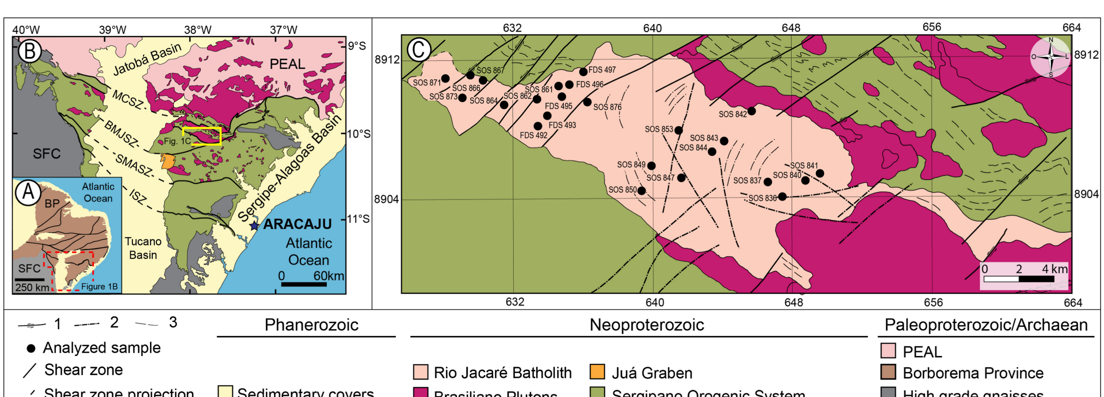

Fig. 1. Schemes contextualizing the regional geology and Rio Jacaré Batholith geology. (A) Simplified map of the Borborema Province in the northeast of Brazil (Van Schmus et al., 2008). (B) Simplified map of the Sergipano Orogenic System (SOS – Pinho Neto et al., 2019). (C) Simplified geological map of the Rio Jacaré Batholith (Sousa et al., 2019). São Francisco Craton (SFC). Pernambuco-Alagoas Massif (PEAL). Shear zones: Macururé (MCSZ); Belo Monte Jeremoabo (BMJSZ); São Miguel do Aleixo (SMASZ); Itaporanga (ISZ). 1- Fault. 2- Fracture. 3- Lineament.

tions like those studied (Table 1): sanidine (Astimex Scientific Ltd®) and plagioclases (Cameca, mineral mount model). The results obtained reveal values close to those provided for the standards and maintained cationic proportions. Dosed iron was in +3 valence. Structural formula of feldspar was calculated based on 8 oxygens, according to the recommendations of Deer et al. (2013).

The obtained BSE images allowed to define the limits of compositional zoning, using the variation of the gray shades. The determination of anorthite contents of each zone was made from several spot chemical analyses using EDS. Several profiles of spot chemical analyses were made through the crystals to delimit areas of the same composition (see Fig. 7A analysis scheme adopted to delimit the compositional zoning). It was noticed that each shade of gray presents a small variation in the anorthite content. To highlight the variations in gray tones of the images obtained with BSE, contrast was applied to the image and to the image tracing filter.

4. Geology and petrography of the Rio Jacaré Batholith

The RJB (Fig. 1) is part of the Poço Redondo Domain (Davison and Santos, 1989) of the Sergipano Orogenic System, being intruded in the Poço Redondo Migmatitic Complex (Santos and Souza, 1988; Carvalho, 2005), in the Sítios Novos Batholith (Pinho Neto et al., 2019) and in granitic gneisses of the Serra Negra Intrusive Suite (Teixeira, 2014; Lima et al., 2019).

According to Sousa et al. (2019), the RJB crystallization age is 617 ± 4 Ma (zircon U-Pb_{SHRIMP}) and it was formed in a post-collisional orogenic environment. It is composed of two petrographic facies: inequigranular (IF) and porphyritic (PF) facies. In both facies there are abundant microgranular enclaves (ME; Fig. 2) that preserve mingling features. According to Sousa et al. (2019), the rocks of these facies correspond to quartz monzonite, monzogranite and granodiorite (Fig. 3), and the PF differs from the IF by the presence of feldspar phenocrysts (Fig. 2). The ME show colors ranging from light to dark gray and present rounded, elongated, and complex shapes. Their size may reach up

Table 1
Comparison between the compositions of CAMECA and Astimex standards and those obtained with EDS-MEV in this study. AST = pattern composition provided by Astimex; CAM = pattern composition provided by CAMECA; 3σ = error calculated in EDS for 3 sigmas; MD = Module of the difference between the analysis of the standards and those obtained with EDS-MEV. Sum of cations obtained with the calculation of the structural formula made for 8 oxygens. % An = percentage of anorthite. The oxide values are presented in weight percentage.

	Sanidine				Plagioclase															
					Labradorite				Andesine				Oligoclase				Albite			
	AST	EDS	*3σ*	*MD*	CAM	EDS	*3σ*	*MD*	CAM	EDS	*3σ*	*MD*	CAM	EDS	*3σ*	*MD*	CAM	EDS	*3σ*	MD
SiO_2	64.67	64.6	*0.3*	*0.07*	50.55	51.0	*0.3*	*0.45*	56.04	55.9	*0.4*	*0.14*	61.41	62.0	*0.3*	*0.59*	66.22	66.06	*0.3*	0.16
Al_2O_3	18.76	18.9	*0.2*	*0.14*	31.69	30.9	*0.2*	*0.79*	27.93	28.1	*0.2*	*0.17*	24.50	25.1	*0.2*	*0.60*	21.12	21.3	*0.3*	0.18
CaO					14.35	14.5	*0.1*	*0.15*	10.12	10.0	*0.1*	*0.12*	6.11	5.9	*0.1*	*0.21*	2.02	2.1	*0.1*	0.08
Na_2O	3.01	2.9	*0.1*	*0.11*	3.40	3.4	*0.1*	*0.0*	5.91	6.0	*0.1*	*0.09*	8.36	8.4	*0.1*	*0.04*	10.64	10.8	*0.1*	0.16
K_2O	12.11	12.1	*0.1*	*0.01*																
FeO	0.18	0.3	*0.1*	*0.12*																
BaO	1.09	1.3	*0.2*	*0.21*																
Total	99.02	100.1			99.99	99.8			100.00	100.0			100.38	101.4			100.00	100.25		
∑Cations	5.003	5.000			5.000	4.995			5.000	5.005			5.002	5.000			5.000	4.996		
% An					70.0	70.2			48.6	47.9			28.8	28.0			9.5	9.7		

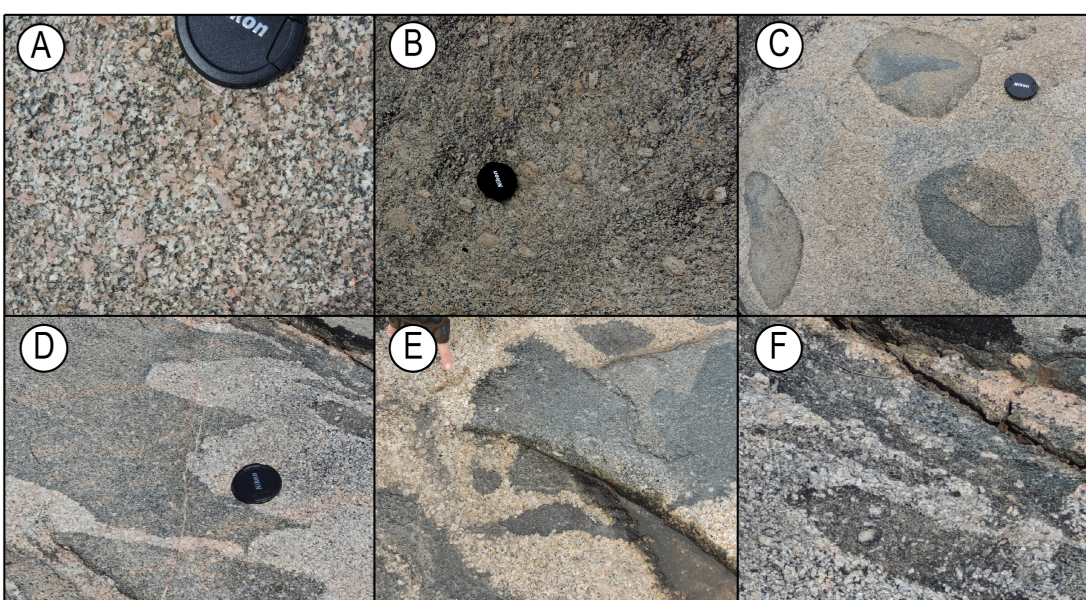

Fig. 2. Field aspects of the RJB rocks. (A) Inequigranular facies. (B) Porphyritic facies. Note the centimetric size of the feldspar phenocrysts. (C) ME with rounded and elongated shapes. Note the lower left corner enclave with finer granulation and darker color in the edge (chilled margin). (D) ME with cuspate contacts. (E) ME with crenulated and lobate edges. (F) Alkali feldspar xenocrysts in ME. Note the feldspar crystals entering the enclave contacts. The diameter of the black circle is 7.0 cm.

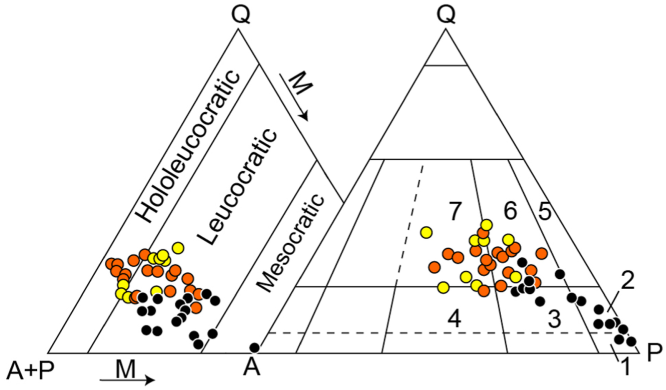

Fig. 3. Streckeisen (1976) QAP and Q(A + P)M diagrams applied to the RJB rocks. Q: quartz, A: alkali feldspar + albite with < 5% anorthite, P: plagioclase (anorthite > 5%), M: total of mafic minerals. Rocks of the Rio Jacaré Batholith of the Inequigranular (orange circle), Porphyritic (yellow circle) facies and the enclaves (black circles). 1: Diorite; 2: quartz diorite; 3: quartz monzodiorite; 4: quartz monzonite; 5: tonalite; 6: granodiorite; 7: monzogranite.

to 2 m in length, with straight, sinuous, and cuspate contacts and chilled margins. Their composition ranges from diorite, quartz diorite, quartz monzodiorite to granodiorite (Fig. 3).

The minerals present in the inequigranular, porphyritic facies and enclaves are the same (plagioclase, alkali feldspar, quartz, biotite, hornblende, titanite, magmatic epidote, zircon, apatite, allanite, magnetite, and ilmenite) (Table 2). However, their volume is different in each facies.

5. Results

5.1. Textures

The rocks of the inequigranular and porphyritic facies of the RJB are medium- to fine- grained (~1 mm) but they in places show phenocrysts of plagioclase, alkali feldspar and quartz with up to 5 mm in the IF and up to 1.5 cm in the PF. The microgranular enclaves are fine-grained (< 1 mm) but locally contain plagioclase phenocrysts (~2.5 mm), and alkali feldspar (~3 mm) and quartz (~2.8 mm) xenocrysts.

Plagioclase is subhedral, anhedral and shows albite and albite-Carlsbad twinning. Compositional zoning is frequent, being characterized by concentric multiple zones parallel to the crystal edge (Fig. 4A and B). Some zoned crystals show sets of tiny inclusions of biotite, hornblende, magnetite, and ilmenite aligned and parallel to the edges of grain faces and located at zone boundaries (Fig. 4B, C and D). This set of inclusions correspond to the inclusion zone, which has a thickness between 10 and 62 μm. There are also crystals with compositional zoning characterized by clear cores without zones and with rounded shapes (Fig. 4E and F); or in cells (boxy cellular texture, Fig. 4A and G). Compositional variation is also marked by intercalations of saussuritized areas with clear areas without plagioclase alteration (Fig. 4H). Some crystals show zoning exclusively at the edges of the crystals and in these cases the grain cores may not be zoned (Fig. 4I). Plagioclase can also form synneusis texture (Fig. 4C and E).

Alkali feldspar, hornblende and titanite crystals also show compositional zoning (Fig. 5A, B, C and D). Microcline is perthitic, with albite-pericline twinning and in places show remnants of Carlsbad twinning. Hornblende is green, subhedral, and may occur in association with mafic mineral agglomerates. It shows inclusions of subhedral and euhedral apatite, ilmenite, epidote, titanite, magnetite and zircon crystal. Clinopyroxene occurs as relict crystals (core) changed to amphibole (edges; Fig. 5C). Biotite is brown, subhedral, may show blade texture and has inclusions of ilmenite, titanite, magnetite, apatite, and zircon.

Quartz is anhedral and shows weak undulose extinction. Brown titanite is anhedral and euhedral. Anhedral titanite (< 2 mm) occurs mainly in biotite cleavage planes; euhedral titanite has larger size (~0.8 mm) and presents complex compositional zoning and shapes that suggest corrosion (corroded texture; Fig. 5D). Magmatic epidote is subhedral, sometimes with allanite core and many crystals show zoning close to grain limits (Fig. 5E). Epidote also occurs as anhedral grains in biotite fractures and in saussuritization zones. Allanite is euhedral and some crystals show compositional zoning at the edges (Fig. 5F). Ilmenite and magnetite are anhedral and associated with titanite, biotite and hornblende. Apatite is euhedral and shows prismatic and acicular habits. Zircon is euhedral.

The textures described above are found in rocks from IF, PF and in the ME. However, some textures are only found in the ME, such as: acicular apatite crystals; compositional zoning limited to the edges of plagioclase crystals; and plagioclase cores with rounded faces (Fig. 4E and F).

Table 2
Representative modal mineralogical compositions of the RJB rocks. HBGd = Hornblende biotite granodiorite. BHGd = Biotite hornblende granodiorite. BGd = Biotite granodiorite. MG = Monzogranite. BMG = Biotite monzogranite. HBD = Hornblende biotite diorite. HBQMD = Hornblende biotite quartz monzodiorite. O.M. = Opaque Minerals (magnetite, ilmenite e pyrite). The values are presented in percentage.

Inequigranular Facies						Porphyritic Facies				Enclaves		
Sample	FDS 492	SOS 836	SOS 841	SOS 849A	SOS 876A	FDS 495	SOS 837	SOS 840A	SOS 847	SOS 843B	SOS 861C	SOS 876B
Rock	HBGd	BHGd	BGd	HBGd	MG	BMG	BMG	BMG	BGd	HBD	HBQMD	HBQMD
Fenocrysts												
Plagioclase						18.4	1.8	5.6	22.1			1.4
Microcline						18.1	11.1	30.1	5.0			0.3
Quartz						7.5			5.7			1.3
Groundmass												
Plagioclase	40.5	42.4	41.4	44.5	31.1	24.3	37.8	28.4	18.9	56.8	46.2	39.5
Hornblende	8.0	14.9		8.7	0.3	3.7	0.5		1.6	17.4	7.4	9.8
Quartz	25.1	14.7	25.0	23.0	24.4	11.2	21.0	17.8	24.0	2.9	11.9	12.3
Muscovite					1.6							
Biotite	12.7	14.1	13.2	14.5	4.2	5.6	6.4	9.7	9.2	18.9	18.7	16.5
Microcline	13.2	11.0	17.2	7.5	36.5	9.6	18.9	5.6	9.3	1.3	12.5	15.6
Titanite	< 0.1	1.6	1.4	0.5	0.7	0.6	1.5	1.6	1.0	1.6	1.5	1.8
Epidote	< 0.1	1.0	0.6	1.0	0.4	0.5	0.3	0.2	2.9	0.8	1.5	1.3
O.M.	< 0.1	< 0.1	1.0	< 0.1	0.6	0.5	0.5	0.8	< 0.1	< 0.1	< 0.1	< 0.1
Apatite	< 0.1	< 0.1	< 0.1	< 0.1	< 0.1	< 0.1	< 0.1	< 0.1	< 0.1	< 0.1	< 0.1	< 0.1
Zircon	< 0.1	< 0.1	< 0.1	< 0.1	< 0.1	< 0.1	< 0.1	< 0.1	< 0.1	< 0.1	< 0.1	
Total	100.0	100.0	100.0	100.0	100.0	100.0	100.0	100.0	100.0	100.0	100.0	100.0

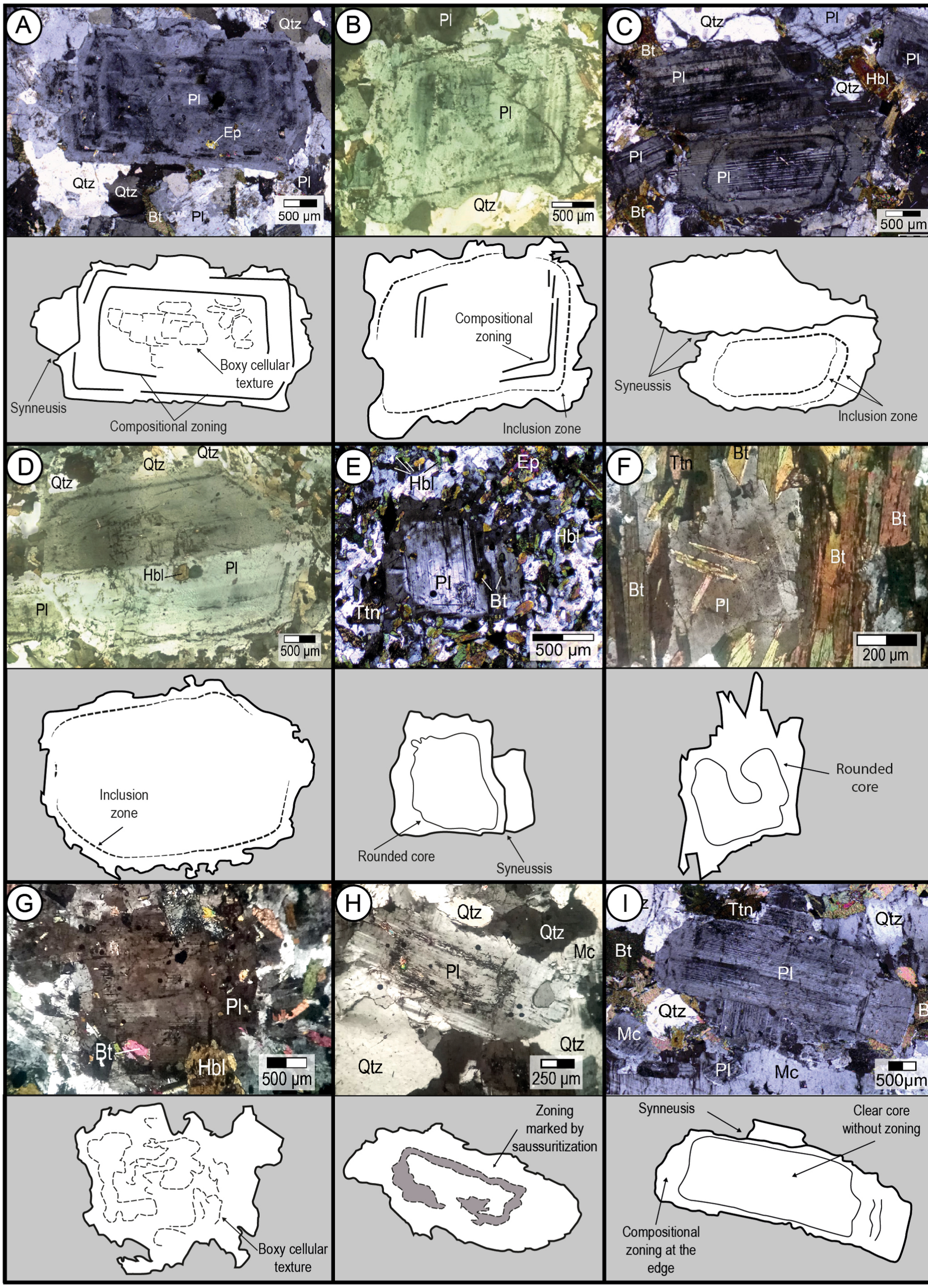

Fig. 4. Images with textures of plagioclase crystals of the RJB rocks and corresponding sketches. (A) Multiple compositional zoning parallel to plagioclase face edges. The central region of the crystal also shows cells with lighter color. (B) Compositional zoning parallel to plagioclase crystal face and to inclusion zone. (C) Plagioclase crystals with synneusis texture and zones with crystal inclusions. (D) Plagioclase with mineral inclusion zone parallel to the crystal faces and close to grain edges. (E) and (F) Plagioclase with compositional zoning at the edges and showing core with rounded faces. Note in Figure F an embayment in the crystal core. (G) Plagioclase crystal with internal features typical of boxy cellular texture. It is possible to observe well-delimited portions that are lighter than others. (H) Plagioclase with compositional zoning well marked by differential saussuritization. (I) Plagioclase exhibiting a clear core without zoning patterns and with compositional zoning at the edges.

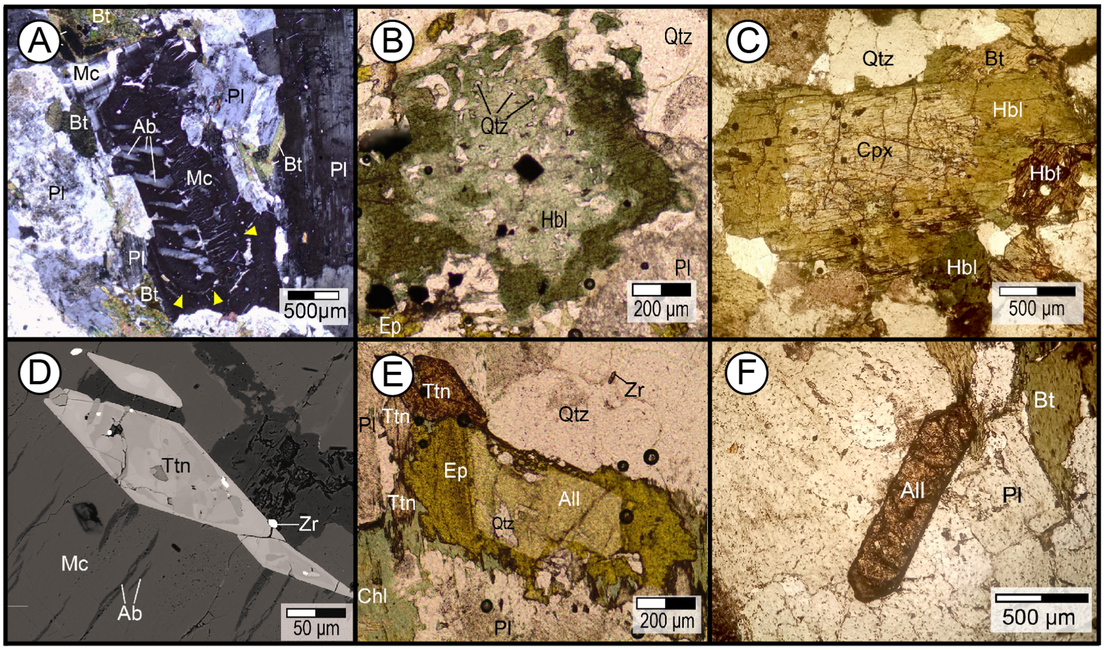

Fig. 5. Compositional zoning features in the RJB crystals. (A) Perthitic microcline exhibiting compositional zoning at the edges. Note the yellow arrows indicating zone limits. (B) Hornblende with compositional zoning at the crystal edges. (C) Hornblende with clinopyroxene core. (D) BSE image of euhedral titanite crystals with compositional zoning parallel to the face edges. (E) Epidote with allanite core. (F) Euhedral allanite with compositional zoning at the edges. Quartz (Qtz). Plagioclase (Pl). Microcline (Mc). Hornblende (Hbl). Biotite (Bt). Clinopyroxene (Cpx). Allanite (All). Epidote (Ep). Titanite (Ttn). Zircon (Zr). Albite (Ab). Chlorite (Chl).

5.2. Mineral chemistry

Table 3 presents representative analyses of plagioclase crystals from the RJB rocks. Plagioclase composition of the IF ranges from albite to andesine ($An_{7\text{-}33}$), whilst in the PF its composition is albite and oligoclase ($An_{5\text{-}23}$) and in the ME the composition varies from albite to labradorite ($An_{6\text{-}51}$). Note that range of plagioclase composition is wider in the ME crystals and smaller in PF crystals (Fig. 6). Albitic compositions in these crystals are limited to grain periphery and suggest action of late fluids, that is, they do not result from magma crystallization and therefore will not be discussed in the next sections.

BSE images of plagioclase crystals allowed better visualization of the geometry of compositional changes (Fig. 7). It can be seen that ME crystals present calcic cores, with resorption features, suggested by amoeba-type shapes, which are outlined by more sodic compositions, configuring a patchy texture (Fig. 7). Obtaining systematic spot chemical analysis in the zones identified with BSE images allowed the quantification of changes in chemical compositions (Fig. 7). It was observed that in the ME crystals the presence of crystals cores with anorthite content higher than in crystals of the inequigranular and porphyritic facies (Figs. 6 and 7).

6. Discussion

The variation in composition of the RJB plagioclase is mainly marked in the crystals present in ME (Fig. 6). According to Hattori and

Table 3
Spot chemical analysis of plagioclase crystals representative of rocks from the Rio Jacaré Batholith. The oxide values are presented in percentage. Cation value are shown in atoms per formula unit. The oxide values are presented in weight percentage. The values of the cations were obtained with the calculation of the structural formula made for 8 oxygens. Or = orthoclase molecule (100.K/(K + Na + Ca)); Ab = albite molecule (100.Na/(K + Na + Ca)); An = anorthite molecule (100.Ca/(K + Na + Ca)).

Inequigranular Facies						Porphyritic Facies			Enclaves		
Sample	FDS 492	SOS 843A	SOS 850A	SOS 866	SOS 866	FDS 495	SOS 840A	SOS 844	SOS 867B	SOS 871B	SOS 871B
SiO_2	60.5	63.1	62.0	64.2	62.2	62.1	63.1	64.4	59.4	61.6	54.8
Al_2O_3	25.3	23.7	24.4	22.5	24.1	24.0	23.6	22.5	26.0	24.4	29.2
CaO	6.1	3.7	4.9	3.4	5.1	5.0	4.0	3.1	7.1	5.4	10.5
Na_2O	8.1	9.2	8.7	9.8	8.7	8.9	9.3	9.9	7.4	8.6	5.5
K_2O		0.2		0.1		0.0					
Total	100.0	99.9	100.0	100.0	100.1	100.0	100.0	99.9	99.9	100.0	100.0
Si	2.687	2.787	2.743	2.831	2.751	2.751	2.785	2.839	2.647	2.731	2.47
Al	1.324	1.234	1.272	1.170	1.256	1.253	1.228	1.169	1.365	1.275	1.55
Ca	0.290	0.175	0.232	0.161	0.242	0.237	0.189	0.146	0.339	0.257	0.51
Na	0.698	0.788	0.746	0838	0.746	0.764	0.796	0.846	0.639	0.739	0.48
K		0.011		0.006							
Total	4.999	4.995	4.994	5.006	4.994	5.005	4.999	5.000	4.990	5.001	5.001
Or		1.1		0.6							
Ab	70.6	80.9	76.3	83.4	75.5	76.3	80.8	85.3	65.3	74.2	48.7
An	29.4	18.0	23.7	16.0	24.5	23.7	19.2	14.7	34.7	25.8	51.3

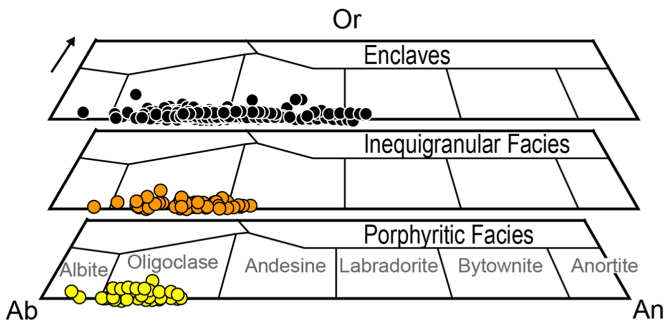

Fig. 6. Or-Ab-Na diagram showing the compositional variation of plagioclase crystals. Inequigranular Facies (orange circles). Porphyritic Facies (yellow circles). and enclaves (black circles).

Sato (1996), the anorthite content in plagioclase depends on temperature (T) and pressure (P) of the magma. Lange et al. (2009) admit that, in addition to temperature, the increase in the content of H_2O dissolved in magma also makes plagioclase crystals more calcic. According to Ustunisik et al. (2014), anorthite content can vary based on the pressure at a rate of 3 mol%/kbar and these variations can be generated by convection in the magmatic chamber, isobaric crystallization, and vertical transport. In the RJB rocks, Sousa et al. (2019) observed amphibole crystallization variation of pressure from 2 to 6 kbar, which suggests magma crystallization at different depths in the crust. According to these pressures, using the 3 mol%/kbar ratio of Ustunisik et al. (2014), the variation in the anorthite content of the RJB plagioclase crystals should be at most 12%. The compositional variation in these crystals (FI: $An_{12\text{-}33}$; PF: $An_{11\text{-}23}$; EM: $An_{11\text{-}51}$) is greater than this value and suggests that in addition to changes in pressure, during the evolution of this batholith, there might have also been changes in the temperature conditions and/or in the H_2O content.

Plagioclase crystals in the RJB rocks present a wide variety of compositional zoning. The presence of compositional zoning in crystals reflects their growth in an open magmatic system, involving processes of mixing between magmas, degassing or hydrothermal processes (Holten et al., 2000). The variations in anorthite content in oscillatory zoning cannot be generated in a stable magmatic chamber (Cao et al., 2019). Granitic plutons are formed by additions of magma pulses (Glazner et al., 2004) and, in a magmatic chamber, magma is affected by several dynamic physical processes, such as the presence of convection or the injection of hotter, calcium-enriched mafic magmas (Yazdi et al., 2019). The plumbing system (e.g. Hildreth, 2004; Annen et al., 2006, 2015; Annen, 2011; Miller et al., 2011; Solano et al., 2012; Cashman et al., 2017) is suggested as the more realistic model to explain the formation of plutons and has been described (e.g. Magee et al., 2018) as sets of interconnected magmatic reservoirs and conduits, which store magma as it evolves into a crystal mush. This model also meets the necessary conditions for the formation of textures in plagioclase (e.g. compositional zoning, inclusion zones in phenocrysts, boxy cellular texture). These textures result from the mixing process of different magmas or magmas pulses (Hibbard, 1981). These interactions between magmas and the identification of multiple magmatic pulses were observed in the RJB by Sousa et al. (2019). These authors identified the presence of different enclave shapes, as well as different morphology of contacts between enclaves and host granites, besides multiplicity of enclave types (dark, light and with varying shades of gray). These features were associated to the existence of different textures (e.g. acicular apatite, compositional zoning in plagioclase).

In the RJB rocks, the presence of plagioclase crystals with homogeneous core and zoning limited to the edges is frequent (Fig. 4I). This texture, according to Anderson (1984), results from crystal core growth under stable physicochemical conditions (Fig. 8A). It suggests a period of initial physicochemical stability during the batholith evolution, probably before the emplacement of mafic magmas that were responsible for the physicochemical instabilities necessary for the formation of zoning.

Sousa et al. (2019) considered the role of mixing processes between magmas in the formation of the RJB based on field, petrographic and geochemical data. Among the petrographic aspects considered by these authors, regular (preferably in ME) and oscillatory chemical zoning were present in the plagioclase crystals of the RJB. The regular zoning was interpreted as a reflection of heat loss from the ME magma to the dominant intermediate-felsic magma in the RJB, whilst the oscillatory zoning could reflect important thermal variations caused by injections of mafic magmas (Fig. 8B). Luhr and Melson (1996) also consider the formation of more calcic zones in oscillatory zoning as a response to recurrent injection of mafic magmas.

According to Hibbard (1981), in a mixing system, magmas do not need to be significantly different in composition and temperature to produce the boxy cellular texture in plagioclase, being necessary the existence of a temperature difference of at least 150 °C between the magmas. In the plagioclase crystals of the ME, great compositional variation ($An_{11\text{-}51}$) and boxy cellular texture are found. However, these characteristics are not found in all ME of the RJB, which suggests that in some locations of the batholith the temperature difference between the mixed magmas was greater (>150 °C). To explain this temperature difference between regions of the magmatic chamber inferred for the RJB, we are suggesting that there were injections of mafic magmas in distinct stages of crystallization of this batholith. This hypothesis may explain the variation of temperature differences between mafic magma pulses and the RJB magma and, consequently, the compositional variation of plagioclase and the presence of boxy cellular texture. Temperature differences between the mafic and RJB magmas can also be inferred from features that indicate rapid cooling in the enclaves, such as: finer granulation than the host granites, chilled margins (Fig. 2C) and acicular apatite crystals.

In some ME plagioclase crystals, the presence of cores with rounded faces or embayment can be observed (Fig. 4E and F). According to Hibbard (1991), Grogan and Reavy (2002) and Bennett et al. (2019), rounded faces or embayment in crystals are characteristic of resorption caused by temperature variations, which can result from repeated recharges of mafic magmas (Hibbard, 1981; Cao et al., 2014). Some authors (e.g. Adamuszek et al., 2009; Kocak et al., 2011; Xiong et al., 2012; Pietranik and Koepke, 2014) suggest that this common texture in ME plagioclase crystals results from the transfer of crystals from the host felsic magma to the mafic magma, in the case of enclaves. However, the cores of ME plagioclase crystals with resorption features (Fig. 7) have higher anorthite content than those of crystals from the RJB rocks (Fig. 6). This fact leads to the hypothesis (the cores with embayment correspond to xenocrysts) to be discarded. We are suggesting that these characteristics, in the plagioclase crystals of the RJB ME result from increase in system temperature due to the subsequent injections of mafic magmas (Fig. 8D).

Synneusis texture in plagioclase crystals is common in the studied rocks (Fig. 4C and E), as well as well-defined zones occupied by inclusions of mafic minerals (Fig. 4B, C and D). Vance (1969), Grogan and Reavy (2002) and Jamshidibadr et al. (2020) propose that synneusis textures and inclusion zones can be formed when there is convection in the magmatic chamber. This convection can be generated by introducing new magmas into an open magmatic system (Fig. 8C), inducing mixing, and mingling.

Patchy zoning, observed in the ME plagioclase crystals (Fig. 7) has been interpreted as a result of magma decompression during crustal ascension (Vance, 1962, 1965; Anderson, 1984) or as a result of interaction between two systems that are compositionally different (e.g. felsic and mafic magmas - L'Heureux and Fowler, 1994) and also as a result of high H_2O content during the crystallization of plagioclase (Cao et al., 2019). According to Blundy and Cashman (2005), decompression under

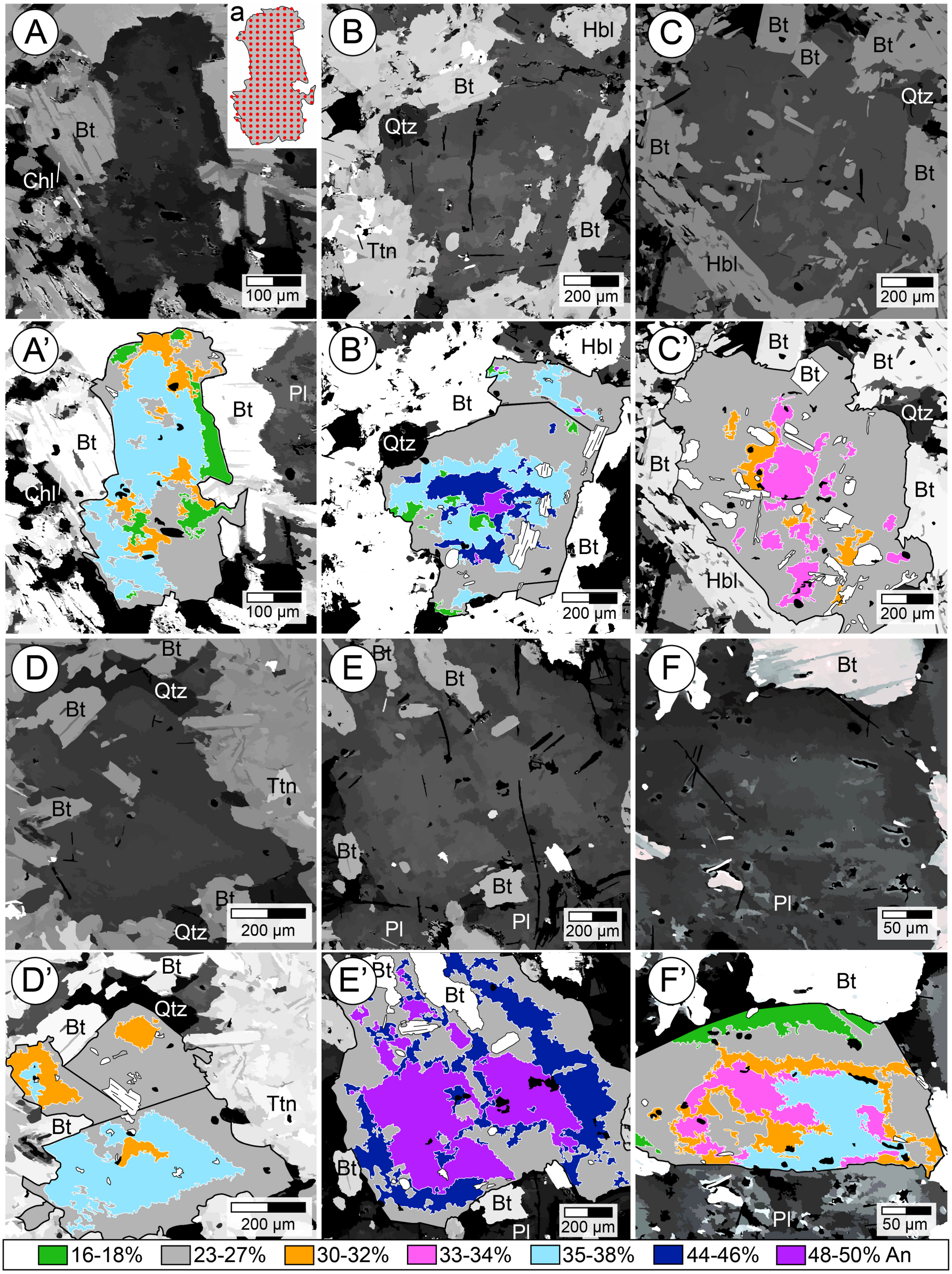

Fig. 7. BSE images of ME plagioclase crystals with application of the image tracing filter to better distinguish the different shades of gray resulting from compositional variations in the plagioclase crystals (A, B, C, D, E and F). Representative scheme of the regular mesh point analyses made to determine the geometry of the zoning (a). Representation of patchy zoning with crystal core exhibiting resorption features (A′, B′, C′, D′, E′ and F′). The images show more than one resorption phase in crystals. These are marked by resorption of portions with different anorthite contents. The percentages represent the anorthite contents of the crystals. Hornblende [Hbl]. Biotite [Bt]. Titanite [Ttn]. Quartz [Qtz]. Chlorite [Chl].

water saturated conditions results in degassing and crystallization of more sodic plagioclase. Pietranik and Koepke (2009) argue that this type of texture in diorite plagioclase is probably formed due to decompression and not due to magma mixing. Sousa et al. (2019) considered the existence of a mixing process in the evolution of the RJB and that this magma rose rapidly along the crust, based on the preservation of magmatic epidote in these rocks. Consequently, these conditions suggest that patchy zonings in ME plagioclase crystals may have been formed not only by mixing between magmas, but also by decompression caused by the rapid ascension of mafic magma (Fig. 8D).

The multiple zones with resorption features (Fig. 7) demonstrate the complexity of the Rio Jacaré magmatic system. These features occur in zones with different anorthite contents and suggest at least five successive moments of resorption in these crystals. In addition to the composi-

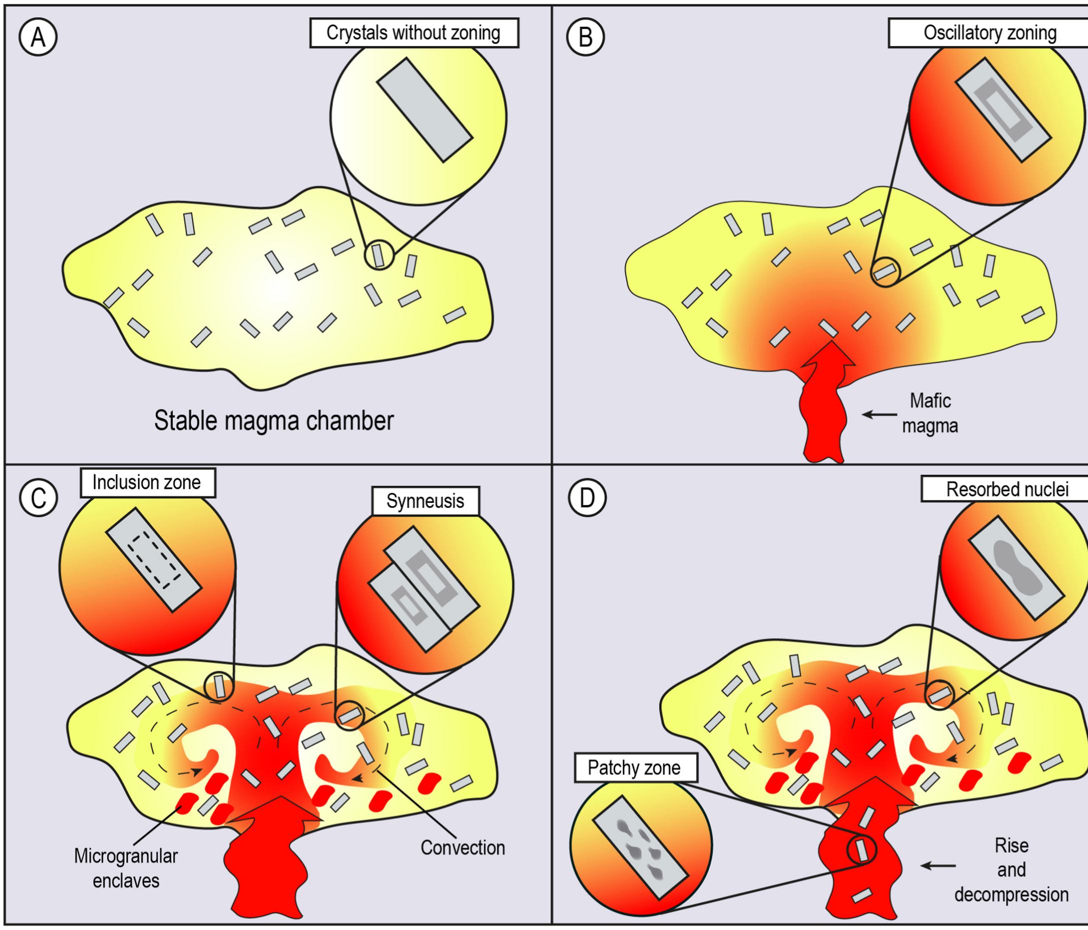

Fig. 8. Schematic model of magmatic processes that occurred for the generation of plagioclase textures in the Rio Jacaré Batholith. (A) Stable magmatic chamber crystallizing plagioclase without zonings. (B) Injection of hotter mafic magma and formation of oscillatory zoning. (C) Convection currents, generated from the injection of mafic magma, originating mafic mineral inclusion zones and synneusis texture. (D) Decompression caused by mafic magma rise and patchy texture formation. The injection of this hotter mafic magma causes previously formed crystals to be partially reabsorbed.

tional zoning of plagioclase crystals described in this work, zoning in alkali feldspar, hornblende, titanite, allanite and epidote crystals are also found (Fig. 5). According to Ginibre et al. (2007), compositional variation in magmatic minerals registers chemical and physical changes in the magma in which they grew. These data suggest that the changes in physicochemical conditions during the formation of the plagioclase crystals are equally registered in several minerals of these rocks (e.g. compositional zoning observed in alkali feldspar, hornblende, titanite and epidote).

7. Conclusions

Compositional variation in plagioclase crystals (Inequigranular Facies: $An_{12\text{-}33}$; Porphyritic Facies: $An_{11\text{-}23}$; Microgranular Enclaves: $An_{11\text{-}51}$) and the presence of compositional zoning and patchy, boxy cellular textures, besides crystal cores with embayment texture, crystal cores with homogeneous composition, inclusion zones of mafic minerals and synneusis texture allowed this work to interpret that:

1. There was a stable period in the Rio Jacaré Batholith magmatic chamber that allowed the crystallization of plagioclase with a homogeneous composition (Fig. 8A).
2. The various injections of mafic magmas modified the physicochemical conditions of the Rio Jacaré magmatic system, promoted convections, allowed mixtures between magmas and as a result, textures and compositional zonings were generated in several minerals, particularly in plagioclase (Fig. 8B).
3. Due to the injections of mafic magmas, convection currents were generated in the RJB magmatic chamber, contributing to the formation of synneusis textures and inclusion zones of mafic minerals (Fig. 8D).

The complexity of the Rio Jacaré magmatic system can also be inferred by the presence of multiple resorption features in the plagioclase crystals of the ME, which suggest at least five successive moments of resorption in these crystals.

CRediT authorship contribution statement

Carlos Santana Sousa : Writing – original draft. **Herbet Conceição :** Supervision, Funding acquisition. **Hiakan Santos Soares :** Investigation. **Diego Melo Fernandes :** Investigation. **Maria de Lourdes da Silva Rosa :** Funding acquisition, Supervision.

Declaration of competing interest

The authors declare that they have no known competing financial interests or personal relationships that could have appeared to influence the work reported in this paper.

Acknowledgments

The authors C.S. Sousa, H.S. Soares and D.M. Fernandes thank CNPq for their PhD scholarships, whose processes are 163770/2018-2, 169765/2018-0 and 140125/2020-5, respectively. M.L.S. Rosa and H. Conceição thank CNPq for their research grants 311008/2017-8, 310391/2017-2. The authors are grateful for the analytical support of the Condominium of Multiuser Laboratories of Geosciences (CLGeo) of the Federal University of Sergipe (UFS). This study was supported by the Coordenação de Aperfeiçoamento de Pessoal de Nível Superior – Brazil (CAPES) – Financing Code 001. This work is part of the first authors' PhD thesis (CSS) at the Postgraduate Program in Geology of the Federal University of Bahia (UFBA), which was carried out at the Laboratory of Petrology Applied to Mineral Research of the Federal University of Sergipe (LAPA-UFS).

Appendix A. Supplementary data

Supplementary data to this article can be found online at https://doi.org/10.1016/j.jsames.2022.103942.

References

Adamuszek, M., John, T., Dabrowski, M., Podladchikov, Y.Y., Gertisser, R., 2009. Assimilation and diffusion during xenolith-magma interaction: a case study of the Variscan Karkonosce granite, Bohemian Massif. Mineral. Petrol. 97, 203–222. https://doi.org/10.1007/s00710-009-0088-8.

Anderson, A.T., 1984. Probable relations between plagioclase zoning and magma dynamics, Fuego Volcano, Guatemala. Am. Mineral. 69 (7), 660–676.

Anderson, U.B., Eklund, O., 1994. Cellular plagioclase intergrowths as a result of crystal-magma mixing in the Proterozoic Åland rapakivi batholith, SW Finland. Contrib. Mineral. Petrol. 117 (2), 124–136. https://doi.org/10.1007/BF00286837.

Annen, C., 2011. Implications of incremental emplacement of magma bodies for magma differentiation, thermal aureole dimensions and plutonism-volcanism relationships. Tectonophysics 500, 3–10. https://doi.org/10.1016/j.tecto.2009.04.010.

Annen, C., Blundy, J.D., Sparks, S.R.J., 2006. The genesis of intermediate and silicic magmas in deep crustal hot zones. J. Petrol. 47, 505–539. https://doi.org/10.1093/petrology/egi084.

Annen, C., Blundy, J.D., Leuthold, J., Sparks, R.S.J., 2015. Construction and evolution of igneous bodies: towards an integrated perspective of crustal magmatism. Lithos 230, 206–221. https://doi.org/10.1016/j.lithos.2015.05.008.

Bennett, E.N., Lissenberg, C.J., Cashman, K.V., 2019. The significance of plagioclase textures in mid-ocean ridge basalt (Gakkel Ridge, Arctic Ocean). Contrib. Mineral. Petrol. 174 (6), 1–22. https://doi.org/10.1007/s00410-019-1587-1.

Blundy, J., Cashman, K., 2005. Rapid decompression-driven crystallization recorded by melt inclusions from Mount St. Helens volcano. Geology 33, 793–796. https://doi.org/10.1130/G21668.1.

Cao, M., Evans, N.J., Reddy, S.M., Fougerouse, D., Hollings, P., Saxey, D.W., McInnes, B.I.A., Cokke, D.R., McDonald, B.J., Qin, K., 2019. Micro and nano-scale textural and compositional zonation in plagioclase at the Black Mountain porphyry Cu deposit: implications for magmatic processes. Am. Mineral. 104 (3), 391–402. https://doi.org/10.2138/am-2019-6609.

Cao, M., Qin, K., Li, G., Yang, Y., Evans, N.J., Zhang, R., Jin, L., 2014. Magmatic process recorded in plagioclase at the Baogutu reduced porphyry Cu deposit, western Junggar, NW-China. J. Asian Earth Sci. 82, 136–150. https://doi.org/10.1016/j.jseaes.2013.12.019.

Carvalho, M.J., 2005. Evolução Tectônica do Domínio Marancó-Poço Redondo: Registro das Orogêneses Cariris Velhos e Brasiliana na Faixa Sergipana, NE do Brasil. Tese de Doutorado. Universidade de Campinas, p. 202.

Cashman, K.V., Sparks, R.S.J., Blundy, J.D., 2017. Vertically extensive and unstable magmatic systems: a unified view of igneous processes. Science 355 (6331). https://doi.org/10.1126/science.aag3055. . eaag3055.

Castro, A., 2001. Plagioclase morphologies in assimilation experiments. Implications for disequilibrium melting in the generation of granodiorite rocks. Mineral. Petrol. 71 (1–2), 31–49. https://doi.org/10.1007/s007100170044.

Conceição, J.A., Rosa, M.L.S., Conceição, H., 2016. Sienogranitos leucocráticos do Domínio Macururé, sistema Orogênicos Sergipano, nordeste do Brasil: stock Glória Sul. Braz. J. Geol. 46, 63–77. https://doi.org/10.1590/2317-4889201620150044.

Davison, I., Santos, R.A., 1989. Tectonic evolution of the Sergipano fold belt, NE Brazil, during the Brasiliano Orogeny. Precambrian Res. 45, 319–342.

Deer, W.A., Howie, R.A., Zussman, J., 2013. An Introduction to the Rock-Forming Minerals, 3° ed. Mineral Society of Great Britain and Ireland.

Donaldson, C.H., Reavy, R.J., O'Mahony, M.J., 2003. Plutonic geology. In: Meyers, R.A. (Ed.), Encyclopaedia of Physical Science and Technology. 3° ed., pp. 491–508. https://doi.org/10.1016/b0-12-227410-5/00588-3.

Fernandez, A.N., Barbarin, B., 1991. Relative rheology of coeval mafic and felsic magmas: nature of resulting interaction processes and shape and mineral fabrics of mafic micro- granular enclaves. In: J. Didier, B. Barbarin (Ed.), Enclaves and Granite Petrology, Developments in Petrology. Elsevier, Amsterdam, pp. 263–275.

Ginibre, C., Worner, G., Kronz, A., 2007. Crystal zoning as an archive for magma evolution. Elements 3 (4), 261–266. https://doi.org/10.2113/gselements.3.4.261.

Glazner, A.F., Bartley, J.M., Coleman, D.S., Gray, W., Taylor, R.Z., 2004. Are plutons assembled over millions of years by amalgamation from small magma chambers? GSA Today 14 (4–5), 4–12. https://doi.org/10.1130/1052-5173(2004)014<0004. . APAOMO>2.0.CO;2.

Gogoi, B., Saikia, A., 2019. Synneusis: does its preservation imply magma mixing? Mineral. Soc. Poland 49 (1–4), 99–117. https://doi.org/10.2478/mipo-2018-0009.

Grogan, S.E., Reavy, R.J., 2002. Disequilibrium textures in the Leinster Granite Complex, SE Ireland: evidence for acid-acid magma mixing. Mineral. Mag. 66 (6), 929–939. https://doi.org/10.1180/0026461026660068.

Hattori, K., Sato, H., 1996. Magma evolution recorded in plagioclase zoning in 1991 Pinatubo eruption products. Am. Mineral. 81, 982–994. https://doi.org/10.2138/am-1996-7-820.

Hibbard, M.J., 1981. The magma mixing origin of mantled feldspars. Contrib. Mineral. Petrol. 76, 158–170. https://doi.org/10.1007/BF00371956.

Hibbard, M.J., 1991. Textural anatomy of twelve magma-mixed granitoid systems. In: Didier, J., Barbarin, B. (Eds.), Enclaves and Granite Petrology, Developments in Petrology. Elsevier, Amsterdam, pp. 431–444.

Hildreth, W., 2004. Volcanological perspectives on long valley, Mammoth Mountain, and Mono Craters: several contiguous but discrete systems. J. Volcanol. Geoth. Res. 136, 169–198. https://doi.org/10.1016/j.jvolgeores.2004.05.019.

Holten, T., Jamtveit, B., Meakin, P., 2000. Noise and oscillatory zoning of minerals. Geochem. Cosmochim. Acta 64 (11), 1893–1904. https://doi.org/10.1016/S0016-7037(99)00444-5.

Humphreys, M.C.S., Blundy, J.D., Sparks, R.S.J., 2006. Magma evolution and open-system processes at Shiveluch Volcano: insights from phenocryst zoning. J. Petrol. 47 (12), 2303–2334. https://doi.org/10.1093/petrology/egl045.

Jamshidibadr, M., Tarabi, S., Gholizadeh, K., 2020. Study of micro-textures and chemistry of East Sarbisheh volcanic complex (Eastern Iran), for evidence of magma chamber process. Iran. J. Earth Sci. 12 (1), 10–31.

Karsli, O., Aydin, F., Sadiklar, M.B., 2004. Magma interaction recorded in plagioclase zoning in granitoid systems, Zigana Granitoid, Eastern Pontides, Turkey. Turk. J. Earth Sci. 13 (3), 287–305.

Kocak, K., Zedef, V., Kansun, G., 2011. Magma mixing/mingling in the Eocene Horoz (Nigde) granitoids, Central Southern Turkey: evidence from mafic microgranular enclaves. Mineral. Petrol. 103, 149–167. https://doi.org/10.1007/s00710-011-0165-7.

Kumar, S., Rino, V., 2006. Mineralogy and geochemistry of microgranular enclaves in Palaeoproterozoic Malanjkhand granitoids, central India: evidence of magma mixing, mingling, and chemical equilibration. Contrib. Mineral. Petrol. 152, 591–609. https://doi.org/10.1007/s00410-006-0122-3.

Kuşcu, G.G., Floyd, P.A., 2001. Mineral compositional and textural evidence for magma mingling in the Saraykent volcanics. Lithos 56 (2–3), 207–230. https://doi.org/10.1016/S0024-4937(00)00051-7.

Lange, R.A., Frey, H.M., Hector, J., 2009. A thermodynamic model for the plagioclase-liquid hygrometer/thermometer. Am. Mineral. 94, 494–506. https://doi.org/10.2138/am.2009.3011.

L'Heureux, I., Fowler, A.D., 1994. A nonlinear dynamical model of oscillatory zoning in plagioclase. Am. Mineral. 79 (9–10), 885–891.

Lima, R.G., Rosa, M.L., Conceição, H., 2019. Caracterização Petrológica Do Batólito Serra Negra, Domínio Marancó, Sistema Orogênico Sergipano. SBG, Aracaju. 28° Simpósio de Geologia do Nordeste (p. 424).

Luhr, J.F., Melson, W.G., 1996. Mineral and glass compositions in June 15, 1991, Pumices: evidence for dynamic disequilibrium. In: Punogbayan, R.S., Newhall, C.G. (Eds.), Fire and Mud Eruptions and Lahars of Mount Pinatubo. pp. 733–750. Philippines.

Magee, C., Stevenson, C.T.E., Ebmeier, S.K., Keir, D., Hammond, J.O.S., Gottsmann, J.H., Whaler, K.A., Schofield, N., Jackson, C.A., Petronis, M.S., O'Driscoll, B., Morgan, J., Cruden, A., Vollgger, S.A., Dering, G., Micklethwaite, S., Jackson, M.D., 2018. Magma plumbling systems: a geophysical perspective. J. Petrol. 59 (6), 1217–1251. https://doi.org/10.1093/petrology/egy064.

Miller, C.F., Furbish, D.J., Walker, B.A., Claiborne, L.L., Koteas, G.C., Bleick, H.A., Miller, J.S., 2011. Growth of plutons by incremental emplacement of sheets in crystal-rich host: evidence from Miocene intrusions of the Colorado River region, Nevada, USA. Tectonophysics 500 (1–4), 65–77. https://doi.org/10.1016/j.tecto.2009.07.011.

Nelson, S.T., Montana, A., 1992. Sieve-textured plagioclase in volcanic rocks produced by rapid decompression. Am. Mineral. 77 (11), 1242–1249.

Perugini, D., Busà, T., Poli, G., Nazzareni, S., 2003. The role of chaotic dynamics and flow fields in the development textures in volcanic rocks. J. Petrol. 44, 733–756. https://doi.org/10.1093/petrology/44.4.733.

Pietranik, A., Koepke, J., 2009. Interactions between dioritic and granodioritic magmas mingling zones: plagioclase record of mixing, mingling and subsolidus interactions in the Gesiniec Intrusion, NE Bohemian Massif, SW Poland. Contrib. Mineral. Petrol. 158, 17–36. https://doi.org/10.1007/s00410-008-0368-z.

Pietranik, A., Koepke, J., 2014. Plagioclase transfer from a host granodiorite to mafic microgranular enclaves: diverse records of magma mixing. Mineral. Petrol. 108, 681–694. https://doi.org/10.1007/s00710-014-0326-6.

Pinho Neto, M.A., Rosa, M.L.S., Conceição, H., 2019. Petrologia do Batólito Sítios Novos, sistema Orogênico Sergipano, Província Borborema, NE do Brasil. Geologia USP. Série Científica 19 (2), 135–150. https://doi.org/10.11606/issn.2316-9095.v19-152469.

Poli, G.E., Tommasini, S., 1991. Model for the origin and significance of microgranular enclaves in calc-alkaline granitoids. J. Petrol. 32 (3), 657–666. https://doi.org/10.1093/petrology/32.3.657.

Santos, R.A., Souza, J.D., 1988. Programa Levantamentos Geológicos Básicos Do Brasil. Carta Geológica Piranhas. Escala 1:100.000. DNPM/CPRM, Brasília.

Sklyarov, E.V., Fedorovskii, V.S., 2006. Magma mingling: tectonic and geodynamic implications. Geotectonics 40 (2), 120–134. https://doi.org/10.1134/S001685210602004X.

Solano, J.M.S., Jackson, M.D., Sparks, R.S.J., Blundy, J.D., Annen, C., 2012. Melt segregation in deep crustal hot zones: a mechanism for chemical differentiation,

crustal assimilation and the formation of evolved magmas. J. Petrol. 53 (10), 1999–2026. https://doi.org/10.1093/petrology/egs041.
Sousa, C.S., Soares, H.S., Rosa, M.L.S., Conceição, H., 2019. Petrologia e Geocronologia do Batólito Rio Jacaré, Domínio Poço Redondo, Sistema Orogênico Sergipano, NE do Brasil. Geologia USP. Série Científica 19 (2), 171–194. https://doi.org/10.11606/issn.2316-9095.v19-152494.
Streckeisen, A., 1976. To each plutonic rock its proper name. Earth Sci. Rev. 12 (1), 121–133. https://doi.org/10.1016/0012-8252(76)90052-0.
Teixeira, L.R., 2014. Mapa Geológico e de Recursos Minerais do Estado de Sergipe. CPRM. Escala 1:250.000.
Tepper, J.H., Kuehner, S.M., 2004. Geochemistry of mafic enclaves and host granitoids from the Chilliwack Batholith, Washington: chemical exchange processes between coexisting mafic and felsic magmas and implications for the interpretation of enclave chemical traits. J. Geol. 112, 349–367.
Ustunisik, G., Kilinc, A., Nielsen, R.L., 2014. New insights into the processes controlling compositional zoning in plagioclase. Lithos 200–201, 80–93. https://doi.org/10.1016/j.lithos.2014.03.021.
Van Schmus, W.R., Oliveira, E.P., Silva Filho, A.F., Toteu, S.F., Penaye, J., Guimarães, I.P., 2008. Proterozoic links between the Borborema Province, NE Brazil, and the central Africa fold belt. Geol. Soc. Lond. 294 (1), 69–99. https://doi.org/10.1144/SP294.5.
Vance, J.A., 1962. Zoning in igneous plagioclase; normal and oscillatory zoning. Am. J. Sci. 260 (10), 746–760. https://doi.org/10.2475/ajs.260.10.746.
Vance, J.A., 1965. Zoning in igneous plagioclase: patchy zoning. J. Geol. 73 (4), 636–651. https://doi.org/10.1086/627099.
Vance, J.A., 1969. On synneusis. Contrib. Mineral. Petrol. 24 (1), 7–29. https://doi.org/10.1007/BF00398750.
Vernon, R.H., 1984. Microgranitoid enclaves in granites - globules of hybrid magma quenched in a plutonic environment. Nature 309, 438–439. https://doi.org/10.1038/309438a0.
Xiong, F.H., Ma, C.Q., Zhang, J.Y., Liu, B., 2012. The origin of mafic microgranular enclaves and their host granodiorites from East Kunlun, Northern Qinghai-Tibet Plateau: implications for magma mixing during subduction of Paleo-Tethyan lithosphere. Mineral. Petrol. 104, 211–224. https://doi.org/10.1007/s00710-011-0187-1.
Yazdi, A., Ardalan, A.A., Emani, M.H., Dabiri, R., Foudazi, M., 2019. Magmatic interactions as recorded in plagioclase phenocrysts of quaternary volcanics in SE Bam (SE Iran). Iran. J. Earth Sci. 11 (3), 215–225.

CAPÍTULO 4
MINERAL CHEMISTRY OF THE RIO JACARÉ BATHOLITH BIOTITE, POÇO REDONDO DOMAIN, SERGIPANO OROGENIC SYSTEM: PETROGENETIC IMPLICATIONS

Carlos Santana Sousa[1,2], Hiakan Santos Soares[1,2], Diego Melo Fernandes[1,2], Maria de Lourdes da Silva Rosa[2,3], Herbet Conceição[1,2,3]

[1] Programa de Pós-graduação em Geologia, Instituto de Geociências, Universidade Federal da Bahia (UFBA), Rua Barão de Jeremoabo, s/n, Federação, 40170-209, Salvador, Bahia, Brazil
[2] Laboratório de Petrologia Aplicada à Pesquisa Mineral (LAPA), Universidade Federal de Sergipe (UFS), Avenida Marechal Rondon, s/n, Jardim Rosa Elze, 49100-000, São Cristóvão, Sergipe, Brazil
[3] Programa de Pós-graduação em Geociências e Análise de Bacias (PGAB), Universidade Federal de Sergipe, Avenida Marechal Rondon, s/n, Jardim Rosa Elze, 49100-000, São Cristóvão, Sergipe, Brazil

karlcss@ufba.br (C.S. Sousa); hiakanss@ufba.br (H.S. Soares); dmfernandes@ufba.br (D.M. Fernandes); lrosa@academico.ufs.br (M.L.S. Rosa) & herbet@academico.ufs.br (H. Conceição)

Abstract

Biotite is the most common mica in igneous rocks and its chemical composition has been used to infer conditions of formation of magmatic rocks. This work presents the results of systematic studies of textures and chemical compositions of biotite crystals from the rocks of the Rio Jacaré Batholith (RJB) inequigranular facies (IF), porphyritic facies (PF) and microgranular enclaves (ME). This intrusion is located in the Sergipano Orogenic System, in the southern part of the Borborema Province, Brazil. Primary and reequilibrated Mg-biotite crystals are found in the RJB rocks. Primary Mg-biotite crystals mainly occur as inclusions in plagioclase crystals whilst the reequilibrated Mg-biotite usually does not occur as inclusions, and typically contains anhedral titanite crystals in the cleavage. Primary Mg-biotite has a typical composition of crystals formed in calc-alkaline orogenic I-type magmas of the magnetite series, indicating high oxygen fugacity. The crystallization temperature of Mg-biotite primary crystals of the RJB ranged from 682 to 713 ºC in the IF, from 678 to 704 ºC in the PF and from 685 to 745 ºC in the ME. This is consistent with crystallization temperature of biotite in granitic systems. Crystallization pressure during magmatic crystallization of Mg-biotite ranges from 1,8 to 2,7 kbar in the IF, from 1,2 to 2,2 kbar in the PF and from 1,2 to 2,9 kbar in the ME. These pressures correspond to depths between 6,6 and 9,9 km in the IF, from 4,4 and 8,1 km in the PF and from 4,4 and 10,7 km in the ME. When compared to crystallization pressure of the RJB amphibole crystals (2 to 6 kbar), one can infer that biotite crystallized in a late stage after amphibole crystallization has ceased. The compositions of the IF and PF primary crystals indicate that they were formed from magmas with H_2O contents between 5 and 7%. The fO_2 during the formation of these crystals could also be estimated and the obtained values range from -16,3 to -15,0 in the IF, from -15,9 to -15,4 in the PF and from -15.6 to -13,9 in the ME. When correlating temperature variation and fO_2 variation of the primary crystals in the different ME samples, it is possible to infer the presence of several mafic magmatic pulses during the evolution of the RJB. Reequilibration of biotite crystals present in most samples resulted from exsolution of Ti associated to hydrothermal fluids containing Ca^{2+}, forming anhedral titanite crystals in cleavage planes and on the borders of biotite grains.

Keywords: Mineral chemistry; Borborema Province; Rebalanced crystals.

1. INTRODUCTION

Determination of the chemical composition of minerals plays an important role in igneous petrology (Binele Betsi and Lentz, 2013). The main factors responsible for the crystallization and mineralogy in rocks are: chemical composition of the magma, pressure, temperature, oxygen fugacity, content and nature of the volatile phase (e.g. Martin, 2007; Papoutsa and Pe-Piper, 2014; Erdman et al., 2014; Bennett et al. 2019; Yu et al., 2021). Thus, the inference of these parameters is relevant to the understanding of processes responsible for the formation of plutons.

Biotite is a very common mafic mineral in all plutonic rocks. It can be formed under different crystallization conditions and has the ability to register in its chemical composition the changes in oxygen fugacity, temperature, pressure and chemical composition of magma (e.g. Speer, 1984). Besides, the tectonic environment and the nature of the magma that generated it influences the composition of biotite (Nachit et al., 1985; Abdel-Rahman, 1994). For these reasons, biotite can be used to infer the physicochemical conditions present in magmas when they crystallize (Dong et al., 2014).

In the Rio Jacaré Batholith (RJB), biotite is the most abundant mafic mineral. In this work, petrographic data and the mineral chemistry of biotite crystals will be presented and discussed, aiming to infer intensive parameters (temperature, pressure, oxygen fugacity) during the crystallization of this mineral.

2. GEOLOGICAL CONTEXT

2.1. Regional Geology

The Sergipano Orogenic System (Conceição et al., 2016) is located in the southern portion of the Borborema Province (Almeida et al., 1977), northeast Brazil and represents the result of collision between the Sanfranciscana Plate and the Pernambuco-Alagoas Superterrain during the Brasiliano Orogeny (Davison and Santos, 1989; D'el Rey Silva, 1992; Oliveira et al., 2006, 2010). During this collision, shear zones that limit the different geological domains of the SOS were generated (Davison and Santos, 1989; Silva Filho and Torres, 2002): Estância, Vaza-Barris, Macururé, Marancó, Poço Redondo, Canindé and Rio Coruripe.

In the Macururé, Marancó, Poço Redondo and Canindé Domains, a number of different plutons occur (e.g. Conceição et al., 2016; Lima et al., 2017; Pinho Neto et al., 2019; Sousa et al., 2019; Soares et al., 2019; Fernandes et al., 2020). They show high-K to shoshonitic calc-alkaline magmatic affinities, some intrusions being emplaced before to the Brasiliano collision and some following it.

2.2. Local Geology

The RJB (Figure 1) intrudes into the Poço Redondo Domain and into Tonian migmatites of the Poço Redondo Migmatitic Complex and in other Ediacaran granites (Brito, 1996; Carvalho, 2005; Oliveira et al., 2015; Sousa et al., 2019). This batholith shows a U-Pb$_{SHRIMP}$ zircon crystallization age of 617 ± 4 Ma (Sousa et al., 2019) and presents two petrographic facies, inequigranular (IF) and porphyritic (PF), which are composed of granodiorites, monzogranite and quartz monzonite. Microgranular enclaves (ME) are ubiquitous in the RJB and correspond to diorite, quartz diorite, quartz monzodiorite and granodiorite. The contact relationships between the MEs and the host granites preserve evidence of interaction between magmas during the evolution of the RJB (Sousa et al., 2022). Magma mixing is considered to be a relevant petrogenetic process which conformed these rocks, as shown by the presence of feldspar xenocrysts, chilled margins and sinuous to embayed contacts and linear chemical evolution with the enclosing felsic rocks in Harker diagrams for the RJB samples (Sousa et al., 2019).

The mineralogy of the RJB rocks is composed of quartz, plagioclase, alkali feldspar, biotite, hornblende, epidote, titanite, apatite, zircon, magnetite and ilmenite. RJB rocks are metaluminous, magnesian high-K rocks of calc-alkaline and shoshonitic series, and have the geochemical signature of post-collisional magmas (Brito, 1996; Sousa et al., 2019).

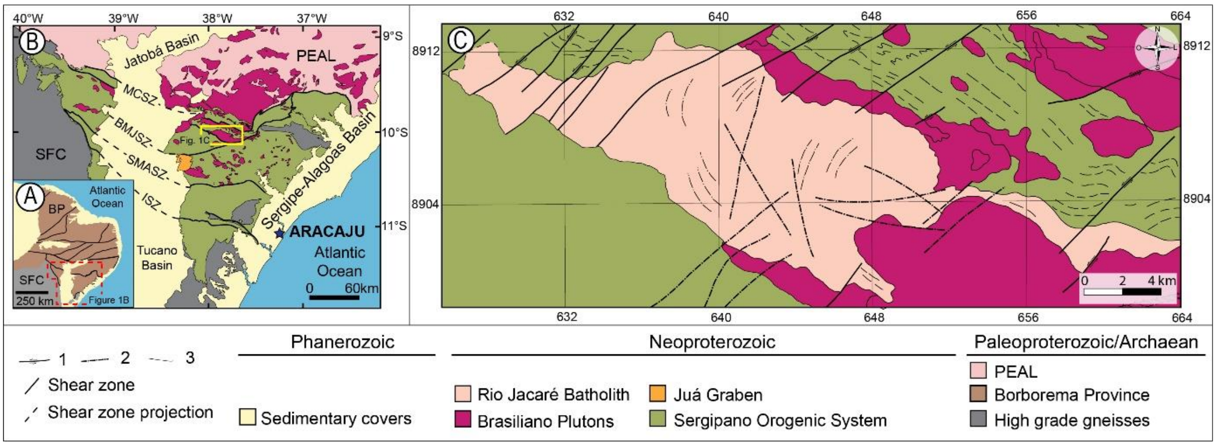

Figure 1. Schematic maps contextualizing the regional geology and the Rio Jacaré Batholith. (A) Simplified map of the Borborema Province in the Northeast of Brazil (Van Schmus et al., 2008). (B) Simplified map of the Sergipano Orogenic System (SOS – Pinho Neto et al., 2019). (C) Geological map of the Rio Jacaré Batholith (Sousa et al., 2019). São Francisco Craton (SFC). Pernambuco-Alagoas Massif (PEAL). Shear zones: Macururé (MCSZ); Belo Monte Jeremoabo (BMJSZ); São Miguel do Aleixo (SMASZ); Itaporanga (ISZ). 1- Fault. 2- Fracture. 3- Lineament.

3. MATERIALS AND METHODS

The mineralogy of the Rio Jacaré Batholith was investigated using polished thin sections from representative samples. Thirty-three polished thin sections where studied, eight from the inequigranular facies, ten from the porphyritic facies and fifteen from the enclaves. Minerals and textures were identified under a OPTON (TNP - 09NT) microscope with transmitted and reflected light at the Laboratory of Microanalysis of Condominium of Multiuser Laboratories of Geosciences (CLGeo), Universidade Federal de Sergipe (UFS).

The polished thin sections were metallized with carbon (8-10 nm thick) with a Quorum® metallizer, model Q150R ES, so that the crystals could be imaged and analyzed. The spot chemical analysis of biotite was determined with X-Act energy dispersive spectrometer (EDS) from Oxford Instruments®, with a resolution of 125 eV and a silicon solid state detector (SSD, 10mm²). This spectrometer is installed in a scanning electron microscope (SEM), brand Tescan - VEGA LMU3 of the CLGeo-UFS. The reliability and reproducibility of the percentages of oxides obtained with the EDS were verified using international standards from *Astimex Scientific Ltd®* and CLGeo-UFS. internal standards. The EDS from the CLGeo-UFS is regularly calibrated using copper energy. The Quant routine of the Aztec 4.0 software, from Oxford Instruments®, was used to convert the intensities of energy to oxide percentage with the ZAF automatic correction factors. Analytical conditions used were: 20 kV voltage, 17 nA beam intensity, 400 nm electron beam diameter, mean analysis time per point of 60s; analysis distance 15 mm.

The internal calibration of the EDS was carried out using standards, energy spectrum and with precision (3σ): albite, NaKα (±0.2); corundum, AlKα (±0.2); metallic chromium, CrKα (±0.4); fluorite, FKα (±0.3); metallic iron, FeKα (±0.4); halite, ClKα (±0.3); metallic manganese, MnKα (±0.2); metallic nickel, NiKα (±0.3); orthoclase, KKα (±0.2); periclase, MgKα (±0.4); quartz, SiKα (±0.4); metallic titanium, TiKα (±0.2); wollastonite, CaKα (±0.2) and barium fluoride, BaLα (±0.3). The comparison between the data obtained with the EDS and those from international Astimec and internal laboratory standards is presented in table 1. The differences observed between the values provided by the standards and those obtained with the EDS are very small (Table 1).

Calculations of the structural formula were carried out based on 22 oxygens and the Fe^{2+} and Fe^{3+} content obtained was based on the empirical equation of Wones (1972), using the Geo-fO_2 software from Li et al (2019).

Table 1. Comparison between compositions of the Astimex standard, from the internal standards (obtained with EPMA = Electron probe micro-analyzer) and those obtained with the EDS-MEV in this study. 3σ = error calculated in the EDS to 3 sigma. MD = modulus of the difference between the analysis of the standards and those obtained with the EDS-MEV.

	Astimex	EDS	*3σ*	MD	EPMA	EDS	*3σ*	MD	EPMA	EDS	*3σ*	MD	EPMA	EDS	*3σ*	MD
SiO_2	38,72	39,04	*0,28*	0,32	37,54	37,50	*0,09*	0,04	39,88	39,53	*0,37*	0,35	40,93	40,20	*0,3*	0,73
TiO_2	1,77	1,73	*0,10*	0,04	2,88	2,86	*0,17*	0,02	1,06	1,11	*0,1*	0,05	0,67	0,74	*0,1*	0,07
Al_2O_3	15,13	15,28	*0,19*	0,15	13,41	13,37	*0,18*	0,04	12,88	12,96	*0,19*	0,08	12,94	13,15	*0,2*	0,21
FeO	10,72	9,64	*0,16*	1,08	17,85	18,07	*0,27*	0,22	13,09	13,91	*0,61*	0,82	13,30	13,21	*0,2*	0,09
MnO	0,04	0,09	*0,07*	0,05	0,89	0,18	*0,09*	0,71	0,22	0,26	*0,07*	0,04	0,30	0,35	*0,1*	0,05
MgO	19,52	19,98	*0,19*	0,46	13,21	13,51	*0,04*	0,30	17,20	17,74	*0,21*	0,54	17,01	17,96	*0,2*	0,95
CaO	0,10	0,15	*0,06*	0,05	0,03	0,06	*0,11*	0,03		0,12	*0,06*	0,12	0,10	0,04	*0,1*	0,06
Na_2O		0,14	*0,08*	0,14	0,01	0,57	*0,06*	0,56	0,01	0,21	*0,09*	0,20		0,09	*0,1*	0,09
K_2O	9,91	9,95	*0,11*	0,04	9,75	9,39	*0,12*	0,36	10,36	9,89	*0,12*	0,47	10,25	10,14	*0,1*	0,11
Cr_2O_3					0,07		*0,07*	0,07	0,09	0,08	*0,07*	0,01		0,08	*0,1*	0,08
	95,91	96,00			95,64	96,00			95,11	96,00			95,50	96,00		

4. RESULTS

4.1. Petrography

Biotite is one of the mafic minerals found in the Rio Jacaré Batholith rocks. Its volume varies from <1,0 to 15,4% in the inequigranular facies, from 2,5 to 11,4% in the porphyritic facies and from 8,5 to 33,5% in the microgranular enclaves.

Biotite crystals of the inequigranular and porphyritic facies show similar textures, being subhedral or euhedral, with diameter between 0,1 and 2,5 mm, those with diameter around 0,8mm being predominant. They show pleochroism varying from brown to yellow (Figures 2A and 2D). Occasionally the pleochroism can range from brown to brownish green. Usually, biotite occurs associated with hornblende, and sometimes, these minerals form agglomerates of crystals with diameters between 2 and 7 mm (Figures 2B and 2C). In places they mark the magmatic flow texture with other minerals. Contacts with the other minerals in the rock are clear-cut, straight or curved. It commonly contains inclusions of zircon, apatite, titanite, opaque minerals and, less often, hornblende. Anhedral magnetite, ilmenite and titanite crystals occur in the cleavage or on grain limits (Figure 2E). Plagioclase, alkali feldspar and quartz crystals have biotite inclusions. However, biotite inclusions in plagioclase phenocrysts have larger sizes when located close to grain limits. On some grains, chlorite is formed as a product of biotite alteration.

The biotite crystals of the microgranular enclaves differ from those of the host rocks by their finer grain size (Figure 2F), which varies from 0,1 to 1,7 mm, with 0,3 mm crystals predominating. As in the porphyritic and inequigranular facies, plagioclase, alkali feldspar and quartz include biotite. While in the plagioclase phenocrysts biotite inclusions are preferentially located close to grain boundaries, in the matrix plagioclase crystals biotite inclusions are distributed throughout the plagioclase grains.

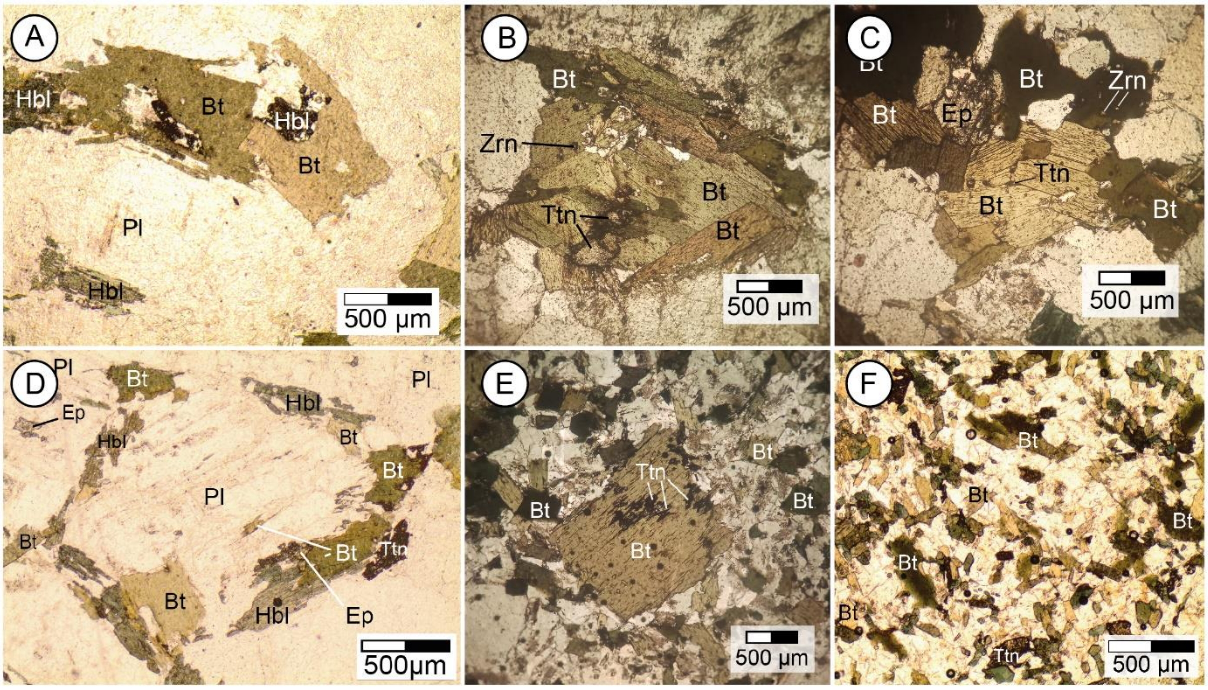

Figure 2. Images with textures observed in biotite crystals of the Rio Jacaré Batholith rocks. (A) Contact between biotite crystals. Hornblende inclusions are observed. (B and C) Cluster of biotite crystals with diameter around 1,5 mm. The presence of titanite among the biotite crystals is noticed. (D) Biotite and hornblende crystals surrounding plagioclase. Note the inclusion of biotite in the plagioclase. (E) Biotite with titanite inclusions in cleavage planes. (F) Fine-grained biotite crystals in a microgranular enclave. Note the abundance of these crystals.

4.2. Biotite chemistry

In this study, 360 point analyses of biotite crystals were obtained, 63 of these in the inequigranular facies, 122 in the porphyritic facies and 175 in the enclaves. Out of the 360 analyses, 93 correspond to primary crystals (12 in the inequigranular facies, 5 in the porphyritic facies and 76 in the enclaves).

The representative results of chemical analyses (Table 2) show that the RJB biotite crystals contain similar MgO concentrations between the inequigranular facies and the microgranular enclaves, of 10,3-14,1% and 9,8-14,5%, respectively, while the crystals of the porphyritic facies have a greater variation of MgO, of 9,4-18,4%. This similarity is also observed in the Mg/(Fe + Mg) ratios, which vary between 0,46 and 0,64 for the IF crystals and between 0,49 and 0,66 for the ME crystals, while those of the PF vary between 0,46 and 0,81. The TiO_2 contents are similar between the IF and PF crystals (1,0-3,5% and 0,9-3,4%, respectively), and with greater variation in the ME crystals (1,1-4,2%). The Al_2O_3 contents 3 (IF: 14,9-17,9 %; PF 14,4-19,4 %; ME: 14,4-19,7 %), FeO (IF: 13,6-19,5 %; PF: 7,6-20,0 %; ME: 12,5-20,0 %) and the Fe/(Fe + Mg) ratio (IF: 0,35-0,51; PF: 0,18-0,53; ME: 0,33-0,51) are similar among those crystals of the inequigranular facies, the porphyritic facies and the microgranular enclaves.

Table 2. Representative chemical analyses of primary biotite crystals from the Rio Jacaré Batholith. Center (C) intermediate (I); edge (B); Spectrum analyzed (Sp); Fe/Fe + Mg (Fe#); Al^{VI}+Al^{IV} (Al^T); H_2O obtained by stoichiometry. T (ºC) = Henry et al. (2005); P (kbar) = Uchida et al. (2007); LogfO_2 = Wones (1972).*

Facies	Inequigranular				Porphyritic				Microgranular enclaves				
Rock	SOS 864	SOS 836	SOS 836	SOS 849A	FDS 497	SOS 876A	SOS 876A	SOS 876A	SOS 849B	SOS 873B	SOS 873B	SOS 861M	SOS 876B
Sp.	33	1	3	64	43	1	2	3	56	31	33	37	60
Position	C	C	C	C	C	C	I	I	C	C	B	C	C
SiO_2	38,2	37,1	37,3	39,0	37,6	37,2	37,6	37,3	38,3	38,3	38,3	38,0	38,1
TiO_2	3,6	3,7	3,7	3,4	3,4	3,1	3,1	3,0	3,3	3,9	3,9	3,0	3,4
Al_2O_3	15,7	15,1	15,3	16,0	14,4	16,2	16,2	16,3	17,9	15,3	15,5	15,7	15,8
FeO	16,9	19,5	19,6	16,5	19,6	19,9	19,6	19,7	15,7	14,5	14,4	16,6	16,0
MnO	0,2	0,4	0,2	0,2	0	0,3	0,3	0,4	0,1	0,2	0	0,2	0,2
MgO	11,6	10,7	10,7	11,3	11,8	9,6	9,4	9,5	10,9	13,5	13,9	12,8	13,2
K_2O	9,7	9,5	9,5	9,2	9,2	9,7	9,7	9,7	9,5	9,4	9,3	9,6	9,2
F	0,2			0,4					0,1	0,8	0,6		
Cl	0,1								0,1	0,2	0,1		
O=F,Cl	- 0,1			- 0,2					- 0,1	- 0,4	- 0,3		
Total	96,1	95,9	96,3	95,9	96,1	96,1	96,0	96,1	95,8	95,8	95,8	95,9	95,9
Si	5,703	5,624	5,635	5,790	5,679	5,640	5,688	5,649	5,667	5,695	5,671	5,668	5,652
Al^{IV}	2,297	2,376	2,365	2,210	2,321	2,360	2,312	2,351	2,333	2,305	2,329	2,332	2,348
T	8,000	8,000	8,000	8,000	8,000	8,000	8,000	8,000	8,000	8,000	8,000	8,000	8,000
Al^{VI}	0,473	0,320	0,350	0,598	0,241	0,535	0,579	0,558	0,780	0,369	0,369	0,435	0,421
Ti	0,399	0,427	0,425	0,375	0,392	0,361	0,360	0,360	0,363	0,440	0,438	0,334	0,375
Fe^{3+}		0,047	0,021		0,144							0,075	0,055
Fe^{2+}	2,096	2,416	2,441	2,029	2,314	2,506	2,461	2,478	1,927	1,790	1,772	1,987	1,921
Mn	0,024	0,049	0,025	0,024		0,037	0,037	0,049	0,012	0,024		0,024	0,024
Mg	2,585	2,411	2,397	2,509	2,656	2,167	2,120	2,143	2,413	3,000	3,072	2,838	2,908
M	5,577	5,671	5,658	5,535	5,747	5,605	5,557	5,589	5,495	5,624	5,651	5,693	5,704
K	1,846	1,840	1,829	1,746	1,774	1,873	1,869	1,871	1,793	1,784	1,759	1,826	1,743
I	1,846	1,840	1,829	1,746	1,774	1,873	1,869	1,871	1,793	1,784	1,759	1,826	1,743
OH*	3,880	4,000	4,000	3,812	4,000	4,000	4,000	4,000	3,928	3,573	3,694	4,000	4,000
F	0,094			0,188					0,047	0,376	0,281		
Cl	0,025								0,025	0,050	0,025		
A	4,000	4,000	4,000	4,000	4,000	4,000	4,000	4,000	4,000	4,000	4,000	4,000	4,000
TOTAL	19,423	19,511	19,487	19,281	19,521	19,478	19,426	19,459	19,289	19,408	19,409	19,519	19,448
Fe#	0,448	0,505	0,507	0,447	0,481	0,536	0,537	0,536	0,444	0,374	0,366	0,421	0,405
Al^T	2,770	2,696	2,715	2,807	2,561	2,895	2,891	2,910	3,114	2,675	2,697	2,767	2,769
T (°C)	713,6	712,3	711,3	704,4	704,6	682,5	681,8	682,3	700,4	744,1	745,7	695,1	715,2
P (kbar)	1,8	1,6	1,7	1,9	1,2	2,2	2,2	2,2	2,8	1,5	1,6	1,8	1,8
LogfO_2	-15,0	-15,1	-15,1	-15,1	-15,4	-15,9	-15,9	-15,9	-14,7	-13,9	-13,9	-15,2	-14,5

5. DISCUSSION

5.1. Classification and compositional variation

Trioctahedral micas have varied composition (e.g. Deer et al., 1992). The Mg, Mn, Fe^{2+}, Fe^{3+}, Ti, Si^{4+} and Al^{VI} contents of the RJB micas allow classifying them as Mg-biotite (Figure 3). A trend is observed (Figure 3) formed in the direction of the Mg and (Fe^{2+} + Mn) poles, suggesting a linear correlation between the concentration of these elements in the studied crystals. This correlation is mainly due to the variation of the Fe^{2+} e Mg contents, once the Mn values are low (Table 2) and have little influence in the formation of this trend. According to Li et al. (2014), the important variation of Mg/(Mg+Fe) in micas suggests that they are not primary.

Nachit et al. (2005) suggest that the distinction between primary/magmatic, reequilibrated and secondary/newly formed biotite crystals can be made using the TiO_2, FeO, MnO and MgO contents (Figure 4). The TiO_2 contents of the RJB analyzed crystals have an important variation (IF: 1,0-3,5 %; PF: 0,9-3,4 %; ME: 1,1-4,2 %) and are typical of primary and reequilibrated crystals, with predominance of reequilibrated grains (Figure 4). The decrease in TiO_2 content in the studied crystals tends to keep the ratio (FeO+Mn)/MgO relatively constant (Figure 4). This evolution can reflect crystal reequilibration. The magmatic biotite crystals of the RJB occur mainly as inclusions in plagioclase. This fact suggests that these crystals have been preserved from the action of hydrothermal fluids. In the next sections the inferences of intensive parameters on biotite crystallization were made using only the primary/magmatic crystals.

The composition of biotite has also been used to infer the nature of the magma from which it crystallized (e.g. Anderson et al., 2008; Karimpour et al., 2011). The Fe/(Fe+Mg) and total Al parameters of the RJB crystals are characteristic of crystals formed in magmas of the magnetite series (Figure 5), which indicates the crystallization under conditions of high oxygen fugacity.

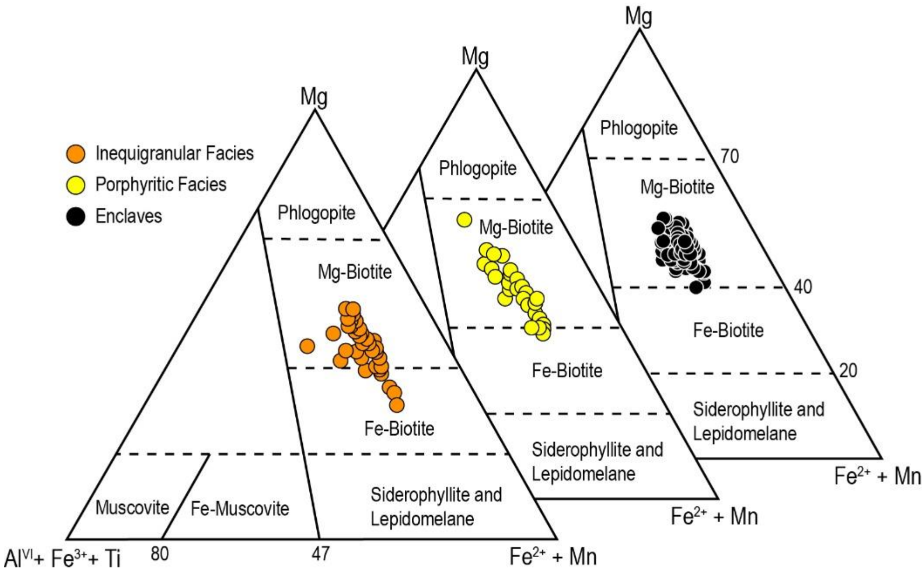

Figure 3. Diagram Mg versus (Fe^{2+} + Mn) versus (Al^{VI} + Fe^{3+} + Mn) after Foster (1960), applied to the biotite crystals of the Rio Jacaré Batholith.

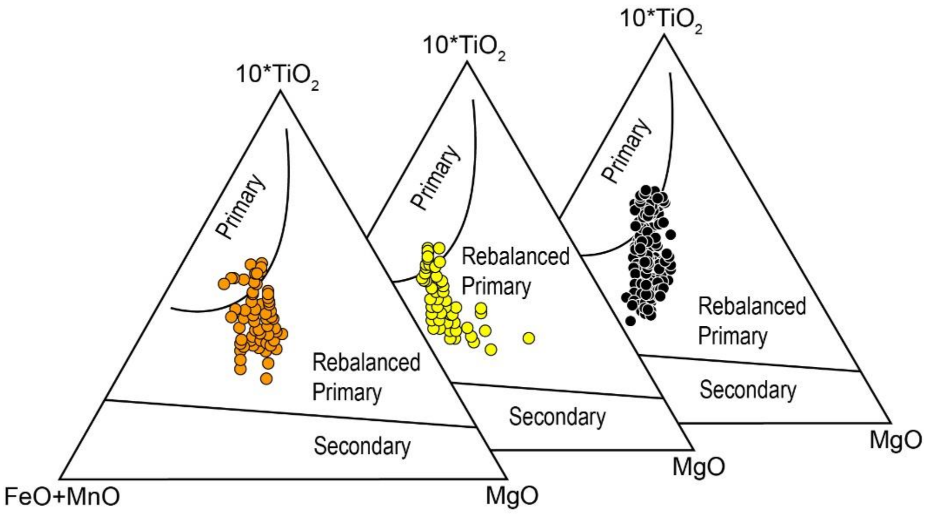

Figure 4. Nachit et al. (2005) diagram for discrimination of primary, reequilibrated and newly-formed biotite applied to biotite crystals from the Rio Jacaré Batholith. Inequigranular facies (orange circle); porphyritic facies (yellow circle); Microgranular enclaves (black circle).

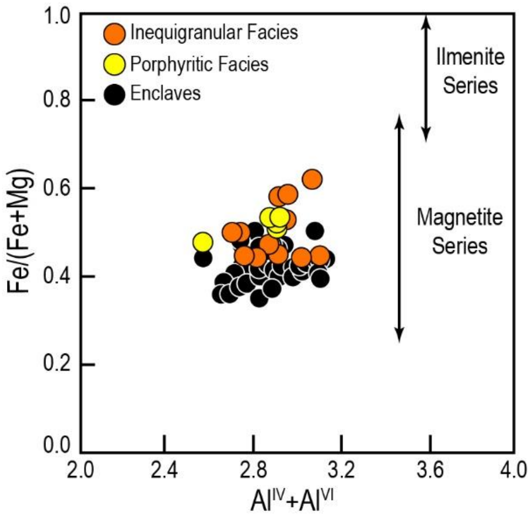

Figure 5. Fe/(Fe+Mg) versus Al^{IV}+Al^{VI} diagram to discriminate between ilmenite and magnetite series magmas by Anderson et al. (2008) applied to primary biotite crystals from the Rio Jacaré Batholith.

5.2. Nature of magmas

Biotite found in the RJB rocks is brown-coloured. According to Lalonde and Bernard (1993), the green or brown color in biotite may be related to the Mg and Fe^{3+} contents and to granites with a magmatic arc signature. The primary biotite crystals of the RJB have a FeO*/MgO ratio that varies from 1,42 to 1,49 in the IF crystals, from 1,65 to 2,08 in the PF crystals and from 1,00 to 1,85 in the ME crystals. According to Abdel-Rahman (1994), biotite with FeO*/MgO ratio around 1,76 is characteristic of I-Type calc-alkaline granites with orogenic signature. The values of Fe/(Fe+Mg) and total Al values of the studied primary crystals have compositions similar to those of biotite from magmatic arc-related metaluminous granites (Figure 6).

The MgO, FeO and Al_2O_3 contents of the RJB primary biotite crystals are similar to those of crystals formed by calc-alkaline orogenic signature magmas (Figure 7) studied by Abdel-Rahman (1994). It is therefore suggested that the RJB biotite was crystallized in Type-I, calc alkaline metaluminous magma, that being consistent with the available data on the regional geological context of the RJB (e.g. Brito, 1996; Oliveira et al., 2015; Sousa et al., 2018, 2019).

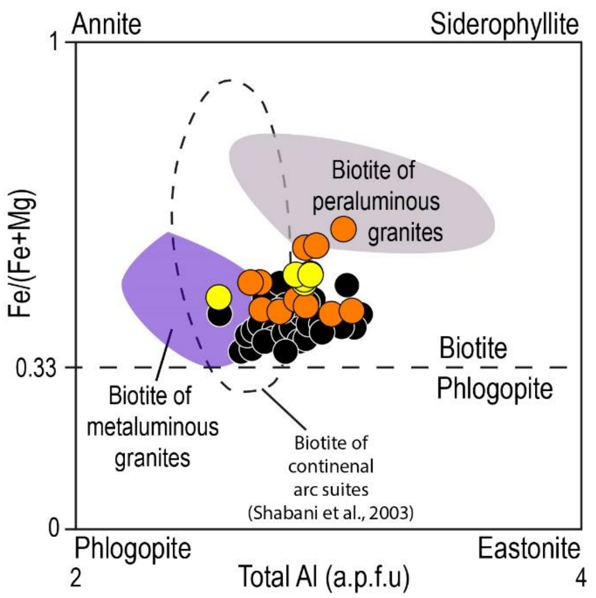

Figure 6. Diagram Fe/(Fe+Mg) versus total Al, after Lalonde and Bernard (1993) applied to primary biotite crystals from the Rio Jacaré Batholith. Porphyritic facies (yellow circle); inequigranular facies (orange circle); microgranular enclaves (black circle).

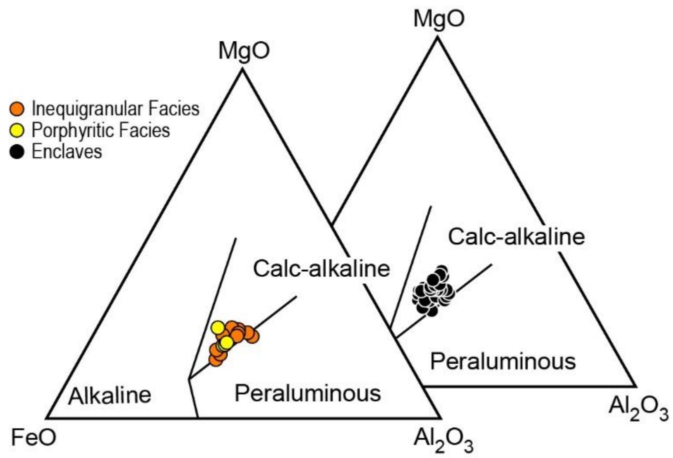

Figure 7. Ternary diagram FeO-MgO-TiO_2 (Abdel-Rahman, 1994) applied to primary biotite crystals from the Rio Jacaré Batholith.

5.3 Crystallization conditions and processes involved

The contents of Ti in biotite seem to follow Le Chatelier's principle (when a force is applied to a system in equilibrium, it tends to readjust itself, seeking to reduce the effects of this force), as some authors describe (e.g., Douce, 1993; Henry et al., 2005) that the concentration of Ti in biotite is sensitive to changes in temperature and for this reason it can be used to infer the crystallization or reequilibration temperature. The Ti geothermometer in biotite by Henry et al. (2005) was applied to the studied crystals. Although this calculation was initially based on biotite compositions from metamorphic rocks, Li et al. (2019) showed that it is possible to apply it to biotite from granites, as good results have been obtained when used in experimental work on magmatic biotite (eg Andújar and Scaillet, 2012; Fabbrizio and Carrol, 2008) and in various intrusions in different terrains (e.g. Hossain and Tsunogae, 2014; Sarjoughian et al., 2012; Wang et al., 2014).

The BRJ primary biotite crystals of the IF and PF facies register similar temperature ranges, from 682 to 713 °C and from 678 to 704 °C, respectively. The primary crystals from the enclaves provided higher temperatures, from 685 to 745 °C. The temperatures obtained for the reequilibrated crystals, with this same geothermometer, were variable and similar between facies (IF: 500 to 682 °C; PF: 514 to 681 °C; ME: 499 to 690 °C).

According to Uchida et al. (2007), it is possible to use the chemical composition of biotite as a geobarometer, as there is a positive correlation between the total aluminum content of biotite and the crystallization pressure of this mineral. By using the calculations proposed by Uchida et al. (2007), crystallization pressures for the primary crystals of 1.8-2.7 kbar in IF, 1.2-2.2 kbar in PF and 1.2-2.9 kbar in ME were obtained. Considering the value of 1 kbar equal to 3.7 km of depth in the continental crust (e.g. Tulloch and Challis, 2000), biotite crystallization depths are estimated to be between 6.6 and 9.9 km in the IF, between 4.4 and 8.1 km in the PF and between 4.4 and 10.7 km in the ME. The pressures obtained in the reequilibrated crystals were 1.4-2.6 kbar in the IF, 1.3-2.9 kbar in the PF and 1.4-3.6 kbar in the ME. In the BRJ rocks, Sousa et al. (2019) identified variation in amphibole crystallization pressure from 2 to 6 kbar. The integration of biotite and amphibole geobarometry data suggests that biotite began to crystallize at the final moments of amphibole crystallization, at shallower levels of the continental crust. This hypothesis is supported by the observed textures, due to the presence of amphibole inclusions in the biotite crystals.

Naney (1983) carried out an experimental study in which he observed the crystallization of a granitic system under conditions of 2 kbar (pressure similar to those found in this work). In this experimental study, when the H2O contents were higher than 4 %, there was the crystallization of the paragenesis biotite + plagioclase + alkali feldspar + liquid + steam between approximate temperatures of 700 and 750 °C and the paragenesis biotite + plagioclase + alkali feldspar + quartz + steam between 670 and 700 °C. These temperatures are similar to those obtained with the RJB primary biotite crystals and suggest that they represent crystallization temperatures.

The temperatures obtained for the rebalanced crystals (499-690 °C) match those of metamorphic biotite (Panchuk, 2019). Petrik and Broska (1994) interpret the low values of

TiO2 in biotite as reequilibration temperatures, and that can be explained by the release of Ti from the crystalline structure of biotite, forming titanite crystals. In the cleavage planes of the RJB biotite, anhedral titanite is found, which may reflect the reequilibration of the studied crystals. According to Shau et al. (1991), during the process the release of biotite components requires that the volume of reagents is equal to the sum of the products. These reactions require dissolution or recrystallization of at least a portion of the original biotite, with gain or loss of components. Also according to Shau et al. (1991), Ti and Ca are stable in the structure of magmatic biotite. It also implies that if magmatic biotite is metamorphosed under conditions of greenschist or amphibolite facies, the Ti and Ca present can be released. Shau et al. (1991) also propose that the destabilization of primary biotite and the topotactic release of Ti is possible leading to formation of titanite during metamorphism. Yui et al. (2001) agree that biotite can provide sufficient Ti, but Ca would need to be provided by an external source (e.g. plagioclase) for the formation of titanite. According to Sousa et al. (2019), the rocks of the BRJ do not have evidence of metamorphism/deformation in the solid state. However, Sousa et al. (2019) when describing saussuritized plagioclase crystals, suggested that they result from the action of late fluids. In this context, it is likely that the formation of titanite in the biotite cleavage in the RJB is not related to regional metamorphism, but to a hydrothermal process at the end of the crystallization process of this batholith.

Holtz et al. (2001) suggest a diagram to estimate the minimum water content dissolved in a granitic magma. To use this diagram, only the temperatures and crystallization pressures of the IF and PF biotite crystals were considered. The RJB ME crystals were not used, as they are considered to be of mantle origin (Oliveira et al., 2015; Sousa et al., 2019), thus not attending the requirements for using this diagram. The values obtained in the FP and FI crystals were similar and according to this estimate, the minimum water content in the magma during the crystallization of biotite was between 5 and 7% (Figure 8).

Evidence of the occurrence of a mixing process between magmas in the RJB were described by Sousa et al. (2019). This hypothesis was based on field data (e.g. contact relationship between ME and host granites), as well as petrographic data (e.g. compositional zoning in plagioclase, ocellar quartz texture in ME, presence of acicular apatite in the ME) and geochemical data (e.g. linear trends between the RJB and ME samples in Harker type diagrams). When relating the values of the FeO/(FeO + MgO) ratio with the MgO contents (Figure 9) of the primary biotite crystals in the Zhou diagram (1986), one can see that the composition of the BRJ crystals is predominantly allocated in the mixed source field (crystal-mantle). These data suggest that the biotite crystals registered the molecular diffusion that occurred between the mixing magmas (mafic magma from the ME and felsic magma from the RJB granites).

Biotite composition is very sensitive to changes in oxygen fugacity, so it has been used as indicator of redox conditions of granitic magmas (e.g. Wones and Eugster, 1965; Wones, 1972; Bónová et al., 2010; Hossain and Tsunogae, 2014). When performing Wones' (1972) calculations with the data of the primary biotite crystals studied, similar values of log fO_2 were obtained between the IF and PF, that is, -16.3 to -15.0 and -15.9 to -15.4, respectively, whilst those found for the ME showed greater variation, -15.6 to -13.9. The results were plotted on the T versus ΔNNO diagram (Figure 10) and were located in an array above the NNO buffer (O'Neil and Pownceby, 1993) showing a trend of increasing fO_2 with temperature decrease. Based on the NNO buffer, fO_2 values range from +0.7 to +1.3 in the IF, between +0.7 to +0.8 in the PF, and from +0.4 to +1.6 in the ME.

It was noted that the ME primary crystals show variations in fO_2 and temperature values. Given this fact, it was decided to analyze these variations in a sample of the ME (Figure 10). It is observed that the set of analyses of each sample of ME presents different variation of temperature and fO_2 (Figure 10). Due to the trends of increasing fO_2 with decreasing temperature, formed with different initial and final values of these parameters in the samples (Figure 10), it is suggested that these variations may indicate the presence of mafic magma (ME) pulses at different stages of the crystallization of the RJB magmatic chamber. Sousa et al. (2019) also inferred the existence of several pulses of mafic magma during the evolution of the RJB magmatic chamber, based on: (i) the identification of a variety of enclave types (dark, light or showing varying shades of gray) in the RJB; (ii) the presence of different shapes and contacts of enclaves with the host granites (indicating differences between the viscosities of the magmas) and (iii) oscillatory zoning in plagioclase crystals.

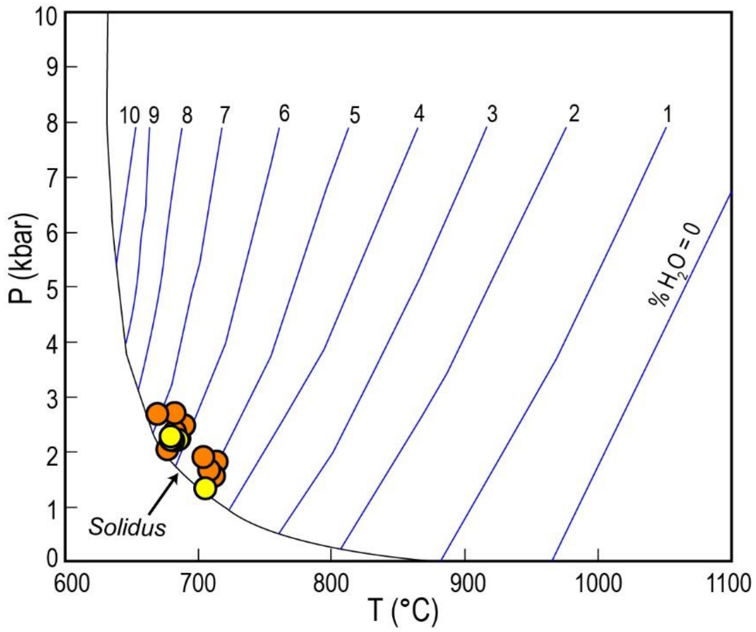

Figure 8. Temperature versus pressure diagram to estimate the minimum content of H_2O dissolved in magma (Holtz et al., 2001) applied to primary biotite crystals of the Rio Jacaré Batholith. Blue lines represent the percentage of water content. Inequigranular facies (orange circle); porphyritic facies (yellow circle).

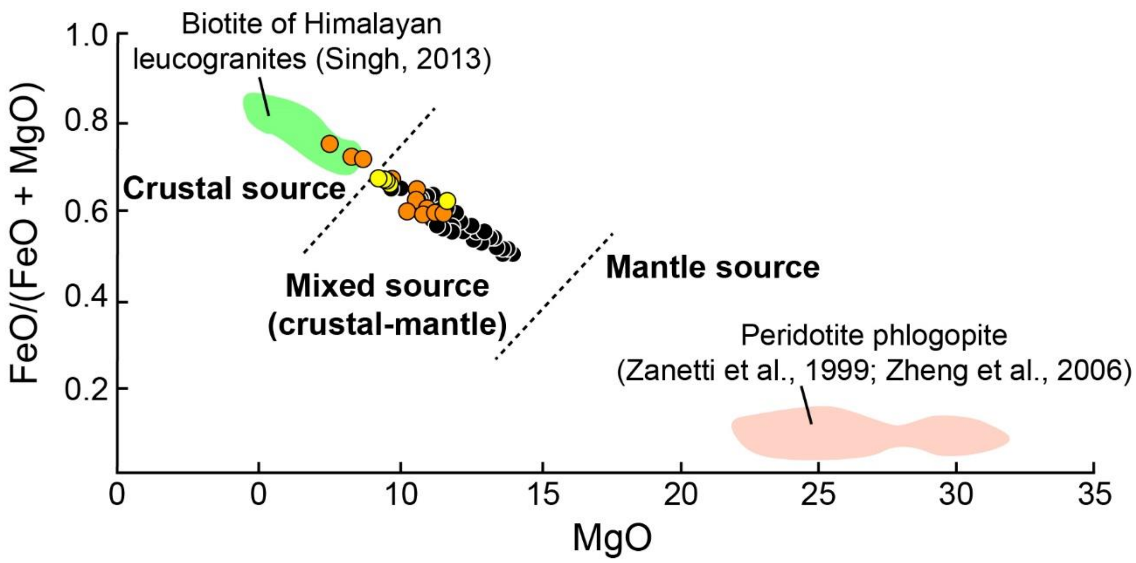

Figure 9. Diagram of the variation in the FeO/(FeO + MgO) ratio and MgO by Zhou (1986) applied to primary biotite crystals from the Rio Jacaré Batholith. Porphyritic facies (yellow circle); inequigranular facies (orange circle); microgranular enclaves (black circle).

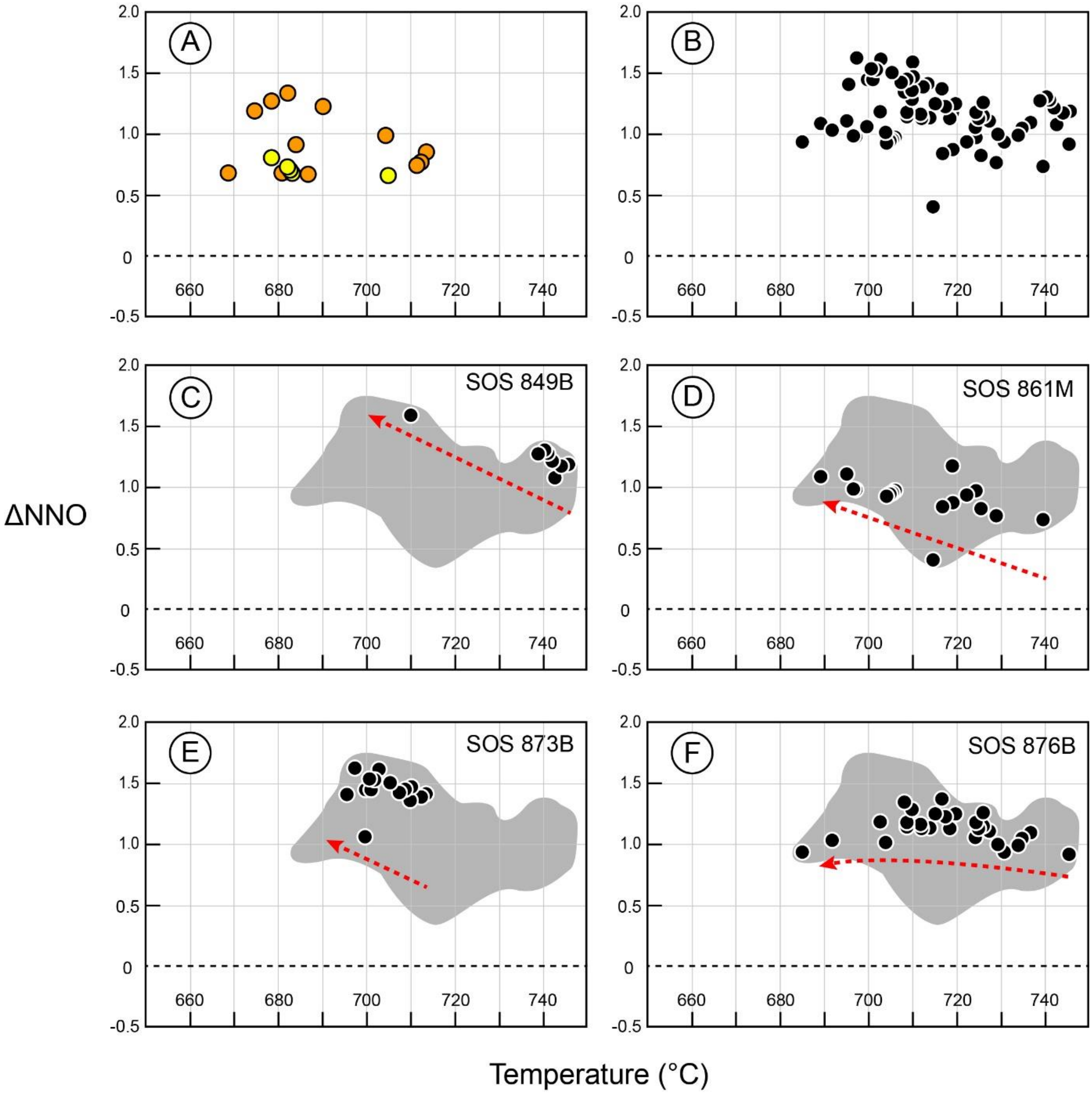

Figure 10. ΔNNO versus temperature diagram applied to primary biotite crystals from the Rio Jacaré Batholith. Porphyritic facies (yellow circle); inequigranular facies (orange circle); microgranular enclaves (black circle). The gray area represents the composition of all analyzed microgranular enclaves. Trends indicated by red arrow.

6. CONCLUSIONS

The micas studied in the RJB correspond to Mg-biotite and are presented as primary and reequilibrated crystals. Primary crystals are found mainly included in plagioclase crystals and have characteristic compositions of crystals formed by type-I magmas from the magnetite series (high oxygen fugacity), being calc-alkaline and showing an orogenic signature.

Magmatic biotite from the RJB crystallized at temperature between 678 and 745 ºC and pressure between 1,2 and 2,9 kbar. These pressures correspond to depths between 4,4 and 10,8 km. The dissolved H_2O content in the magma (5 to 7%) and the oxygen fugacity (log fO_2: -16,3 to -13,9) also varied during the crystallization of primary biotite.

Different mafic magma pulses during the evolution of the RJB were identified by observing different variations in temperature and fO_2 in the different ME samples.

The reequilibrium of biotite crystals resulted from the release of Ti from its crystalline structure. The released Ti, together with Ca from plagioclase that was altered by late fluids, gave origin to anhedral titanite crystals in biotite cleavage planes.

7. ACKNOWLEDGMENTS

This work was carried out with the support of the Coordenação de Aperfeiçoamento de Pessoal de Nível Superior (CAPES) 001. The authors Carlos Santana Sousa, Diego Melo Fernandes and Hiakan Santos Soares thank CNPq for their PHD scholarships, whose processes are 163770/2018-2, 140125/2020-5 and 169765/2018-0, respectively. H. Conceição and MLS Rosa thank CNPq (Processes numbers 019.203.02538/2009-7; 311008/2017-8; 310391/2017-2; 403797/2016-0; 310740/2021-5; 311023/2021-5) for supporting the research in the Sergipano Orogenic System. This work is a part of the first author's PhD thesis at the Geology Postgraduate Program of the Federal University of Bahia (UFBA), which was carried out at the Laboratory of Petrology Applied to Mineral Research at the Federal University of Sergipe (LAPA-UFS). I also thank Dr. Weikai Li from the Academy of Geological Sciences, China, for sparing no effort in helping to use the Geo-fO_2 software.

8. BIBLIOGRAPHY

Abdel-Rahman, A. M. (1994). Nature of biotites from alkaline, calcalcaline and peraluminous magmas. *Journal of Petrology*, **35**(2), 525-541. doi:10.1093/petrology/35.2.525

Almeida, F. F., Hasuí, Y., Brito Neves, B. B., Fuck, R. A. (1977). Províncias estruturais brasileiras. In: Simpósio de Geologia do Nordeste. Campina Grande, 363-391.

Anderson, J. L., Barth, A. P., Wooden, J. L., Mazdab, F. (2008). Thermometers and thermobarometers in granitic systems. *Reviews in Mineralogy and Geochemistry*, **69**(1), 121-142. doi:https://doi.org/10.2138/rmg.2008.69.4.

Andújar, J., Scaillet, B. (2012). Experimental constraints on parameters controlling the difference in the eruptive dynamics of phonolitic magmas: The case of Tenerife (Canary Islands). *Journal of Petrology*, **53**(9), 1777-1806. doi:10.1093/petrology/egs033

Bennett, E. N., Lissenberg, C. J., Cashman, K. V. (2019). The significance of plagioclase textures in mid-ocean ridge basalt (Gakkel Ridge, Arctic Ocean). *Contributions of Mineralogy and Petrology*, **174**(6), 1-22. doi:10.1007/s00410-019-1587-1

Bineli Betsi, T., Lentz, D. R. (2013). Chemical composition of rock-forming minerals in granitoids associated with Au–Bi–Cu, Cu–Mo, and Au–Ag mineralization at the Freegold Mountain, Yukon, Canada: magmatic and hydrothermal fluid chemistry and petrogenetic implications. *International Geology Review*, **55**(6), 657-691. doi:10.1080/00206814.2012.731767

Bónová, K., Broska, I., Petrík, I. (2010). Biotite from Čierna hora Mountains granitoids (Western Carpathians, Slovakia) and estimation of water contents in granitoid melts. *Geologica Carpathica*, **61**, 3-17. Doi: https://doi.org/10.2478/v10096-009-0040-1

Brito, M. F. (1996). *Geologia, geoquímica e petrologia do Complexo Granítico Sítios Novos, Sistema de Dobramentos Sergipano*. MS Dissertation, Universidade Federal de Pernambuco, Recife, .

Carvalho, M. J. (2005). *Evolução Tectônica do Domínio Marancó-Poço Redondo: Registro das Orogêneses Cariris Velhos e Brasiliana na Faixa Sergipana, NE do Brasil*. PhD Thesis, Universidade de Campinas, Campinas, 202 p.

Conceição, J. A., Rosa, M. L., Conceição, H. (2016). Sienogranitos leucocráticos do Domínio Macururé, sistema Orogênicos Sergipano, nordeste do Brasil: stock Glória Sul. *Brazilian Journal of Geology*, **46**, 63-77. doi:http://dx.doi.org/10.1590/2317-4889201620150044

Davison , I., Santos, R. A. (1989). Tectonic evolution of the Sergipano fold belt, NE Brazil, during the Brasiliano Orogeny. *Precambrian Research*, **45**, 319-342. Doi: 10.1016/0301-9268(89)90068-5

Deer, W. A., Howie, R. A., & Zussman, J. (1992). *Rock-forming minerals (2° ed.).* London: Longman. 969 p.

D'el Rey Silva, L. J. (1992). Tectonic Evolution of the Southern Part of the Sergipano Fold Belt, Northeastern Brazil. PhD Thesis, University of London, London, 288 p.

Dong, Q., Du, Y., Pang, Z., Miao, W., Tu, W. (2014). Composition of biotite within the Wushan granodiorite, Jiangxi Province, China: Petrogenetic and metallogenetic implications. *Earth Sciences Research Journal*, **18**(1), 39-44. doi:10.15446/esrj.v18n1.40830

Douce, A. P. (1993). Titanium substituion in biotite: an empirical model with applications to thermometry, O_2 and H_2O barometries, and consequences form biotite stability. *Chemical Geology*, **108**, 133-162. Doi: 10.1016/0009-2541(93)90321-9

Erdmann, S., Martel, C., Pichavant, M., Kushnir, A. (2014). Amphibole as an archivist of magmatic crystallization conditions: problems, potential, and implications for inferring magma storage prior to the paroxysmal 2010 eruption of Mount Merapi, Indonesia. *Contributions to Mineralogy and Petrology*, **167**, 1-23. doi:10.1007/s00410-014-1016-4

Fabbrizio, A., Carrol, M. R. (2008). Experimental constraints on the differentiation process and pre-eruptive conditions in the magmatic system of phlegraean fields (Naples, Italy). *Journal of Volcanology and Geothermal Research*, **171**(1), 88-102. doi:10.1016/j.jvolgeores.2007.11.002

Fernandes, D. M., Lisboa, V. A., Rosa, M. L., Conceição, H. (2020). Petrologia e idade do Stock Fazenda Lagoas, Domínio Macururé, Sistema Orogênico Sergipano, NE-Brasil. *Geologia USP. Série Científica*, **20**(1), 39-60. doi:10.11606/issn.2316-9095.v20-160040

Foster, M. D. (1960). Interpretation of the composition of trioctahedral micas. *Geological Survey Professional Paper*(354-B), 11-49. doi:10.3133/pp354B

Henry, D. J., Guidotti, C. V., Thomoson, J. A. (2005). The Ti-saturation surface for low-to-medium pressure metapelitic biotites: implications for geothermonmetry and Ti-substitution mechanisms. *American Mineralogist*, **90**, 316-328. Doi: 10.2138/am.2005.1498

Holtz, F., Johannes, W., Tamic, N., Behrens, H. (2001). Maximum and minimum water contents of granitic melts generated in the crust: a reevaluation and implications. *Lithos*, **56**, 1-14. doi:10.1016/S0024-4937(00)00056-6

Hossain, I., Tsunogae, T. (2014). Crystallization conditions and petrogenesis of the paleoproterozoic basement rocks in Bangladesh: An evaluation of biotite and coexisting amphibole mineral chemistry. *Journal of Earth Science*, **90**, 87-97. doi:10.1007/s12583-014-0402-1

Karimpour, M. H., Stern, C. R., Mouradi, M. (2011). Chemical composition of biotites as a guide to petrogenesis of granitic rocks from Maherabad, Dehnow, Gheshlagh, Khajehmourad and Najmabad, Iran. *Iranian Journal of Crystallography and Mineralogy*, **18**, 89-100.

Lalonde, A. E., Bernard, P. (1993). Composition and color of biotite from granites: two useful properties in the characterization of plutonic suites from the Hepburn internal zone of Wopmay Orogen, Northwest territories. *The Canadian Mineralogist*, **31**, 203-217.

Li, S., Yang, X., Huang, Y., Sun, W. (2014). Petrogenesis and mineralization of the Fenghuangshan skarn Cu–Au deposit, Tongling ore cluster field. Lower Yangtze metallogenic belt. *Ore Geology Reviews*, **58**, 148-162. doi:10.1016/j.oregeorev.2013.11.004

Li, W., Cheng, Y., Yang, Z. (2019). Geo-fO2: Integrated software for analysis of magmatic oxygen fugacity. *Geochemistry, Geophysics, Geosystems*, **20**, 2542-2555. Doi: https://doi.org/10.1029/2019GC008273

Lima, R. G., Rosa, M. L., & Conceição, H. (2017). Petrografia e química mineral do Batólito Serra Negra, Domínio Poço Redondo, Sistema Orogênivo Sergipano. In: 27° Simpósio de Geologia do Nordeste. João Pessoa.

Martin, R. F. (2007). Amphiboles in the Igneous Environment. *Reviews in Mineralogy and Geochemistry*, **67**(1), 323-358. doi:10.2138/rmg.2007.67.9

Nachit, H., Ibhi, A., Abia, E. H., Ohoud, M. B. (2005). Discrimination between primary magmatic biotites, reequilibrated and neoformed biotites. *Comptus Rendus Geoscience*, **337**, 1415-1420. doi:10.1016/j.crte.2005.09.002

Nachit, H., Razafimahefa, N., Stussi, J. M., Carron, J. P. (1985). Composition chimique des biotites et typologie magmatique des granitoides. *Comptes rendus Académie des Sciences Paris*, **301**, 813-818.

Naney, M. T. (1983). Phase equilibria of rock-forming ferro-magnesian silicates in granitic systems. *American Journal of Science*, **283**, 993-1033. Doi: 10.2475/ajs.283.10.993

O'Neill, H. S., Pownceby, M. I. (1993). Thermodynamic data from redox reactions at high temperatures. I. An experimental and theoretical assessment of the electrochemical method using stabilized zirconia electrolytes, with revised values for the Fe–“FeO”, Co–CoO, Ni–NiO, and Cu–Cu2O oxygen buffers, and new data for the W–WO2 buffer. *Contributions to Mineralogy and Petrology*, **114**, 296–314. https://doi.org/10.1007/BF01046533

Oliveira, E. P., Bueno, J. F., McNaughton, N. J., Silva Filho, A. F., Nascimento, R. S., Donatti-Filho, J. P. (2015). Age, composition, and source of continental arc- and syn-collision granites of the Neoproterozoic Sergipano Belt, Southern Borborema Province, Brazil. *Journal of South American Earth Sciences*, **58**, 257-280. doi:https://doi.org/10.1016/j.jsames.2014.08.003

Oliveira, E. P., Toteu, S. F., Araújo, M. N., Carvalho, M. J., Nascimento, R. S., Bueno, J. F., Mcnaughton, N., Basilici, G. (2006). Geologic correlation between the Neoproteroxoic

Sergipano belt (NE Brazil) and the Yaoundé belt (Cameron, Africa). *Journal of African Earth Sciences*, **44**, 470-478. doi:10.1016/j.jafrearsci.2005.11.014

Oliveira, E. P., Windley, B. F., Araújo, M. N. (2010). The Neoproterozoic Sergipano orogenic belt, NE Brazil: a complete plate tectonic cycle in western Gondwana. *Precambrian Research*, **181**, 64-84. Doi: https://doi.org/10.1016/j.precamres.2010.05.014

Panchuk, K. (2019). *Physical Geology (1 ed.).* First University of Saskatchewan Edition. 602 p.

Papoutsa, A., Pe-Piper, G. (2014). Geochemical variation of amphiboles in A-type granites as an indicator of complex magmatic systems: Wentworth pluton, Nova Scotia, Canada. *Chemical Geology*, **384**, 120-134. doi:10.1016/j.chemgeo.2014.07.001

Petrík, I., Broska, I. (1994). Petrology of two granite types from the Tríbeč Mountains, Western Carpathians: an example of allanite (+ magnetite) versus monazite dichotomy. *Geological Journal*, **29**, 59-78. doi:10.1002/gj.3350290106

Pinho Neto, M. A., Rosa, M. L., Conceição, H. (2019). Petrologia do Batólito Sítios Novos, Sistema Orogênico Sergipano, Província Borborema, NE do Brasil. *Geologia USP. Série Científica*, **19**(2), 135-150. doi:10.11606/issn.2316-9095.v19-152469

Sarjoughian, F., Kananian, A., Haschke, M., Ahmadian, J., Ling, W., Zong, K. (2012). Magma mingling and hybridization in the Kuh-e Dom pluton, Central Iran. *Journal of Asian Earth Sciences*, **54**, 49-63. doi:10.1016/j.jseaes.2012.03.013

Shabani, A.A.T., Lalonde, A.E., Whalen J. B. (2003). Composition of biotite from granitic rocks of the Canadian Appalachian Orogen: A potential tectonomagmatic indicator?. *The Canadian Mineralogist*, **41**(6), 1381-1396. Doi: 10.2113/gscanmin.41.6.1381

Shau, Y. H., Yang, H. Y., Peacor, D. R. (1991). On oriented titanite and rutile inclusions in sagenitic biotite. *American Mineralogist*, **76**, 1205-1217.

Silva Filho, M. A., Torres, H. H. (2002). A new interpretation on the Sergipano Belt domains. *An. Acad. Bras. Cienc. Anais*, **74**(3), 556-557. Doi: https://doi.org/10.1590/S0001-37652002000300049

Singh, R. K. (2013). Origin and emplacement of the Higher Himalayan Leucogranite in the eastern Himalaya: Constraints from geochemistry and mineral chemistry. *Journal of the Geological Society of India*, **81**, 791-803. doi:10.1007/s12594-013-0104-9

Soares, H. S., Sousa, C. S., Rosa, M. L. S., Conceição, H. (2019). Petrologia dos Stocks Santa Maria, Monte Pedral, Bom Jardim, Boa Esperança e Niterói, Suíte Intrusiva Serra do Catu, Estado de Sergipe, NE Sergipe. *Geologia USP. Série Científica*, **19**(4), 63-84. doi:10.11606/issn.2316-9095.v19-156598

Sousa, C. S., Soares, H. S., Rosa, M. L. S., Conceição, H. (2019). Petrologia e Geocronologia do Batólito Rio Jacaré, Domínio Poço Redondo, Sistema Orogênico Sergipano, NE do Brasil. *Geologia USP. Série Científica*, **19**(2), 171-194. doi:10.11606/issn.2316-9095.v19-152494

Sousa, C. S., Soares, H. S., Rosa, M. L. S., Conceição, H. (2018). Petrografia e Geoquímica da Região Oeste do Batólito Bela Vista, Domínio Poço Redondo, Sistema Orogênico Sergipano. *REVISTA DE GEOLOGIA (FORTALEZA)*, **31**, 105-120.

Sousa, C. S., Soares, H. S., Rosa, M. L. S., Conceição, H. (2022). Injections of enriched lithospheric mantle magmas explains the formation of microgranular enclaves in the Rio Jacaré Batholith, Borborema Province, Brazil. Brazilian Journal of Geology, **52**(4), e2022033. doi: 10.1590/2317-4889202220220033

Speer, J. A. (1984). Micas in igneous rocks. *Reviews in Mineralogy and Geochesmistry*, **13**(1), pp. 299-356.

Tulloch, A. J., Challis, G. A. (2000). Emplacement depths of Paleozoic-Mesozoic plutons from western New Zealand estimated by hornblende-AI geobarometry. *New Zealand Journal of Geology and Geophysics*, **43**(4), 555-567. doi:10.1080/00288306.2000.9514908

Uchida, E., Endo, S., Makino, M. (2007). Relationship between solidification depth of granitic rocks and formation of hydrothermal ore deposits. *Resource Geology*, **57**(1), 47-56. doi:10.1111/j.1751-3928.2006.00004.x

Van Schmus, W.R., Oliveira, E.P., Silva Filho, A.F., Toteu, S.F., Penaye, J., Guimarães, I.P. (2008). Proterozoic links between the Bororema Province, NE Brazil, and the Central African Fold Belt. *Geological Society, London, Special Publications*, **294**, 69-99. Doi: https://doi.org/10.1144/SP294.5

Wang, R., Richards, J. P., Hou, Z. Q., Yang, Z. M., Gou, Z. B., DuFrane, S. A. (2014). Increasing magmatic oxidation state from Paleocene to Miocene in the eastern Gangdese Belt, Tibet: implication for collision-related porphyry Cu-Mo+-Au mineralization. *Economic Geology*, **109**, 1943-1965. Doi: https://doi.org/10.2113/econgeo.109.7.1943

Wones, D. R. (1972). Stability of biotite: A reply. *American Mineralogist*, **57**(1-2), 316-317.

Wones, D. R., Eugster, H. P. (1965). Stability of biotite: Experiment, theory and application. *American Mineralogist*, **50**, 1228-1272.

Yu, M., Xia, Q., Zheng, Y., Zhao, Z., Chen, Y., Chen, R., Luo, X., Li, W., Xu, H. (2021). The composition of garnet in granite and pegmatite from the Gangdese orogen in southeastern Tibet: Constrains on pegmatite petrogenesis. *American Mineralogist*, **106**(2), 265-281. doi:10.2138/am-2020-7388

Yui, T. F., Shen, P., Liu, H. H. (2001). Titanite inclusions in altered biotite from granitoids of Taiwan: microstructures and origins. *Journal of Asian Earth Sciences*, **19**, 165-175. doi:10.1016/S1367-9120(00)00025-0

Zanetti, A., Mazzucchelli, M., Rivalenti, G., Vannucci, R. (1999). The Finero phlogopite-peridotite massif: an example of subduction-related metasomatism. *Contribution to Mineralogy and Petrology*, **134**(2-3), 107-122. doi:10.1007/s004100050472

Zheng, J., Griffin, W., O'Reilly, S., Yang, J., Li, T., Zhang, M., Zhang, R.Y., Liou, J. (2006). Mineral chemistry of peridotites from Paleozoic, Mesozoic and Cenozoic lithosphere: constraints on mantle evolution beneath eastern China. *Journal of Petrology*, **47**(11), 2233-2256. doi:10.1093/petrology/egl042

Zhou, Z. X. (1986). The origin of intrusive mass in Fengshandong, Hubei province. *Acta Petrologica Sinica*, **2**(2), 59-70.

CAPÍTULO 5
CONCLUSÕES

Com este estudo, pode-se perceber que o Batólito Rio Jacaré (BRJ) é uma intrusão importante e peculiar do Domínio Poço Redondo, no Sistema Orogênico Sergipano. O BRJ é composto por quartzo monzodioritos, monzogranitos e granodioritos, que estão dispostos na fácies inequigranular e porfirítica. Essas rochas possuem abundantes enclaves microgranulares (EM) que preservam feições de *mixing* e *mingling*. Os EM têm composição diorítica, monzodiorítica, quartzo monzodiorítica e monzonítica.

Os EM do BRJ foram formados por magma máfico shoshonítico, originado de taxa de 3% de fusão parcial do manto litosférico enriquecido em elementos incompatíveis. Esse magma foi injetado em vários pulsos magmáticos, durante etapas distintas da cristalização da câmara magmática do BRJ. A interação do magma máfico com o magma BRJ em etapas distintas da cristalização originou enclaves com formas globulares, alongadas e complexas, enclaves com contatos retos, crenulados, sinuosos e cúspides, e diques sin-plutônicos. Dados químicos sugerem que o grau de hibridização máxima dos EM foi de 57%.

Os cristais de plagioclásio do BRJ possuem variação composicional (fácies inequigranular: An_{7-33}; fácies porfirítica: An_{5-23}; enclaves microgranulares: An_{6-51}) e uma gama variada de texturas: zoneamentos composicionais, *patchy zoning*, *boxy cellular*, cristais com núcleos embaiados, cristais com núcleos com composição homogênea, zonas de inclusões de minerais máficos e *synneusis*. A partir dessas características infere-se que durante a cristalização houve um período estável na câmara magmática do BRJ, seguido por várias injeções de magma máfico que modificaram as condições físico-químicas do sistema magmático BRJ. As perturbações geradas pelas injeções de magma máfico ocasionaram provavelmente correntes de convecção e permitiram o *mixing* e *mingling* entre magmas. Além disso, infere-se pelo menos 5 momentos sucessivos de reabsorção nos cristais de plagioclásio.

Os cristais de Mg-biotita do BRJ são primários/magmáticos e primários reequilibrados. Os cristais primários são encontrados principalmente inclusos em cristais de plagioclásio e os reequilibrados possuem, em seus planos de clivagem, titanita anédrica. As composições da Mg-biotita estudada são típicas de cristais formados por magmas com assinatura orogênica. A Mg-biotita magmática cristalizou-se em temperaturas entre 678 e 745 °C e pressões entre 1,2 e 2,9 kbar. Durante a cristalização da Mg-biotita o conteúdo de H_2O dissolvido no magma foi estimado entre 5 e 7 % e a fugacidade de oxigênio (log fO_2) variou de -16,3 a -13,9. O reequilíbrio dos cristais de Mg-biotita resultou da liberação do Ti da estrutura cristalina. Os cristais de titanita anédricos dispostos nos planos de clivagem da biotita foram formados pelo Ti liberado junto com o Ca (resultante do plagioclásio que foi alterado por fluidos tardios).

APÊNDICE A – JUSTIFICATIVA DA PARTICIPAÇÃO DOS CO-AUTORES

Professor Dr. Herbet Conceição

Auxiliou no desenvolvimento dos trabalhos de campo e os custos analíticos foram em boa parte financiados por projetos sob a sua coordenação. Contribuiu com as discussões e sugestões durante o andamento da pesquisa. É o orientador do trabalho, possui graduação em Geologia pela Universidade Federal da Bahia (1982), mestrado em Geoquímica pela Universidade Federal da Bahia (1986), doutorado em Ciências da Terra - Université Paris Sud - Centre d'Orsay (1990) e pós-doutorado em Geoquímica Isotópica pela Université Blaise Pascal (1996). É Professor Titular desde 1999. Atualmente é docente da Universidade Federal de Sergipe, pesquisador do Programa de Pós-Graduação e Análises de Bacias da UFS, colaborador do Programa de Pós-Graduação em Geologia da UFBA e membro do corpo editorial de revistas científicas. Tem experiência na área de Geociências, com ênfase em Petrologia, atuando principalmente em Petrologia Ígnea: sienitos e granitos.

Professora Dra. Maria de Lourdes da Silva Rosa

Auxiliou no desenvolvimento dos trabalhos de campo e os custos analíticos foram em boa parte financiados por projetos sob a sua coordenação. Contribuiu com as discussões e sugestões durante o andamento da pesquisa. É a coorientadora desta pesquisa e contribuiu na obtenção dos dados geoquímicos deste trabalho. É graduada em Geologia pela Universidade Federal da Bahia (1991), mestre em Geologia pela Universidade Federal da Bahia (1994) e doutora em Geologia pela Universidade Federal da Bahia (1999), com estágios no Swiss Federal Institute of Technology de Zurique (ETHZ) e Université Blaise Pascal (UBP-Clermont Ferrand). Foi pesquisadora DCR-CNPq, DTI-CNPq e PRODOC-CAPES pela Universidade Federal da Bahia. Atualmente é Professora Associada II do Departamento de Geologia da Universidade Federal de Sergipe e Coordenadora Adjunta do Programa de Pós-Graduação em Geociências e Análise de Bacias da UFS. Tem experiência na área de Geociências, com ênfase em Geologia Isotópica, Geoquímica e Petrologia de Rochas Alcalinas.

Msc. Hiakan Santos Soares

Auxiliou em trabalhos de campo, no tratamento e processamento de amostras, na elaboração de alguns diagramas e discussões construtivas acerca do tema abordado. É graduado em Geologia pela Universidade Federal de Sergipe (2016) e mestre pelo Programa de Pós-Graduação em Análises de Bacias da UFS (2018). Atualmente é aluno de doutorado do Programa de Pós-Graduação em Geologia da UFBA. Possui afinidade com as áreas da Petrologia Ígnea, Química Mineral e Geoquímica.

Msc. Diego Melo Fernandes

Auxiliou no tratamento e processamento de amostras, na elaboração de alguns diagramas e discussões. Possui graduação em Geologia pela Universidade Federal da Bahia (2012). Foi professor substituto da Universidade Federal da Bahia no ano de 2016. É mestre em Geociências pela Universidade Federal de Sergipe na área de Petrologia. Atualmente é aluno de doutorado no Programa de Pós-graduação em Geologia da Universidade Federal da Bahia. Tem experiência na área de Geociências, com ênfase nos seguintes temas: Petrologia Ígnea, Química Mineral, Geoquímica e Prospeccão Mineral.

APÊNDICE B – DETALHAMENTO DO MÉTODO DE TRABALHO DESENVOLVIDO

Para desenvolver esta pesquisa aplicou-se uma metodologia que permitiu a coleta de dados, análises, reflexões e conclusões. O presente trabalho foi dividido em várias etapas para atingir as metas propostas nesta pesquisa. Desta forma, iniciaram-se os estudos com a reunião de dados bibliográficos, seguido da realização de missões de campo; preparação de amostras e etapa laboratorial.

Levantamento Bibliográfico

Consistiu do levantamento de dados disponíveis sobre a relação entre granitos e enclaves microganulares, sobre os granitos que possuem enclaves microgranulares no Sistema Orogênico Sergipano e sobre significado de texturas e variações composicionais em minerais. Nesta etapa foram consultados artigos científicos, dissertações, teses, projetos de mapeamento e anais de eventos que abordassem o tema.

Trabalhos de Campo

Realizou-se 2 missões de campo para fazer o reconhecimento das diferentes rochas presentes na área de estudo. Foram visitados cerca de 53 afloramentos, onde coletou-se as coordenadas geográficas em UTM com o GPS, utilizando o Datum SAD69 (South American Datum 1969) como referência. Identificou-se com o auxílio de lupa os aspectos textuais e mineralógicos nas rochas estudadas. Medidas estruturais (mergulho, direção, acamamento, lineação mineral, etc.) foram coletadas com auxílio de uma bússola geológica. 80 amostras de rochas, representativas dos tipos petrográficos identificados, foram coletadas, identificadas e acondicionadas em sacos plásticos.

Preparação das amostras

As amostras coletadas foram lavadas em água corrente para eliminar os resíduos orgânicos ou de solo e tiveram as superfícies de alteração removidas. Após estes processos, foram escolhidas amostras representativas para os estudos petrográfico, mineraloquímico, geoquímico e isotópico. As amostras selecionadas para o estudo petrográfico foram reduzidas a tamanhos de 10x5 cm para a confecção de lâminas delgado-polidas. Essas lâminas foram feitas no Laboratório de Laminação da Superintendência de Salvador do Serviço Geológico do Brasil. Para o estudo geoquímico utilizou-se a parte central dos enclaves, descartando as possíveis interações da periferia com o magma hospedeiro. Após a britagem, tirou-se manualmente os xenocristais de feldspatos presentes em alguns enclaves microgranulares com o objetivo de obter dados químicos que correspondessem à composição mais próxima do magma original. As análises geoquímicas de elementos maiores foram obtidas a partir de pastilhas prensadas utilizando a fluorescência de raios-X Shimadzu XRF-1800, no Condomínio de Laboratórios Multiusuários das Geociências da Universidade Federal de Sergipe (CLGeo-UFS). As pastilhas foram confeccionadas misturando as amostras pulverizadas com ácido bórico, na proporção 3:1 (amostra:ácido bórico), e prensadas posteriormente em prensa hidráulica com pressão de 60 kN por 30 segundos.

Estudo Petrográfico

Nesta etapa, fez-se a descrição de lâminas delgado-polidas, utilizando o microscópio de luz refletida e transmitida da marca Opton, modelo TNP-09T, no Laboratório de Petrografia e Metalografia do CLGeo-UFS. A análise petrográfica consistiu da identificação dos minerais, do reconhecimento e descrição de texturas, estruturas e morfologia dos cristais. Nomeou-se as rochas seguindo a terminologia proposta pela International Union of Geological Sciences (IUGS) para as rochas ígneas plutônicas. Utilizou-se para isso, o diagrama QAP, onde: Q corresponde ao percentual de quartzo; A representa o percentual de feldspato alcalino mais plagioclásio com menos de 5% da molécula de anortita (An) e P corresponde ao percentual de plagioclásio com mais de 5% de An. As fotomicrografias foram obtidas com uma câmera Olympus SC30 acoplada ao microscópio da marca Olympus BX 41, utilizando-se o software Cell^B Olympus (2008).

Estudo Mineraloquímico

As lâminas delgado-polidas foram metalizadas com ouro (espessura de metalização de 8 a 10 nm) para serem investigadas utilizando microscópio eletrônico de varredura (MEV), usando detectores de elétrons retroespalhados (BSE), elétrons secundários, catodoluminescência e espectrômetro de energia dispersiva (EDS). Esses detectores permitiram uma melhor visualização das texturas e variação composicional nos minerais. Esses equipamentos estão instalados em um MEV da marca TESCAN, modelo Vega-3 LMU, no Laboratório de Microanálises do CLGeo-UFS.

Os parâmetros analíticos usados para as análises químicas foram voltagem de 20 kV, corrente de 15-17 nA, diâmetro do feixe de elétrons entre 20-40 μm e tempo de contagem de 60 segundos. As linhas espectrais usadas para a quantificação de elementos, dos padrões internos do EDS e as incertezas associadas (3σ) foram: albita, NaKα (±0.2); coríndon, AlKα

(±0.2); cromo metálico, CrKα (±0.4); fluorita, FKα (±0.3); ferro metálico, FeKα (±0.4); halita, ClKα (±0.3); manganês metálico, MnKα (±0.2); níquel metálico, NiKα (±0.3); ortoclásio, KKα (±0.2); periclásio, MgKα (±0.4); quartzo, SiKα (±0.4); titânio metálico, TiKα (±0.2); wollastonita, CaKα (±0.2) e; fluoreto de bário, BaLα (±0.3).

A confiabilidade e reprodutibilidade das porcentagens dos óxidos obtidos com o EDS foram verificados usando padrões internacionais da *Astimex Scientific Ltd*® e padrões internos do CLGeo-UFS.

Para a obtenção de análises de elementos traço em minerais, retirou-se a metalização das lâminas delgado-polidas e demarcou-se a localização dos minerais a serem analisados (titanita, biotita, plagioclásio e hornblenda). Em seguida, enviou-se as lâminas para a Universidade Federal de Ouro Preto (UFOP) para serem obtidas as análises utilizando o LA-ICP-MS.

Estudo Geoquímico

As análises geoquímicas de elementos maiores foram obtidas a partir de pastilhas prensadas utilizando a fluorescência de raios-X Shimadzu XRF-1800, no CLGeo-UFS. Avaliou-se o grau de confiança das análises comparando com materiais de referência certificados (e.g. AVG-1, DTS-1, QLO-1). A perda ao fogo foi determinada calcinando as amostras em temperatura constante de 1000 °C em forno mufla por 2 h. As análises de elementos traços foram obtidas no laboratório comercial ALS, Brasil, utilizando o ICP-MS e pacote analítico para fins petrológicos (ME-MS81D).

Estudo Isotópico

Para a obtenção de isótopos de U-Pb em titanita, retirou-se a metalização das lâminas delgado-polidas e demarcou-se a localização dos cristais a serem analisados. Em seguida, enviou-se as lâminas para a UFOP para serem analisadas utilizando o LA-ICP-MS.

Os isótopos de Lu-Hf foram obtidos em cristais de zircão concordantes cujas idades foram obtidas por SHRIMP. O mount de cristais de zircão, junto com suas imagens de catodoluminescência, foram enviados para a UFOP para se analisar os isótopos de Lu-Hf usando o LA-ICP-MS.

APÊNDICE C – TABELAS COM DADOS

Apêndice C.1. Análises químicas pontuais em plagioclásio. Os valores dos cations foram obtidos com o cálculo da formula estrutural feita para 8 oxigênios. Or = molécula de ortoclásio (100.K/(K+Na+Ca)); Ab = molécula de albita (100.Na/(K+Na+Ca)); An = molécula de anortita (100.Ca/(K+Na+Ca)). [a, b, c, d, e] representa análises químicas pontuais obtidas em diferentes datas e cristais.

Amostra	FDS 492	FDS 492	FDS 492	FDS 492	FDS 492	FDS 492	FDS 492	FDS 493	FDS 493	FDS 493	FDS 493	FDS 493	FDS 493	FDS 493	FDS 493	FDS 495	FDS 495
Espectro	30	61	62	63	84	96	97	27	28	29	37	43	45	72	83	3	4
UTM	633449	633449	633449	633449	633449	633449	633449	634090	634090	634090	634090	634090	634090	634090	634090	634902	634902
	8908274	8908274	8908274	8908274	8908274	8908274	8908274	8908750	8908750	8908750	8908750	8908750	8908750	8908750	8908750	8909915	8909915
SiO_2	66,6	61,5	61,1	62,0	61,6	61,8	60,5	61,2	65,5	66,1	65,7	65,3	61,0	64,8	64,3	63,6	65,4
Al_2O_3	20,9	24,5	24,8	24,1	24,5	24,2	25,3	24,6	21,7	21,3	21,6	22,3	23,9	22,4	22,3	22,7	21,8
FeO	0,0	0,0	0,0	0,0	0,0	0,0	0,0	0,0	0,0	0,0	0,0	0,0	0,0	0,0	0,0	0,0	0,0
CaO	1,3	5,2	5,7	4,6	5,4	4,8	6,1	5,5	1,8	1,8	2,1	1,3	6,5	3,0	3,4	4,0	2,5
Na_2O	11,2	8,7	8,4	8,9	8,4	8,4	8,1	8,5	10,7	10,8	10,7	10,2	8,7	9,8	9,8	9,8	10,4
K_2O	0,0	0,0	0,0	0,4	0,0	0,0	0,0	0,2	0,3	0,0	0,0	0,9	0,0	0,0	0,2	0,0	0,0
BaO	0,0	0,0	0,0	0,0	0,0	0,0	0,0	0,0	0,0	0,0	0,0	0,0	0,0	0,0	0,0	0,0	0,0
Total	100,0	99,9	100,0	100,0	99,9	100,1	100,0	100,0	100,0	100,0	100,1	100,0	100,1	100,0	100,0	100,1	100,1
Si	2,921	2,728	2,711	2,749	2,731	2,731	2,687	2,718	2,881	2,901	2,885	2,872	2,716	2,850	2,837	2,809	2,873
Al	1,080	1,281	1,297	1,260	1,280	1,261	1,324	1,288	1,125	1,102	1,118	1,156	1,254	1,161	1,160	1,182	1,129
Fe	0,000	0,000	0,000	0,000	0,000	0,000	0,000	0,000	0,000	0,000	0,000	0,000	0,000	0,000	0,000	0,000	0,000
Ca	0,061	0,247	0,271	0,219	0,257	0,227	0,290	0,262	0,085	0,085	0,099	0,061	0,310	0,141	0,161	0,189	0,118
Na	0,952	0,748	0,723	0,765	0,722	0,720	0,698	0,732	0,913	0,919	0,911	0,870	0,751	0,836	0,838	0,839	0,886
K	0,000	0,000	0,000	0,023	0,000	0,000	0,000	0,011	0,017	0,000	0,000	0,050	0,000	0,000	0,011	0,000	0,000
Ba	0,000	0,000	0,000	0,000	0,000	0,000	0,000	0,000	0,000	0,000	0,000	0,000	0,000	0,000	0,000	0,000	0,000
Total	5,015	5,005	5,002	5,015	4,990	4,998	4,999	5,010	5,021	5,007	5,012	5,010	5,032	4,988	5,008	5,020	5,005
Or	0,0	0,0	0,0	2,2	0,0	0,0	0,0	1,1	1,7	0,0	0,0	5,1	0,0	0,0	1,1	0,0	0,0
Ab	94,0	75,2	72,7	76,0	73,8	76,0	70,6	72,8	90,0	91,6	90,2	88,6	70,8	85,5	83,0	81,6	88,3
An	6,0	24,8	27,3	21,7	26,2	24,0	29,4	26,0	8,4	8,4	9,8	6,2	29,2	14,5	15,9	18,4	11,7

Apêndice C.1. Análises químicas pontuais em plagioclásio (continuação).

Amostra	FDS 495	FDS 495	FDS 495	FDS 495	FDS 495	FDS 495	FDS 495	FDS 495	FDS 495	FDS 495	FDS 495	FDS 495	FDS 495	FDS 495	FDS 495	FDS 495	FDS 495
Espectro	5	6	37	38	44	46	47	53	62	66	69	83	86	132	133	138	174
UTM	634902	634902	634902	634902	634902	634902	634902	634902	634902	634902	634902	634902	634902	634902	634902	634902	634902
	8909915	8909915	8909915	8909915	8909915	8909915	8909915	8909915	8909915	8909915	8909915	8909915	8909915	8909915	8909915	8909915	8909915
SiO_2	62,1	64,8	63,4	65,3	63,4	64,3	62,3	64,6	63,1	62,6	62,8	63,4	62,8	61,6	62,6	63,6	62,4
Al_2O_3	24,0	22,1	22,9	21,8	23,5	22,6	23,8	23,4	23,1	23,4	23,3	23,2	23,9	24,3	23,7	23,0	23,8
FeO	0,0	0,0	0,0	0,0	0,0	0,0	0,0	0,0	0,0	0,0	0,0	0,0	0,0	0,0	0,0	0,0	0,0
CaO	5,0	2,9	4,0	2,5	3,8	2,5	5,0	1,2	3,8	5,0	4,7	4,1	3,5	5,0	4,3	3,6	4,7
Na_2O	8,9	10,0	9,5	10,3	9,3	10,0	8,9	10,4	9,7	9,0	9,2	9,2	9,0	9,1	9,1	9,8	8,8
K_2O	0,0	0,3	0,3	0,0	0,0	0,6	0,0	0,4	0,3	0,0	0,0	0,0	0,7	0,0	0,2	0,0	0,2
BaO	0,0	0,0	0,0	0,0	0,0	0,0	0,0	0,0	0,0	0,0	0,0	0,0	0,0	0,0	0,0	0,0	0,0
Total	100,0	100,1	100,1	99,9	100,0	100,0	100,0	100,0	100,0	100,0	100,0	99,9	99,9	100,0	99,9	100,0	99,9
Si	2,751	2,854	2,803	2,873	2,795	2,837	2,759	2,837	2,793	2,772	2,780	2,800	2,779	2,733	2,772	2,808	2,765
Al	1,253	1,147	1,193	1,131	1,221	1,175	1,242	1,211	1,205	1,221	1,216	1,208	1,247	1,271	1,237	1,197	1,243
Fe	0,000	0,000	0,000	0,000	0,000	0,000	0,000	0,000	0,000	0,000	0,000	0,000	0,000	0,000	0,000	0,000	0,000
Ca	0,237	0,137	0,189	0,118	0,180	0,118	0,237	0,056	0,180	0,237	0,223	0,194	0,166	0,238	0,204	0,170	0,223
Na	0,764	0,854	0,814	0,879	0,795	0,856	0,764	0,885	0,833	0,773	0,790	0,788	0,772	0,783	0,781	0,839	0,756
K	0,000	0,017	0,017	0,000	0,000	0,034	0,000	0,022	0,017	0,000	0,000	0,000	0,040	0,000	0,011	0,000	0,011
Ba	0,000	0,000	0,000	0,000	0,000	0,000	0,000	0,000	0,000	0,000	0,000	0,000	0,000	0,000	0,000	0,000	0,000
Total	5,005	5,008	5,016	5,001	4,991	5,020	5,002	5,012	5,029	5,004	5,007	4,990	5,003	5,024	5,006	5,013	4,998
Or	0,0	1,7	1,7	0,0	0,0	3,4	0,0	2,3	1,6	0,0	0,0	0,0	4,0	0,0	1,1	0,0	1,1
Ab	76,3	84,7	79,8	88,2	81,6	84,9	76,3	91,8	80,9	76,5	78,0	80,2	79,0	76,7	78,4	83,1	76,3
An	23,7	13,6	18,6	11,8	18,4	11,7	23,7	5,9	17,5	23,5	22,0	19,8	17,0	23,3	20,5	16,9	22,5

Apêndice C.1. Análises químicas pontuais em plagioclásio (continuação).

Amostra	FDS 495	FDS 495	FDS 495	FDS 495	FDS 495	FDS 495	FDS 495	FDS 496A	FDS 496A	FDS 496A	FDS 496A	FDS 496A	FDS 496A	FDS 496A	FDS 496A	FDS 496A	FDS 496A
Espectro	175	176	177	178	179	180	209	21	22	28	29	34	35	36	37	38	41
UTM	634902	634902	634902	634902	634902	634902	634902	635353	635353	635353	635353	635353	635353	635353	635353	635353	635353
	8909915	8909915	8909915	8909915	8909915	8909915	8909915	8910609	8910609	8910609	8910609	8910609	8910609	8910609	8910609	8910609	8910609
SiO_2	62,6	63,4	64,8	63,1	62,8	63,2	64,0	68,3	65,8	62,5	64,8	61,7	62,0	61,7	63,6	65,7	62,4
Al_2O_3	23,5	23,5	22,1	23,5	23,4	23,3	22,6	22,1	22,0	24,8	22,6	24,4	24,6	24,6	23,2	21,9	24,0
FeO	0,0	0,0	0,0	0,0	0,0	0,0	0,0	0,0	0,0	0,0	0,0	0,0	0,0	0,0	0,0	0,0	0,0
CaO	4,9	4,1	2,8	3,9	4,3	3,8	3,6	4,4	2,8	4,5	3,8	5,8	5,8	6,7	4,5	3,0	5,3
Na_2O	9,0	9,0	10,2	9,3	9,5	9,7	9,8	5,3	9,1	8,1	8,7	7,8	7,6	6,9	8,7	9,4	7,8
K_2O	0,0	0,0	0,0	0,2	0,0	0,0	0,0	0,0	0,2	0,0	0,0	0,4	0,0	0,0	0,0	0,0	0,4
BaO	0,0	0,0	0,0	0,0	0,0	0,0	0,0	0,0	0,0	0,0	0,0	0,0	0,0	0,0	0,0	0,0	0,0
Total	100,0	100,0	99,9	100,0	100,0	100,0	100,0	100,1	99,9	99,9	99,9	100,1	100,0	99,9	100,0	100,0	99,9
Si	2,771	2,795	2,855	2,788	2,779	2,792	2,824	2,945	2,885	2,754	2,847	2,734	2,739	2,731	2,804	2,881	2,762
Al	1,226	1,221	1,148	1,224	1,220	1,213	1,175	1,123	1,137	1,288	1,171	1,274	1,281	1,283	1,205	1,132	1,252
Fe	0,000	0,000	0,000	0,000	0,000	0,000	0,000	0,000	0,000	0,000	0,000	0,000	0,000	0,000	0,000	0,000	0,000
Ca	0,232	0,194	0,132	0,185	0,204	0,180	0,170	0,203	0,132	0,213	0,179	0,275	0,275	0,318	0,213	0,141	0,251
Na	0,772	0,769	0,871	0,797	0,815	0,831	0,838	0,443	0,774	0,692	0,741	0,670	0,651	0,592	0,744	0,799	0,669
K	0,000	0,000	0,000	0,011	0,000	0,000	0,000	0,000	0,011	0,000	0,000	0,023	0,000	0,000	0,000	0,000	0,023
Ba	0,000	0,000	0,000	0,000	0,000	0,000	0,000	0,000	0,000	0,000	0,000	0,000	0,000	0,000	0,000	0,000	0,000
Total	5,002	4,979	5,007	5,004	5,018	5,017	5,008	4,715	4,939	4,947	4,938	4,976	4,946	4,924	4,965	4,953	4,958
Or	0,0	0,0	0,0	1,1	0,0	0,0	0,0	0,0	1,2	0,0	0,0	2,3	0,0	0,0	0,0	0,0	2,4
Ab	76,9	79,9	86,8	80,3	80,0	82,2	83,1	68,6	84,4	76,5	80,6	69,2	70,3	65,1	77,8	85,0	71,0
An	23,1	20,1	13,2	18,6	20,0	17,8	16,9	31,4	14,4	23,5	19,4	28,4	29,7	34,9	22,2	15,0	26,6

Apêndice C.1. Análises químicas pontuais em plagioclásio (continuação).

Amostra	FDS 496A	FDS 496A	FDS 496A	FDS 496A	FDS 496A	FDS 496A	FDS 496B	FDS 496B	FDS 496B	FDS 496B	FDS 496B	FDS 496B	FDS 496B	FDS 496B	FDS 496B	FDS 496B	FDS 496B
Espectro	42	43	44	45	80	82	6	7	9	15	19	21	57	58	59	62	63
UTM	635353	635353	635353	635353	635353	635353	635353	635353	635353	635353	635353	635353	635353	635353	635353	635353	635353
	8910609	8910609	8910609	8910609	8910609	8910609	8910609	8910609	8910609	8910609	8910609	8910609	8910609	8910609	8910609	8910609	8910609
SiO_2	60,8	61,3	60,7	63,1	64,1	63,8	62,9	63,1	64,4	64,3	66,1	64,3	63,1	63,0	62,1	62,4	62,0
Al_2O_3	25,2	25,1	25,2	23,7	23,1	22,6	23,2	23,0	22,7	22,4	21,2	22,3	23,3	23,2	24,3	23,5	23,9
FeO	0,0	0,0	0,0	0,0	0,0	0,6	0,0	0,0	0,0	0,0	0,0	0,0	0,0	0,0	0,0	0,0	0,0
CaO	6,8	6,3	6,8	4,8	4,3	3,9	4,6	4,4	2,7	3,9	1,5	4,1	4,5	4,2	4,3	5,0	5,0
Na_2O	6,9	7,3	7,0	8,2	8,5	8,8	9,1	9,4	9,6	9,4	11,2	9,3	8,8	9,3	9,1	8,8	8,8
K_2O	0,3	0,0	0,2	0,2	0,0	0,3	0,3	0,0	0,7	0,0	0,0	0,0	0,2	0,3	0,3	0,2	0,3
BaO	0,0	0,0	0,0	0,0	0,0	0,0	0,0	0,0	0,0	0,0	0,0	0,0	0,0	0,0	0,0	0,0	0,0
Total	100,0	100,0	99,9	100,0	100,0	100,0	100,1	99,9	100,1	100,0	100,0	100,0	99,9	100,0	100,1	99,9	100,0
Si	2,697	2,712	2,695	2,784	2,819	2,820	2,784	2,794	2,837	2,834	2,903	2,835	2,791	2,789	2,748	2,768	2,750
Al	1,318	1,309	1,319	1,232	1,198	1,178	1,210	1,200	1,179	1,164	1,097	1,159	1,215	1,210	1,267	1,229	1,250
Fe	0,000	0,000	0,000	0,000	0,000	0,022	0,000	0,000	0,000	0,000	0,000	0,000	0,000	0,000	0,000	0,000	0,000
Ca	0,323	0,299	0,324	0,227	0,203	0,185	0,218	0,209	0,127	0,184	0,071	0,194	0,213	0,199	0,204	0,238	0,238
Na	0,594	0,626	0,603	0,702	0,725	0,754	0,781	0,807	0,820	0,803	0,954	0,795	0,755	0,798	0,781	0,757	0,757
K	0,017	0,000	0,011	0,011	0,000	0,017	0,017	0,000	0,039	0,000	0,000	0,000	0,011	0,017	0,017	0,011	0,017
Ba	0,000	0,000	0,000	0,000	0,000	0,000	0,000	0,000	0,000	0,000	0,000	0,000	0,000	0,000	0,000	0,000	0,000
Total	4,949	4,946	4,952	4,956	4,944	4,976	5,010	5,010	5,003	4,986	5,025	4,983	4,985	5,014	5,017	5,002	5,012
Or	1,8	0,0	1,2	1,2	0,0	1,8	1,7	0,0	4,0	0,0	0,0	0,0	1,2	1,7	1,7	1,1	1,7
Ab	63,6	67,7	64,3	74,7	78,2	78,9	76,9	79,4	83,1	81,3	93,1	80,4	77,1	78,7	78,0	75,2	74,8
An	34,6	32,3	34,5	24,1	21,8	19,3	21,5	20,6	12,9	18,7	6,9	19,6	21,8	19,6	20,4	23,6	23,5

Apêndice C.1. Análises químicas pontuais em plagioclásio (continuação).

Amostra	FDS 496B	FDS 496B	FDS 496B	FDS 496B	FDS 496B	FDS 496B	FDS 496B	FDS 496B	FDS 497	FDS 497	FDS 497	FDS 497	FDS 497	SOS 836	SOS 836	SOS 836	SOS 836
Espectro	70	74	75	86	87	88	92	93	31	32	33	34	58	4	5	5	6
UTM	635353	635353	635353	635353	635353	635353	635353	635353	636006	636006	636006	636006	636006	647702	647702	647702	647702
	8910609	8910609	8910609	8910609	8910609	8910609	8910609	8910609	8911340	8911340	8911340	8911340	8911340	8904050	8904050	8904050	8904050
SiO_2	62,2	61,7	65,4	63,1	60,8	60,8	63,0	62,6	64,8	62,5	61,9	63,1	61,5	60,4	60,4	62,1	61,0
Al_2O_3	23,9	24,1	21,7	23,2	24,6	24,6	23,1	23,6	22,0	23,5	23,9	23,1	24,1	26,1	26,3	24,1	25,6
FeO	0,0	0,0	0,0	0,0	0,0	0,0	0,0	0,0	0,0	0,0	0,0	0,0	0,0	0,0	0,0	0,0	0,0
CaO	5,0	5,5	2,1	4,2	5,9	5,7	4,8	5,3	3,3	4,7	5,2	4,7	5,4	5,0	5,0	4,4	4,4
Na_2O	9,0	8,4	10,5	9,2	8,4	8,6	8,9	8,5	9,8	8,9	8,7	9,2	8,6	8,5	8,4	8,1	8,9
K_2O	0,0	0,3	0,3	0,2	0,3	0,4	0,3	0,0	0,0	0,3	0,4	0,0	0,3	0,0	0,0	1,1	0,0
BaO	0,0	0,0	0,0	0,0	0,0	0,0	0,0	0,0	0,0	0,0	0,0	0,0	0,0	0,0	0,0	0,0	0,0
Total	100,1	100,0	100,0	99,9	100,0	100,1	100,1	100,0	99,9	99,9	100,1	100,1	99,9	100,0	100,1	99,8	99,9
Si	2,753	2,739	2,878	2,793	2,706	2,705	2,788	2,769	2,856	2,772	2,746	2,789	2,734	2,676	2,673	2,759	2,702
Al	1,247	1,261	1,126	1,210	1,290	1,290	1,205	1,231	1,143	1,228	1,250	1,203	1,263	1,363	1,372	1,262	1,337
Fe	0,000	0,000	0,000	0,000	0,000	0,000	0,000	0,000	0,000	0,000	0,000	0,000	0,000	0,000	0,000	0,000	0,000
Ca	0,237	0,262	0,099	0,199	0,281	0,272	0,228	0,251	0,156	0,223	0,247	0,223	0,257	0,237	0,237	0,209	0,209
Na	0,772	0,723	0,896	0,789	0,725	0,742	0,764	0,729	0,837	0,765	0,748	0,788	0,741	0,730	0,721	0,698	0,764
K	0,000	0,017	0,017	0,011	0,017	0,023	0,017	0,000	0,000	0,017	0,023	0,000	0,017	0,000	0,000	0,062	0,000
Ba	0,000	0,000	0,000	0,000	0,000	0,000	0,000	0,000	0,000	0,000	0,000	0,000	0,000	0,000	0,000	0,000	0,000
Total	5,010	5,001	5,016	5,003	5,020	5,032	5,000	4,980	4,992	5,005	5,014	5,004	5,013	5,007	5,002	4,990	5,012
Or	0,0	1,7	1,7	1,1	1,7	2,2	1,7	0,0	0,0	1,7	2,2	0,0	1,7	0,0	0,0	6,4	0,0
Ab	76,5	72,2	88,5	79,0	70,8	71,6	75,7	74,4	84,3	76,1	73,5	78,0	73,0	75,5	75,2	72,0	78,5
An	23,5	26,1	9,8	19,9	27,5	26,2	22,6	25,6	15,7	22,2	24,3	22,0	25,3	24,5	24,8	21,6	21,5

Apêndice C.1. Análises químicas pontuais em plagioclásio (continuação).

Amostra	SOS 836	SOS 836	SOS 836	SOS 836	SOS 836	SOS 836	SOS 836	SOS 836	SOS 836	SOS 836	SOS 836	SOS 836	SOS 836	SOS 836	SOS 836	SOS 836	SOS 836
Espectro	6	7[a]	7[b]	8[a]	8[b]	9[a]	9[b]	10[a]	10[b]	11	12	13	29	30	31	34	35
UTM	647702	647702	647702	647702	647702	647702	647702	647702	647702	647702	647702	647702	647702	647702	647702	647702	647702
	8904050	8904050	8904050	8904050	8904050	8904050	8904050	8904050	8904050	8904050	8904050	8904050	8904050	8904050	8904050	8904050	8904050
SiO_2	61,6	60,7	61,6	60,9	64,5	60,9	61,9	60,9	61,8	60,8	60,7	65,6	61,1	61,3	61,3	64,1	61,7
Al_2O_3	24,4	25,9	24,3	25,8	22,1	25,6	24,2	25,9	24,2	25,9	25,8	21,8	24,6	24,9	24,7	23,1	24,4
FeO	0,0	0,0	0,0	0,0	0,0	0,0	0,0	0,0	0,0	0,0	0,0	0,0	0,0	0,0	0,0	0,0	0,0
CaO	5,3	4,4	4,9	4,7	2,7	4,6	4,8	4,4	4,7	4,7	4,6	1,5	4,7	4,6	4,6	1,3	4,5
Na_2O	8,5	8,9	9,0	8,6	10,5	8,9	8,9	8,8	8,9	8,5	8,8	10,5	9,4	9,3	9,4	10,5	9,4
K_2O	0,2	0,0	0,3	0,0	0,2	0,0	0,1	0,0	0,4	0,0	0,0	0,6	0,2	0,0	0,0	1,1	0,0
BaO	0,0	0,0	0,0	0,0	0,0	0,0	0,0	0,0	0,0	0,0	0,0	0,0	0,0	0,0	0,0	0,0	0,0
Total	100,0	99,9	100,1	100,0	100,0	100,0	99,9	100,0	100,0	99,9	99,9	100,0	100,0	100,1	100,0	100,1	100,0
Si	2,732	2,690	2,733	2,695	2,847	2,697	2,745	2,694	2,742	2,692	2,691	2,885	2,716	2,716	2,720	2,828	2,735
Al	1,275	1,353	1,271	1,346	1,150	1,336	1,265	1,351	1,266	1,352	1,348	1,130	1,289	1,300	1,292	1,201	1,275
Fe	0,000	0,000	0,000	0,000	0,000	0,000	0,000	0,000	0,000	0,000	0,000	0,000	0,000	0,000	0,000	0,000	0,000
Ca	0,252	0,209	0,233	0,223	0,128	0,218	0,228	0,209	0,223	0,223	0,218	0,071	0,224	0,218	0,219	0,061	0,214
Na	0,731	0,765	0,774	0,738	0,899	0,764	0,765	0,755	0,766	0,730	0,756	0,895	0,810	0,799	0,809	0,898	0,808
K	0,011	0,000	0,017	0,000	0,011	0,000	0,006	0,000	0,023	0,000	0,000	0,034	0,011	0,000	0,000	0,062	0,000
Ba	0,000	0,000	0,000	0,000	0,000	0,000	0,000	0,000	0,000	0,000	0,000	0,000	0,000	0,000	0,000	0,000	0,000
Total	5,001	5,016	5,027	5,001	5,034	5,017	5,008	5,008	5,019	4,997	5,014	5,015	5,050	5,033	5,039	5,051	5,032
Or	1,1	0,0	1,7	0,0	1,1	0,0	0,6	0,0	2,2	0,0	0,0	3,4	1,1	0,0	0,0	6,1	0,0
Ab	73,5	78,5	75,6	76,8	86,6	77,8	76,6	78,4	75,7	76,6	77,6	89,6	77,5	78,5	78,7	87,9	79,1
Na	25,3	21,5	22,7	23,2	12,3	22,2	22,8	21,6	22,1	23,4	22,4	7,1	21,4	21,5	21,3	6,0	20,9

Apêndice C.1. Análises químicas pontuais em plagioclásio (continuação).

Amostra	SOS 836	SOS 836	SOS 836	SOS 836	SOS 836	SOS 836	SOS 836	SOS 836	SOS 836	SOS 836	SOS 836	SOS 836	SOS 837	SOS 837	SOS 837	SOS 837	SOS 837
Espectro	36	37	38	39	40	48	49	51	52	53	60	71	20	21	22	23	24
UTM	647702	647702	647702	647702	647702	647702	647702	647702	647702	647702	647702	647702	646665	646665	646665	646665	646665
	8904050	8904050	8904050	8904050	8904050	8904050	8904050	8904050	8904050	8904050	8904050	8904050	8905027	8905027	8905027	8905027	8905027
SiO_2	61,8	62,0	61,8	61,2	63,3	59,8	61,7	64,8	61,4	62,0	59,7	60,1	62,6	62,9	62,9	63,1	63,2
Al_2O_3	24,3	24,3	24,4	24,8	23,3	25,9	24,3	21,8	24,8	24,2	26,0	25,7	23,5	23,4	23,2	22,9	23,1
FeO	0,0	0,0	0,0	0,0	0,0	0,0	0,0	0,0	0,0	0,0	0,0	0,0	0,0	0,0	0,0	0,0	0,0
CaO	4,2	4,2	4,2	4,8	3,1	5,0	4,3	1,7	4,6	4,1	5,9	5,3	3,6	3,4	3,5	3,0	3,3
Na_2O	9,7	9,5	9,6	9,2	9,9	8,7	9,5	11,5	9,3	9,5	8,4	8,9	10,1	10,2	10,2	10,7	10,1
K_2O	0,0	0,0	0,0	0,0	0,4	0,5	0,2	0,2	0,0	0,2	0,0	0,0	0,2	0,2	0,2	0,2	0,3
BaO	0,0	0,0	0,0	0,0	0,0	0,0	0,0	0,0	0,0	0,0	0,0	0,0	0,0	0,0	0,0	0,0	0,0
Total	100,0	100,0	100,0	100,0	100,0	99,9	100,0	100,0	100,1	100,0	100,0	100,0	100,0	100,1	100,0	99,9	100,0
Si	2,740	2,745	2,738	2,715	2,798	2,665	2,738	2,860	2,720	2,748	2,656	2,672	2,774	2,783	2,786	2,798	2,797
Al	1,270	1,268	1,274	1,297	1,214	1,361	1,271	1,134	1,295	1,264	1,363	1,347	1,227	1,220	1,211	1,197	1,205
Fe	0,000	0,000	0,000	0,000	0,000	0,000	0,000	0,000	0,000	0,000	0,000	0,000	0,000	0,000	0,000	0,000	0,000
Ca	0,199	0,199	0,199	0,228	0,147	0,239	0,204	0,080	0,218	0,195	0,281	0,252	0,171	0,161	0,166	0,143	0,156
Na	0,834	0,816	0,825	0,791	0,849	0,752	0,817	0,984	0,799	0,816	0,725	0,767	0,868	0,875	0,876	0,920	0,867
K	0,000	0,000	0,000	0,000	0,023	0,028	0,011	0,011	0,000	0,011	0,000	0,000	0,011	0,011	0,011	0,011	0,017
Ba	0,000	0,000	0,000	0,000	0,000	0,000	0,000	0,000	0,000	0,000	0,000	0,000	0,000	0,000	0,000	0,000	0,000
Total	5,042	5,028	5,037	5,032	5,030	5,045	5,041	5,070	5,032	5,034	5,025	5,038	5,052	5,050	5,052	5,069	5,042
Or	0,0	0,0	0,0	0,0	2,2	2,8	1,1	1,0	0,0	1,1	0,0	0,0	1,1	1,1	1,1	1,1	1,6
Ab	80,7	80,4	80,5	77,6	83,4	73,8	79,1	91,5	78,5	79,9	72,0	75,2	82,6	83,5	83,2	85,7	83,3
An	19,3	19,6	19,5	22,4	14,4	23,4	19,8	7,5	21,5	19,0	28,0	24,8	16,3	15,4	15,8	13,3	15,0

Apêndice C.1. Análises químicas pontuais em plagioclásio (continuação).

Amostra	SOS 837	SOS 837	SOS 837	SOS 837	SOS 837	SOS 837	SOS 837	SOS 837	SOS 837	SOS 840A	SOS 840A	SOS 840A	SOS 840A	SOS 840A	SOS 840A	SOS 840A	SOS 841
Espectro	25	28	29	30	31	32	35	41	43	13	28	29	30	31	32	41	23
UTM	646665	646665	646665	646665	646665	646665	646665	646665	646665	648617	648617	648617	648617	648617	648617	648617	649295
	8905027	8905027	8905027	8905027	8905027	8905027	8905027	8905027	8905027	8905079	8905079	8905079	8905079	8905079	8905079	8905079	8905517
SiO_2	64,1	63,1	63,5	63,7	63,6	63,7	65,7	63,6	64,9	63,1	63,7	61,4	63,0	62,7	63,1	63,2	63,9
Al_2O_3	22,6	23,0	22,8	22,6	22,6	22,6	18,6	22,9	22,0	23,5	23,4	25,2	23,6	22,4	23,6	23,6	23,1
FeO	0,0	0,0	0,0	0,0	0,0	0,0	0,0	0,0	0,0	0,0	0,0	0,0	0,0	0,0	0,0	0,0	0,0
CaO	2,7	3,6	3,2	3,2	3,1	3,0	1,2	3,2	2,5	4,2	3,7	4,8	4,3	2,0	4,0	3,9	3,6
Na_2O	10,5	10,1	10,4	10,4	10,5	10,5	1,0	10,3	10,7	9,2	9,3	8,7	9,0	12,7	9,3	9,3	9,4
K_2O	0,2	0,2	0,2	0,2	0,2	0,2	13,4	0,0	0,0	0,0	0,0	0,0	0,0	0,2	0,0	0,0	0,0
BaO	0,0	0,0	0,0	0,0	0,0	0,0	0,0	0,0	0,0	0,0	0,0	0,0	0,0	0,0	0,0	0,0	0,0
Total	100,1	100,0	100,1	100,1	100,0	100,0	99,9	100,0	100,1	100,0	100,1	100,1	99,9	100,0	100,0	100,0	100,0
Si	2,828	2,794	2,807	2,816	2,814	2,817	3,002	2,809	2,857	2,786	2,804	2,715	2,784	2,793	2,785	2,788	2,815
Al	1,175	1,201	1,188	1,177	1,179	1,178	1,002	1,192	1,141	1,223	1,214	1,313	1,229	1,176	1,228	1,227	1,199
Fe	0,000	0,000	0,000	0,000	0,000	0,000	0,000	0,000	0,000	0,000	0,000	0,000	0,000	0,000	0,000	0,000	0,000
Ca	0,128	0,171	0,152	0,152	0,147	0,142	0,059	0,151	0,118	0,199	0,175	0,227	0,204	0,095	0,189	0,184	0,170
Na	0,898	0,867	0,892	0,891	0,901	0,900	0,089	0,882	0,913	0,788	0,794	0,746	0,771	1,097	0,796	0,796	0,803
K	0,011	0,011	0,011	0,011	0,011	0,011	0,781	0,000	0,000	0,000	0,000	0,000	0,000	0,011	0,000	0,000	0,000
Ba	0,000	0,000	0,000	0,000	0,000	0,000	0,000	0,000	0,000	0,000	0,000	0,000	0,000	0,000	0,000	0,000	0,000
Total	5,040	5,045	5,050	5,047	5,052	5,049	4,932	5,035	5,029	4,996	4,986	5,001	4,987	5,173	4,999	4,996	4,987
Or	1,1	1,1	1,1	1,1	1,1	1,1	84,1	0,0	0,0	0,0	0,0	0,0	0,0	0,9	0,0	0,0	0,0
Ab	86,6	82,6	84,6	84,6	85,1	85,4	9,5	85,3	88,6	79,9	82,0	76,6	79,1	91,1	80,8	81,2	82,5
An	12,3	16,3	14,4	14,4	13,9	13,5	6,3	14,7	11,4	20,1	18,0	23,4	20,9	7,9	19,2	18,8	17,5

Apêndice C.1. Análises químicas pontuais em plagioclásio (continuação).

Amostra	SOS 841	SOS 841	SOS 841	SOS 841	SOS 841	SOS 841	SOS 841	SOS 841	SOS 841	SOS 841	SOS 841	SOS 841	SOS 841	SOS 842A	SOS 842B	SOS 842B	SOS 842B
Espectro	24	25	26	27	32	33	34	35	36	37	38	39	40	18	21	22	31
UTM	649295	649295	649295	649295	649295	649295	649295	649295	649295	649295	649295	649295	649295	645657	645657	645657	645657
	8905517	8905517	8905517	8905517	8905517	8905517	8905517	8905517	8905517	8905517	8905517	8905517	8905517	8909076	8909076	8909076	8909076
SiO_2	64,1	64,7	63,9	64,3	63,4	63,5	63,6	62,9	63,7	64,3	64,4	63,9	64,1	64,5	61,8	61,9	61,9
Al_2O_3	22,8	22,4	22,7	22,5	23,2	23,0	23,0	23,8	23,1	22,6	22,4	22,8	22,8	21,8	24,3	24,1	24,0
FeO	0,0	0,0	0,0	0,0	0,0	0,0	0,0	0,0	0,0	0,0	0,0	0,0	0,0	0,0	0,0	0,0	0,0
CaO	3,5	2,7	3,7	3,6	3,9	3,9	3,8	3,8	3,8	3,5	3,4	3,7	3,6	1,7	3,8	3,1	4,0
Na_2O	9,6	10,0	9,4	9,4	9,2	9,3	9,4	8,9	9,4	9,4	9,5	9,5	9,5	11,9	10,2	10,9	10,1
K_2O	0,0	0,2	0,2	0,2	0,2	0,2	0,3	0,6	0,0	0,2	0,2	0,2	0,0	0,2	0,0	0,0	0,0
BaO	0,0	0,0	0,0	0,0	0,0	0,0	0,0	0,0	0,0	0,0	0,0	0,0	0,0	0,0	0,0	0,0	0,0
Total	100,0	100,0	99,9	100,0	99,9	99,9	100,1	100,0	100,0	100,0	99,9	100,1	100,0	100,1	100,1	100,0	100,0
Si	2,824	2,848	2,822	2,834	2,802	2,807	2,807	2,781	2,809	2,833	2,840	2,818	2,824	2,850	2,739	2,747	2,746
Al	1,184	1,162	1,182	1,169	1,208	1,198	1,197	1,240	1,201	1,174	1,164	1,185	1,184	1,136	1,269	1,260	1,255
Fe	0,000	0,000	0,000	0,000	0,000	0,000	0,000	0,000	0,000	0,000	0,000	0,000	0,000	0,000	0,000	0,000	0,000
Ca	0,165	0,127	0,175	0,170	0,185	0,185	0,180	0,180	0,180	0,165	0,161	0,175	0,170	0,080	0,180	0,147	0,190
Na	0,820	0,854	0,805	0,803	0,788	0,797	0,805	0,763	0,804	0,803	0,812	0,812	0,812	1,020	0,876	0,938	0,869
K	0,000	0,011	0,011	0,011	0,011	0,011	0,017	0,034	0,000	0,011	0,011	0,011	0,000	0,011	0,000	0,000	0,000
Ba	0,000	0,000	0,000	0,000	0,000	0,000	0,000	0,000	0,000	0,000	0,000	0,000	0,000	0,000	0,000	0,000	0,000
Total	4,994	5,003	4,995	4,988	4,994	4,998	5,005	4,998	4,993	4,987	4,989	5,001	4,990	5,097	5,065	5,092	5,061
Or	0,0	1,1	1,1	1,1	1,1	1,1	1,7	3,5	0,0	1,1	1,1	1,1	0,0	1,0	0,0	0,0	0,0
Ab	83,2	86,0	81,2	81,6	80,1	80,3	80,4	78,1	81,7	82,0	82,5	81,4	82,7	91,7	82,9	86,4	82,0
An	16,8	12,8	17,7	17,3	18,8	18,6	18,0	18,4	18,3	16,9	16,3	17,5	17,3	7,2	17,1	13,6	18,0

Apêndice C.1. Análises químicas pontuais em plagioclásio (continuação).

Amostra	SOS 842B	SOS 842B	SOS 842B	SOS 842B	SOS 842B	SOS 842B	SOS 842B	SOS 842B	SOS 842B	SOS 842B	SOS 843A	SOS 843A	SOS 843A	SOS 843A	SOS 843A	SOS 843A	SOS 843A
Espectro	34	36	38	39	40	41	42	43	44	46	35	36	37	38	39	40	41
UTM	645657	645657	645657	645657	645657	645657	645657	645657	645657	645657	644105	644105	644105	644105	644105	644105	644105
	8909076	8909076	8909076	8909076	8909076	8909076	8909076	8909076	8909076	8909076	8907367	8907367	8907367	8907367	8907367	8907367	8907367
SiO_2	61,6	60,1	63,7	63,1	66,7	62,8	60,9	61,9	62,5	61,5	64,1	63,3	63,3	63,1	63,4	63,3	62,8
Al_2O_3	24,2	27,3	22,4	22,7	22,5	23,4	25,9	23,7	22,9	24,3	22,9	23,2	23,2	23,7	23,2	23,4	23,4
FeO	0,0	0,0	0,0	0,0	0,0	0,0	0,0	0,0	0,0	0,0	0,0	0,0	0,0	0,0	0,0	0,0	0,0
CaO	2,7	1,7	2,1	2,3	2,0	3,4	2,6	3,1	2,8	3,7	4,0	3,8	4,0	3,7	4,2	4,0	3,9
Na_2O	11,4	10,5	11,8	11,8	8,8	10,3	8,9	11,2	11,6	10,5	8,9	9,5	9,2	9,2	9,0	9,1	9,6
K_2O	0,2	0,4	0,0	0,2	0,0	0,2	1,7	0,0	0,1	0,0	0,2	0,2	0,2	0,2	0,1	0,2	0,2
BaO	0,0	0,0	0,0	0,0	0,0	0,0	0,0	0,0	0,0	0,0	0,0	0,0	0,0	0,0	0,0	0,0	0,0
Total	100,1	100,0	100,0	100,1	100,0	100,1	100,0	99,9	99,9	100,0	100,1	100,0	99,9	99,9	99,9	100,0	99,9
Si	2,737	2,660	2,820	2,799	2,902	2,780	2,705	2,753	2,781	2,732	2,822	2,797	2,799	2,787	2,801	2,795	2,782
Al	1,267	1,424	1,169	1,187	1,154	1,221	1,356	1,242	1,201	1,272	1,188	1,208	1,209	1,234	1,208	1,218	1,222
Fe	0,000	0,000	0,000	0,000	0,000	0,000	0,000	0,000	0,000	0,000	0,000	0,000	0,000	0,000	0,000	0,000	0,000
Ca	0,129	0,081	0,100	0,109	0,093	0,161	0,124	0,148	0,133	0,176	0,189	0,180	0,189	0,175	0,199	0,189	0,185
Na	0,982	0,901	1,013	1,015	0,742	0,884	0,767	0,966	1,001	0,904	0,760	0,814	0,789	0,788	0,771	0,779	0,825
K	0,011	0,023	0,000	0,011	0,000	0,011	0,096	0,000	0,006	0,000	0,011	0,011	0,011	0,011	0,006	0,011	0,011
Ba	0,000	0,000	0,000	0,000	0,000	0,000	0,000	0,000	0,000	0,000	0,000	0,000	0,000	0,000	0,000	0,000	0,000
Total	5,126	5,089	5,102	5,121	4,892	5,057	5,048	5,109	5,122	5,084	4,970	5,011	4,997	4,995	4,984	4,992	5,025
Or	1,0	2,2	0,0	1,0	0,0	1,1	9,8	0,0	0,5	0,0	1,2	1,1	1,1	1,2	0,6	1,1	1,1
Ab	87,5	89,7	91,0	89,4	88,8	83,7	77,7	86,7	87,8	83,7	79,2	81,0	79,7	80,9	79,0	79,5	80,8
An	11,5	8,0	9,0	9,6	11,2	15,3	12,5	13,3	11,7	16,3	19,7	17,9	19,2	18,0	20,4	19,3	18,1

Apêndice C.1. Análises químicas pontuais em plagioclásio (continuação).

Amostra	SOS 843A	SOS 844	SOS 844	SOS 844	SOS 844	SOS 844B	SOS 844B	SOS 844B	SOS 844B	SOS 844B	SOS 844B	SOS 844B	SOS 844B	SOS 847	SOS 847	SOS 847	SOS 847
Espectro	42	45	47	49	51	23	24	27	83	86	87	88	89	14	21	22	23
UTM	644105	643535	643535	643535	643535	643535	643535	643535	643535	643535	643535	643535	643535	641702	641702	641702	641702
	8907367	8906655	8906655	8906655	8906655	8906655	8906655	8906655	8906655	8906655	8906655	8906655	8906655	8905086	8905086	8905086	8905086
SiO_2	64,1	64,4	66,3	66,3	66,8	65,2	65,6	66,2	63,4	62,3	60,8	62,4	62,9	62,8	61,3	62,3	61,2
Al_2O_3	22,9	22,5	21,2	21,3	21,0	23,2	23,0	22,2	24,0	24,2	24,0	24,8	24,5	23,4	24,5	24,1	25,0
FeO	0,0	0,0	0,0	0,0	0,0	0,0	0,0	0,0	0,0	0,0	0,0	0,0	0,0	0,0	0,0	0,0	0,0
CaO	3,8	3,1	1,6	1,9	1,5	2,4	2,1	1,5	3,2	4,2	5,8	4,0	3,8	3,3	4,3	3,7	4,5
Na_2O	9,3	9,9	10,8	10,4	10,6	9,3	9,4	10,1	9,4	9,3	9,5	8,8	8,7	10,4	10,0	9,7	9,4
K_2O	0,0	0,0	0,0	0,1	0,2	0,0	0,0	0,0	0,0	0,0	0,0	0,0	0,0	0,0	0,0	0,3	0,0
BaO	0,0	0,0	0,0	0,0	0,0	0,0	0,0	0,0	0,0	0,0	0,0	0,0	0,0	0,0	0,0	0,0	0,0
Total	100,1	99,9	99,9	100,0	100,1	100,1	100,1	100,0	100,0	100,0	100,1	100,0	99,9	99,9	100,1	100,1	100,1
Si	2,821	2,839	2,910	2,907	2,924	2,850	2,864	2,893	2,790	2,755	2,710	2,751	2,771	2,782	2,721	2,757	2,712
Al	1,188	1,169	1,097	1,101	1,084	1,195	1,184	1,144	1,245	1,261	1,261	1,289	1,272	1,222	1,282	1,257	1,306
Fe	0,000	0,000	0,000	0,000	0,000	0,000	0,000	0,000	0,000	0,000	0,000	0,000	0,000	0,000	0,000	0,000	0,000
Ca	0,179	0,146	0,075	0,089	0,070	0,112	0,098	0,070	0,151	0,199	0,277	0,189	0,179	0,157	0,205	0,175	0,214
Na	0,794	0,846	0,919	0,884	0,900	0,788	0,796	0,856	0,802	0,797	0,821	0,752	0,743	0,893	0,861	0,832	0,808
K	0,000	0,000	0,000	0,006	0,011	0,000	0,000	0,000	0,000	0,000	0,000	0,000	0,000	0,000	0,000	0,017	0,000
Ba	0,000	0,000	0,000	0,000	0,000	0,000	0,000	0,000	0,000	0,000	0,000	0,000	0,000	0,000	0,000	0,000	0,000
Total	4,982	5,000	5,001	4,987	4,989	4,946	4,942	4,963	4,988	5,013	5,070	4,981	4,965	5,054	5,068	5,039	5,039
Or	0,0	0,0	0,0	0,6	1,1	0,0	0,0	0,0	0,0	0,0	0,0	0,0	0,0	0,0	0,0	1,7	0,0
Ab	81,6	85,2	92,4	90,3	91,7	87,5	89,0	92,4	84,2	80,0	74,8	79,9	80,6	85,1	80,8	81,2	79,1
An	18,4	14,8	7,6	9,1	7,2	12,5	11,0	7,6	15,8	20,0	25,2	20,1	19,4	14,9	19,2	17,1	20,9

Apêndice C.1. Análises químicas pontuais em plagioclásio (continuação).

Amostra	SOS 847	SOS 847	SOS 847	SOS 847	SOS 847	SOS 847	SOS 847	SOS 847	SOS 847	SOS 847	SOS 847	SOS 847	SOS 847	SOS 847	SOS 849A	SOS 849A	SOS 849A
Espectro	24	25	26	42	65	66	67	68	71	72	73	74	75	76	21	22	49
UTM	641702	641702	641702	641702	641702	641702	641702	641702	641702	641702	641702	641702	641702	641702	639957	639957	639957
	8905086	8905086	8905086	8905086	8905086	8905086	8905086	8905086	8905086	8905086	8905086	8905086	8905086	8905086	8905640	8905640	8905640
SiO_2	62,3	59,6	65,7	63,2	61,7	62,3	64,8	63,3	61,0	60,8	61,3	61,3	62,3	63,0	62,4	63,1	61,0
Al_2O_3	23,8	26,4	21,1	22,9	24,5	23,1	22,3	23,0	24,8	24,8	24,7	24,9	23,3	23,2	23,8	23,3	25,0
FeO	0,0	0,0	0,0	0,0	0,0	0,0	0,0	0,0	0,0	0,0	0,0	0,0	0,0	0,0	0,0	0,0	0,0
CaO	3,7	3,5	1,1	2,9	4,2	3,3	1,4	2,8	4,3	3,9	3,9	3,8	3,1	2,3	3,8	3,1	4,8
Na_2O	10,2	10,2	12,0	10,8	9,7	11,0	10,9	10,7	9,9	10,3	10,1	9,9	11,0	11,1	9,7	10,5	9,0
K_2O	0,0	0,2	0,0	0,2	0,0	0,3	0,6	0,2	0,0	0,3	0,0	0,3	0,2	0,4	0,3	0,0	0,3
BaO	0,0	0,0	0,0	0,0	0,0	0,0	0,0	0,0	0,0	0,0	0,0	0,0	0,0	0,0	0,0	0,0	0,0
Total	100,0	99,9	99,9	100,0	100,1	100,0	100,0	100,0	100,0	100,1	100,0	100,2	99,9	100,0	100,0	100,0	100,1
Si	2,761	2,654	2,896	2,800	2,733	2,771	2,857	2,801	2,710	2,706	2,721	2,717	2,770	2,792	2,765	2,791	2,707
Al	1,243	1,386	1,096	1,196	1,279	1,211	1,159	1,200	1,299	1,301	1,292	1,301	1,221	1,212	1,243	1,215	1,308
Fe	0,000	0,000	0,000	0,000	0,000	0,000	0,000	0,000	0,000	0,000	0,000	0,000	0,000	0,000	0,000	0,000	0,000
Ca	0,176	0,167	0,052	0,138	0,199	0,157	0,066	0,133	0,205	0,185	0,185	0,180	0,148	0,109	0,180	0,147	0,228
Na	0,876	0,881	1,025	0,928	0,833	0,949	0,932	0,918	0,853	0,889	0,869	0,851	0,948	0,954	0,833	0,900	0,774
K	0,000	0,011	0,000	0,011	0,000	0,017	0,034	0,011	0,000	0,017	0,000	0,017	0,011	0,023	0,017	0,000	0,017
Ba	0,000	0,000	0,000	0,000	0,000	0,000	0,000	0,000	0,000	0,000	0,000	0,000	0,000	0,000	0,000	0,000	0,000
Total	5,056	5,099	5,069	5,072	5,044	5,106	5,047	5,063	5,067	5,097	5,068	5,066	5,099	5,090	5,039	5,052	5,035
Or	0,0	1,1	0,0	1,0	0,0	1,5	3,3	1,1	0,0	1,6	0,0	1,6	1,0	2,1	1,6	0,0	1,7
Ab	83,3	83,2	95,2	86,2	80,7	84,5	90,3	86,4	80,6	81,5	82,4	81,2	85,6	87,9	80,9	86,0	76,0
An	16,7	15,8	4,8	12,8	19,3	14,0	6,4	12,5	19,4	17,0	17,6	17,2	13,3	10,1	17,5	14,0	22,4

Apêndice C.1. Análises químicas pontuais em plagioclásio (continuação).

Amostra	SOS 849B	SOS 849B	SOS 849B	SOS 849B	SOS 849B	SOS 849B	SOS 849B	SOS 849B	SOS 849B	SOS 849B	SOS 849B	SOS 849B	SOS 849B	SOS 849B	SOS 849B	SOS 849B	SOS 849B
Espectro	1	2	3	4	5	6	7	8	9	10	11	12[a]	12[b]	13[a]	13[b]	14	15
UTM	639957	639957	639957	639957	639957	639957	639957	639957	639957	639957	639957	639957	639957	639957	639957	639957	639957
	8905640	8905640	8905640	8905640	8905640	8905640	8905640	8905640	8905640	8905640	8905640	8905640	8905640	8905640	8905640	8905640	8905640
SiO_2	59,0	60,1	59,5	59,4	61,1	60,0	60,0	59,5	57,0	60,5	61,1	61,0	61,8	63,3	62,3	62,0	62,0
Al_2O_3	26,9	26,3	26,8	26,6	25,7	26,3	26,4	26,6	28,7	26,6	25,7	25,7	24,2	24,0	24,1	24,0	24,1
FeO	0,0	0,0	0,0	0,0	0,0	0,0	0,0	0,0	0,0	0,0	0,0	0,0	0,0	0,0	0,0	0,0	0,0
CaO	5,8	4,8	5,4	5,5	4,5	5,1	5,2	5,2	6,9	4,4	4,4	4,3	4,8	2,4	4,7	4,7	4,6
Na_2O	8,3	8,9	8,3	8,4	8,7	8,6	8,4	8,6	7,4	8,5	8,9	9,0	9,0	10,2	8,8	9,0	9,1
K_2O	0,0	0,0	0,0	0,0	0,0	0,0	0,0	0,0	0,0	0,0	0,0	0,0	0,2	0,0	0,2	0,3	0,2
BaO	0,0	0,0	0,0	0,0	0,0	0,0	0,0	0,0	0,0	0,0	0,0	0,0	0,0	0,0	0,0	0,0	0,0
Total	100,0	100,1	100,0	99,9	100,0	100,0	100,0	99,9	100,0	100,0	100,1	100,0	100,0	99,9	100,1	100,0	100,0
Si	2,625	2,664	2,641	2,642	2,702	2,662	2,661	2,645	2,543	2,674	2,701	2,700	2,741	2,790	2,755	2,750	2,748
Al	1,411	1,374	1,402	1,395	1,340	1,375	1,380	1,394	1,509	1,386	1,339	1,341	1,265	1,247	1,256	1,255	1,259
Fe	0,000	0,000	0,000	0,000	0,000	0,000	0,000	0,000	0,000	0,000	0,000	0,000	0,000	0,000	0,000	0,000	0,000
Ca	0,276	0,228	0,257	0,262	0,213	0,242	0,247	0,248	0,330	0,208	0,208	0,204	0,228	0,113	0,223	0,223	0,218
Na	0,716	0,765	0,714	0,724	0,746	0,740	0,722	0,741	0,640	0,729	0,763	0,772	0,774	0,872	0,755	0,774	0,782
K	0,000	0,000	0,000	0,000	0,000	0,000	0,000	0,000	0,000	0,000	0,000	0,000	0,011	0,000	0,011	0,017	0,011
Ba	0,000	0,000	0,000	0,000	0,000	0,000	0,000	0,000	0,000	0,000	0,000	0,000	0,000	0,000	0,000	0,000	0,000
Total	5,028	5,031	5,015	5,023	5,001	5,020	5,010	5,028	5,022	4,997	5,011	5,016	5,019	5,022	5,000	5,019	5,019
Or	0,0	0,0	0,0	0,0	0,0	0,0	0,0	0,0	0,0	0,0	0,0	0,0	1,1	0,0	1,1	1,7	1,1
Ab	72,1	77,0	73,6	73,4	77,8	75,3	74,5	75,0	66,0	77,8	78,5	79,1	76,4	88,5	76,3	76,3	77,3
An	27,9	23,0	26,4	26,6	22,2	24,7	25,5	25,0	34,0	22,2	21,5	20,9	22,5	11,5	22,5	22,0	21,6

Apêndice C.1. Análises químicas pontuais em plagioclásio (continuação).

Amostra	SOS 849B	SOS 849B	SOS 849B	SOS 850A	SOS 850A	SOS 850A	SOS 850A	SOS 850A	SOS 850B	SOS 850B	SOS 850B	SOS 850B	SOS 850B	SOS 850B	SOS 850B	SOS 850B	SOS 850B
Espectro	16	17	18	23	24	25	26	27	1	2	3	4	5	6	7	8	9
UTM	639957	639957	639957	639285	639285	639285	639285	639285	639285	639285	639285	639285	639285	639285	639285	639285	639285
	8905640	8905640	8905640	8904524	8904524	8904524	8904524	8904524	8904524	8904524	8904524	8904524	8904524	8904524	8904524	8904524	8904524
SiO_2	61,9	62,2	62,1	62,0	61,7	59,6	60,1	60,6	60,9	59,8	59,6	59,1	59,7	59,3	59,8	59,9	60,3
Al_2O_3	24,2	23,9	24,0	24,4	24,7	25,9	25,8	25,3	25,5	26,4	26,3	26,9	26,0	26,7	26,4	26,1	25,8
FeO	0,0	0,0	0,0	0,0	0,0	0,0	0,0	0,0	0,0	0,0	0,0	0,0	0,0	0,0	0,0	0,0	0,0
CaO	4,6	4,5	4,7	4,9	5,4	6,3	6,2	5,1	3,6	4,6	4,6	5,0	4,6	4,8	5,0	4,4	4,3
Na_2O	9,1	9,2	9,0	8,7	8,3	8,1	8,0	8,5	10,1	9,3	9,5	9,0	9,8	9,2	8,8	9,5	9,7
K_2O	0,2	0,1	0,2	0,0	0,0	0,0	0,0	0,6	0,0	0,0	0,0	0,0	0,0	0,0	0,0	0,0	0,0
BaO	0,0	0,0	0,0	0,0	0,0	0,0	0,0	0,0	0,0	0,0	0,0	0,0	0,0	0,0	0,0	0,0	0,0
Total	100,0	99,9	100,0	100,0	100,1	99,9	100,1	100,1	100,1	100,1	100,0	100,0	100,1	100,0	100,0	99,9	100,1
Si	2,744	2,757	2,752	2,743	2,729	2,655	2,668	2,693	2,699	2,655	2,651	2,629	2,656	2,637	2,655	2,664	2,677
Al	1,264	1,249	1,254	1,272	1,287	1,360	1,350	1,325	1,332	1,381	1,379	1,410	1,364	1,400	1,382	1,368	1,350
Fe	0,000	0,000	0,000	0,000	0,000	0,000	0,000	0,000	0,000	0,000	0,000	0,000	0,000	0,000	0,000	0,000	0,000
Ca	0,218	0,214	0,223	0,232	0,256	0,301	0,295	0,243	0,171	0,219	0,219	0,238	0,219	0,229	0,238	0,210	0,205
Na	0,782	0,791	0,773	0,746	0,712	0,700	0,689	0,732	0,868	0,800	0,819	0,776	0,845	0,793	0,758	0,819	0,835
K	0,011	0,006	0,011	0,000	0,000	0,000	0,000	0,034	0,000	0,000	0,000	0,000	0,000	0,000	0,000	0,000	0,000
Ba	0,000	0,000	0,000	0,000	0,000	0,000	0,000	0,000	0,000	0,000	0,000	0,000	0,000	0,000	0,000	0,000	0,000
Total	5,020	5,016	5,013	4,994	4,984	5,015	5,001	5,028	5,069	5,055	5,069	5,054	5,085	5,059	5,033	5,061	5,066
Or	1,1	0,6	1,1	0,0	0,0	0,0	0,0	3,4	0,0	0,0	0,0	0,0	0,0	0,0	0,0	0,0	0,0
Ab	77,3	78,3	76,7	76,3	73,6	69,9	70,0	72,6	83,5	78,5	78,9	76,5	79,4	77,6	76,1	79,6	80,3
An	21,6	21,2	22,1	23,7	26,4	30,1	30,0	24,1	16,5	21,5	21,1	23,5	20,6	22,4	23,9	20,4	19,7

Apêndice C.1. Análises químicas pontuais em plagioclásio (continuação).

Amostra	SOS 850B	SOS 850B	SOS 850B	SOS 850B	SOS 850B	SOS 850B	SOS 850B	SOS 850B	SOS 850B	SOS 850B	SOS 850B	SOS 850B	SOS 850B	SOS 850B	SOS 850B	SOS 850B	SOS 850B
Espectro	10	11	12	13	14	15	16	17	18	20	21	22	23	24	25	26	27
UTM	639285	639285	639285	639285	639285	639285	639285	639285	639285	639285	639285	639285	639285	639285	639285	639285	639285
	8904524	8904524	8904524	8904524	8904524	8904524	8904524	8904524	8904524	8904524	8904524	8904524	8904524	8904524	8904524	8904524	8904524
SiO_2	60,2	59,8	59,6	59,3	59,9	60,0	60,4	57,5	57,9	58,6	59,5	58,4	59,2	59,3	59,5	59,4	60,0
Al_2O_3	25,8	26,2	26,5	26,4	26,0	26,1	25,8	28,3	27,9	27,2	26,4	27,5	26,8	26,7	26,6	26,5	25,9
FeO	0,0	0,0	0,0	0,0	0,0	0,0	0,0	0,0	0,0	0,0	0,0	0,0	0,0	0,0	0,0	0,0	0,0
CaO	4,4	4,5	4,5	4,5	4,2	4,4	4,4	5,9	5,8	5,3	4,8	5,9	4,8	4,7	4,7	4,7	4,2
Na_2O	9,6	9,4	9,5	9,8	9,8	9,6	9,4	8,3	8,4	8,9	9,3	8,2	9,2	9,4	9,3	9,3	9,8
K_2O	0,0	0,0	0,0	0,0	0,0	0,0	0,0	0,0	0,0	0,0	0,0	0,0	0,0	0,0	0,0	0,0	0,0
BaO	0,0	0,0	0,0	0,0	0,0	0,0	0,0	0,0	0,0	0,0	0,0	0,0	0,0	0,0	0,0	0,0	0,0
Total	100,0	99,9	100,1	100,0	99,9	100,1	100,0	100,0	100,0	100,0	100,0	100,0	100,0	100,1	100,1	99,9	99,9
Si	2,675	2,660	2,648	2,641	2,666	2,664	2,681	2,564	2,581	2,610	2,647	2,600	2,633	2,636	2,643	2,644	2,670
Al	1,351	1,374	1,388	1,386	1,364	1,366	1,350	1,487	1,466	1,428	1,384	1,443	1,405	1,399	1,393	1,391	1,358
Fe	0,000	0,000	0,000	0,000	0,000	0,000	0,000	0,000	0,000	0,000	0,000	0,000	0,000	0,000	0,000	0,000	0,000
Ca	0,209	0,214	0,214	0,215	0,200	0,209	0,209	0,282	0,277	0,253	0,229	0,281	0,229	0,224	0,224	0,224	0,200
Na	0,827	0,811	0,818	0,846	0,846	0,827	0,809	0,718	0,726	0,769	0,802	0,708	0,794	0,810	0,801	0,803	0,846
K	0,000	0,000	0,000	0,000	0,000	0,000	0,000	0,000	0,000	0,000	0,000	0,000	0,000	0,000	0,000	0,000	0,000
Ba	0,000	0,000	0,000	0,000	0,000	0,000	0,000	0,000	0,000	0,000	0,000	0,000	0,000	0,000	0,000	0,000	0,000
Total	5,063	5,059	5,068	5,089	5,075	5,066	5,049	5,051	5,049	5,060	5,062	5,032	5,061	5,069	5,061	5,062	5,074
Or	0,0	0,0	0,0	0,0	0,0	0,0	0,0	0,0	0,0	0,0	0,0	0,0	0,0	0,0	0,0	0,0	0,0
Ab	79,8	79,1	79,3	79,8	80,9	79,8	79,4	71,8	72,4	75,2	77,8	71,6	77,6	78,4	78,2	78,2	80,9
An	20,2	20,9	20,7	20,2	19,1	20,2	20,6	28,2	27,6	24,8	22,2	28,4	22,4	21,6	21,8	21,8	19,1

Apêndice C.1. Análises químicas pontuais em plagioclásio (continuação).

Amostra	SOS 850B	SOS 850B	SOS 850B	SOS 850B	SOS 850B	SOS 850B	SOS 853D	SOS 853D	SOS 853D	SOS 853D	SOS 853D	SOS 853D	SOS 853D	SOS 853D	SOS 853D	SOS 853D	SOS 853D
Espectro	28	29	30	56	57	58	1	2	3	4	5	6	7	8	9	11	12
UTM	639285 8904524	639285 8904524	639285 8904524	639285 8904524	639285 8904524	639285 8904524	641608 8908298	641608 8908298	641608 8908298	641608 8908298	641608 8908298	641608 8908298	641608 8908298	641608 8908298	641608 8908298	641608 8908298	641608 8908298
SiO_2	59,5	59,8	59,6	59,7	60,5	61,9	61,1	65,5	62,3	61,6	61,7	61,9	61,5	61,8	62,1	62,1	62,1
Al_2O_3	26,3	26,3	26,3	26,4	25,7	24,5	25,8	22,7	24,7	25,2	25,2	25,0	25,2	25,6	25,4	24,8	24,8
FeO	0,0	0,0	0,0	0,0	0,0	0,0	0,0	0,0	0,0	0,0	0,0	0,0	0,0	0,0	0,0	0,0	0,0
CaO	4,6	4,6	4,6	4,2	4,0	2,7	4,2	1,5	4,3	4,2	4,1	4,2	4,2	4,0	4,3	3,9	3,7
Na_2O	9,5	9,3	9,5	9,7	9,9	10,9	9,0	10,3	8,7	9,0	9,1	8,8	9,1	8,6	8,2	9,2	9,4
K_2O	0,0	0,0	0,0	0,0	0,0	0,0	0,0	0,0	0,0	0,0	0,0	0,0	0,0	0,0	0,0	0,0	0,0
BaO	0,0	0,0	0,0	0,0	0,0	0,0	0,0	0,0	0,0	0,0	0,0	0,0	0,0	0,0	0,0	0,0	0,0
Total	99,9	100,0	100,0	100,0	100,1	100,0	100,1	100,0	100,0	100,0	100,1	99,9	100,0	100,0	100,0	100,0	100,0
Si	2,650	2,657	2,651	2,654	2,684	2,742	2,700	2,868	2,749	2,723	2,725	2,735	2,720	2,724	2,735	2,743	2,743
Al	1,381	1,377	1,379	1,383	1,344	1,279	1,344	1,171	1,285	1,313	1,312	1,302	1,314	1,330	1,318	1,291	1,291
Fe	0,000	0,000	0,000	0,000	0,000	0,000	0,000	0,000	0,000	0,000	0,000	0,000	0,000	0,000	0,000	0,000	0,000
Ca	0,220	0,219	0,219	0,200	0,190	0,128	0,199	0,070	0,203	0,199	0,194	0,199	0,199	0,189	0,203	0,185	0,175
Na	0,820	0,801	0,819	0,836	0,852	0,936	0,771	0,874	0,744	0,771	0,779	0,754	0,780	0,735	0,700	0,788	0,805
K	0,000	0,000	0,000	0,000	0,000	0,000	0,000	0,000	0,000	0,000	0,000	0,000	0,000	0,000	0,000	0,000	0,000
Ba	0,000	0,000	0,000	0,000	0,000	0,000	0,000	0,000	0,000	0,000	0,000	0,000	0,000	0,000	0,000	0,000	0,000
Total	5,070	5,055	5,069	5,073	5,070	5,086	5,014	4,984	4,981	5,006	5,009	4,991	5,013	4,978	4,956	5,006	5,014
Or	0,0	0,0	0,0	0,0	0,0	0,0	0,0	0,0	0,0	0,0	0,0	0,0	0,0	0,0	0,0	0,0	0,0
Ab	78,9	78,5	78,9	80,7	81,7	88,0	79,5	92,6	78,5	79,5	80,1	79,1	79,7	79,6	77,5	81,0	82,1
An	21,1	21,5	21,1	19,3	18,3	12,0	20,5	7,4	21,5	20,5	19,9	20,9	20,3	20,4	22,5	19,0	17,9

Apêndice C.1. Análises químicas pontuais em plagioclásio (continuação).

Amostra	SOS 853D	SOS 853D	SOS 853D	SOS 853D	SOS 853D	SOS 853D	SOS 861C	SOS 861C	SOS 861C	SOS 861C	SOS 861E	SOS 861E	SOS 861E	SOS 861E	SOS 861E	SOS 861E	SOS 861E
Espectro	13	58	59	60	61	62	10	11	12	13	28	29	38	39	40	41	42
UTM	641608	641608	641608	641608	641608	641608	634708	634708	634708	634708	634708	634708	634708	634708	634708	634708	634708
	8908298	8908298	8908298	8908298	8908298	8908298	8910522	8910522	8910522	8910522	8910522	8910522	8910522	8910522	8910522	8910522	8910522
SiO_2	62,6	63,7	64,6	64,5	65,6	64,6	60,8	63,5	63,8	62,9	63,2	63,9	66,4	62,0	62,1	61,2	61,5
Al_2O_3	24,6	25,3	23,0	23,2	22,7	23,3	25,0	23,1	22,9	23,4	24,3	23,9	21,4	25,2	25,1	25,8	25,6
FeO	0,0	0,0	0,0	0,0	0,0	0,0	0,0	0,0	0,0	0,0	0,0	0,0	0,7	0,0	0,0	0,0	0,0
CaO	3,8	1,7	2,5	2,4	1,4	2,3	5,9	3,8	3,6	4,4	4,0	3,5	1,2	5,1	4,8	5,7	5,5
Na_2O	9,0	9,3	10,0	9,9	10,3	9,8	8,3	9,5	9,5	9,2	8,5	8,7	10,3	7,7	7,9	7,2	7,4
K_2O	0,0	0,0	0,0	0,0	0,0	0,0	0,0	0,2	0,2	0,2	0,0	0,0	0,0	0,0	0,0	0,0	0,0
BaO	0,0	0,0	0,0	0,0	0,0	0,0	0,0	0,0	0,0	0,0	0,0	0,0	0,0	0,0	0,0	0,0	0,0
Total	100,0	100,0	100,1	100,0	100,0	100,0	100,0	100,1	100,0	100,1	100,0	100,0	100,0	100,0	99,9	99,9	100,0
Si	2,759	2,785	2,836	2,832	2,871	2,834	2,700	2,803	2,815	2,781	2,780	2,805	2,911	2,733	2,739	2,703	2,713
Al	1,278	1,304	1,190	1,201	1,171	1,205	1,308	1,202	1,191	1,220	1,260	1,237	1,106	1,309	1,305	1,343	1,331
Fe	0,000	0,000	0,000	0,000	0,000	0,000	0,000	0,000	0,000	0,000	0,000	0,000	0,026	0,000	0,000	0,000	0,000
Ca	0,179	0,080	0,118	0,113	0,066	0,108	0,281	0,180	0,170	0,208	0,189	0,165	0,056	0,241	0,227	0,270	0,260
Na	0,769	0,788	0,851	0,843	0,874	0,834	0,715	0,813	0,813	0,789	0,725	0,741	0,876	0,658	0,676	0,617	0,633
K	0,000	0,000	0,000	0,000	0,000	0,000	0,000	0,011	0,011	0,011	0,000	0,000	0,000	0,000	0,000	0,000	0,000
Ba	0,000	0,000	0,000	0,000	0,000	0,000	0,000	0,000	0,000	0,000	0,000	0,000	0,000	0,000	0,000	0,000	0,000
Total	4,986	4,957	4,995	4,989	4,981	4,980	5,003	5,009	5,001	5,009	4,953	4,947	4,974	4,941	4,946	4,933	4,938
Or	0,0	0,0	0,0	0,0	0,0	0,0	0,0	1,1	1,1	1,1	0,0	0,0	0,0	0,0	0,0	0,0	0,0
Ab	81,1	90,8	87,9	88,2	93,0	88,5	71,8	81,0	81,7	78,2	79,4	81,8	94,0	73,2	74,9	69,6	70,9
An	18,9	9,2	12,1	11,8	7,0	11,5	28,2	17,9	17,1	20,7	20,6	18,2	6,0	26,8	25,1	30,4	29,1

Apêndice C.1. Análises químicas pontuais em plagioclásio (continuação).

Amostra	SOS 861E	SOS 861M	SOS 861M	SOS 861M	SOS 861M	SOS 861M	SOS 861M	SOS 861M	SOS 861M	SOS 861M	SOS 861M	SOS 861M	SOS 861M	SOS 861M	SOS 861M	SOS 861M	SOS 861M
Espectro	43	1	2	3	4[a]	4[b]	5[a]	5[b]	6[a]	6[b]	6[c]	7	8[a]	8[b]	9[a]	9[b]	10[a]
UTM	634708	634708	634708	634708	634708	634708	634708	634708	634708	634708	634708	634708	634708	634708	634708	634708	634708
	8910522	8910522	8910522	8910522	8910522	8910522	8910522	8910522	8910522	8910522	8910522	8910522	8910522	8910522	8910522	8910522	8910522
SiO_2	63,1	61,1	62,6	59,7	58,7	58,0	63,5	59,6	60,5	59,0	60,2	60,4	61,4	59,7	61,1	60,2	61,4
Al_2O_3	25,2	24,7	27,1	25,9	26,5	24,8	27,1	25,7	25,1	26,1	25,4	25,3	24,5	25,7	24,5	25,3	24,1
FeO	0,0	0,0	0,0	0,0	0,0	0,0	0,0	0,0	0,0	0,0	0,0	0,0	0,0	0,0	0,0	0,0	0,0
CaO	3,6	5,5	2,0	6,4	7,2	8,5	1,3	6,6	5,9	7,1	6,2	6,1	5,1	6,3	5,4	6,3	5,3
Na_2O	8,1	8,6	8,3	8,0	7,6	8,7	8,1	7,9	8,2	7,8	8,1	8,3	8,8	8,1	8,7	8,2	9,0
K_2O	0,0	0,1	0,0	0,0	0,0	0,0	0,0	0,2	0,2	0,0	0,0	0,0	0,2	0,2	0,3	0,0	0,2
BaO	0,0	0,0	0,0	0,0	0,0	0,0	0,0	0,0	0,0	0,0	0,0	0,0	0,0	0,0	0,0	0,0	0,0
Total	100,0	100,0	100,0	100,0	100,0	100,0	100,0	100,0	99,9	100,0	99,9	100,1	100,0	100,0	100,0	100,0	100,0
Si	2,767	2,713	2,732	2,656	2,619	2,616	2,758	2,656	2,692	2,632	2,678	2,683	2,725	2,660	2,717	2,678	2,730
Al	1,302	1,293	1,394	1,358	1,393	1,318	1,388	1,350	1,317	1,372	1,332	1,325	1,282	1,350	1,284	1,327	1,263
Fe	0,000	0,000	0,000	0,000	0,000	0,000	0,000	0,000	0,000	0,000	0,000	0,000	0,000	0,000	0,000	0,000	0,000
Ca	0,169	0,262	0,094	0,305	0,344	0,411	0,061	0,315	0,281	0,339	0,296	0,290	0,243	0,301	0,257	0,300	0,252
Na	0,689	0,740	0,702	0,690	0,657	0,761	0,682	0,683	0,708	0,675	0,699	0,715	0,757	0,700	0,750	0,707	0,776
K	0,000	0,006	0,000	0,000	0,000	0,000	0,000	0,011	0,011	0,000	0,000	0,000	0,011	0,011	0,017	0,000	0,011
Ba	0,000	0,000	0,000	0,000	0,000	0,000	0,000	0,000	0,000	0,000	0,000	0,000	0,000	0,000	0,000	0,000	0,000
Total	4,927	5,014	4,922	5,010	5,013	5,106	4,889	5,016	5,009	5,019	5,005	5,012	5,018	5,021	5,025	5,012	5,032
Or	0,0	0,6	0,0	0,0	0,0	0,0	0,0	1,1	1,1	0,0	0,0	0,0	1,1	1,1	1,7	0,0	1,1
Ab	80,3	73,5	88,2	69,3	65,6	64,9	91,9	67,6	70,7	66,5	70,3	71,1	74,9	69,2	73,2	70,2	74,6
An	19,7	26,0	11,8	30,7	34,4	35,1	8,1	31,2	28,1	33,5	29,7	28,9	24,0	29,7	25,1	29,8	24,3

Apêndice C.1. Análises químicas pontuais em plagioclásio (continuação).

Amostra	SOS 861M	SOS 861M	SOS 861M	SOS 861M	SOS 861M	SOS 861M	SOS 861M	SOS 861M	SOS 861M	SOS 861M	SOS 861M	SOS 861M	SOS 861M	SOS 861M	SOS 861M	SOS 861M	SOS 861M
Espectro	10[b]	10[c]	11[a]	11[b]	11[c]	12[a]	12[b]	13[a]	13[b]	15	16	17	18	19	20	26	27
UTM	634708	634708	634708	634708	634708	634708	634708	634708	634708	634708	634708	634708	634708	634708	634708	634708	634708
	8910522	8910522	8910522	8910522	8910522	8910522	8910522	8910522	8910522	8910522	8910522	8910522	8910522	8910522	8910522	8910522	8910522
SiO_2	60,5	60,9	61,4	60,8	60,9	61,1	60,6	61,1	59,7	58,6	58,0	56,9	60,6	61,4	61,7	59,5	61,2
Al_2O_3	25,0	24,8	24,6	25,0	24,9	24,8	25,1	24,6	25,6	26,6	27,0	27,7	25,1	24,5	24,5	25,8	24,7
FeO	0,0	0,0	0,0	0,0	0,0	0,0	0,0	0,0	0,0	0,0	0,0	0,0	0,0	0,0	0,0	0,0	0,0
CaO	5,8	5,4	5,2	5,5	5,6	4,6	5,8	5,0	6,4	7,5	7,6	8,6	5,9	4,9	4,8	6,3	5,2
Na_2O	8,6	8,9	8,8	8,8	8,5	8,9	8,3	9,0	8,1	7,3	7,4	6,7	8,3	9,1	8,9	8,0	9,0
K_2O	0,2	0,0	0,0	0,0	0,0	0,5	0,1	0,2	0,2	0,0	0,0	0,0	0,2	0,2	0,2	0,4	0,0
BaO	0,0	0,0	0,0	0,0	0,0	0,0	0,0	0,0	0,0	0,0	0,0	0,0	0,0	0,0	0,0	0,0	0,0
Total	100,1	100,0	100,0	100,1	99,9	99,9	99,9	99,9	100,0	100,0	100,0	99,9	100,1	100,1	100,1	100,0	100,1
Si	2,691	2,706	2,723	2,699	2,706	2,717	2,695	2,717	2,661	2,614	2,591	2,550	2,692	2,724	2,733	2,654	2,714
Al	1,311	1,299	1,286	1,308	1,304	1,300	1,316	1,289	1,345	1,399	1,422	1,463	1,314	1,281	1,279	1,356	1,291
Fe	0,000	0,000	0,000	0,000	0,000	0,000	0,000	0,000	0,000	0,000	0,000	0,000	0,000	0,000	0,000	0,000	0,000
Ca	0,276	0,257	0,247	0,262	0,267	0,219	0,276	0,238	0,306	0,358	0,364	0,413	0,281	0,233	0,228	0,301	0,247
Na	0,742	0,767	0,757	0,757	0,732	0,767	0,716	0,776	0,700	0,631	0,641	0,582	0,715	0,783	0,764	0,692	0,774
K	0,011	0,000	0,000	0,000	0,000	0,028	0,006	0,011	0,011	0,000	0,000	0,000	0,011	0,011	0,011	0,023	0,000
Ba	0,000	0,000	0,000	0,000	0,000	0,000	0,000	0,000	0,000	0,000	0,000	0,000	0,000	0,000	0,000	0,000	0,000
Total	5,031	5,028	5,013	5,026	5,008	5,031	5,008	5,032	5,023	5,002	5,018	5,009	5,014	5,032	5,015	5,026	5,027
Or	1,1	0,0	0,0	0,0	0,0	2,8	0,6	1,1	1,1	0,0	0,0	0,0	1,1	1,1	1,1	2,2	0,0
Ab	72,0	74,9	75,4	74,3	73,3	75,6	71,7	75,7	68,8	63,8	63,8	58,5	71,0	76,2	76,2	68,1	75,8
An	26,9	25,1	24,6	25,7	26,7	21,6	27,7	23,2	30,1	36,2	36,2	41,5	27,9	22,7	22,7	29,6	24,2

Apêndice C.1. Análises químicas pontuais em plagioclásio (continuação).

Amostra	SOS 861M	SOS 861M	SOS 861M	SOS 861M	SOS 861M	SOS 861M	SOS 861M	SOS 861M	SOS 861M	SOS 861M	SOS 861M	SOS 861M	SOS 861P	SOS 861P	SOS 861P	SOS 861P	SOS 861P
Espectro	27	28	29	30	31	31	32	32	33	33	34	34	7	8	9	23	24
UTM	634708	634708	634708	634708	634708	634708	634708	634708	634708	634708	634708	634708	634708	634708	634708	634708	634708
	8910522	8910522	8910522	8910522	8910522	8910522	8910522	8910522	8910522	8910522	8910522	8910522	8910522	8910522	8910522	8910522	8910522
SiO_2	62,3	61,6	60,2	61,0	59,7	60,1	60,8	60,4	60,0	59,9	60,9	60,4	64,0	62,7	63,4	64,3	63,3
Al_2O_3	24,8	24,4	25,2	24,5	26,2	25,4	24,9	25,0	25,7	25,5	24,8	25,2	22,7	23,5	22,9	22,5	23,0
FeO	0,0	0,0	0,0	0,0	0,0	0,0	0,0	0,0	0,0	0,0	0,0	0,0	0,0	0,0	0,0	0,0	0,3
CaO	1,3	5,4	6,3	5,6	6,0	6,0	5,7	5,7	6,5	6,1	5,7	5,8	3,3	4,4	3,9	3,6	3,9
Na_2O	9,1	8,6	8,2	8,7	7,9	8,5	8,5	8,7	7,8	8,5	8,5	8,5	10,0	9,3	9,6	9,4	9,4
K_2O	2,5	0,0	0,2	0,2	0,2	0,0	0,0	0,1	0,0	0,0	0,2	0,2	0,0	0,2	0,2	0,1	0,2
BaO	0,0	0,0	0,0	0,0	0,0	0,0	0,0	0,0	0,0	0,0	0,0	0,0	0,0	0,0	0,0	0,0	0,0
Total	100,0	100,0	100,1	100,0	100,0	100,0	99,9	99,9	100,0	100,0	100,1	100,1	100,0	100,1	100,0	99,9	100,1
Si	2,765	2,731	2,679	2,713	2,654	2,674	2,703	2,690	2,667	2,667	2,705	2,685	2,823	2,774	2,804	2,835	2,799
Al	1,297	1,275	1,322	1,284	1,373	1,332	1,305	1,313	1,347	1,338	1,298	1,321	1,180	1,226	1,194	1,169	1,199
Fe	0,000	0,000	0,000	0,000	0,000	0,000	0,000	0,000	0,000	0,000	0,000	0,000	0,000	0,000	0,000	0,000	0,011
Ca	0,062	0,257	0,300	0,267	0,286	0,286	0,271	0,272	0,310	0,291	0,271	0,276	0,156	0,209	0,185	0,170	0,185
Na	0,783	0,739	0,708	0,750	0,681	0,733	0,733	0,751	0,672	0,734	0,732	0,733	0,855	0,798	0,823	0,804	0,806
K	0,142	0,000	0,011	0,011	0,011	0,000	0,000	0,006	0,000	0,000	0,011	0,011	0,000	0,011	0,011	0,006	0,011
Ba	0,000	0,000	0,000	0,000	0,000	0,000	0,000	0,000	0,000	0,000	0,000	0,000	0,000	0,000	0,000	0,000	0,000
Total	5,049	5,001	5,020	5,026	5,005	5,026	5,011	5,032	4,996	5,031	5,018	5,026	5,015	5,018	5,017	4,984	5,010
Or	14,3	0,0	1,1	1,1	1,2	0,0	0,0	0,6	0,0	0,0	1,1	1,1	0,0	1,1	1,1	0,6	1,1
Ab	79,4	74,2	69,4	72,9	69,6	71,9	73,0	73,0	68,5	71,6	72,1	71,8	84,6	78,4	80,8	82,1	80,4
An	6,3	25,8	29,5	25,9	29,2	28,1	27,0	26,4	31,5	28,4	26,7	27,1	15,4	20,5	18,1	17,4	18,4

Apêndice C.1. Análises químicas pontuais em plagioclásio (continuação).

Amostra	SOS 861P	SOS 861P	SOS 861P	SOS 861P	SOS 861P	SOS 861P	SOS 861P	SOS 861P	SOS 861P	SOS 861Q	SOS 861Q	SOS 861Q	SOS 861Q	SOS 861Q	SOS 861Q	SOS 861Q	SOS 861Q
Espectro	25	26	27	35	36	44	45	46	47	1	2	3	4	5	19	20	23
UTM	634708	634708	634708	634708	634708	634708	634708	634708	634708	634708	634708	634708	634708	634708	634708	634708	634708
	8910522	8910522	8910522	8910522	8910522	8910522	8910522	8910522	8910522	8910522	8910522	8910522	8910522	8910522	8910522	8910522	8910522
SiO_2	64,0	63,8	63,3	62,9	63,6	62,8	63,6	60,0	62,2	61,8	63,0	63,9	64,7	64,0	63,9	64,7	66,9
Al_2O_3	22,7	22,8	23,2	23,3	22,9	23,3	23,3	25,5	24,3	24,3	23,4	23,0	22,0	22,4	22,9	22,1	20,7
FeO	0,0	0,0	0,0	0,0	0,0	0,0	0,0	0,0	0,0	0,0	0,0	0,0	0,0	0,0	0,0	0,0	0,0
CaO	3,6	2,8	3,9	4,4	3,8	3,7	3,9	6,4	4,8	5,1	3,8	3,6	2,9	3,1	3,6	3,1	1,3
Na_2O	9,7	10,6	9,4	9,3	9,7	10,1	9,2	7,9	8,4	8,8	9,7	9,5	10,2	10,3	9,6	10,2	10,9
K_2O	0,0	0,0	0,2	0,1	0,0	0,2	0,0	0,2	0,3	0,0	0,0	0,0	0,2	0,2	0,0	0,0	0,2
BaO	0,0	0,0	0,0	0,0	0,0	0,0	0,0	0,0	0,0	0,0	0,0	0,0	0,0	0,0	0,0	0,0	0,0
Total	100,0	100,0	100,0	100,0	100,0	100,1	100,0	100,0	100,0	100,0	99,9	100,0	100,0	100,0	100,0	100,1	100,0
Si	2,823	2,817	2,797	2,783	2,809	2,781	2,803	2,671	2,752	2,738	2,787	2,816	2,853	2,828	2,817	2,849	2,933
Al	1,180	1,187	1,208	1,215	1,192	1,216	1,211	1,338	1,267	1,269	1,220	1,195	1,143	1,167	1,190	1,147	1,070
Fe	0,000	0,000	0,000	0,000	0,000	0,000	0,000	0,000	0,000	0,000	0,000	0,000	0,000	0,000	0,000	0,000	0,000
Ca	0,170	0,132	0,185	0,209	0,180	0,176	0,184	0,305	0,228	0,242	0,180	0,170	0,137	0,147	0,170	0,146	0,061
Na	0,829	0,908	0,805	0,798	0,831	0,867	0,786	0,682	0,721	0,756	0,832	0,812	0,872	0,883	0,821	0,871	0,927
K	0,000	0,000	0,011	0,006	0,000	0,011	0,000	0,011	0,017	0,000	0,000	0,000	0,011	0,011	0,000	0,000	0,011
Ba	0,000	0,000	0,000	0,000	0,000	0,000	0,000	0,000	0,000	0,000	0,000	0,000	0,000	0,000	0,000	0,000	0,000
Total	5,002	5,044	5,007	5,011	5,011	5,051	4,984	5,007	4,984	5,005	5,019	4,993	5,017	5,035	4,998	5,013	5,001
Or	0,0	0,0	1,1	0,6	0,0	1,1	0,0	1,1	1,8	0,0	0,0	0,0	1,1	1,1	0,0	0,0	1,1
Ab	83,0	87,3	80,4	78,8	82,2	82,3	81,0	68,3	74,7	75,7	82,2	82,7	85,5	84,8	82,8	85,6	92,8
An	17,0	12,7	18,4	20,6	17,8	16,7	19,0	30,6	23,6	24,3	17,8	17,3	13,4	14,1	17,2	14,4	6,1

Apêndice C.1. Análises químicas pontuais em plagioclásio (continuação).

Amostra	SOS 861Q	SOS 861Q	SOS 861Q	SOS 861Q	SOS 861Q	SOS 861Q	SOS 861Q	SOS 861Q	SOS 861Q	SOS 861Q	SOS 861T	SOS 861T	SOS 861T	SOS 861T	SOS 861T	SOS 861T	SOS 861T
Espectro	25	26	27	27	28	69	71	72	73	74	34	35	36	37	38	39	41
UTM	634708	634708	634708	634708	634708	634708	634708	634708	634708	634708	634708	634708	634708	634708	634708	634708	634708
	8910522	8910522	8910522	8910522	8910522	8910522	8910522	8910522	8910522	8910522	8910522	8910522	8910522	8910522	8910522	8910522	8910522
SiO_2	66,1	66,2	63,2	65,7	63,6	63,2	62,7	61,5	62,6	63,2	62,7	63,6	64,1	64,4	64,2	64,5	64,7
Al_2O_3	21,0	21,2	23,3	21,5	22,9	22,8	23,6	24,8	23,5	23,1	25,0	24,2	23,9	23,6	23,7	23,5	23,4
FeO	0,0	0,0	0,0	0,0	0,0	0,0	0,0	0,0	0,0	0,0	0,0	0,0	0,0	0,0	0,0	0,0	0,0
CaO	1,7	1,6	4,1	1,6	3,9	3,6	4,1	4,4	4,2	3,8	5,0	3,9	3,6	3,4	3,5	3,3	3,1
Na_2O	10,9	10,8	9,3	10,7	9,6	10,4	9,4	9,2	9,2	9,7	7,4	8,2	8,4	8,6	8,6	8,7	8,7
K_2O	0,3	0,2	0,0	0,5	0,0	0,0	0,2	0,2	0,4	0,2	0,0	0,0	0,0	0,0	0,0	0,0	0,0
BaO	0,0	0,0	0,0	0,0	0,0	0,0	0,0	0,0	0,0	0,0	0,0	0,0	0,0	0,0	0,0	0,0	0,0
Total	100,0	100,0	99,9	100,0	100,0	100,0	100,0	100,1	99,9	100,0	100,1	99,9	100,0	100,0	100,0	100,0	99,9
Si	2,907	2,907	2,793	2,891	2,808	2,799	2,775	2,724	2,776	2,796	2,754	2,794	2,811	2,823	2,816	2,827	2,836
Al	1,089	1,097	1,214	1,115	1,192	1,190	1,231	1,295	1,228	1,204	1,294	1,253	1,235	1,219	1,225	1,214	1,209
Fe	0,000	0,000	0,000	0,000	0,000	0,000	0,000	0,000	0,000	0,000	0,000	0,000	0,000	0,000	0,000	0,000	0,000
Ca	0,080	0,075	0,194	0,075	0,185	0,171	0,194	0,209	0,200	0,180	0,235	0,184	0,169	0,160	0,164	0,155	0,146
Na	0,929	0,920	0,797	0,913	0,822	0,893	0,807	0,790	0,791	0,832	0,630	0,698	0,714	0,731	0,731	0,739	0,739
K	0,017	0,011	0,000	0,028	0,000	0,000	0,011	0,011	0,023	0,011	0,000	0,000	0,000	0,000	0,000	0,000	0,000
Ba	0,000	0,000	0,000	0,000	0,000	0,000	0,000	0,000	0,000	0,000	0,000	0,000	0,000	0,000	0,000	0,000	0,000
Total	5,022	5,010	4,998	5,022	5,007	5,053	5,018	5,029	5,017	5,024	4,914	4,929	4,929	4,933	4,937	4,936	4,930
Or	1,6	1,1	0,0	2,8	0,0	0,0	1,1	1,1	2,2	1,1	0,0	0,0	0,0	0,0	0,0	0,0	0,0
Ab	90,6	91,4	80,4	89,8	81,7	83,9	79,7	78,2	78,1	81,3	72,8	79,2	80,9	82,1	81,6	82,7	83,5
An	7,8	7,5	19,6	7,4	18,3	16,1	19,2	20,7	19,7	17,6	27,2	20,8	19,1	17,9	18,4	17,3	16,5

Apêndice C.1. Análises químicas pontuais em plagioclásio (continuação).

Amostra	SOS 861T	SOS 861T	SOS 861T	SOS 861T	SOS 861T	SOS 861T	SOS 861T	SOS 861T	SOS 861T	SOS 862	SOS 862	SOS 864	SOS 864	SOS 864	SOS 864	SOS 864	SOS 864
Espectro	51	52	53	54	55	56	57	58	59	23	25	21	21	22[a]	22[b]	23[a]	23[b]
UTM	634708	634708	634708	634708	634708	634708	634708	634708	634708	633389	633389	631485	631485	631485	631485	631485	631485
	8910522	8910522	8910522	8910522	8910522	8910522	8910522	8910522	8910522	8909807	8909807	8909369	8909369	8909369	8909369	8909369	8909369
SiO_2	61,2	63,6	64,3	63,8	64,0	63,9	63,6	64,5	63,8	65,1	63,1	60,4	59,8	61,4	60,1	60,4	60,5
Al_2O_3	25,6	24,4	23,8	24,1	24,0	24,2	24,2	23,5	24,0	22,1	24,2	25,2	25,7	24,4	25,5	25,2	25,2
FeO	0,0	0,0	0,0	0,0	0,0	0,0	0,0	0,0	0,0	0,0	0,0	0,0	0,0	0,0	0,0	0,0	0,0
CaO	5,6	3,9	3,7	4,0	3,4	3,8	3,8	3,5	3,5	1,5	1,5	6,3	6,7	5,3	6,4	6,2	6,2
Na_2O	7,6	8,2	8,3	8,2	8,6	8,1	8,4	8,5	8,7	10,6	9,6	8,0	7,6	8,7	7,9	8,1	8,0
K_2O	0,0	0,0	0,0	0,0	0,0	0,0	0,0	0,0	0,0	0,6	1,6	0,2	0,2	0,2	0,2	0,1	0,2
BaO	0,0	0,0	0,0	0,0	0,0	0,0	0,0	0,0	0,0	0,0	0,0	0,0	0,0	0,0	0,0	0,0	0,0
Total	100,0	100,1	100,1	100,1	100,0	100,0	100,0	100,0	100,0	99,9	100,0	100,1	100,0	100,0	100,1	100,0	100,1
Si	2,705	2,788	2,816	2,798	2,807	2,801	2,793	2,827	2,801	2,869	2,790	2,685	2,662	2,726	2,672	2,686	2,688
Al	1,333	1,261	1,228	1,246	1,241	1,250	1,252	1,214	1,242	1,148	1,261	1,320	1,348	1,277	1,336	1,321	1,320
Fe	0,000	0,000	0,000	0,000	0,000	0,000	0,000	0,000	0,000	0,000	0,000	0,000	0,000	0,000	0,000	0,000	0,000
Ca	0,265	0,183	0,174	0,188	0,160	0,178	0,179	0,164	0,165	0,071	0,071	0,300	0,320	0,252	0,305	0,295	0,295
Na	0,651	0,697	0,705	0,697	0,731	0,688	0,715	0,722	0,741	0,906	0,823	0,689	0,656	0,749	0,681	0,698	0,689
K	0,000	0,000	0,000	0,000	0,000	0,000	0,000	0,000	0,000	0,034	0,090	0,011	0,011	0,011	0,011	0,006	0,011
Ba	0,000	0,000	0,000	0,000	0,000	0,000	0,000	0,000	0,000	0,000	0,000	0,000	0,000	0,000	0,000	0,000	0,000
Total	4,954	4,930	4,922	4,928	4,939	4,918	4,939	4,927	4,948	5,027	5,036	5,006	4,997	5,016	5,006	5,006	5,003
Or	0,0	0,0	0,0	0,0	0,0	0,0	0,0	0,0	0,0	3,3	9,2	1,1	1,2	1,1	1,1	0,6	1,1
Ab	71,1	79,2	80,2	78,8	82,1	79,4	80,0	81,5	81,8	89,7	83,6	68,9	66,5	74,0	68,3	69,9	69,2
An	28,9	20,8	19,8	21,2	17,9	20,6	20,0	18,5	18,2	7,0	7,2	30,0	32,4	24,9	30,6	29,6	29,6

Apêndice C.1. Análises químicas pontuais em plagioclásio (continuação).

Amostra	SOS 864	SOS 864	SOS 864	SOS 864	SOS 864	SOS 864	SOS 864	SOS 864	SOS 864	SOS 864	SOS 864	SOS 864	SOS 864	SOS 864	SOS 864	SOS 864	SOS 864
Espectro	24[a]	24[b]	25[a]	25[b]	26[a]	26[b]	27	28	29	30	31	32	33	34	35	36	38
UTM	631485	631485	631485	631485	631485	631485	631485	631485	631485	631485	631485	631485	631485	631485	631485	631485	631485
	8909369	8909369	8909369	8909369	8909369	8909369	8909369	8909369	8909369	8909369	8909369	8909369	8909369	8909369	8909369	8909369	8909369
SiO_2	61,1	60,4	61,3	60,3	62,5	61,2	62,1	61,8	63,7	66,3	59,9	59,9	60,0	59,7	60,0	59,6	61,0
Al_2O_3	24,8	25,3	24,7	25,1	24,0	24,4	24,2	24,4	23,1	21,1	25,7	25,6	25,7	25,6	25,5	25,7	24,7
FeO	0,0	0,0	0,0	0,0	0,0	0,0	0,0	0,0	0,0	0,0	0,0	0,0	0,0	0,0	0,0	0,0	0,0
CaO	5,8	6,1	5,4	6,3	5,2	4,9	4,6	4,8	3,5	1,6	6,5	6,5	6,4	6,8	6,7	6,8	5,5
Na_2O	8,3	8,1	8,6	8,2	8,3	9,4	9,0	9,1	9,7	10,9	7,8	8,0	8,0	7,9	7,8	7,8	8,6
K_2O	0,0	0,1	0,0	0,2	0,0	0,2	0,2	0,0	0,0	0,1	0,2	0,0	0,0	0,0	0,0	0,2	0,2
BaO	0,0	0,0	0,0	0,0	0,0	0,0	0,0	0,0	0,0	0,0	0,0	0,0	0,0	0,0	0,0	0,0	0,0
Total	100,0	100,0	100,0	100,1	100,0	100,1	100,1	100,1	100,0	100,0	100,1	100,0	100,1	100,0	100,0	100,1	100,0
Si	2,711	2,685	2,718	2,683	2,762	2,720	2,748	2,736	2,809	2,910	2,664	2,665	2,666	2,659	2,669	2,655	2,711
Al	1,297	1,325	1,291	1,316	1,250	1,278	1,262	1,273	1,201	1,092	1,347	1,343	1,346	1,344	1,337	1,349	1,294
Fe	0,000	0,000	0,000	0,000	0,000	0,000	0,000	0,000	0,000	0,000	0,000	0,000	0,000	0,000	0,000	0,000	0,000
Ca	0,276	0,291	0,257	0,300	0,246	0,233	0,218	0,228	0,165	0,075	0,310	0,310	0,305	0,325	0,319	0,325	0,262
Na	0,714	0,698	0,740	0,707	0,711	0,810	0,772	0,781	0,829	0,928	0,673	0,690	0,689	0,682	0,673	0,674	0,741
K	0,000	0,006	0,000	0,011	0,000	0,011	0,011	0,000	0,000	0,006	0,011	0,000	0,000	0,000	0,000	0,011	0,011
Ba	0,000	0,000	0,000	0,000	0,000	0,000	0,000	0,000	0,000	0,000	0,000	0,000	0,000	0,000	0,000	0,000	0,000
Total	4,998	5,004	5,006	5,018	4,969	5,052	5,012	5,018	5,005	5,011	5,005	5,008	5,006	5,010	4,999	5,013	5,019
Or	0,0	0,6	0,0	1,1	0,0	1,1	1,1	0,0	0,0	0,6	1,1	0,0	0,0	0,0	0,0	1,1	1,1
Ab	72,1	70,2	74,2	69,4	74,3	76,8	77,1	77,4	83,4	92,0	67,7	69,0	69,3	67,8	67,8	66,7	73,1
An	27,9	29,2	25,8	29,5	25,7	22,1	21,8	22,6	16,6	7,5	31,2	31,0	30,7	32,2	32,2	32,1	25,8

Apêndice C.1. Análises químicas pontuais em plagioclásio (continuação).

Amostra	SOS 864	SOS 864	SOS 864	SOS 864	SOS 864	SOS 864	SOS 864	SOS 864	SOS 864	SOS 864	SOS 864	SOS 864	SOS 864	SOS 864	SOS 864	SOS 864	SOS 864
Espectro	39	40	41	42	43	44	45	46	47	48	49	50	51	52	53	54	55
UTM	631485	631485	631485	631485	631485	631485	631485	631485	631485	631485	631485	631485	631485	631485	631485	631485	631485
	8909369	8909369	8909369	8909369	8909369	8909369	8909369	8909369	8909369	8909369	8909369	8909369	8909369	8909369	8909369	8909369	8909369
SiO_2	61,5	60,7	61,5	61,0	61,3	60,9	60,7	59,3	60,3	60,2	61,5	56,4	61,3	60,0	60,2	60,0	59,9
Al_2O_3	24,5	25,3	24,2	24,2	24,5	24,9	24,9	26,3	25,3	25,2	24,5	23,3	24,7	25,6	25,3	25,4	25,7
FeO	0,0	0,0	0,0	0,0	0,0	0,0	0,0	0,0	0,0	0,0	0,0	0,0	0,0	0,0	0,0	0,0	0,0
CaO	5,3	5,8	5,3	6,1	5,3	5,8	5,7	6,6	6,0	6,3	5,4	12,6	5,1	6,4	6,1	6,3	6,4
Na_2O	8,7	8,2	8,9	8,5	8,8	8,3	8,5	7,7	8,3	8,1	8,6	7,5	8,7	7,9	8,3	8,1	7,8
K_2O	0,0	0,0	0,1	0,3	0,1	0,1	0,2	0,1	0,1	0,2	0,0	0,2	0,2	0,0	0,2	0,2	0,2
BaO	0,0	0,0	0,0	0,0	0,0	0,0	0,0	0,0	0,0	0,0	0,0	0,0	0,0	0,0	0,0	0,0	0,0
Total	100,0	100,0	100,0	100,1	100,0	100,0	100,0	100,0	100,0	100,0	100,0	100,0	100,0	99,9	100,1	100,0	100,0
Si	2,727	2,693	2,731	2,715	2,722	2,704	2,699	2,640	2,682	2,680	2,727	2,580	2,720	2,670	2,678	2,672	2,665
Al	1,280	1,323	1,267	1,269	1,282	1,303	1,305	1,380	1,326	1,322	1,280	1,256	1,292	1,343	1,327	1,333	1,348
Fe	0,000	0,000	0,000	0,000	0,000	0,000	0,000	0,000	0,000	0,000	0,000	0,000	0,000	0,000	0,000	0,000	0,000
Ca	0,252	0,276	0,252	0,291	0,252	0,276	0,272	0,315	0,286	0,301	0,257	0,618	0,242	0,305	0,291	0,301	0,305
Na	0,748	0,706	0,766	0,734	0,758	0,715	0,733	0,665	0,716	0,699	0,739	0,665	0,749	0,682	0,716	0,699	0,673
K	0,000	0,000	0,006	0,017	0,006	0,006	0,011	0,006	0,006	0,011	0,000	0,012	0,011	0,000	0,011	0,011	0,011
Ba	0,000	0,000	0,000	0,000	0,000	0,000	0,000	0,000	0,000	0,000	0,000	0,000	0,000	0,000	0,000	0,000	0,000
Total	5,007	4,998	5,022	5,026	5,019	5,004	5,020	5,005	5,016	5,014	5,003	5,130	5,014	5,000	5,022	5,017	5,003
Or	0,0	0,0	0,6	1,6	0,6	0,6	1,1	0,6	0,6	1,1	0,0	0,9	1,1	0,0	1,1	1,1	1,1
Ab	74,8	71,9	74,8	70,4	74,6	71,7	72,1	67,5	71,1	69,2	74,2	51,4	74,7	69,1	70,3	69,2	68,0
An	25,2	28,1	24,6	27,9	24,8	27,7	26,7	32,0	28,4	29,7	25,8	47,7	24,2	30,9	28,6	29,7	30,8

Apêndice C.1. Análises químicas pontuais em plagioclásio (continuação).

Amostra	SOS 864	SOS 864	SOS 864	SOS 864	SOS 864	SOS 864	SOS 864	SOS 864	SOS 864	SOS 864	SOS 864	SOS 864	SOS 864	SOS 864	SOS 864	SOS 864	SOS 864
Espectro	56	57	58	59	60	61	62	63	64	65	66	67	68	69	70	71	72
UTM	631485	631485	631485	631485	631485	631485	631485	631485	631485	631485	631485	631485	631485	631485	631485	631485	631485
	8909369	8909369	8909369	8909369	8909369	8909369	8909369	8909369	8909369	8909369	8909369	8909369	8909369	8909369	8909369	8909369	8909369
SiO_2	60,8	60,1	61,3	60,9	59,1	64,5	60,9	61,3	60,8	59,8	61,0	61,0	61,3	61,0	61,4	61,7	63,0
Al_2O_3	25,1	25,5	24,6	24,5	24,6	22,5	24,7	24,7	25,1	25,7	24,8	24,7	24,7	25,0	24,6	24,2	23,5
FeO	0,0	0,0	0,0	0,2	0,3	0,0	0,0	0,0	0,0	0,0	0,0	0,0	0,0	0,0	0,0	0,0	0,0
CaO	6,1	6,3	5,2	5,4	7,7	3,0	5,7	5,4	5,9	6,3	5,7	5,4	5,5	5,5	5,1	5,2	4,0
Na_2O	8,1	7,9	8,7	8,7	8,1	10,1	8,6	8,5	8,1	8,0	8,5	8,7	8,5	8,5	8,8	8,7	9,3
K_2O	0,0	0,2	0,2	0,2	0,1	0,0	0,2	0,2	0,1	0,2	0,0	0,2	0,0	0,0	0,2	0,1	0,2
BaO	0,0	0,0	0,0	0,0	0,0	0,0	0,0	0,0	0,0	0,0	0,0	0,0	0,0	0,0	0,0	0,0	0,0
Total	100,1	100,0	100,0	99,9	99,9	100,1	100,1	100,1	100,0	100,0	100,0	100,0	100,0	100,0	100,1	99,9	100,0
Si	2,697	2,674	2,721	2,712	2,655	2,838	2,706	2,718	2,699	2,663	2,708	2,711	2,718	2,706	2,723	2,738	2,785
Al	1,312	1,337	1,287	1,286	1,302	1,167	1,294	1,291	1,313	1,349	1,298	1,294	1,291	1,307	1,286	1,266	1,224
Fe	0,000	0,000	0,000	0,007	0,011	0,000	0,000	0,000	0,000	0,000	0,000	0,000	0,000	0,000	0,000	0,000	0,000
Ca	0,290	0,300	0,247	0,258	0,371	0,141	0,271	0,257	0,281	0,301	0,271	0,257	0,261	0,261	0,242	0,247	0,189
Na	0,697	0,681	0,749	0,751	0,705	0,862	0,741	0,731	0,697	0,691	0,732	0,750	0,731	0,731	0,757	0,749	0,797
K	0,000	0,011	0,011	0,011	0,006	0,000	0,011	0,011	0,006	0,011	0,000	0,011	0,000	0,000	0,011	0,006	0,011
Ba	0,000	0,000	0,000	0,000	0,000	0,000	0,000	0,000	0,000	0,000	0,000	0,000	0,000	0,000	0,000	0,000	0,000
Total	4,995	5,004	5,016	5,026	5,050	5,009	5,023	5,008	4,996	5,014	5,009	5,023	5,002	5,006	5,019	5,006	5,007
Or	0,0	1,1	1,1	1,1	0,5	0,0	1,1	1,1	0,6	1,1	0,0	1,1	0,0	0,0	1,1	0,6	1,1
Ab	70,6	68,6	74,3	73,6	65,2	85,9	72,4	73,2	70,9	68,9	73,0	73,6	73,7	73,7	74,9	74,7	79,9
An	29,4	30,2	24,5	25,3	34,3	14,1	26,5	25,7	28,5	30,0	27,0	25,3	26,3	26,3	24,0	24,7	19,0

Apêndice C.1. Análises químicas pontuais em plagioclásio (continuação).

Amostra	SOS 864	SOS 864	SOS 864	SOS 864	SOS 864	SOS 864	SOS 864	SOS 864	SOS 864	SOS 864	SOS 864	SOS 864	SOS 864	SOS 864	SOS 864	SOS 864	SOS 864
Espectro	73	74	75	76	77	78	79	80	81	82	83	84	85	86	87	89	90
UTM	631485 8909369	631485 8909369	631485 8909369	631485 8909369	631485 8909369	631485 8909369	631485 8909369	631485 8909369	631485 8909369	631485 8909369	631485 8909369	631485 8909369	631485 8909369	631485 8909369	631485 8909369	631485 8909369	631485 8909369
SiO_2	61,6	59,1	59,6	59,7	58,4	59,9	59,9	61,4	61,1	59,8	59,7	59,5	60,3	60,6	60,1	61,7	59,8
Al_2O_3	24,3	26,8	25,9	26,0	27,2	25,8	25,6	24,5	24,6	25,6	25,4	25,6	25,2	25,1	25,4	24,4	25,4
FeO	0,0	0,0	0,0	0,0	0,0	0,0	0,0	0,0	0,0	0,0	0,0	0,5	0,0	0,0	0,0	0,0	0,0
CaO	5,1	6,1	6,5	6,5	5,3	5,9	6,5	5,3	5,8	6,7	6,4	6,2	6,2	6,2	6,2	5,2	6,6
Na_2O	8,9	7,9	7,8	7,9	8,8	7,9	7,9	8,7	8,3	7,7	8,0	8,0	8,3	8,0	8,1	8,6	8,0
K_2O	0,2	0,0	0,2	0,0	0,0	0,5	0,1	0,0	0,1	0,2	0,2	0,2	0,0	0,1	0,2	0,2	0,2
BaO	0,0	0,0	0,0	0,0	0,0	0,0	0,0	0,0	0,0	0,0	0,0	0,0	0,0	0,0	0,0	0,0	0,0
Total	100,1	99,9	100,0	100,1	99,7	100,0	100,0	99,9	99,9	100,0	99,7	100,0	100,0	100,0	100,0	100,1	100,0
Si	2,732	2,630	2,654	2,653	2,609	2,666	2,666	2,725	2,715	2,663	2,667	2,656	2,682	2,693	2,675	2,733	2,666
Al	1,270	1,406	1,359	1,362	1,432	1,354	1,343	1,282	1,289	1,344	1,338	1,347	1,321	1,315	1,333	1,274	1,335
Fe	0,000	0,000	0,000	0,000	0,000	0,000	0,000	0,000	0,000	0,000	0,000	0,019	0,000	0,000	0,000	0,000	0,000
Ca	0,242	0,291	0,310	0,310	0,254	0,281	0,310	0,252	0,276	0,320	0,306	0,297	0,296	0,295	0,296	0,247	0,315
Na	0,765	0,682	0,674	0,681	0,762	0,682	0,682	0,749	0,715	0,665	0,693	0,692	0,716	0,689	0,699	0,739	0,691
K	0,011	0,000	0,011	0,000	0,000	0,028	0,006	0,000	0,006	0,011	0,011	0,011	0,000	0,006	0,011	0,011	0,011
Ba	0,000	0,000	0,000	0,000	0,000	0,000	0,000	0,000	0,000	0,000	0,000	0,000	0,000	0,000	0,000	0,000	0,000
Total	5,021	5,008	5,009	5,006	5,056	5,012	5,006	5,008	5,001	5,003	5,016	5,022	5,015	4,997	5,014	5,005	5,018
Or	1,1	0,0	1,1	0,0	0,0	2,9	0,6	0,0	0,6	1,1	1,1	1,1	0,0	0,6	1,1	1,1	1,1
Ab	75,1	70,1	67,7	68,7	75,0	68,8	68,4	74,8	71,7	66,8	68,6	69,2	70,8	69,6	69,5	74,1	67,9
An	23,8	29,9	31,2	31,3	25,0	28,4	31,1	25,2	27,7	32,1	30,3	29,6	29,2	29,8	29,4	24,8	31,0

Apêndice C.1. Análises químicas pontuais em plagioclásio (continuação).

Amostra	SOS 864	SOS 864	SOS 864	SOS 864	SOS 864	SOS 864	SOS 866	SOS 866	SOS 866	SOS 866	SOS 866	SOS 866	SOS 866	SOS 866	SOS 866	SOS 866	SOS 867A
Espectro	91	92	93	94	95	96	1	2	3	4	5	6	7	44	45	46	4
UTM	631485	631485	631485	631485	631485	631485	630266	630266	630266	630266	630266	630266	630266	630266	630266	630266	629494
	8909369	8909369	8909369	8909369	8909369	8909369	8910933	8910933	8910933	8910933	8910933	8910933	8910933	8910933	8910933	8910933	8911129
SiO_2	57,5	59,6	60,3	61,4	61,7	60,9	60,6	61,5	60,5	62,3	62,3	62,4	66,7	62,5	64,2	62,2	61,8
Al_2O_3	28,0	15,5	25,2	24,6	24,4	24,8	25,4	24,7	25,2	23,9	23,8	23,8	21,0	23,8	22,5	24,1	24,0
FeO	0,5	0,0	0,0	0,0	0,0	0,0	0,0	0,0	0,0	0,0	0,0	0,0	0,0	0,0	0,0	0,0	0,0
CaO	5,8	6,6	6,5	5,3	5,0	5,5	5,8	6,5	6,4	4,8	4,9	4,7	1,5	5,0	3,4	5,1	3,8
Na_2O	7,1	8,1	7,7	8,5	8,8	8,6	8,0	7,1	8,0	8,9	8,8	8,9	10,8	8,7	9,8	8,7	10,2
K_2O	1,2	0,2	0,2	0,2	0,2	0,2	0,3	0,2	0,0	0,0	0,2	0,2	0,0	0,0	0,1	0,0	0,2
BaO	0,0	0,0	0,0	0,0	0,0	0,0	0,0	0,0	0,0	0,0	0,0	0,0	0,0	0,0	0,0	0,0	0,0
Total	100,1	90,0	99,9	100,0	100,1	100,0	100,1	100,0	100,1	99,9	100,0	100,0	100,0	100,0	100,0	100,1	100,0
Si	2,573	2,949	2,684	2,724	2,734	2,707	2,689	2,724	2,686	2,759	2,760	2,763	2,922	2,764	2,831	2,751	2,745
Al	1,477	0,904	1,322	1,286	1,274	1,299	1,329	1,289	1,319	1,248	1,243	1,242	1,084	1,241	1,170	1,256	1,256
Fe	0,019	0,000	0,000	0,000	0,000	0,000	0,000	0,000	0,000	0,000	0,000	0,000	0,000	0,000	0,000	0,000	0,000
Ca	0,278	0,350	0,310	0,252	0,237	0,262	0,276	0,308	0,304	0,228	0,233	0,223	0,070	0,237	0,161	0,242	0,181
Na	0,616	0,777	0,665	0,731	0,756	0,741	0,688	0,610	0,689	0,764	0,756	0,764	0,917	0,746	0,838	0,746	0,878
K	0,068	0,013	0,011	0,011	0,011	0,011	0,017	0,011	0,000	0,000	0,011	0,011	0,000	0,000	0,006	0,000	0,011
Ba	0,000	0,000	0,000	0,000	0,000	0,000	0,000	0,000	0,000	0,000	0,000	0,000	0,000	0,000	0,000	0,000	0,000
Total	5,031	4,993	4,993	5,004	5,013	5,020	4,999	4,942	4,999	4,999	5,002	5,004	4,994	4,988	5,006	4,994	5,072
Or	7,1	1,1	1,2	1,1	1,1	1,1	1,7	1,2	0,0	0,0	1,1	1,1	0,0	0,0	0,6	0,0	1,1
Ab	64,0	68,2	67,4	73,5	75,2	73,1	70,2	65,6	69,3	77,0	75,6	76,5	92,9	75,9	83,4	75,5	82,0
An	28,9	30,7	31,4	25,3	23,6	25,8	28,1	33,2	30,7	23,0	23,3	22,3	7,1	24,1	16,0	24,5	16,9

Apêndice C.1. Análises químicas pontuais em plagioclásio (continuação).

Amostra	SOS 867A	SOS 867A	SOS 867A	SOS 867A	SOS 867A	SOS 867A	SOS 867A	SOS 867A	SOS 867A	SOS 867A	SOS 867A	SOS 867A	SOS 867A	SOS 867A	SOS 867A	SOS 867A	SOS 867A
Espectro	11	14	15	16	17	18	21	22	25	45	46	47	48	49	50	51	52
UTM	629494	629494	629494	629494	629494	629494	629494	629494	629494	629494	629494	629494	629494	629494	629494	629494	629494
	8911129	8911129	8911129	8911129	8911129	8911129	8911129	8911129	8911129	8911129	8911129	8911129	8911129	8911129	8911129	8911129	8911129
SiO_2	65,1	59,5	62,2	61,9	60,0	61,6	63,4	63,5	63,3	65,1	63,6	62,7	63,3	63,1	63,6	63,0	61,8
Al_2O_3	22,1	26,3	23,5	23,9	24,4	23,5	23,3	23,0	23,0	22,1	22,7	22,1	24,3	23,6	23,3	22,8	24,1
FeO	0,0	0,0	0,0	0,0	0,0	0,0	0,0	0,0	0,0	0,0	0,0	0,0	0,0	0,0	0,0	0,0	0,0
CaO	1,5	2,1	2,1	2,8	2,8	2,7	1,7	1,9	3,0	2,2	2,8	2,5	3,2	3,2	2,3	3,0	4,1
Na_2O	11,3	10,7	12,2	11,4	12,8	12,2	11,6	11,6	10,6	10,6	10,9	12,7	9,1	9,7	10,8	11,2	10,0
K_2O	0,0	1,4	0,0	0,0	0,0	0,0	0,0	0,0	0,2	0,0	0,0	0,0	0,0	0,4	0,0	0,0	0,0
BaO	0,0	0,0	0,0	0,0	0,0	0,0	0,0	0,0	0,0	0,0	0,0	0,0	0,0	0,0	0,0	0,0	0,0
Total	100,0	100,0	100,0	100,0	100,0	100,0	100,0	100,0	100,1	100,0	100,0	100,0	99,9	100,0	100,0	100,0	100,0
Si	2,864	2,659	2,764	2,749	2,688	2,746	2,801	2,807	2,800	2,863	2,813	2,795	2,785	2,789	2,806	2,794	2,742
Al	1,146	1,385	1,231	1,251	1,289	1,235	1,213	1,199	1,199	1,146	1,183	1,161	1,260	1,229	1,212	1,192	1,260
Fe	0,000	0,000	0,000	0,000	0,000	0,000	0,000	0,000	0,000	0,000	0,000	0,000	0,000	0,000	0,000	0,000	0,000
Ca	0,071	0,101	0,100	0,133	0,134	0,129	0,080	0,090	0,142	0,104	0,133	0,119	0,151	0,152	0,109	0,143	0,195
Na	0,964	0,927	1,051	0,982	1,112	1,054	0,994	0,994	0,909	0,904	0,935	1,098	0,776	0,831	0,924	0,963	0,860
K	0,000	0,080	0,000	0,000	0,000	0,000	0,000	0,000	0,011	0,000	0,000	0,000	0,000	0,023	0,000	0,000	0,000
Ba	0,000	0,000	0,000	0,000	0,000	0,000	0,000	0,000	0,000	0,000	0,000	0,000	0,000	0,000	0,000	0,000	0,000
Total	5,045	5,152	5,146	5,116	5,223	5,164	5,089	5,090	5,061	5,016	5,063	5,173	4,973	5,023	5,050	5,092	5,058
Or	0,0	7,2	0,0	0,0	0,0	0,0	0,0	0,0	1,1	0,0	0,0	0,0	0,0	2,2	0,0	0,0	0,0
Ab	93,2	83,7	91,3	88,0	89,2	89,1	92,5	91,7	85,6	89,7	87,6	90,2	83,7	82,7	89,5	87,1	81,5
An	6,8	9,1	8,7	12,0	10,8	10,9	7,5	8,3	13,4	10,3	12,4	9,8	16,3	15,1	10,5	12,9	18,5

Apêndice C.1. Análises químicas pontuais em plagioclásio (continuação).

Amostra	SOS 867A	SOS 867A	SOS 867A	SOS 871A	SOS 871A	SOS 871A	SOS 871A	SOS 871A	SOS 871B	SOS 871B	SOS 871B	SOS 871B	SOS 871B	SOS 871B	SOS 871B	SOS 871B	SOS 871B
Espectro	53	54	55	11	12	13	14	27	1[a]	1[b]	2[a]	2[b]	3[a]	3[b]	4[a]	4[b]	5[a]
UTM	629494	629494	629494	628349	628349	628349	628349	628349	628349	628349	628349	628349	628349	628349	628349	628349	628349
	8911129	8911129	8911129	8911047	8911047	8911047	8911047	8911047	8911047	8911047	8911047	8911047	8911047	8911047	8911047	8911047	8911047
SiO_2	64,5	63,6	63,8	60,0	59,2	59,2	61,5	61,1	62,0	56,1	62,1	55,7	62,7	58,3	63,5	61,1	61,3
Al_2O_3	22,3	23,1	22,6	25,7	26,4	25,7	24,5	24,7	24,3	28,3	24,1	28,5	23,7	26,8	24,5	24,7	24,9
FeO	0,0	0,0	0,0	0,0	0,0	0,4	0,0	0,0	0,0	0,0	0,0	0,0	0,0	0,0	0,0	0,0	0,0
CaO	2,6	2,4	2,4	6,1	6,9	4,9	5,1	5,2	4,9	9,5	4,9	9,5	4,4	7,9	5,4	5,5	4,8
Na_2O	10,6	10,8	11,2	8,3	7,5	7,0	8,9	8,7	8,9	6,1	8,9	6,2	9,0	7,0	8,6	8,5	8,5
K_2O	0,0	0,0	0,0	0,0	0,0	0,0	0,0	0,3	0,0	0,0	0,0	0,2	0,2	0,0	0,0	0,2	0,5
BaO	0,0	0,0	0,0	0,0	0,0	0,0	0,0	0,0	0,0	0,0	0,0	0,0	0,0	0,0	0,0	0,0	0,0
Total	100,0	99,9	100,0	100,1	100,0	98,0	100,0	100,0	100,1	100,0	100,0	100,1	100,0	100,0	102,0	100,0	100,0
Si	2,843	2,810	2,820	2,666	2,635	2,670	2,727	2,715	2,743	2,517	2,749	2,502	2,773	2,602	2,754	2,714	2,720
Al	1,159	1,203	1,177	1,346	1,385	1,366	1,281	1,293	1,267	1,496	1,258	1,509	1,236	1,410	1,253	1,293	1,302
Fe	0,000	0,000	0,000	0,000	0,000	0,015	0,000	0,000	0,000	0,000	0,000	0,000	0,000	0,000	0,000	0,000	0,000
Ca	0,123	0,114	0,114	0,290	0,329	0,237	0,242	0,248	0,232	0,457	0,232	0,457	0,209	0,378	0,251	0,262	0,228
Na	0,906	0,925	0,960	0,715	0,647	0,612	0,765	0,749	0,763	0,531	0,764	0,540	0,772	0,606	0,723	0,732	0,731
K	0,000	0,000	0,000	0,000	0,000	0,000	0,000	0,017	0,000	0,000	0,000	0,011	0,011	0,000	0,000	0,011	0,028
Ba	0,000	0,000	0,000	0,000	0,000	0,000	0,000	0,000	0,000	0,000	0,000	0,000	0,000	0,000	0,000	0,000	0,000
Total	5,031	5,051	5,071	5,018	4,996	4,953	5,015	5,022	5,005	5,000	5,004	5,019	5,001	4,996	4,981	5,012	5,009
Or	0,0	0,0	0,0	0,0	0,0	0,0	0,0	1,7	0,0	0,0	0,0	1,1	1,1	0,0	0,0	1,1	2,9
Ab	88,1	89,1	89,4	71,1	66,3	72,1	75,9	73,9	76,7	53,7	76,7	53,5	77,8	61,6	74,2	72,8	74,0
An	11,9	10,9	10,6	28,9	33,7	27,9	24,1	24,4	23,3	46,3	23,3	45,3	21,0	38,4	25,8	26,0	23,1

Apêndice C.1. Análises químicas pontuais em plagioclásio (continuação).

Amostra	SOS 871B	SOS 871B	SOS 871B	SOS 871B	SOS 871B	SOS 871B	SOS 871B	SOS 871B	SOS 871B	SOS 871B	SOS 871B	SOS 871B	SOS 871B	SOS 871B	SOS 871B	SOS 871B	SOS 871B
Espectro	5[b]	6[a]	6[b]	7[a]	7[b]	7[c]	8[a]	8[b]	8[c]	9[a]	9[b]	9[c]	10[a]	10[b]	10[c]	11[a]	11[b]
UTM	628349 8911047	628349 8911047	628349 8911047	628349 8911047	628349 8911047	628349 8911047	628349 8911047	628349 8911047	628349 8911047	628349 8911047	628349 8911047	628349 8911047	628349 8911047	628349 8911047	628349 8911047	628349 8911047	628349 8911047
SiO_2	61,4	62,4	61,1	55,1	60,7	55,1	55,0	61,7	57,0	55,4	61,3	56,3	55,9	55,7	61,8	56,2	55,9
Al_2O_3	24,6	23,8	24,7	28,8	24,7	31,5	29,0	24,2	27,6	28,9	24,1	28,1	28,1	28,2	24,5	28,2	28,5
FeO	0,0	0,0	0,0	0,0	0,0	0,0	0,0	0,0	0,0	0,0	0,0	0,0	0,0	0,0	0,0	0,0	0,0
CaO	5,3	4,6	5,3	10,1	5,1	8,8	10,3	5,0	8,9	9,8	4,7	9,1	9,8	9,7	4,3	9,5	9,6
Na_2O	8,6	9,0	8,7	6,0	9,4	4,6	5,7	8,9	6,5	5,9	9,6	6,4	6,2	6,5	9,3	6,2	6,0
K_2O	0,0	0,2	0,2	0,0	0,0	0,0	0,0	0,3	0,0	0,0	0,3	0,0	0,0	0,0	0,0	0,0	0,0
BaO	0,0	0,0	0,0	0,0	0,0	0,0	0,0	0,0	0,0	0,0	0,0	0,0	0,0	0,0	0,0	0,0	0,0
Total	99,9	100,0	100,0	100,0	99,9	100,0	100,0	100,1	100,0	100,0	100,0	99,9	100,0	100,1	99,9	100,1	100,0
Si	2,724	2,763	2,714	2,480	2,703	2,452	2,474	2,737	2,553	2,488	2,728	2,527	2,512	2,504	2,738	2,519	2,508
Al	1,286	1,242	1,293	1,528	1,296	1,652	1,538	1,265	1,457	1,530	1,264	1,487	1,489	1,494	1,280	1,490	1,507
Fe	0,000	0,000	0,000	0,000	0,000	0,000	0,000	0,000	0,000	0,000	0,000	0,000	0,000	0,000	0,000	0,000	0,000
Ca	0,252	0,218	0,252	0,487	0,243	0,420	0,496	0,238	0,427	0,472	0,224	0,438	0,472	0,467	0,204	0,456	0,462
Na	0,740	0,773	0,749	0,524	0,812	0,397	0,497	0,765	0,564	0,514	0,828	0,557	0,540	0,567	0,799	0,539	0,522
K	0,000	0,011	0,011	0,000	0,000	0,000	0,000	0,017	0,000	0,000	0,017	0,000	0,000	0,000	0,000	0,000	0,000
Ba	0,000	0,000	0,000	0,000	0,000	0,000	0,000	0,000	0,000	0,000	0,000	0,000	0,000	0,000	0,000	0,000	0,000
Total	5,002	5,008	5,020	5,018	5,055	4,921	5,006	5,022	5,001	5,004	5,062	5,008	5,013	5,032	5,021	5,005	4,999
Or	0,0	1,1	1,1	0,0	0,0	0,0	0,0	1,7	0,0	0,0	1,6	0,0	0,0	0,0	0,0	0,0	0,0
Ab	74,6	77,1	74,0	51,8	76,9	48,6	50,0	75,0	56,9	52,1	77,5	56,0	53,4	54,8	79,6	54,1	53,1
An	25,4	21,8	24,9	48,2	23,1	51,4	50,0	23,3	43,1	47,9	21,0	44,0	46,6	45,2	20,4	45,9	46,9

Apêndice C.1. Análises químicas pontuais em plagioclásio (continuação).

Amostra	SOS 871B	SOS 871B	SOS 871B	SOS 871B	SOS 871B	SOS 871B	SOS 871B	SOS 871B	SOS 871B	SOS 871B	SOS 871B	SOS 871B	SOS 871B	SOS 871B	SOS 871B	SOS 871B	SOS 871B
Espectro	11c	12a	12b	12c	13a	13b	13c	14a	14b	14c	15a	15b	15c	15d	16a	16b	16c
UTM	628349 8911047	628349 8911047	628349 8911047	628349 8911047	628349 8911047	628349 8911047	628349 8911047	628349 8911047	628349 8911047	628349 8911047	628349 8911047	628349 8911047	628349 8911047	628349 8911047	628349 8911047	628349 8911047	628349 8911047
SiO_2	67,5	55,9	56,4	62,1	58,2	55,7	61,7	59,9	55,8	65,4	63,8	60,8	56,0	62,4	62,7	61,5	58,4
Al_2O_3	25,8	28,4	28,5	24,1	26,8	28,0	24,2	25,4	28,3	21,8	23,6	24,7	28,2	23,9	25,8	24,1	26,6
FeO	0,0	0,0	0,0	0,0	0,0	0,0	0,0	0,0	0,0	0,0	0,0	0,0	0,0	0,0	0,0	0,0	0,0
CaO	1,6	9,6	8,3	4,7	7,9	9,2	4,8	6,5	9,5	2,3	1,3	6,0	9,5	4,7	2,1	5,5	7,3
Na_2O	5,0	6,1	6,1	8,9	7,1	7,1	9,1	8,1	6,3	10,4	9,6	8,3	6,2	9,0	7,3	8,7	7,5
K_2O	0,0	0,0	0,7	0,2	0,0	0,0	0,2	0,2	0,1	0,2	1,7	0,1	0,0	0,0	2,1	0,2	0,2
BaO	0,0	0,0	0,0	0,0	0,0	0,0	0,0	0,0	0,0	0,0	0,0	0,0	0,0	0,0	0,0	0,0	0,0
Total	99,9	100,0	100,0	100,0	100,0	100,0	100,0	100,1	100,0	100,1	100,0	99,9	99,9	100,0	100,0	100,0	100,0
Si	2,885	2,509	2,529	2,751	2,599	2,508	2,738	2,667	2,508	2,874	2,818	2,705	2,516	2,761	2,761	2,732	2,609
Al	1,300	1,503	1,506	1,258	1,411	1,486	1,266	1,333	1,499	1,129	1,229	1,295	1,493	1,246	1,339	1,262	1,401
Fe	0,000	0,000	0,000	0,000	0,000	0,000	0,000	0,000	0,000	0,000	0,000	0,000	0,000	0,000	0,000	0,000	0,000
Ca	0,073	0,462	0,399	0,223	0,378	0,444	0,228	0,310	0,458	0,108	0,062	0,286	0,457	0,223	0,099	0,262	0,349
Na	0,414	0,531	0,530	0,764	0,615	0,620	0,783	0,699	0,549	0,886	0,822	0,716	0,540	0,772	0,623	0,749	0,650
K	0,000	0,000	0,040	0,011	0,000	0,000	0,011	0,011	0,006	0,011	0,096	0,006	0,000	0,000	0,118	0,011	0,011
Ba	0,000	0,000	0,000	0,000	0,000	0,000	0,000	0,000	0,000	0,000	0,000	0,000	0,000	0,000	0,000	0,000	0,000
Total	4,672	5,005	5,004	5,008	5,003	5,059	5,026	5,021	5,020	5,010	5,026	5,008	5,007	5,002	4,940	5,017	5,021
Or	0,0	0,0	4,1	1,1	0,0	0,0	1,1	1,1	0,6	1,1	9,8	0,6	0,0	0,0	14,0	1,1	1,1
Ab	85,0	53,5	54,7	76,5	61,9	58,3	76,6	68,5	54,2	88,1	83,9	71,1	54,1	77,6	74,2	73,3	64,3
An	15,0	46,5	41,1	22,3	38,1	41,7	22,3	30,4	45,2	10,8	6,3	28,4	45,9	22,4	11,8	25,6	34,6

Apêndice C.1. Análises químicas pontuais em plagioclásio (continuação).

Amostra	SOS 871B	SOS 871B	SOS 871B	SOS 871B	SOS 871B	SOS 871B	SOS 871B	SOS 871B	SOS 871B	SOS 871B	SOS 871B	SOS 871B	SOS 871B	SOS 871B	SOS 871B	SOS 871B	SOS 871B
Espectro	16[d]	17[a]	17[b]	17[c]	17[d]	18[a]	18[b]	19[a]	19[b]	19[c]	19[d]	20[a]	20[b]	20[c]	20[d]	21[a]	21[b]
UTM	628349	628349	628349	628349	628349	628349	628349	628349	628349	628349	628349	628349	628349	628349	628349	628349	628349
	8911047	8911047	8911047	8911047	8911047	8911047	8911047	8911047	8911047	8911047	8911047	8911047	8911047	8911047	8911047	8911047	8911047
SiO_2	62,4	61,7	60,2	60,6	62,7	60,3	61,2	61,5	55,5	60,8	61,4	61,7	55,6	60,4	61,3	55,1	58,9
Al_2O_3	23,8	25,3	25,9	25,0	23,4	25,7	24,8	25,0	26,3	25,1	24,4	24,5	28,5	25,1	24,4	29,0	26,2
FeO	0,0	0,0	0,0	0,0	0,0	0,0	0,0	0,0	0,0	0,0	0,0	0,0	0,0	0,0	0,0	0,0	0,0
CaO	4,6	2,1	5,5	5,9	4,3	5,0	5,5	4,5	11,8	6,0	5,4	5,1	9,9	6,0	5,5	10,1	7,1
Na_2O	9,1	8,7	8,5	8,3	9,3	8,2	8,3	8,5	6,3	8,1	8,6	8,7	5,9	8,4	8,6	5,6	7,7
K_2O	0,2	2,3	0,0	0,2	0,2	0,7	0,2	0,5	0,2	0,0	0,2	0,0	0,0	0,2	0,3	0,2	0,1
BaO	0,0	0,0	0,0	0,0	0,0	0,0	0,0	0,0	0,0	0,0	0,0	0,0	0,0	0,0	0,0	0,0	0,0
Total	100,1	100,1	100,1	100,0	99,9	99,9	100,0	100,0	100,1	100,0	100,0	100,0	99,9	100,1	100,1	100,0	100,0
Si	2,762	2,738	2,671	2,695	2,779	2,683	2,715	2,725	2,517	2,698	2,726	2,733	2,500	2,686	2,722	2,478	2,629
Al	1,242	1,323	1,354	1,310	1,222	1,348	1,297	1,305	1,406	1,313	1,277	1,279	1,510	1,316	1,277	1,538	1,378
Fe	0,000	0,000	0,000	0,000	0,000	0,000	0,000	0,000	0,000	0,000	0,000	0,000	0,000	0,000	0,000	0,000	0,000
Ca	0,218	0,100	0,261	0,281	0,204	0,238	0,261	0,214	0,573	0,285	0,257	0,242	0,477	0,286	0,262	0,487	0,340
Na	0,781	0,749	0,731	0,716	0,799	0,707	0,714	0,730	0,554	0,697	0,740	0,747	0,514	0,724	0,740	0,488	0,666
K	0,011	0,130	0,000	0,011	0,011	0,040	0,011	0,028	0,012	0,000	0,011	0,000	0,000	0,011	0,017	0,011	0,006
Ba	0,000	0,000	0,000	0,000	0,000	0,000	0,000	0,000	0,000	0,000	0,000	0,000	0,000	0,000	0,000	0,000	0,000
Total	5,014	5,040	5,018	5,013	5,015	5,017	4,999	5,002	5,062	4,994	5,011	5,001	5,002	5,024	5,018	5,003	5,018
Or	1,1	13,3	0,0	1,1	1,1	4,0	1,1	2,9	1,0	0,0	1,1	0,0	0,0	1,1	1,7	1,2	0,6
Ab	77,3	76,5	73,7	71,0	78,8	71,8	72,4	75,1	48,6	71,0	73,4	75,5	51,9	70,9	72,7	49,5	65,9
An	21,6	10,2	26,3	27,9	20,1	24,2	26,5	22,0	50,3	29,0	25,5	24,5	48,1	28,0	25,7	49,3	33,6

Apêndice C.1. Análises químicas pontuais em plagioclásio (continuação).

Amostra	SOS 871B	SOS 871B	SOS 871B	SOS 871B	SOS 871B	SOS 871B	SOS 871B	SOS 871B	SOS 871B	SOS 871B	SOS 871B	SOS 871B	SOS 871B	SOS 871B	SOS 871B	SOS 871B	SOS 871B
Espectro	21[c]	22[a]	22[b]	22[c]	23[a]	23[b]	23[c]	24[a]	24[b]	25[a]	25[b]	25[c]	26[a]	26[b]	26[c]	27	28[a]
UTM	628349	628349	628349	628349	628349	628349	628349	628349	628349	628349	628349	628349	628349	628349	628349	628349	628349
	8911047	8911047	8911047	8911047	8911047	8911047	8911047	8911047	8911047	8911047	8911047	8911047	8911047	8911047	8911047	8911047	8911047
SiO_2	60,7	54,8	58,0	60,2	56,3	60,3	60,4	56,8	60,8	59,4	55,0	60,9	59,3	55,2	61,9	61,8	62,2
Al_2O_3	24,8	30,9	26,8	25,3	27,9	25,2	28,2	27,7	24,9	25,8	29,0	24,8	25,4	28,9	25,4	24,1	23,8
FeO	0,0	0,0	0,0	0,0	0,0	0,0	0,0	0,0	0,0	0,0	0,0	0,0	0,0	0,0	0,0	0,0	0,0
CaO	5,9	8,7	7,8	6,2	9,4	6,2	5,2	9,0	6,0	7,1	10,3	5,6	6,8	10,3	4,3	5,0	4,9
Na_2O	8,4	5,6	7,3	8,4	6,2	8,1	6,2	6,6	8,1	7,7	5,7	8,5	8,0	5,7	8,4	9,0	9,1
K_2O	0,2	0,0	0,0	0,0	0,1	0,3	0,0	0,0	0,1	0,0	0,0	0,2	0,2	0,0	0,0	0,1	0,0
BaO	0,0	0,0	0,0	0,0	0,0	0,0	0,0	0,0	0,0	0,0	0,0	0,0	0,0	0,0	0,0	0,0	0,0
Total	100,0	100,0	99,9	100,1	99,9	100,1	100,0	100,1	99,9	100,0	100,0	100,0	99,7	100,1	100,0	100,0	100,0
Si	2,700	2,449	2,595	2,677	2,529	2,682	2,651	2,544	2,703	2,648	2,474	2,706	2,655	2,480	2,729	2,741	2,756
Al	1,300	1,628	1,413	1,326	1,477	1,321	1,459	1,462	1,305	1,355	1,538	1,299	1,340	1,530	1,320	1,260	1,243
Fe	0,000	0,000	0,000	0,000	0,000	0,000	0,000	0,000	0,000	0,000	0,000	0,000	0,000	0,000	0,000	0,000	0,000
Ca	0,281	0,417	0,374	0,295	0,452	0,296	0,245	0,432	0,286	0,339	0,496	0,267	0,326	0,496	0,203	0,238	0,233
Na	0,725	0,485	0,633	0,724	0,540	0,699	0,528	0,573	0,698	0,665	0,497	0,732	0,695	0,497	0,718	0,774	0,782
K	0,011	0,000	0,000	0,000	0,006	0,017	0,000	0,000	0,006	0,000	0,000	0,011	0,011	0,000	0,000	0,006	0,000
Ba	0,000	0,000	0,000	0,000	0,000	0,000	0,000	0,000	0,000	0,000	0,000	0,000	0,000	0,000	0,000	0,000	0,000
Total	5,018	4,979	5,015	5,022	5,005	5,015	4,883	5,011	4,997	5,007	5,006	5,016	5,028	5,003	4,970	5,019	5,013
Or	1,1	0,0	0,0	0,0	0,6	1,7	0,0	0,0	0,6	0,0	0,0	1,1	1,1	0,0	0,0	0,6	0,0
Ab	71,2	53,8	62,9	71,0	54,1	69,1	68,3	57,0	70,5	66,2	50,0	72,5	67,3	50,0	77,9	76,1	77,1
An	27,6	46,2	37,1	29,0	45,3	29,2	31,7	43,0	28,9	33,8	50,0	26,4	31,6	50,0	22,1	23,4	22,9

Apêndice C.1. Análises químicas pontuais em plagioclásio (continuação).

Amostra	SOS 871B	SOS 871B	SOS 871B	SOS 871B	SOS 871B	SOS 871B	SOS 871B	SOS 871B	SOS 871B	SOS 871B	SOS 871B	SOS 871B	SOS 871B	SOS 871B	SOS 871B	SOS 871B	SOS 871B
Espectro	28[b]	29[a]	29[b]	31[a]	31[b]	31[c]	32[a]	32[b]	33[a]	33[b]	34[a]	34[b]	35[a]	35[b]	36[a]	36[b]	36[c]
UTM	628349	628349	628349	628349	628349	628349	628349	628349	628349	628349	628349	628349	628349	628349	628349	628349	628349
	8911047	8911047	8911047	8911047	8911047	8911047	8911047	8911047	8911047	8911047	8911047	8911047	8911047	8911047	8911047	8911047	8911047
SiO_2	57,2	62,2	61,6	62,6	55,2	61,0	54,6	61,5	55,7	61,8	55,9	61,9	61,1	62,0	61,8	62,2	61,8
Al_2O_3	27,6	24,1	24,1	23,8	28,6	24,9	28,0	24,2	28,2	24,2	28,5	24,2	24,8	24,2	24,4	24,0	24,6
FeO	0,0	0,0	0,0	0,3	0,0	0,0	0,0	0,0	0,0	0,0	0,0	0,0	0,0	0,0	0,0	0,0	0,0
CaO	8,6	4,8	5,3	4,3	10,2	5,7	10,5	5,2	9,9	5,2	9,6	5,2	5,6	4,6	5,2	4,7	4,6
Na_2O	6,7	8,9	8,8	9,1	6,0	8,4	6,7	8,8	6,2	8,6	6,1	8,7	8,6	8,9	8,6	9,0	8,7
K_2O	0,0	0,0	0,3	0,0	0,0	0,0	0,0	0,2	0,0	0,1	0,0	0,0	0,0	0,3	0,0	0,0	0,3
BaO	0,0	0,0	0,0	0,0	0,0	0,0	0,0	0,0	0,0	0,0	0,0	0,0	0,0	0,0	0,0	0,0	0,0
Total	100,1	100,0	100,1	100,1	100,0	100,0	99,8	99,9	100,0	99,9	100,1	100,0	100,1	100,0	100,0	99,9	100,0
Si	2,558	2,752	2,735	2,767	2,485	2,707	2,475	2,733	2,505	2,741	2,507	2,742	2,710	2,747	2,737	2,755	2,737
Al	1,455	1,257	1,261	1,240	1,518	1,302	1,496	1,268	1,495	1,265	1,506	1,264	1,296	1,264	1,274	1,253	1,284
Fe	0,000	0,000	0,000	0,011	0,000	0,000	0,000	0,000	0,000	0,000	0,000	0,000	0,000	0,000	0,000	0,000	0,000
Ca	0,412	0,228	0,252	0,204	0,492	0,271	0,510	0,248	0,477	0,247	0,461	0,247	0,266	0,218	0,247	0,223	0,218
Na	0,581	0,764	0,757	0,780	0,524	0,723	0,589	0,758	0,541	0,740	0,530	0,747	0,740	0,765	0,738	0,773	0,747
K	0,000	0,000	0,017	0,000	0,000	0,000	0,000	0,011	0,000	0,006	0,000	0,000	0,000	0,017	0,000	0,000	0,017
Ba	0,000	0,000	0,000	0,000	0,000	0,000	0,000	0,000	0,000	0,000	0,000	0,000	0,000	0,000	0,000	0,000	0,000
Total	5,005	5,001	5,022	5,002	5,018	5,003	5,071	5,018	5,018	4,999	5,005	5,000	5,012	5,011	4,996	5,005	5,003
Or	0,0	0,0	1,7	0,0	0,0	0,0	0,0	1,1	0,0	0,6	0,0	0,0	0,0	1,7	0,0	0,0	1,7
Ab	58,5	77,0	73,8	79,3	51,6	72,7	53,6	74,5	53,1	74,5	53,5	75,2	73,5	76,5	75,0	77,6	76,1
An	41,5	23,0	24,6	20,7	48,4	27,3	46,4	24,3	46,9	24,9	46,5	24,8	26,5	21,8	25,0	22,4	22,2

Apêndice C.1. Análises químicas pontuais em plagioclásio (continuação).

Amostra	SOS 871B	SOS 871B	SOS 871B	SOS 871B	SOS 871B	SOS 871B	SOS 871B	SOS 871B	SOS 871B	SOS 871B	SOS 871B	SOS 871B	SOS 871B	SOS 871B	SOS 871B	SOS 871B	SOS 871B
Espectro	37[a]	37[b]	37[c]	38[a]	38[b]	39[a]	39[b]	40[a]	40[b]	41[a]	41[b]	42[a]	42[b]	43	44[a]	44[b]	45[a]
UTM	628349	628349	628349	628349	628349	628349	628349	628349	628349	628349	628349	628349	628349	628349	628349	628349	628349
	8911047	8911047	8911047	8911047	8911047	8911047	8911047	8911047	8911047	8911047	8911047	8911047	8911047	8911047	8911047	8911047	8911047
SiO_2	61,6	62,1	62,3	60,0	62,0	60,8	62,1	62,1	62,7	61,4	63,1	55,5	59,2	55,8	55,9	61,9	56,3
Al_2O_3	24,4	23,9	23,7	25,2	23,8	24,9	24,0	24,1	23,7	24,3	23,4	28,1	28,8	28,5	28,3	28,8	27,9
FeO	0,0	0,0	0,0	0,0	0,3	0,0	0,0	0,0	0,0	0,0	0,0	0,4	0,0	0,0	0,0	0,0	0,4
CaO	5,4	4,8	4,5	6,9	4,6	5,4	4,7	4,9	4,4	5,3	3,8	9,6	4,2	9,6	9,6	4,2	9,1
Na_2O	8,6	9,0	9,3	7,9	9,2	8,8	9,1	9,0	9,0	9,0	9,5	6,1	7,8	6,0	6,2	5,1	6,3
K_2O	0,0	0,2	0,1	0,0	0,2	0,1	0,2	0,0	0,2	0,0	0,2	0,3	0,0	0,1	0,0	0,0	0,0
BaO	0,0	0,0	0,0	0,0	0,0	0,0	0,0	0,0	0,0	0,0	0,0	0,0	0,0	0,0	0,0	0,0	0,0
Total	100,0	100,0	99,9	100,0	100,1	100,0	100,1	100,1	100,0	100,0	100,0	100,0	100,0	100,0	100,0	100,0	100,0
Si	2,731	2,753	2,763	2,673	2,751	2,702	2,751	2,748	2,773	2,726	2,789	2,503	2,611	2,506	2,510	2,689	2,529
Al	1,275	1,249	1,239	1,323	1,245	1,304	1,253	1,257	1,236	1,272	1,219	1,494	1,497	1,508	1,498	1,475	1,477
Fe	0,000	0,000	0,000	0,000	0,011	0,000	0,000	0,000	0,000	0,000	0,000	0,015	0,000	0,000	0,000	0,000	0,015
Ca	0,257	0,228	0,214	0,329	0,219	0,257	0,223	0,232	0,209	0,252	0,180	0,464	0,198	0,462	0,462	0,195	0,438
Na	0,739	0,774	0,800	0,682	0,791	0,758	0,782	0,772	0,772	0,775	0,814	0,533	0,667	0,522	0,540	0,430	0,549
K	0,000	0,011	0,006	0,000	0,011	0,006	0,011	0,000	0,011	0,000	0,011	0,017	0,000	0,006	0,000	0,000	0,000
Ba	0,000	0,000	0,000	0,000	0,000	0,000	0,000	0,000	0,000	0,000	0,000	0,000	0,000	0,000	0,000	0,000	0,000
Total	5,001	5,015	5,021	5,007	5,028	5,028	5,019	5,010	5,001	5,025	5,014	5,026	4,974	5,004	5,010	4,789	5,007
Or	0,0	1,1	0,6	0,0	1,1	0,6	1,1	0,0	1,1	0,0	1,1	1,7	0,0	0,6	0,0	0,0	0,0
Ab	74,2	76,4	78,5	67,4	77,5	74,3	76,9	76,9	77,8	75,4	81,0	52,6	77,1	52,8	53,9	68,7	55,6
An	25,8	22,5	21,0	32,6	21,4	25,2	22,0	23,1	21,0	24,6	17,9	45,7	22,9	46,7	46,1	31,3	44,4

Apêndice C.1. Análises químicas pontuais em plagioclásio (continuação).

Amostra	SOS 871B	SOS 871B	SOS 871B	SOS 871B	SOS 871B	SOS 871B	SOS 871B	SOS 871B	SOS 871B	SOS 871B	SOS 871B	SOS 871B	SOS 871B	SOS 871B	SOS 871B	SOS 871B	SOS 871B
Espectro	45[b]	46[a]	46[b]	47[a]	47[b]	48[a]	48[b]	49[a]	49[b]	50[a]	50[b]	51[a]	51[b]	52[a]	52[b]	53[a]	53[b]
UTM	628349	628349	628349	628349	628349	628349	628349	628349	628349	628349	628349	628349	628349	628349	628349	628349	628349
	8911047	8911047	8911047	8911047	8911047	8911047	8911047	8911047	8911047	8911047	8911047	8911047	8911047	8911047	8911047	8911047	8911047
SiO_2	59,6	56,1	56,7	56,5	60,1	58,1	60,8	59,7	61,6	57,6	57,6	61,5	56,0	61,6	58,3	68,4	61,9
Al_2O_3	24,9	27,8	27,9	27,8	25,5	26,7	24,8	27,1	24,5	27,8	24,4	24,4	28,3	24,3	26,6	19,8	24,2
FeO	0,6	0,0	0,0	0,0	0,0	0,0	0,0	0,0	0,0	0,0	0,0	0,0	0,0	0,0	0,0	0,0	0,0
CaO	6,8	9,5	9,1	9,3	6,4	8,1	5,7	7,6	5,3	8,3	10,1	5,3	9,1	5,0	7,5	2,3	5,0
Na_2O	7,9	6,4	6,3	6,3	7,9	7,1	8,7	5,7	8,7	6,3	7,9	8,7	6,4	8,9	7,5	9,5	8,7
K_2O	0,3	0,2	0,0	0,0	0,0	0,0	0,0	0,0	0,0	0,0	0,0	0,0	0,1	0,2	0,2	0,0	0,2
BaO	0,0	0,0	0,0	0,0	0,0	0,0	0,0	0,0	0,0	0,0	0,0	0,0	0,0	0,0	0,0	0,0	0,0
Total	100,1	100,0	100,0	99,9	99,9	100,0	100,0	100,1	100,1	100,0	100,0	99,9	99,9	100,0	100,1	100,0	100,0
Si	2,666	2,523	2,540	2,536	2,674	2,597	2,702	2,639	2,728	2,569	2,606	2,729	2,516	2,734	2,605	2,982	2,743
Al	1,313	1,474	1,473	1,471	1,337	1,407	1,299	1,412	1,279	1,462	1,301	1,276	1,499	1,271	1,401	1,018	1,264
Fe	0,022	0,000	0,000	0,000	0,000	0,000	0,000	0,000	0,000	0,000	0,000	0,000	0,000	0,000	0,000	0,000	0,000
Ca	0,326	0,458	0,437	0,447	0,305	0,388	0,271	0,360	0,252	0,397	0,490	0,252	0,438	0,238	0,359	0,107	0,237
Na	0,685	0,558	0,547	0,548	0,682	0,615	0,750	0,489	0,747	0,545	0,693	0,749	0,558	0,766	0,650	0,803	0,748
K	0,017	0,011	0,000	0,000	0,000	0,000	0,000	0,000	0,000	0,000	0,000	0,000	0,006	0,011	0,011	0,000	0,011
Ba	0,000	0,000	0,000	0,000	0,000	0,000	0,000	0,000	0,000	0,000	0,000	0,000	0,000	0,000	0,000	0,000	0,000
Total	5,029	5,025	4,997	5,003	4,998	5,007	5,023	4,899	5,006	4,972	5,090	5,007	5,016	5,019	5,026	4,910	5,004
Or	1,7	1,1	0,0	0,0	0,0	0,0	0,0	0,0	0,0	0,0	0,0	0,0	0,6	1,1	1,1	0,0	1,1
Ab	66,6	54,3	55,6	55,1	69,1	61,3	73,4	57,6	74,8	57,9	58,6	74,8	55,7	75,5	63,7	88,2	75,0
An	31,7	44,6	44,4	44,9	30,9	38,7	26,6	42,4	25,2	42,1	41,4	25,2	43,7	23,4	35,2	11,8	23,8

Apêndice C.1. Análises químicas pontuais em plagioclásio (continuação).

Amostra	SOS 871B	SOS 871B	SOS 871B	SOS 871B	SOS 871B	SOS 871B	SOS 871B	SOS 871B	SOS 871B	SOS 871B	SOS 871B	SOS 871B	SOS 871B	SOS 871B	SOS 871B	SOS 871B	SOS 871B
Espectro	54[a]	54[b]	55[a]	55[b]	56[a]	56[b]	57[a]	57[b]	58[a]	58[b]	59[a]	59[b]	60[a]	60[b]	61[a]	61[b]	62
UTM	628349	628349	628349	628349	628349	628349	628349	628349	628349	628349	628349	628349	628349	628349	628349	628349	628349
	8911047	8911047	8911047	8911047	8911047	8911047	8911047	8911047	8911047	8911047	8911047	8911047	8911047	8911047	8911047	8911047	8911047
SiO_2	61,4	62,2	56,9	61,8	56,0	62,1	58,4	62,2	59,0	62,0	59,7	64,3	59,1	57,6	58,4	60,5	57,6
Al_2O_3	24,4	23,9	27,5	24,3	28,3	24,2	26,4	24,0	26,1	24,0	25,4	23,9	25,9	29,5	26,3	26,7	27,1
FeO	0,0	0,0	0,0	0,0	0,0	0,0	0,0	0,0	0,0	0,0	0,0	0,0	0,0	0,0	0,0	0,0	0,0
CaO	5,5	4,8	8,8	4,9	9,5	4,9	7,8	4,8	7,0	4,7	6,8	2,2	7,1	7,1	7,7	5,4	8,4
Na_2O	8,5	8,9	6,8	8,9	6,1	8,7	7,4	9,0	7,6	9,1	7,8	9,6	7,6	5,8	7,4	7,5	6,9
K_2O	0,2	0,2	0,0	0,2	0,0	0,2	0,0	0,0	0,3	0,2	0,2	0,0	0,2	0,0	0,2	0,0	0,0
BaO	0,0	0,0	0,0	0,0	0,0	0,0	0,0	0,0	0,0	0,0	0,0	0,0	0,0	0,0	0,0	0,0	0,0
Total	100,0	100,0	100,0	100,1	99,9	100,1	100,0	100,0	100,0	100,0	99,9	100,0	99,9	100,0	100,0	100,1	100,0
Si	2,726	2,756	2,551	2,738	2,515	2,748	2,610	2,754	2,634	2,749	2,664	2,818	2,640	2,552	2,612	2,670	2,577
Al	1,277	1,248	1,453	1,269	1,498	1,262	1,391	1,252	1,373	1,254	1,336	1,235	1,364	1,540	1,387	1,389	1,429
Fe	0,000	0,000	0,000	0,000	0,000	0,000	0,000	0,000	0,000	0,000	0,000	0,000	0,000	0,000	0,000	0,000	0,000
Ca	0,262	0,228	0,423	0,233	0,457	0,232	0,374	0,228	0,335	0,223	0,325	0,103	0,340	0,337	0,369	0,255	0,403
Na	0,732	0,765	0,591	0,765	0,531	0,746	0,641	0,773	0,658	0,782	0,675	0,816	0,658	0,498	0,642	0,642	0,599
K	0,011	0,011	0,000	0,011	0,000	0,011	0,000	0,000	0,017	0,011	0,011	0,000	0,011	0,000	0,011	0,000	0,000
Ba	0,000	0,000	0,000	0,000	0,000	0,000	0,000	0,000	0,000	0,000	0,000	0,000	0,000	0,000	0,000	0,000	0,000
Total	5,007	5,008	5,018	5,015	5,002	5,000	5,015	5,006	5,017	5,021	5,011	4,972	5,013	4,927	5,021	4,956	5,008
Or	1,1	1,1	0,0	1,1	0,0	1,1	0,0	0,0	1,7	1,1	1,1	0,0	1,1	0,0	1,1	0,0	0,0
Ab	72,8	76,2	58,3	75,8	53,7	75,4	63,2	77,2	65,1	76,9	66,7	88,8	65,2	59,6	62,8	71,5	59,8
An	26,0	22,7	41,7	23,1	46,3	23,5	36,8	22,8	33,2	22,0	32,1	11,2	33,7	40,4	36,1	28,5	40,2

Apêndice C.1. Análises químicas pontuais em plagioclásio (continuação).

Amostra	SOS 871B	SOS 871B	SOS 871B	SOS 871B	SOS 871B	SOS 871B	SOS 871B	SOS 871B	SOS 871B	SOS 871B	SOS 871B	SOS 871B	SOS 871B	SOS 871B	SOS 871B	SOS 871B	SOS 871B
Espectro	63[a]	63[b]	64[a]	64[b]	65[a]	65[b]	66[a]	66[b]	67[a]	67[b]	68[a]	68[b]	69[a]	69[b]	70[a]	70[b]	71[a]
UTM	628349	628349	628349	628349	628349	628349	628349	628349	628349	628349	628349	628349	628349	628349	628349	628349	628349
	8911047	8911047	8911047	8911047	8911047	8911047	8911047	8911047	8911047	8911047	8911047	8911047	8911047	8911047	8911047	8911047	8911047
SiO_2	55,8	55,9	55,2	57,6	56,8	59,9	59,2	58,6	56,1	58,4	62,4	56,3	61,4	55,6	55,8	56,1	55,1
Al_2O_3	28,5	28,1	28,9	27,1	27,9	25,7	26,0	26,6	30,5	26,0	23,6	28,0	24,6	28,4	28,4	28,4	28,8
FeO	0,0	0,0	0,0	0,0	0,0	0,0	0,0	0,0	0,0	0,0	0,0	0,0	0,0	0,0	0,0	0,0	0,0
CaO	9,6	8,8	10,1	8,3	8,2	6,9	7,0	6,9	5,9	7,7	4,7	9,0	5,4	9,6	9,9	9,5	10,2
Na_2O	5,6	7,0	5,8	6,9	6,4	7,6	7,8	7,3	7,1	7,9	9,1	6,6	8,6	6,2	5,9	5,9	5,9
K_2O	0,2	0,1	0,0	0,1	0,7	0,0	0,0	0,7	0,3	0,0	0,1	0,0	0,0	0,1	0,0	0,0	0,0
BaO	0,0	0,0	0,0	0,0	0,0	0,0	0,0	0,0	0,0	0,0	0,0	0,0	0,0	0,0	0,0	0,0	0,0
Total	99,7	99,9	100,0	100,0	100,0	100,1	100,0	100,1	99,9	100,0	99,9	99,9	100,0	99,9	100,0	99,9	100,0
Si	2,510	2,516	2,482	2,578	2,548	2,662	2,639	2,617	2,500	2,615	2,766	2,528	2,723	2,502	2,506	2,517	2,480
Al	1,511	1,491	1,531	1,430	1,475	1,346	1,366	1,400	1,602	1,372	1,233	1,482	1,286	1,506	1,503	1,502	1,528
Fe	0,000	0,000	0,000	0,000	0,000	0,000	0,000	0,000	0,000	0,000	0,000	0,000	0,000	0,000	0,000	0,000	0,000
Ca	0,463	0,424	0,487	0,398	0,394	0,329	0,334	0,330	0,282	0,369	0,223	0,433	0,257	0,463	0,476	0,457	0,492
Na	0,488	0,611	0,506	0,599	0,557	0,655	0,674	0,632	0,613	0,686	0,782	0,575	0,739	0,541	0,514	0,513	0,515
K	0,011	0,006	0,000	0,006	0,040	0,000	0,000	0,040	0,017	0,000	0,006	0,000	0,000	0,006	0,000	0,000	0,000
Ba	0,000	0,000	0,000	0,000	0,000	0,000	0,000	0,000	0,000	0,000	0,000	0,000	0,000	0,000	0,000	0,000	0,000
Total	4,984	5,047	5,005	5,010	5,013	4,992	5,015	5,019	5,014	5,042	5,011	5,018	5,004	5,018	4,999	4,989	5,014
Or	1,2	0,6	0,0	0,6	4,0	0,0	0,0	4,0	1,9	0,0	0,6	0,0	0,0	0,6	0,0	0,0	0,0
Ab	50,7	58,7	51,0	59,7	56,2	66,6	66,8	63,1	67,2	65,0	77,4	57,0	74,2	53,6	51,9	52,9	51,1
An	48,1	40,8	49,0	39,7	39,8	33,4	33,2	32,9	30,9	35,0	22,1	43,0	25,8	45,8	48,1	47,1	48,9

Apêndice C.1. Análises químicas pontuais em plagioclásio (continuação).

Amostra	SOS 871B	SOS 871B	SOS 871B	SOS 871B	SOS 871B	SOS 871B	SOS 871B	SOS 871B	SOS 871B	SOS 871B	SOS 871B	SOS 871B	SOS 871B	SOS 871B	SOS 871B	SOS 871B	SOS 871B
Espectro	71[b]	72	73[a]	73[b]	74[a]	74[b]	75[a]	75[b]	76[a]	76[b]	77[a]	77[b]	78[a]	78[b]	79[a]	79[b]	80[a]
UTM	628349	628349	628349	628349	628349	628349	628349	628349	628349	628349	628349	628349	628349	628349	628349	628349	628349
	8911047	8911047	8911047	8911047	8911047	8911047	8911047	8911047	8911047	8911047	8911047	8911047	8911047	8911047	8911047	8911047	8911047
SiO_2	55,7	55,3	55,0	58,2	56,0	60,5	53,9	60,7	56,2	60,8	62,5	60,4	57,4	61,4	56,8	60,0	55,4
Al_2O_3	28,3	28,7	28,9	28,1	30,7	25,4	30,5	25,0	28,3	25,0	23,6	25,2	27,5	27,1	27,9	25,5	28,4
FeO	0,0	0,0	0,3	0,0	0,0	0,0	0,0	0,0	0,0	0,0	0,0	0,0	0,0	0,0	0,4	0,0	0,0
CaO	9,7	10,2	10,3	6,6	8,5	6,2	10,0	5,9	9,2	5,7	4,6	6,1	8,5	4,3	8,1	6,4	10,0
Na_2O	6,3	5,8	5,5	7,1	4,9	8,0	5,6	8,1	6,3	8,5	9,2	8,4	6,7	7,2	6,5	8,0	6,2
K_2O	0,0	0,0	0,0	0,0	0,0	0,0	0,0	0,2	0,0	0,0	0,1	0,0	0,0	0,0	0,3	0,2	0,0
BaO	0,0	0,0	0,0	0,0	0,0	0,0	0,0	0,0	0,0	0,0	0,0	0,0	0,0	0,0	0,0	0,0	0,0
Total	100,0	100,0	100,0	100,0	100,1	100,1	100,0	99,9	100,0	100,0	100,0	100,1	100,1	100,0	100,0	100,1	100,0
Si	2,504	2,487	2,476	2,586	2,487	2,684	2,424	2,699	2,520	2,700	2,768	2,684	2,565	2,694	2,547	2,669	2,494
Al	1,500	1,521	1,533	1,472	1,607	1,328	1,617	1,310	1,496	1,309	1,232	1,320	1,448	1,402	1,474	1,337	1,507
Fe	0,000	0,000	0,011	0,000	0,000	0,000	0,000	0,000	0,000	0,000	0,000	0,000	0,000	0,000	0,015	0,000	0,000
Ca	0,467	0,491	0,497	0,314	0,404	0,295	0,482	0,281	0,442	0,271	0,218	0,290	0,407	0,202	0,389	0,305	0,482
Na	0,549	0,506	0,480	0,612	0,422	0,688	0,488	0,698	0,548	0,732	0,790	0,724	0,581	0,613	0,565	0,690	0,541
K	0,000	0,000	0,000	0,000	0,000	0,000	0,000	0,011	0,000	0,000	0,006	0,000	0,000	0,000	0,017	0,011	0,000
Ba	0,000	0,000	0,000	0,000	0,000	0,000	0,000	0,000	0,000	0,000	0,000	0,000	0,000	0,000	0,000	0,000	0,000
Total	5,020	5,005	4,997	4,984	4,920	4,996	5,011	5,000	5,006	5,012	5,014	5,018	5,001	4,911	5,007	5,013	5,024
Or	0,0	0,0	0,0	0,0	0,0	0,0	0,0	1,1	0,0	0,0	0,6	0,0	0,0	0,0	1,8	1,1	0,0
Ab	54,0	50,7	49,1	66,1	51,1	70,0	50,3	70,5	55,3	73,0	77,9	71,4	58,8	75,2	58,2	68,6	52,9
An	46,0	49,3	50,9	33,9	48,9	30,0	49,7	28,4	44,7	27,0	21,5	28,6	41,2	24,8	40,1	30,3	47,1

Apêndice C.1. Análises químicas pontuais em plagioclásio (continuação).

Amostra	SOS 871B	SOS 871B	SOS 871B	SOS 871B	SOS 871B	SOS 871B	SOS 871B	SOS 871B	SOS 871B	SOS 871B	SOS 871B	SOS 871B	SOS 871B	SOS 871B	SOS 871B	SOS 871B	SOS 871B
Espectro	80[b]	81	82[a]	82[b]	83	84[a]	84[b]	85[a]	85[b]	86[a]	86[b]	87[a]	87[b]	88[a]	88[b]	89[a]	89[b]
UTM	628349	628349	628349	628349	628349	628349	628349	628349	628349	628349	628349	628349	628349	628349	628349	628349	628349
	8911047	8911047	8911047	8911047	8911047	8911047	8911047	8911047	8911047	8911047	8911047	8911047	8911047	8911047	8911047	8911047	8911047
SiO_2	56,1	60,8	55,1	64,6	55,2	61,9	56,2	58,5	56,3	59,4	57,0	59,8	56,9	61,1	60,0	62,5	59,4
Al_2O_3	29,1	24,8	28,9	23,9	28,9	24,2	28,1	26,6	27,7	26,0	27,4	25,6	27,3	24,5	25,4	24,0	25,8
FeO	0,0	0,0	0,0	0,0	0,0	0,0	0,0	0,0	0,0	0,0	0,0	0,0	0,0	0,0	0,0	0,0	0,0
CaO	6,0	5,7	10,4	3,2	10,2	5,0	9,2	7,6	9,3	6,9	8,6	6,7	8,7	5,9	6,6	3,9	7,0
Na_2O	8,8	8,6	5,7	8,2	5,7	8,9	6,5	7,3	6,7	7,8	6,9	7,9	7,1	8,4	8,0	9,1	7,9
K_2O	0,0	0,2	0,0	0,0	0,0	0,0	0,0	0,0	0,0	0,0	0,0	0,0	0,0	0,2	0,0	0,5	0,0
BaO	0,0	0,0	0,0	0,0	0,0	0,0	0,0	0,0	0,0	0,0	0,0	0,0	0,0	0,0	0,0	0,0	0,0
Total	100,0	100,1	100,1	99,9	100,0	100,0	100,0	100,0	100,0	100,1	99,9	100,0	100,0	100,1	100,0	100,0	100,1
Si	2,513	2,702	2,477	2,827	2,482	2,742	2,522	2,611	2,530	2,644	2,557	2,662	2,553	2,714	2,671	2,766	2,646
Al	1,536	1,299	1,531	1,233	1,531	1,264	1,487	1,399	1,467	1,364	1,449	1,343	1,444	1,283	1,333	1,252	1,355
Fe	0,000	0,000	0,000	0,000	0,000	0,000	0,000	0,000	0,000	0,000	0,000	0,000	0,000	0,000	0,000	0,000	0,000
Ca	0,288	0,271	0,501	0,150	0,491	0,237	0,442	0,363	0,448	0,329	0,413	0,320	0,418	0,281	0,315	0,185	0,334
Na	0,764	0,741	0,497	0,696	0,497	0,765	0,566	0,632	0,584	0,673	0,600	0,682	0,618	0,723	0,690	0,781	0,682
K	0,000	0,011	0,000	0,000	0,000	0,000	0,000	0,000	0,000	0,000	0,000	0,000	0,000	0,011	0,000	0,028	0,000
Ba	0,000	0,000	0,000	0,000	0,000	0,000	0,000	0,000	0,000	0,000	0,000	0,000	0,000	0,000	0,000	0,000	0,000
Total	5,101	5,025	5,006	4,905	5,001	5,008	5,017	5,005	5,028	5,010	5,019	5,007	5,034	5,012	5,008	5,012	5,018
Or	0,0	1,1	0,0	0,0	0,0	0,0	0,0	0,0	0,0	0,0	0,0	0,0	0,0	1,1	0,0	2,8	0,0
Ab	72,6	72,4	49,8	82,3	50,3	76,3	56,1	63,5	56,6	67,2	59,2	68,1	59,6	71,2	68,7	78,6	67,1
An	27,4	26,5	50,2	17,7	49,7	23,7	43,9	36,5	43,4	32,8	40,8	31,9	40,4	27,6	31,3	18,6	32,9

Apêndice C.1. Análises químicas pontuais em plagioclásio (continuação).

Amostra	SOS 871B	SOS 871B	SOS 871B	SOS 871B	SOS 871B	SOS 871B	SOS 871B	SOS 871B	SOS 871B	SOS 871B	SOS 871B	SOS 871B	SOS 871B	SOS 871B	SOS 871B	SOS 873B	SOS 873B
Espectro	90	91[a]	91[b]	92[a]	92[b]	93	94	95	96	97	98	99	100	101	102	1[a]	1[b]
UTM	628349	628349	628349	628349	628349	628349	628349	628349	628349	628349	628349	628349	628349	628349	628349	629288	629288
	8911047	8911047	8911047	8911047	8911047	8911047	8911047	8911047	8911047	8911047	8911047	8911047	8911047	8911047	8911047	8909896	8909896
SiO_2	61,1	57,5	60,6	58,6	59,9	62,2	62,2	62,1	62,3	62,4	65,1	61,1	63,0	61,9	62,9	61,6	57,4
Al_2O_3	24,6	27,4	24,7	26,6	27,7	24,2	24,0	23,8	23,7	23,7	21,3	24,5	23,3	24,3	23,5	28,4	28,1
FeO	0,0	0,0	0,3	0,0	0,0	0,0	0,0	0,0	0,0	0,0	0,8	0,0	0,0	0,0	0,0	0,0	0,0
CaO	5,7	8,2	5,6	7,4	5,4	4,7	4,9	4,8	4,8	4,8	1,9	4,3	4,2	4,4	4,4	1,8	7,4
Na_2O	8,5	6,8	8,6	7,3	7,0	8,9	8,9	9,1	9,0	8,9	10,7	9,8	9,5	9,2	9,3	8,2	7,1
K_2O	0,2	0,0	0,2	0,0	0,0	0,0	0,0	0,2	0,1	0,2	0,2	0,2	0,0	0,3	0,0	0,0	0,0
BaO	0,0	0,0	0,0	0,0	0,0	0,0	0,0	0,0	0,0	0,0	0,0	0,0	0,0	0,0	0,0	0,0	0,0
Total	100,1	99,9	100,0	99,9	100,0	100,0	100,0	100,0	99,9	100,0	100,0	99,9	100,0	100,1	100,1	100,0	100,0
Si	2,713	2,572	2,700	2,616	2,642	2,751	2,754	2,754	2,762	2,764	2,876	2,719	2,786	2,742	2,779	2,689	2,561
Al	1,287	1,445	1,297	1,399	1,440	1,262	1,252	1,244	1,239	1,237	1,109	1,285	1,214	1,269	1,224	1,461	1,478
Fe	0,000	0,000	0,011	0,000	0,000	0,000	0,000	0,000	0,000	0,000	0,030	0,000	0,000	0,000	0,000	0,000	0,000
Ca	0,271	0,393	0,267	0,354	0,255	0,223	0,232	0,228	0,228	0,228	0,090	0,205	0,199	0,209	0,208	0,084	0,354
Na	0,732	0,590	0,743	0,632	0,599	0,763	0,764	0,783	0,774	0,764	0,917	0,846	0,815	0,790	0,797	0,694	0,614
K	0,011	0,000	0,011	0,000	0,000	0,000	0,000	0,011	0,006	0,011	0,011	0,011	0,000	0,017	0,000	0,000	0,000
Ba	0,000	0,000	0,000	0,000	0,000	0,000	0,000	0,000	0,000	0,000	0,000	0,000	0,000	0,000	0,000	0,000	0,000
Total	5,015	5,000	5,029	5,001	4,937	4,999	5,002	5,021	5,008	5,005	5,033	5,067	5,014	5,027	5,008	4,928	5,007
Or	1,1	0,0	1,1	0,0	0,0	0,0	0,0	1,1	0,6	1,1	1,1	1,1	0,0	1,7	0,0	0,0	0,0
Ab	72,1	60,0	72,7	64,1	70,1	77,4	76,7	76,6	76,8	76,2	90,1	79,6	80,4	77,8	79,3	89,2	63,5
An	26,7	40,0	26,2	35,9	29,9	22,6	23,3	22,3	22,6	22,7	8,8	19,3	19,6	20,6	20,7	10,8	36,5

Apêndice C.1. Análises químicas pontuais em plagioclásio (continuação).

Amostra	SOS 873B	SOS 873B	SOS 873B	SOS 873B	SOS 873B	SOS 873B	SOS 873B	SOS 873B	SOS 873B	SOS 873B	SOS 873B	SOS 873B	SOS 873B	SOS 873B	SOS 873B	SOS 873B	SOS 873B
Espectro	1^{c}	1^{d}	2^{a}	2^{b}	2^{c}	2^{d}	3^{a}	3^{b}	3^{c}	3^{d}	4^{a}	4^{b}	4^{c}	4^{d}	5^{a}	5^{b}	5^{c}
UTM	629288	629288	629288	629288	629288	629288	629288	629288	629288	629288	629288	629288	629288	629288	629288	629288	629288
	8909896	8909896	8909896	8909896	8909896	8909896	8909896	8909896	8909896	8909896	8909896	8909896	8909896	8909896	8909896	8909896	8909896
SiO_2	58,1	57,4	57,3	57,5	61,0	57,8	57,7	57,6	58,4	61,1	61,9	57,9	57,9	57,4	61,4	60,5	61,0
Al_2O_3	26,6	27,0	28,2	28,2	24,7	26,9	27,9	27,7	26,7	24,6	24,6	27,7	27,2	26,7	26,5	26,0	24,7
FeO	0,0	0,0	0,0	0,0	0,0	0,0	0,0	0,0	0,0	0,0	0,0	0,0	0,0	0,0	0,0	0,0	0,0
CaO	7,6	8,2	6,8	7,4	5,5	7,9	6,9	7,5	7,7	5,2	3,9	7,1	8,0	8,3	3,7	5,0	5,3
Na_2O	7,6	7,3	7,7	7,0	8,5	7,5	7,4	7,2	7,3	9,0	9,7	7,3	7,0	7,5	8,4	8,6	8,9
K_2O	0,0	0,0	0,0	0,0	0,2	0,0	0,0	0,0	0,0	0,2	0,0	0,0	0,0	0,1	0,0	0,0	0,1
BaO	0,0	0,0	0,0	0,0	0,0	0,0	0,0	0,0	0,0	0,0	0,0	0,0	0,0	0,0	0,0	0,0	0,0
Total	99,9	99,9	100,0	100,1	99,9	100,1	99,9	100,0	100,1	100,1	100,1	100,0	100,1	100,0	100,0	100,1	100,0
Si	2,600	2,574	2,558	2,562	2,712	2,585	2,575	2,572	2,605	2,714	2,738	2,581	2,584	2,576	2,702	2,679	2,710
Al	1,403	1,427	1,484	1,481	1,294	1,418	1,467	1,458	1,404	1,288	1,282	1,455	1,431	1,413	1,375	1,357	1,294
Fe	0,000	0,000	0,000	0,000	0,000	0,000	0,000	0,000	0,000	0,000	0,000	0,000	0,000	0,000	0,000	0,000	0,000
Ca	0,364	0,394	0,325	0,353	0,262	0,379	0,330	0,359	0,368	0,247	0,185	0,339	0,383	0,399	0,174	0,237	0,252
Na	0,660	0,635	0,666	0,605	0,733	0,650	0,640	0,623	0,631	0,775	0,832	0,631	0,606	0,653	0,717	0,738	0,767
K	0,000	0,000	0,000	0,000	0,011	0,000	0,000	0,000	0,000	0,011	0,000	0,000	0,000	0,006	0,000	0,000	0,006
Ba	0,000	0,000	0,000	0,000	0,000	0,000	0,000	0,000	0,000	0,000	0,000	0,000	0,000	0,000	0,000	0,000	0,000
Total	5,028	5,030	5,033	5,000	5,013	5,031	5,012	5,011	5,009	5,036	5,037	5,007	5,003	5,047	4,969	5,012	5,029
Or	0,0	0,0	0,0	0,0	1,1	0,0	0,0	0,0	0,0	1,1	0,0	0,0	0,0	0,5	0,0	0,0	0,6
Ab	64,4	61,7	67,2	63,1	72,8	63,2	66,0	63,5	63,2	75,0	81,8	65,0	61,3	61,7	80,4	75,7	74,8
An	35,6	38,3	32,8	36,9	26,0	36,8	34,0	36,5	36,8	23,9	18,2	35,0	38,7	37,7	19,6	24,3	24,6

Apêndice C.1. Análises químicas pontuais em plagioclásio (continuação).

Amostra	SOS 873B	SOS 873B	SOS 873B	SOS 873B	SOS 873B	SOS 873B	SOS 873B	SOS 873B	SOS 873B	SOS 873B	SOS 873B	SOS 873B	SOS 873B	SOS 873B	SOS 873B	SOS 873B	SOS 873B
Espectro	5[d]	6[a]	6[b]	6[c]	6[d]	7[a]	7[b]	7[c]	7[d]	8[a]	8[b]	8[c]	8[d]	9[a]	9[b]	9[c]	9[d]
UTM	629288	629288	629288	629288	629288	629288	629288	629288	629288	629288	629288	629288	629288	629288	629288	629288	629288
	8909896	8909896	8909896	8909896	8909896	8909896	8909896	8909896	8909896	8909896	8909896	8909896	8909896	8909896	8909896	8909896	8909896
SiO_2	58,5	62,9	60,8	58,0	61,3	56,1	60,9	61,6	61,3	58,2	61,6	61,1	58,8	59,3	57,2	61,3	59,9
Al_2O_3	26,3	24,1	25,6	26,8	24,3	28,7	25,4	25,1	24,4	27,6	25,0	24,6	26,2	26,6	28,2	24,2	25,3
FeO	0,0	0,0	0,0	0,0	0,0	0,0	0,0	0,0	0,0	0,0	0,0	0,0	0,0	0,0	0,0	0,0	0,0
CaO	7,2	3,0	5,1	7,8	5,4	8,0	4,9	2,3	5,0	6,2	4,4	4,4	7,2	5,7	7,5	5,2	6,0
Na_2O	7,8	10,0	8,5	7,4	8,8	7,1	8,8	9,0	9,2	8,0	9,0	9,2	7,4	8,4	7,0	9,1	8,7
K_2O	0,1	0,0	0,0	0,0	0,2	0,0	0,0	2,0	0,2	0,0	0,0	0,7	0,3	0,0	0,0	0,1	0,2
BaO	0,0	0,0	0,0	0,0	0,0	0,0	0,0	0,0	0,0	0,0	0,0	0,0	0,0	0,0	0,0	0,0	0,0
Total	99,9	100,0	100,0	100,0	100,0	99,9	100,0	100,0	100,1	100,0	100,0	100,0	99,9	100,0	99,9	99,9	100,1
Si	2,617	2,775	2,694	2,593	2,724	2,516	2,699	2,737	2,722	2,592	2,725	2,719	2,628	2,637	2,555	2,727	2,669
Al	1,387	1,253	1,337	1,412	1,273	1,517	1,327	1,315	1,277	1,449	1,304	1,290	1,380	1,394	1,485	1,269	1,329
Fe	0,000	0,000	0,000	0,000	0,000	0,000	0,000	0,000	0,000	0,000	0,000	0,000	0,000	0,000	0,000	0,000	0,000
Ca	0,345	0,142	0,242	0,374	0,257	0,384	0,233	0,110	0,238	0,296	0,209	0,210	0,345	0,272	0,359	0,248	0,286
Na	0,677	0,856	0,730	0,642	0,758	0,617	0,756	0,775	0,792	0,691	0,772	0,794	0,641	0,724	0,606	0,785	0,752
K	0,006	0,000	0,000	0,000	0,011	0,000	0,000	0,113	0,011	0,000	0,000	0,040	0,017	0,000	0,000	0,006	0,011
Ba	0,000	0,000	0,000	0,000	0,000	0,000	0,000	0,000	0,000	0,000	0,000	0,000	0,000	0,000	0,000	0,000	0,000
Total	5,031	5,026	5,003	5,021	5,024	5,034	5,015	5,050	5,041	5,028	5,009	5,053	5,011	5,028	5,005	5,034	5,048
Or	0,6	0,0	0,0	0,0	1,1	0,0	0,0	11,4	1,1	0,0	0,0	3,8	1,7	0,0	0,0	0,5	1,1
Ab	65,9	85,8	75,1	63,2	73,9	61,6	76,5	77,7	76,1	70,0	78,7	76,1	63,9	72,7	62,8	75,6	71,6
An	33,6	14,2	24,9	36,8	25,0	38,4	23,5	11,0	22,8	30,0	21,3	20,1	34,4	27,3	37,2	23,9	27,3

Apêndice C.1. Análises químicas pontuais em plagioclásio (continuação).

Amostra	SOS 873B	SOS 873B	SOS 873B	SOS 873B	SOS 873B	SOS 873B	SOS 873B	SOS 873B	SOS 873B	SOS 873B	SOS 873B	SOS 873B	SOS 873B	SOS 873B	SOS 873B	SOS 873B	SOS 873B
Espectro	10[a]	10[b]	10[c]	10[d]	11[a]	11[b]	11[c]	11[d]	12[a]	12[b]	12[c]	12[d]	13[a]	13[b]	13[c]	13[d]	14[a]
UTM	629288	629288	629288	629288	629288	629288	629288	629288	629288	629288	629288	629288	629288	629288	629288	629288	629288
	8909896	8909896	8909896	8909896	8909896	8909896	8909896	8909896	8909896	8909896	8909896	8909896	8909896	8909896	8909896	8909896	8909896
SiO_2	61,1	57,0	58,1	61,2	59,9	57,1	59,2	57,7	56,7	58,5	58,3	57,5	58,6	57,9	55,7	58,0	56,3
Al_2O_3	25,4	28,3	26,3	24,4	26,0	28,2	26,4	27,3	28,5	27,9	26,8	27,1	28,0	27,8	29,2	26,7	28,6
FeO	0,0	0,0	0,0	0,0	0,0	0,0	0,0	0,0	0,0	0,0	0,0	0,0	0,0	0,0	0,0	0,0	0,0
CaO	4,0	7,5	7,2	5,3	5,0	7,6	6,6	7,9	7,5	5,8	7,3	7,8	6,0	7,0	7,3	7,9	7,7
Na_2O	9,5	7,1	8,2	8,9	9,1	7,0	7,6	7,2	7,3	7,8	7,5	7,4	7,4	7,3	7,6	7,4	7,4
K_2O	0,0	0,0	0,2	0,2	0,0	0,0	0,2	0,0	0,0	0,0	0,1	0,2	0,0	0,0	0,2	0,0	0,0
BaO	0,0	0,0	0,0	0,0	0,0	0,0	0,0	0,0	0,0	0,0	0,0	0,0	0,0	0,0	0,0	0,0	0,0
Total	100,0	99,9	100,0	100,0	100,0	99,9	100,0	100,1	100,0	100,0	100,0	100,0	100,0	100,0	100,0	100,0	100,0
Si	2,706	2,548	2,604	2,720	2,663	2,552	2,636	2,577	2,535	2,598	2,604	2,576	2,600	2,580	2,499	2,594	2,522
Al	1,326	1,491	1,389	1,278	1,362	1,486	1,386	1,437	1,502	1,461	1,411	1,431	1,464	1,460	1,544	1,408	1,510
Fe	0,000	0,000	0,000	0,000	0,000	0,000	0,000	0,000	0,000	0,000	0,000	0,000	0,000	0,000	0,000	0,000	0,000
Ca	0,190	0,359	0,346	0,252	0,238	0,364	0,315	0,378	0,359	0,276	0,349	0,374	0,285	0,334	0,351	0,379	0,370
Na	0,816	0,615	0,713	0,767	0,784	0,607	0,656	0,624	0,633	0,672	0,649	0,643	0,637	0,631	0,661	0,642	0,643
K	0,000	0,000	0,011	0,011	0,000	0,000	0,011	0,000	0,000	0,000	0,006	0,011	0,000	0,000	0,011	0,000	0,000
Ba	0,000	0,000	0,000	0,000	0,000	0,000	0,000	0,000	0,000	0,000	0,000	0,000	0,000	0,000	0,000	0,000	0,000
Total	5,038	5,014	5,063	5,030	5,048	5,008	5,005	5,016	5,030	5,007	5,019	5,036	4,986	5,005	5,066	5,023	5,044
Or	0,0	0,0	1,1	1,1	0,0	0,0	1,2	0,0	0,0	0,0	0,6	1,1	0,0	0,0	1,1	0,0	0,0
Ab	81,1	63,1	66,6	74,4	76,7	62,5	66,8	62,3	63,8	70,9	64,7	62,5	69,1	65,4	64,6	62,9	63,5
An	18,9	36,9	32,3	24,5	23,3	37,5	32,1	37,7	36,2	29,1	34,8	36,4	30,9	34,6	34,3	37,1	36,5

Apêndice C.1. Análises químicas pontuais em plagioclásio (continuação).

Amostra	SOS 873B	SOS 873B	SOS 873B	SOS 873B	SOS 873B	SOS 873B	SOS 873B	SOS 873B	SOS 873B	SOS 873B	SOS 873B	SOS 873B	SOS 873B	SOS 873B	SOS 873B	SOS 873B	SOS 873B
Espectro	14[b]	14[c]	14[d]	15[a]	15[b]	15[c]	15[d]	16[a]	16[b]	16[c]	16[d]	17[a]	17[b]	17[c]	17[d]	17[e]	18[a]
UTM	629288	629288	629288	629288	629288	629288	629288	629288	629288	629288	629288	629288	629288	629288	629288	629288	629288
	8909896	8909896	8909896	8909896	8909896	8909896	8909896	8909896	8909896	8909896	8909896	8909896	8909896	8909896	8909896	8909896	8909896
SiO_2	60,4	61,4	60,2	57,6	59,9	61,4	60,8	59,0	59,6	57,5	61,4	57,4	57,4	61,3	58,7	60,1	58,5
Al_2O_3	25,8	24,4	25,1	27,8	26,0	24,3	24,7	27,2	26,5	27,2	24,0	28,4	28,0	24,5	26,5	25,4	28,0
FeO	0,0	0,0	0,0	0,0	0,0	0,0	0,0	0,0	0,0	0,0	0,0	0,0	0,0	0,0	0,0	0,0	0,0
CaO	5,5	5,1	6,1	6,7	5,4	5,3	5,4	5,8	5,8	8,0	5,3	7,1	7,3	5,3	7,4	6,0	6,4
Na_2O	8,2	8,9	8,4	7,9	8,7	8,7	8,9	8,0	8,1	7,3	9,0	7,1	7,2	8,7	7,5	8,3	7,1
K_2O	0,0	0,2	0,2	0,0	0,0	0,3	0,2	0,0	0,0	0,0	0,2	0,0	0,0	0,1	0,0	0,2	0,0
BaO	0,0	0,0	0,0	0,0	0,0	0,0	0,0	0,0	0,0	0,0	0,0	0,0	0,0	0,0	0,0	0,0	0,0
Total	99,9	100,0	100,0	100,0	100,0	100,0	100,0	100,0	100,0	100,0	99,9	100,0	99,9	99,9	100,1	100,0	100,0
Si	2,681	2,726	2,682	2,572	2,662	2,728	2,705	2,621	2,647	2,574	2,732	2,558	2,564	2,723	2,617	2,675	2,596
Al	1,350	1,277	1,318	1,463	1,362	1,272	1,295	1,424	1,387	1,435	1,259	1,492	1,474	1,283	1,392	1,333	1,465
Fe	0,000	0,000	0,000	0,000	0,000	0,000	0,000	0,000	0,000	0,000	0,000	0,000	0,000	0,000	0,000	0,000	0,000
Ca	0,262	0,243	0,291	0,321	0,257	0,252	0,257	0,276	0,276	0,384	0,253	0,339	0,349	0,252	0,353	0,286	0,304
Na	0,706	0,766	0,726	0,684	0,750	0,749	0,768	0,689	0,698	0,634	0,777	0,614	0,624	0,749	0,648	0,716	0,611
K	0,000	0,011	0,011	0,000	0,000	0,017	0,011	0,000	0,000	0,000	0,011	0,000	0,000	0,006	0,000	0,011	0,000
Ba	0,000	0,000	0,000	0,000	0,000	0,000	0,000	0,000	0,000	0,000	0,000	0,000	0,000	0,000	0,000	0,000	0,000
Total	4,997	5,024	5,028	5,039	5,031	5,019	5,037	5,011	5,008	5,026	5,032	5,003	5,011	5,013	5,011	5,022	4,977
Or	0,0	1,1	1,1	0,0	0,0	1,7	1,1	0,0	0,0	0,0	1,1	0,0	0,0	0,6	0,0	1,1	0,0
Ab	73,0	75,1	70,6	68,1	74,5	73,6	74,1	71,4	71,6	62,3	74,6	64,4	64,1	74,4	64,7	70,7	66,8
An	27,0	23,8	28,3	31,9	25,5	24,8	24,8	28,6	28,4	37,7	24,3	35,6	35,9	25,0	35,3	28,2	33,2

Apêndice C.1. Análises químicas pontuais em plagioclásio (continuação).

Amostra	SOS 873B	SOS 873B	SOS 873B	SOS 873B	SOS 873B	SOS 873B	SOS 873B	SOS 873B	SOS 873B	SOS 873B	SOS 873B	SOS 873B	SOS 873B	SOS 873B	SOS 873B	SOS 873B	SOS 873B
Espectro	18^{b}	18^{c}	18^{d}	18^{e}	19^{a}	19^{b}	19^{c}	19^{d}	19^{e}	20^{a}	20^{b}	20^{c}	20^{d}	20^{e}	21^{a}	21^{b}	21^{c}
UTM	629288	629288	629288	629288	629288	629288	629288	629288	629288	629288	629288	629288	629288	629288	629288	629288	629288
	8909896	8909896	8909896	8909896	8909896	8909896	8909896	8909896	8909896	8909896	8909896	8909896	8909896	8909896	8909896	8909896	8909896
SiO_2	60,1	61,2	61,0	59,9	56,7	60,3	61,3	61,4	59,6	57,4	60,4	60,7	59,1	58,7	56,8	60,6	57,5
Al_2O_3	26,0	24,3	24,5	25,4	28,8	25,9	24,6	24,6	25,4	28,2	25,9	24,6	26,0	25,9	28,4	25,7	26,9
FeO	0,0	0,0	0,0	0,0	0,0	0,0	0,0	0,0	0,0	0,0	0,0	0,0	0,0	0,0	0,0	0,0	0,0
CaO	5,4	5,0	5,4	6,3	7,7	4,9	5,3	5,3	6,4	7,1	5,1	5,6	6,8	7,4	7,6	5,0	8,2
Na_2O	8,6	9,6	8,9	8,5	6,9	8,8	8,8	8,8	8,6	7,3	8,6	9,0	8,1	7,8	7,3	8,7	7,3
K_2O	0,0	0,0	0,2	0,0	0,0	0,0	0,0	0,0	0,0	0,0	0,0	0,2	0,0	0,2	0,0	0,0	0,0
BaO	0,0	0,0	0,0	0,0	0,0	0,0	0,0	0,0	0,0	0,0	0,0	0,0	0,0	0,0	0,0	0,0	0,0
Total	100,1	100,1	100,0	100,1	100,1	99,9	100,0	100,1	100,0	100,0	100,0	100,1	100,0	100,0	100,1	100,0	99,9
Si	2,667	2,720	2,713	2,667	2,530	2,677	2,720	2,721	2,659	2,560	2,679	2,702	2,637	2,626	2,538	2,687	2,578
Al	1,360	1,273	1,284	1,333	1,515	1,355	1,287	1,285	1,336	1,483	1,354	1,291	1,367	1,366	1,496	1,343	1,422
Fe	0,000	0,000	0,000	0,000	0,000	0,000	0,000	0,000	0,000	0,000	0,000	0,000	0,000	0,000	0,000	0,000	0,000
Ca	0,257	0,238	0,257	0,301	0,368	0,233	0,252	0,252	0,306	0,339	0,242	0,267	0,325	0,355	0,364	0,238	0,394
Na	0,740	0,827	0,768	0,734	0,597	0,758	0,757	0,756	0,744	0,631	0,740	0,777	0,701	0,677	0,633	0,748	0,635
K	0,000	0,000	0,011	0,000	0,000	0,000	0,000	0,000	0,000	0,000	0,000	0,011	0,000	0,011	0,000	0,000	0,000
Ba	0,000	0,000	0,000	0,000	0,000	0,000	0,000	0,000	0,000	0,000	0,000	0,000	0,000	0,000	0,000	0,000	0,000
Total	5,023	5,058	5,034	5,034	5,011	5,024	5,015	5,014	5,045	5,014	5,014	5,047	5,030	5,035	5,030	5,016	5,028
Or	0,0	0,0	1,1	0,0	0,0	0,0	0,0	0,0	0,0	0,0	0,0	1,1	0,0	1,1	0,0	0,0	0,0
Ab	74,2	77,7	74,1	70,9	61,9	76,5	75,0	75,0	70,9	65,0	75,3	73,6	68,3	64,9	63,5	75,9	61,7
An	25,8	22,3	24,8	29,1	38,1	23,5	25,0	25,0	29,1	35,0	24,7	25,3	31,7	34,0	36,5	24,1	38,3

Apêndice C.1. Análises químicas pontuais em plagioclásio (continuação).

Amostra	SOS 873B	SOS 873B	SOS 873B	SOS 873B	SOS 873B	SOS 873B	SOS 873B	SOS 873B	SOS 873B	SOS 873B	SOS 873B	SOS 873B	SOS 873B	SOS 873B	SOS 873B	SOS 873B	SOS 873B
Espectro	21^{d}	21^{e}	22^{a}	22^{b}	22^{c}	22^{d}	22^{e}	23^{a}	23^{b}	23^{c}	23^{d}	24^{a}	24^{b}	24^{c}	24^{d}	25^{a}	25^{b}
UTM	629288	629288	629288	629288	629288	629288	629288	629288	629288	629288	629288	629288	629288	629288	629288	629288	629288
	8909896	8909896	8909896	8909896	8909896	8909896	8909896	8909896	8909896	8909896	8909896	8909896	8909896	8909896	8909896	8909896	8909896
SiO_2	58,6	58,4	57,6	60,9	56,4	60,2	57,9	63,5	60,9	58,4	59,1	61,9	58,1	57,7	61,0	59,6	61,0
Al_2O_3	26,5	26,6	28,0	25,6	27,3	32,4	27,0	23,6	25,4	26,4	25,9	24,8	26,7	26,3	24,6	26,7	24,5
FeO	0,0	0,0	0,0	0,0	0,0	0,0	0,0	0,0	0,0	0,0	0,0	0,0	0,0	0,0	0,0	0,0	0,0
CaO	7,5	7,6	6,6	4,9	8,9	0,8	6,7	2,4	4,9	7,4	6,8	3,8	7,8	7,4	5,5	5,5	5,2
Na_2O	7,5	7,4	7,8	8,6	7,4	6,6	8,2	10,5	8,8	7,5	8,3	9,6	7,2	8,6	8,8	8,3	9,1
K_2O	0,0	0,0	0,0	0,0	0,0	0,0	0,2	0,0	0,0	0,2	0,0	0,0	0,2	0,0	0,2	0,0	0,2
BaO	0,0	0,0	0,0	0,0	0,0	0,0	0,0	0,0	0,0	0,0	0,0	0,0	0,0	0,0	0,0	0,0	0,0
Total	100,1	100,0	100,0	100,0	100,0	100,0	100,0	100,0	100,0	99,9	100,1	100,1	100,0	100,0	100,1	100,1	100,0
Si	2,614	2,608	2,569	2,697	2,538	2,604	2,591	2,799	2,699	2,613	2,637	2,736	2,599	2,591	2,710	2,644	2,714
Al	1,393	1,400	1,472	1,336	1,448	1,652	1,424	1,226	1,327	1,392	1,362	1,292	1,408	1,392	1,288	1,396	1,285
Fe	0,000	0,000	0,000	0,000	0,000	0,000	0,000	0,000	0,000	0,000	0,000	0,000	0,000	0,000	0,000	0,000	0,000
Ca	0,358	0,364	0,315	0,233	0,429	0,037	0,321	0,113	0,233	0,355	0,325	0,180	0,374	0,356	0,262	0,261	0,248
Na	0,649	0,641	0,675	0,738	0,646	0,554	0,711	0,898	0,756	0,651	0,718	0,823	0,624	0,749	0,758	0,714	0,785
K	0,000	0,000	0,000	0,000	0,000	0,000	0,011	0,000	0,000	0,011	0,000	0,000	0,011	0,000	0,011	0,000	0,011
Ba	0,000	0,000	0,000	0,000	0,000	0,000	0,000	0,000	0,000	0,000	0,000	0,000	0,000	0,000	0,000	0,000	0,000
Total	5,014	5,012	5,032	5,004	5,061	4,847	5,059	5,036	5,015	5,022	5,041	5,030	5,016	5,088	5,030	5,015	5,042
Or	0,0	0,0	0,0	0,0	0,0	0,0	1,1	0,0	0,0	1,1	0,0	0,0	1,1	0,0	1,1	0,0	1,1
Ab	64,4	63,8	68,1	76,1	60,1	93,7	68,1	88,8	76,5	64,0	68,8	82,1	61,8	67,8	73,5	73,2	75,2
An	35,6	36,2	31,9	23,9	39,9	6,3	30,8	11,2	23,5	34,9	31,2	17,9	37,0	32,2	25,4	26,8	23,7

Apêndice C.1. Análises químicas pontuais em plagioclásio (continuação).

Amostra	SOS 873B	SOS 873B	SOS 873B	SOS 873B	SOS 873B	SOS 873B	SOS 873B	SOS 873B	SOS 873B	SOS 873B	SOS 873B	SOS 873B	SOS 873B	SOS 873B	SOS 873B	SOS 873B	SOS 873B
Espectro	25[c]	26[a]	26[b]	26[c]	27[a]	27[b]	28[a]	28[b]	28[c]	29[a]	29[b]	29[c]	30[a]	30[b]	30[c]	31[a]	31[b]
UTM	629288	629288	629288	629288	629288	629288	629288	629288	629288	629288	629288	629288	629288	629288	629288	629288	629288
	8909896	8909896	8909896	8909896	8909896	8909896	8909896	8909896	8909896	8909896	8909896	8909896	8909896	8909896	8909896	8909896	8909896
SiO_2	58,1	60,4	60,0	56,9	57,7	60,7	57,1	58,2	57,6	58,5	57,4	61,0	58,8	60,9	58,1	57,4	62,6
Al_2O_3	26,2	26,0	25,4	25,7	27,8	24,8	28,3	26,6	26,9	27,2	27,1	24,4	27,0	24,6	26,6	28,3	23,6
FeO	0,0	0,0	0,0	0,0	0,0	0,0	0,0	0,0	0,0	0,0	0,0	0,0	0,0	0,0	0,0	0,0	0,0
CaO	7,6	4,6	6,2	12,9	6,8	5,6	7,3	7,5	7,5	6,4	8,3	5,6	6,0	5,6	7,6	7,0	4,2
Na_2O	8,1	9,0	8,3	4,3	7,6	8,8	7,3	7,5	8,0	7,9	7,1	8,9	8,2	8,8	7,6	7,3	9,6
K_2O	0,0	0,0	0,0	0,2	0,0	0,2	0,0	0,2	0,0	0,0	0,0	0,0	0,0	0,1	0,1	0,0	0,0
BaO	0,0	0,0	0,0	0,0	0,0	0,0	0,0	0,0	0,0	0,0	0,0	0,0	0,0	0,0	0,0	0,0	0,0
Total	100,0	100,0	99,9	100,0	99,9	100,1	100,0	100,0	100,0	100,0	99,9	99,9	100,0	100,0	100,0	100,0	100,0
Si	2,604	2,678	2,673	2,567	2,576	2,699	2,550	2,603	2,581	2,606	2,573	2,715	2,617	2,708	2,599	2,559	2,771
Al	1,384	1,359	1,334	1,366	1,463	1,300	1,490	1,402	1,421	1,428	1,432	1,280	1,417	1,289	1,403	1,487	1,231
Fe	0,000	0,000	0,000	0,000	0,000	0,000	0,000	0,000	0,000	0,000	0,000	0,000	0,000	0,000	0,000	0,000	0,000
Ca	0,365	0,219	0,296	0,623	0,325	0,267	0,349	0,359	0,360	0,305	0,399	0,267	0,286	0,267	0,364	0,334	0,199
Na	0,704	0,774	0,717	0,376	0,658	0,759	0,632	0,650	0,695	0,682	0,617	0,768	0,708	0,759	0,659	0,631	0,824
K	0,000	0,000	0,000	0,012	0,000	0,011	0,000	0,011	0,000	0,000	0,000	0,000	0,000	0,006	0,006	0,000	0,000
Ba	0,000	0,000	0,000	0,000	0,000	0,000	0,000	0,000	0,000	0,000	0,000	0,000	0,000	0,000	0,000	0,000	0,000
Total	5,056	5,029	5,019	4,944	5,022	5,036	5,021	5,027	5,056	5,021	5,020	5,029	5,028	5,029	5,032	5,012	5,025
Or	0,0	0,0	0,0	1,1	0,0	1,1	0,0	1,1	0,0	0,0	0,0	0,0	0,0	0,6	0,6	0,0	0,0
Ab	65,9	78,0	70,8	37,2	66,9	73,2	64,4	63,7	65,9	69,1	60,8	74,2	71,2	73,6	64,1	65,4	80,5
An	34,1	22,0	29,2	61,7	33,1	25,7	35,6	35,2	34,1	30,9	39,2	25,8	28,8	25,9	35,4	34,6	19,5

Apêndice C.1. Análises químicas pontuais em plagioclásio (continuação).

Amostra	SOS 873B	SOS 873B	SOS 873B	SOS 873B	SOS 873B	SOS 873B	SOS 873B	SOS 873B	SOS 873B	SOS 873B	SOS 873B	SOS 873B	SOS 873B	SOS 873B	SOS 873B	SOS 873B	SOS 873B
Espectro	31[c]	32[a]	32[b]	32[c]	32[d]	33[a]	33[b]	33[c]	34[a]	34[b]	34[c]	34[d]	35[a]	35[b]	35[c]	35[d]	36[a]
UTM	629288	629288	629288	629288	629288	629288	629288	629288	629288	629288	629288	629288	629288	629288	629288	629288	629288
	8909896	8909896	8909896	8909896	8909896	8909896	8909896	8909896	8909896	8909896	8909896	8909896	8909896	8909896	8909896	8909896	8909896
SiO_2	62,2	57,1	63,5	59,4	57,6	57,8	61,3	57,5	57,8	58,4	62,3	58,1	57,3	58,8	60,9	60,6	57,3
Al_2O_3	23,8	28,3	22,7	25,7	27,1	27,9	24,1	27,2	27,8	26,5	27,0	26,7	28,2	26,1	24,8	25,1	28,1
FeO	0,0	0,0	0,0	0,0	0,0	0,0	0,0	0,0	0,0	0,0	0,0	0,0	0,0	0,0	0,0	0,0	0,0
CaO	4,3	7,4	3,1	6,9	8,0	6,8	5,5	8,0	6,9	7,2	4,5	8,1	7,1	7,1	5,3	5,9	7,2
Na_2O	9,4	7,2	10,5	8,1	7,2	7,5	8,9	7,3	7,5	7,8	6,3	7,1	7,5	8,1	9,0	8,3	7,4
K_2O	0,2	0,0	0,2	0,0	0,1	0,0	0,2	0,0	0,0	0,1	0,0	0,0	0,0	0,0	0,0	0,2	0,0
BaO	0,0	0,0	0,0	0,0	0,0	0,0	0,0	0,0	0,0	0,0	0,0	0,0	0,0	0,0	0,0	0,0	0,0
Total	99,9	100,0	100,0	100,1	100,0	100,0	100,0	100,0	100,0	100,0	100,1	100,0	100,1	100,1	100,0	100,1	100,0
Si	2,759	2,550	2,810	2,648	2,578	2,576	2,727	2,574	2,577	2,610	2,720	2,597	2,556	2,625	2,706	2,692	2,558
Al	1,245	1,490	1,184	1,350	1,430	1,466	1,263	1,435	1,461	1,396	1,389	1,407	1,483	1,373	1,299	1,314	1,479
Fe	0,000	0,000	0,000	0,000	0,000	0,000	0,000	0,000	0,000	0,000	0,000	0,000	0,000	0,000	0,000	0,000	0,000
Ca	0,204	0,354	0,147	0,330	0,384	0,325	0,262	0,384	0,330	0,345	0,210	0,388	0,339	0,340	0,252	0,281	0,344
Na	0,809	0,623	0,901	0,700	0,625	0,648	0,768	0,634	0,648	0,676	0,533	0,615	0,649	0,701	0,775	0,715	0,641
K	0,011	0,000	0,011	0,000	0,006	0,000	0,011	0,000	0,000	0,006	0,000	0,000	0,000	0,000	0,000	0,011	0,000
Ba	0,000	0,000	0,000	0,000	0,000	0,000	0,000	0,000	0,000	0,000	0,000	0,000	0,000	0,000	0,000	0,000	0,000
Total	5,028	5,017	5,054	5,027	5,022	5,015	5,031	5,026	5,016	5,033	4,852	5,007	5,027	5,039	5,032	5,014	5,022
Or	1,1	0,0	1,1	0,0	0,6	0,0	1,1	0,0	0,0	0,6	0,0	0,0	0,0	0,0	0,0	1,1	0,0
Ab	78,9	63,8	85,1	68,0	61,6	66,6	73,7	62,3	66,3	65,9	71,7	61,3	65,7	67,4	75,4	71,0	65,0
An	20,0	36,2	13,9	32,0	37,8	33,4	25,2	37,7	33,7	33,6	28,3	38,7	34,3	32,6	24,6	27,9	35,0

Apêndice C.1. Análises químicas pontuais em plagioclásio (continuação).

Amostra	SOS 873B	SOS 873B	SOS 873B	SOS 873B	SOS 873B	SOS 873B	SOS 873B	SOS 873B	SOS 873B	SOS 873B	SOS 873B	SOS 873B	SOS 873B	SOS 873B	SOS 873B	SOS 873B	SOS 873B
Espectro	36^{b}	36^{c}	36^{d}	37^{a}	37^{b}	37^{c}	37^{d}	38^{a}	38^{b}	38^{c}	38^{d}	39^{a}	39^{b}	39^{c}	39^{d}	40^{a}	40^{b}
UTM	629288	629288	629288	629288	629288	629288	629288	629288	629288	629288	629288	629288	629288	629288	629288	629288	629288
	8909896	8909896	8909896	8909896	8909896	8909896	8909896	8909896	8909896	8909896	8909896	8909896	8909896	8909896	8909896	8909896	8909896
SiO_2	61,6	61,6	61,3	56,8	61,9	67,5	61,4	56,6	61,1	61,7	61,3	57,7	61,6	61,0	61,2	57,0	61,7
Al_2O_3	26,2	24,1	24,5	28,5	23,9	26,9	24,7	28,8	24,4	23,9	24,4	28,0	24,4	24,7	24,4	28,6	24,3
FeO	0,0	0,0	0,0	0,0	0,0	0,0	0,0	0,0	0,0	0,0	0,0	0,0	0,0	0,0	0,3	0,0	0,0
CaO	4,9	5,1	5,3	7,5	4,4	1,6	5,2	7,7	5,3	4,7	5,3	6,8	5,7	5,0	5,2	7,0	5,0
Na_2O	7,3	9,1	8,8	7,2	9,6	4,0	8,7	6,9	9,0	9,7	8,8	7,6	8,2	9,2	8,9	7,4	9,0
K_2O	0,0	0,2	0,2	0,0	0,2	0,0	0,0	0,0	0,2	0,0	0,1	0,0	0,2	0,2	0,0	0,0	0,0
BaO	0,0	0,0	0,0	0,0	0,0	0,0	0,0	0,0	0,0	0,0	0,0	0,0	0,0	0,0	0,0	0,0	0,0
Total	100,0	100,1	100,1	100,0	100,0	100,0	100,0	100,0	100,0	100,0	99,9	100,1	100,1	100,1	100,0	100,0	100,0
Si	2,710	2,734	2,721	2,538	2,748	2,870	2,722	2,529	2,717	2,741	2,724	2,571	2,730	2,710	2,720	2,544	2,735
Al	1,359	1,261	1,282	1,501	1,251	1,348	1,291	1,517	1,279	1,251	1,278	1,470	1,275	1,293	1,278	1,505	1,270
Fe	0,000	0,000	0,000	0,000	0,000	0,000	0,000	0,000	0,000	0,000	0,000	0,000	0,000	0,000	0,011	0,000	0,000
Ca	0,231	0,243	0,252	0,359	0,209	0,073	0,247	0,369	0,253	0,224	0,252	0,325	0,271	0,238	0,248	0,335	0,238
Na	0,623	0,783	0,757	0,624	0,826	0,330	0,748	0,598	0,776	0,835	0,758	0,657	0,705	0,793	0,767	0,640	0,774
K	0,000	0,011	0,011	0,000	0,011	0,000	0,000	0,000	0,011	0,000	0,006	0,000	0,011	0,011	0,000	0,000	0,000
Ba	0,000	0,000	0,000	0,000	0,000	0,000	0,000	0,000	0,000	0,000	0,000	0,000	0,000	0,000	0,000	0,000	0,000
Total	4,922	5,032	5,023	5,023	5,046	4,621	5,007	5,012	5,037	5,051	5,019	5,022	4,991	5,045	5,024	5,024	5,016
Or	0,0	1,1	1,1	0,0	1,1	0,0	0,0	0,0	1,1	0,0	0,6	0,0	1,1	1,1	0,0	0,0	0,0
Ab	72,9	75,5	74,2	63,5	78,9	81,9	75,2	61,9	74,6	78,9	74,6	66,9	71,4	76,1	75,6	65,7	76,5
An	27,1	23,4	24,7	36,5	20,0	18,1	24,8	38,1	24,3	21,1	24,8	33,1	27,4	22,8	24,4	34,3	23,5

Apêndice C.1. Análises químicas pontuais em plagioclásio (continuação).

Amostra	SOS 873B	SOS 873B	SOS 873B	SOS 873B	SOS 873B	SOS 873B	SOS 873B	SOS 873B	SOS 873B	SOS 873B	SOS 873B	SOS 873B	SOS 873B	SOS 873B	SOS 873B	SOS 873B	SOS 873B
Espectro	40[c]	40[d]	41[a]	41[b]	41[c]	41[d]	42[a]	42[b]	42[c]	42[d]	43[a]	43[b]	43[c]	43[d]	44[a]	44[b]	44[c]
UTM	629288	629288	629288	629288	629288	629288	629288	629288	629288	629288	629288	629288	629288	629288	629288	629288	629288
	8909896	8909896	8909896	8909896	8909896	8909896	8909896	8909896	8909896	8909896	8909896	8909896	8909896	8909896	8909896	8909896	8909896
SiO_2	60,9	61,4	60,8	60,9	60,8	58,0	62,4	59,8	63,2	60,6	60,1	57,6	58,8	60,9	60,0	57,6	58,7
Al_2O_3	24,8	24,5	25,6	24,8	24,8	27,0	28,9	25,6	30,5	25,2	25,9	27,4	26,2	24,6	26,1	27,3	26,2
FeO	0,0	0,0	0,0	0,0	0,0	0,0	0,0	0,0	0,0	0,0	0,0	0,0	0,0	0,0	0,0	0,0	0,0
CaO	5,3	5,1	4,7	5,4	5,4	7,8	1,5	6,7	1,2	5,6	5,0	8,0	6,9	5,6	5,0	8,1	7,1
Na_2O	8,8	9,0	8,9	8,6	8,8	7,2	7,2	8,0	5,1	8,5	8,9	7,0	8,1	8,8	9,0	7,0	8,0
K_2O	0,2	0,0	0,0	0,2	0,1	0,0	0,0	0,0	0,0	0,0	0,0	0,0	0,0	0,0	0,0	0,0	0,0
BaO	0,0	0,0	0,0	0,0	0,0	0,0	0,0	0,0	0,0	0,0	0,0	0,0	0,0	0,0	0,0	0,0	0,0
Total	100,0	100,0	100,0	99,9	99,9	100,0	100,0	100,1	100,0	99,9	99,9	100,0	100,0	99,9	100,1	100,0	100,0
Si	2,707	2,724	2,694	2,708	2,705	2,591	2,706	2,661	2,710	2,693	2,671	2,574	2,625	2,709	2,663	2,575	2,622
Al	1,299	1,281	1,337	1,300	1,300	1,422	1,477	1,343	1,542	1,320	1,357	1,443	1,379	1,290	1,366	1,439	1,380
Fe	0,000	0,000	0,000	0,000	0,000	0,000	0,000	0,000	0,000	0,000	0,000	0,000	0,000	0,000	0,000	0,000	0,000
Ca	0,252	0,242	0,223	0,257	0,257	0,373	0,070	0,319	0,055	0,267	0,238	0,383	0,330	0,267	0,238	0,388	0,340
Na	0,758	0,774	0,765	0,742	0,759	0,624	0,605	0,690	0,424	0,733	0,767	0,607	0,701	0,759	0,775	0,607	0,693
K	0,011	0,000	0,000	0,011	0,006	0,000	0,000	0,000	0,000	0,000	0,000	0,000	0,000	0,000	0,000	0,000	0,000
Ba	0,000	0,000	0,000	0,000	0,000	0,000	0,000	0,000	0,000	0,000	0,000	0,000	0,000	0,000	0,000	0,000	0,000
Total	5,028	5,022	5,019	5,018	5,027	5,010	4,858	5,013	4,731	5,013	5,034	5,007	5,036	5,025	5,041	5,009	5,035
Or	1,1	0,0	0,0	1,1	0,6	0,0	0,0	0,0	0,0	0,0	0,0	0,0	0,0	0,0	0,0	0,0	0,0
Ab	74,2	76,2	77,4	73,4	74,3	62,6	89,7	68,4	88,5	73,3	76,3	61,3	68,0	74,0	76,5	61,0	67,1
An	24,7	23,8	22,6	25,5	25,2	37,4	10,3	31,6	11,5	26,7	23,7	38,7	32,0	26,0	23,5	39,0	32,9

Apêndice C.1. Análises químicas pontuais em plagioclásio (continuação).

Amostra	SOS 873B	SOS 873B	SOS 873B	SOS 873B	SOS 873B	SOS 873B	SOS 873B	SOS 873B	SOS 873B	SOS 873B	SOS 873B	SOS 873B	SOS 873B	SOS 873B	SOS 873B	SOS 873B	SOS 873B
Espectro	44[d]	45[a]	45[b]	45[c]	45[d]	46[a]	46[b]	46[c]	46[d]	47[a]	47[b]	47[c]	47[d]	48[a]	48[b]	48[c]	48[d]
UTM	629288	629288	629288	629288	629288	629288	629288	629288	629288	629288	629288	629288	629288	629288	629288	629288	629288
	8909896	8909896	8909896	8909896	8909896	8909896	8909896	8909896	8909896	8909896	8909896	8909896	8909896	8909896	8909896	8909896	8909896
SiO_2	61,6	60,7	57,8	58,3	59,1	60,2	58,6	59,1	60,4	60,5	58,6	62,2	61,3	62,0	60,7	61,0	61,2
Al_2O_3	24,2	25,5	27,0	26,7	26,3	25,6	26,5	26,2	25,2	25,7	26,5	24,7	24,4	24,7	25,0	24,6	24,6
FeO	0,0	0,0	0,0	0,0	0,0	0,0	0,0	0,0	0,0	0,0	0,0	0,0	0,0	0,0	0,0	0,0	0,0
CaO	4,6	4,6	8,0	7,7	7,1	4,7	7,2	7,1	5,8	4,7	7,1	4,3	5,1	4,0	5,6	5,4	5,3
Na_2O	9,5	9,2	7,2	7,3	7,4	9,5	7,5	7,6	8,4	9,1	7,7	8,9	9,0	9,4	8,5	8,9	8,8
K_2O	0,0	0,0	0,0	0,0	0,0	0,0	0,2	0,0	0,2	0,0	0,1	0,0	0,1	0,0	0,2	0,0	0,2
BaO	0,0	0,0	0,0	0,0	0,0	0,0	0,0	0,0	0,0	0,0	0,0	0,0	0,0	0,0	0,0	0,0	0,0
Total	99,9	100,0	100,0	100,0	99,9	100,0	100,0	100,0	100,0	100,0	100,0	100,1	99,9	100,1	100,0	99,9	100,1
Si	2,736	2,693	2,585	2,604	2,634	2,677	2,617	2,634	2,687	2,684	2,616	2,745	2,725	2,739	2,698	2,712	2,717
Al	1,267	1,333	1,423	1,405	1,382	1,342	1,395	1,376	1,321	1,344	1,395	1,285	1,278	1,286	1,310	1,289	1,287
Fe	0,000	0,000	0,000	0,000	0,000	0,000	0,000	0,000	0,000	0,000	0,000	0,000	0,000	0,000	0,000	0,000	0,000
Ca	0,219	0,219	0,383	0,368	0,339	0,224	0,344	0,339	0,276	0,223	0,340	0,203	0,243	0,189	0,267	0,257	0,252
Na	0,818	0,791	0,624	0,632	0,640	0,819	0,649	0,657	0,725	0,783	0,667	0,761	0,776	0,805	0,733	0,767	0,757
K	0,000	0,000	0,000	0,000	0,000	0,000	0,011	0,000	0,011	0,000	0,006	0,000	0,006	0,000	0,011	0,000	0,011
Ba	0,000	0,000	0,000	0,000	0,000	0,000	0,000	0,000	0,000	0,000	0,000	0,000	0,000	0,000	0,000	0,000	0,000
Total	5,040	5,036	5,016	5,010	4,995	5,062	5,016	5,006	5,020	5,035	5,023	4,994	5,027	5,020	5,019	5,027	5,024
Or	0,0	0,0	0,0	0,0	0,0	0,0	1,1	0,0	1,1	0,0	0,6	0,0	0,6	0,0	1,1	0,0	1,1
Ab	78,9	78,4	62,0	63,2	65,4	78,5	64,6	66,0	71,6	77,8	65,9	78,9	75,7	81,0	72,5	74,9	74,2
An	21,1	21,6	38,0	36,8	34,6	21,5	34,3	34,0	27,3	22,2	33,6	21,1	23,7	19,0	26,4	25,1	24,7

Apêndice C.1. Análises químicas pontuais em plagioclásio (continuação).

Amostra	SOS 873B	SOS 873B	SOS 873B	SOS 873B	SOS 873B	SOS 873B	SOS 873B	SOS 873B	SOS 873B	SOS 873B	SOS 873B	SOS 873B	SOS 873B	SOS 873B	SOS 873B	SOS 873B	SOS 873B
Espectro	49[a]	49[b]	49[c]	49[d]	50[a]	50[b]	50[c]	50[d]	51[a]	51[b]	51[c]	51[d]	52[a]	52[b]	52[c]	53[a]	53[b]
UTM	629288	629288	629288	629288	629288	629288	629288	629288	629288	629288	629288	629288	629288	629288	629288	629288	629288
	8909896	8909896	8909896	8909896	8909896	8909896	8909896	8909896	8909896	8909896	8909896	8909896	8909896	8909896	8909896	8909896	8909896
SiO_2	61,8	57,7	60,9	59,0	61,9	60,9	61,3	59,7	57,0	60,7	61,3	62,8	56,7	61,0	59,1	56,5	61,2
Al_2O_3	24,8	26,9	24,4	26,0	25,0	24,6	24,3	25,4	28,6	24,9	24,4	24,8	28,6	24,2	27,9	28,7	24,4
FeO	0,0	0,0	0,0	0,0	0,0	0,0	0,0	0,0	0,0	0,0	0,0	0,0	0,0	0,3	0,0	0,0	0,0
CaO	3,9	7,8	5,3	6,9	3,7	5,3	5,1	6,2	7,4	5,3	6,0	3,2	7,6	5,3	3,0	7,7	5,3
Na_2O	9,4	7,4	9,1	7,9	9,4	9,1	9,1	8,5	6,9	9,1	8,2	9,2	7,1	9,1	6,6	7,1	8,9
K_2O	0,0	0,2	0,2	0,2	0,0	0,2	0,1	0,2	0,0	0,0	0,0	0,0	0,0	0,1	3,4	0,0	0,1
BaO	0,0	0,0	0,0	0,0	0,0	0,0	0,0	0,0	0,0	0,0	0,0	0,0	0,0	0,0	0,0	0,0	0,0
Total	99,9	100,0	99,9	100,0	100,0	100,1	99,9	100,0	99,9	100,0	99,9	100,0	100,0	100,0	100,0	100,0	99,9
Si	2,735	2,584	2,713	2,635	2,735	2,708	2,726	2,663	2,545	2,699	2,723	2,764	2,534	2,717	2,637	2,527	2,721
Al	1,294	1,420	1,281	1,369	1,302	1,289	1,274	1,336	1,505	1,305	1,277	1,286	1,507	1,271	1,467	1,513	1,279
Fe	0,000	0,000	0,000	0,000	0,000	0,000	0,000	0,000	0,000	0,000	0,000	0,000	0,000	0,011	0,000	0,000	0,000
Ca	0,185	0,374	0,253	0,330	0,175	0,253	0,243	0,296	0,354	0,253	0,286	0,151	0,364	0,253	0,143	0,369	0,253
Na	0,807	0,643	0,786	0,684	0,805	0,785	0,785	0,735	0,597	0,785	0,706	0,785	0,615	0,786	0,571	0,616	0,767
K	0,000	0,011	0,011	0,011	0,000	0,011	0,006	0,011	0,000	0,000	0,000	0,000	0,000	0,006	0,193	0,000	0,006
Ba	0,000	0,000	0,000	0,000	0,000	0,000	0,000	0,000	0,000	0,000	0,000	0,000	0,000	0,000	0,000	0,000	0,000
Total	5,021	5,033	5,045	5,029	5,017	5,045	5,033	5,042	5,001	5,041	4,992	4,986	5,020	5,043	5,012	5,025	5,026
Or	0,0	1,1	1,1	1,1	0,0	1,1	0,5	1,1	0,0	0,0	0,0	0,0	0,0	0,5	21,3	0,0	0,6
Ab	81,3	62,5	74,8	66,7	82,1	74,8	75,9	70,5	62,8	75,7	71,2	83,9	62,8	75,2	62,9	62,5	74,8
An	18,7	36,4	24,1	32,2	17,9	24,1	23,5	28,4	37,2	24,3	28,8	16,1	37,2	24,2	15,8	37,5	24,6

Apêndice C.1. Análises químicas pontuais em plagioclásio (continuação).

Amostra	SOS 873B	SOS 873B	SOS 873B	SOS 873B	SOS 873B	SOS 873B	SOS 873B	SOS 873B	SOS 873B	SOS 873B	SOS 873B	SOS 873B	SOS 873B	SOS 873B	SOS 873B	SOS 873B	SOS 873B
Espectro	53[c]	54[a]	54[b]	54[c]	55[a]	55[b]	55[c]	55[d]	56[a]	56[b]	56[c]	56[d]	57[a]	57[b]	57[c]	58[a]	58[b]
UTM	629288	629288	629288	629288	629288	629288	629288	629288	629288	629288	629288	629288	629288	629288	629288	629288	629288
	8909896	8909896	8909896	8909896	8909896	8909896	8909896	8909896	8909896	8909896	8909896	8909896	8909896	8909896	8909896	8909896	8909896
SiO_2	57,2	58,4	61,1	58,3	57,8	61,3	61,0	65,3	61,2	60,3	62,6	64,7	57,5	57,9	61,3	61,2	58,3
Al_2O_3	27,3	27,3	24,9	26,5	27,8	24,5	24,7	25,7	30,6	25,1	23,6	22,6	28,1	26,7	24,3	25,5	26,5
FeO	0,0	0,0	0,0	0,0	0,0	0,0	0,0	0,0	0,0	0,0	0,3	0,0	0,0	0,0	0,0	0,0	0,0
CaO	8,0	6,2	5,3	7,3	6,9	5,5	5,4	1,0	1,2	6,1	2,6	1,8	7,0	7,8	5,2	4,4	7,7
Na_2O	7,5	8,2	8,7	7,9	7,5	8,6	8,7	8,0	7,0	8,5	9,6	10,2	7,3	7,6	8,9	8,9	7,5
K_2O	0,0	0,0	0,0	0,0	0,0	0,0	0,2	0,0	0,0	0,0	0,9	0,7	0,0	0,0	0,2	0,0	0,0
BaO	0,0	0,0	0,0	0,0	0,0	0,0	0,0	0,0	0,0	0,0	0,0	0,0	0,0	0,0	0,0	0,0	0,0
Total	100,0	100,1	100,0	100,0	100,0	99,9	100,0	100,0	100,0	100,0	99,6	100,0	99,9	100,0	99,9	100,0	100,0
Si	2,563	2,600	2,710	2,607	2,577	2,722	2,711	2,826	2,653	2,684	2,785	2,850	2,566	2,592	2,726	2,708	2,606
Al	1,442	1,433	1,302	1,397	1,461	1,282	1,294	1,311	1,563	1,317	1,237	1,173	1,478	1,409	1,274	1,330	1,396
Fe	0,000	0,000	0,000	0,000	0,000	0,000	0,000	0,000	0,000	0,000	0,011	0,000	0,000	0,000	0,000	0,000	0,000
Ca	0,384	0,296	0,252	0,350	0,330	0,262	0,257	0,046	0,056	0,291	0,124	0,085	0,335	0,374	0,248	0,209	0,369
Na	0,652	0,708	0,748	0,685	0,648	0,741	0,750	0,671	0,588	0,734	0,828	0,871	0,632	0,660	0,767	0,763	0,650
K	0,000	0,000	0,000	0,000	0,000	0,000	0,011	0,000	0,000	0,000	0,051	0,039	0,000	0,000	0,011	0,000	0,000
Ba	0,000	0,000	0,000	0,000	0,000	0,000	0,000	0,000	0,000	0,000	0,000	0,000	0,000	0,000	0,000	0,000	0,000
Total	5,041	5,037	5,013	5,038	5,016	5,007	5,023	4,854	4,860	5,025	5,036	5,019	5,011	5,034	5,026	5,009	5,021
Or	0,0	0,0	0,0	0,0	0,0	0,0	1,1	0,0	0,0	0,0	5,1	4,0	0,0	0,0	1,1	0,0	0,0
Ab	62,9	70,5	74,8	66,2	66,3	73,9	73,6	93,5	91,3	71,6	82,6	87,5	65,4	63,8	74,8	78,5	63,8
An	37,1	29,5	25,2	33,8	33,7	26,1	25,3	6,5	8,7	28,4	12,4	8,5	34,6	36,2	24,1	21,5	36,2

Apêndice C.1. Análises químicas pontuais em plagioclásio (continuação).

Amostra	SOS 873B	SOS 873B	SOS 873B	SOS 873B	SOS 873B	SOS 873B	SOS 873B	SOS 873B	SOS 873B	SOS 873B	SOS 873B	SOS 873B	SOS 873B	SOS 873B	SOS 873B	SOS 873B	SOS 873B
Espectro	58[ca]	59[a]	59[b]	59[c]	60[a]	60[b]	60[c]	61[a]	61[b]	61[c]	62[a]	62[b]	62[c]	63[a]	63[b]	63[c]	64[a]
UTM	629288	629288	629288	629288	629288	629288	629288	629288	629288	629288	629288	629288	629288	629288	629288	629288	629288
	8909896	8909896	8909896	8909896	8909896	8909896	8909896	8909896	8909896	8909896	8909896	8909896	8909896	8909896	8909896	8909896	8909896
SiO_2	61,4	59,0	57,9	62,3	56,6	58,1	57,9	56,8	57,9	59,2	57,8	57,6	60,9	64,3	57,9	60,7	60,1
Al_2O_3	24,5	27,0	26,6	24,0	28,8	26,9	26,6	28,6	27,1	26,1	28,0	26,8	24,6	23,6	27,1	24,9	26,1
FeO	0,0	0,0	0,0	0,0	0,0	0,0	0,0	0,0	0,0	0,0	0,0	0,0	0,0	0,0	0,0	0,0	0,0
CaO	5,2	6,2	7,6	4,7	7,6	7,8	7,6	7,5	7,2	6,7	6,8	8,1	5,2	1,5	7,9	5,8	4,9
Na_2O	8,9	7,9	7,7	9,1	7,0	7,3	7,7	7,1	7,9	7,7	7,5	7,3	9,1	10,7	7,1	8,6	8,8
K_2O	0,0	0,0	0,2	0,0	0,0	0,0	0,2	0,0	0,0	0,3	0,0	0,2	0,2	0,0	0,0	0,0	0,0
BaO	0,0	0,0	0,0	0,0	0,0	0,0	0,0	0,0	0,0	0,0	0,0	0,0	0,0	0,0	0,0	0,0	0,0
Total	100,0	100,1	100,0	100,1	100,0	100,1	100,0	100,0	100,1	100,0	100,1	100,0	100,0	100,1	100,0	100,0	99,9
Si	2,724	2,622	2,594	2,755	2,529	2,594	2,594	2,537	2,586	2,640	2,574	2,582	2,709	2,822	2,587	2,698	2,669
Al	1,281	1,414	1,405	1,251	1,517	1,416	1,405	1,506	1,427	1,372	1,470	1,416	1,290	1,221	1,427	1,305	1,366
Fe	0,000	0,000	0,000	0,000	0,000	0,000	0,000	0,000	0,000	0,000	0,000	0,000	0,000	0,000	0,000	0,000	0,000
Ca	0,247	0,295	0,365	0,223	0,364	0,373	0,365	0,359	0,345	0,320	0,324	0,389	0,248	0,071	0,378	0,276	0,233
Na	0,766	0,681	0,669	0,780	0,606	0,632	0,669	0,615	0,684	0,666	0,648	0,635	0,785	0,910	0,615	0,741	0,758
K	0,000	0,000	0,011	0,000	0,000	0,000	0,011	0,000	0,000	0,017	0,000	0,011	0,011	0,000	0,000	0,000	0,000
Ba	0,000	0,000	0,000	0,000	0,000	0,000	0,000	0,000	0,000	0,000	0,000	0,000	0,000	0,000	0,000	0,000	0,000
Total	5,018	5,012	5,044	5,009	5,016	5,014	5,044	5,017	5,042	5,015	5,015	5,033	5,044	5,023	5,007	5,020	5,027
Or	0,0	0,0	1,1	0,0	0,0	0,0	1,1	0,0	0,0	1,7	0,0	1,1	1,1	0,0	0,0	0,0	0,0
Ab	75,6	69,8	64,0	77,8	62,5	62,9	64,0	63,1	66,5	66,4	66,6	61,3	75,2	92,8	61,9	72,8	76,5
An	24,4	30,2	34,9	22,2	37,5	37,1	34,9	36,9	33,5	31,9	33,4	37,6	23,7	7,2	38,1	27,2	23,5

Apêndice C.1. Análises químicas pontuais em plagioclásio (continuação).

Amostra	SOS 873B	SOS 873B	SOS 873B	SOS 873B	SOS 873B	SOS 873B	SOS 873B	SOS 873B	SOS 873B	SOS 873B	SOS 873B	SOS 873B	SOS 873B	SOS 873B	SOS 873B	SOS 873B	SOS 873B
Espectro	64[b]	64[c]	65[a]	65[b]	66	67	68[a]	68[b]	69[a]	69[b]	70[a]	70[b]	71[a]	71[b]	72[a]	72[b]	73[a]
UTM	629288	629288	629288	629288	629288	629288	629288	629288	629288	629288	629288	629288	629288	629288	629288	629288	629288
	8909896	8909896	8909896	8909896	8909896	8909896	8909896	8909896	8909896	8909896	8909896	8909896	8909896	8909896	8909896	8909896	8909896
SiO_2	57,7	58,0	59,9	61,8	64,5	62,1	60,6	61,0	60,5	61,0	60,6	60,4	60,8	59,9	60,9	60,5	62,0
Al_2O_3	27,0	26,5	26,0	23,7	24,3	24,2	25,7	24,4	25,6	25,0	25,6	25,1	25,5	25,2	25,5	25,2	24,9
FeO	0,0	0,0	0,0	0,4	0,0	0,0	0,0	0,0	0,0	0,0	0,0	0,0	0,0	0,0	0,0	0,0	0,0
CaO	7,7	7,7	5,4	4,7	2,4	4,2	4,6	5,5	4,8	5,4	4,8	5,9	4,6	6,2	4,3	6,0	3,7
Na_2O	7,4	7,8	8,6	9,3	8,7	9,1	9,1	8,9	9,1	8,6	9,0	8,5	9,2	8,5	9,3	8,4	9,4
K_2O	0,2	0,0	0,0	0,0	0,0	0,4	0,0	0,2	0,0	0,0	0,0	0,1	0,0	0,2	0,0	0,0	0,0
BaO	0,0	0,0	0,0	0,0	0,0	0,0	0,0	0,0	0,0	0,0	0,0	0,0	0,0	0,0	0,0	0,0	0,0
Total	100,0	100,0	99,9	99,9	99,9	100,0	100,0	100,0	100,0	100,0	100,0	100,0	100,1	100,0	100,0	100,1	100,0
Si	2,583	2,597	2,664	2,748	2,820	2,751	2,688	2,714	2,685	2,706	2,688	2,687	2,694	2,672	2,699	2,687	2,739
Al	1,425	1,399	1,363	1,242	1,252	1,264	1,343	1,280	1,339	1,307	1,339	1,316	1,332	1,325	1,332	1,319	1,296
Fe	0,000	0,000	0,000	0,015	0,000	0,000	0,000	0,000	0,000	0,000	0,000	0,000	0,000	0,000	0,000	0,000	0,000
Ca	0,369	0,369	0,257	0,224	0,112	0,199	0,219	0,262	0,228	0,257	0,228	0,281	0,218	0,296	0,204	0,286	0,175
Na	0,642	0,677	0,742	0,802	0,738	0,782	0,783	0,768	0,783	0,740	0,774	0,733	0,790	0,735	0,799	0,723	0,805
K	0,011	0,000	0,000	0,000	0,000	0,023	0,000	0,011	0,000	0,000	0,000	0,006	0,000	0,011	0,000	0,000	0,000
Ba	0,000	0,000	0,000	0,000	0,000	0,000	0,000	0,000	0,000	0,000	0,000	0,000	0,000	0,000	0,000	0,000	0,000
Total	5,031	5,042	5,026	5,031	4,922	5,019	5,032	5,035	5,036	5,010	5,029	5,024	5,035	5,039	5,035	5,015	5,016
Or	1,1	0,0	0,0	0,0	0,0	2,3	0,0	1,1	0,0	0,0	0,0	0,6	0,0	1,1	0,0	0,0	0,0
Ab	62,8	64,7	74,2	78,2	86,8	77,9	78,2	73,7	77,4	74,2	77,2	71,9	78,4	70,5	79,6	71,7	82,1
An	36,1	35,3	25,8	21,8	13,2	19,9	21,8	25,2	22,6	25,8	22,8	27,6	21,6	28,4	20,4	28,3	17,9

Apêndice C.1. Análises químicas pontuais em plagioclásio (continuação).

Amostra	SOS 873B	SOS 873B	SOS 873B	SOS 873B	SOS 873B	SOS 873B	SOS 873B	SOS 873B	SOS 873B	SOS 873B	SOS 873B	SOS 873B	SOS 873B	SOS 873B	SOS 873B	SOS 873B	SOS 873B
Espectro	73[b]	74[a]	74[b]	75	76	77	78	79	80	81	82	83	84	85	86	87	88
UTM	629288	629288	629288	629288	629288	629288	629288	629288	629288	629288	629288	629288	629288	629288	629288	629288	629288
	8909896	8909896	8909896	8909896	8909896	8909896	8909896	8909896	8909896	8909896	8909896	8909896	8909896	8909896	8909896	8909896	8909896
SiO_2	59,0	64,0	57,2	56,8	59,4	58,1	61,2	60,8	60,7	60,6	59,6	57,8	57,2	57,7	57,8	58,6	58,9
Al_2O_3	26,1	23,6	27,1	27,9	25,6	26,9	24,4	24,6	24,5	24,9	25,4	26,9	27,1	26,9	27,0	26,6	26,0
FeO	0,0	0,0	0,0	0,0	0,0	0,0	0,3	0,0	0,0	0,0	0,0	0,0	0,0	0,0	0,0	0,0	0,0
CaO	6,8	2,7	8,2	8,6	7,0	7,7	5,2	5,6	5,4	5,6	6,5	7,9	8,3	8,1	7,8	7,1	6,7
Na_2O	7,9	9,6	7,5	6,7	8,0	7,3	8,6	8,9	9,1	8,8	8,3	7,4	7,2	7,4	7,4	7,6	8,4
K_2O	0,2	0,0	0,0	0,0	0,0	0,0	0,3	0,2	0,2	0,2	0,2	0,0	0,2	0,0	0,0	0,0	0,0
BaO	0,0	0,0	0,0	0,0	0,0	0,0	0,0	0,0	0,0	0,0	0,0	0,0	0,0	0,0	0,0	0,0	0,0
Total	100,0	99,9	100,0	100,0	100,0	100,0	100,0	100,1	99,9	100,1	100,0	100,0	100,0	100,1	100,0	99,9	100,0
Si	2,634	2,814	2,565	2,544	2,650	2,595	2,722	2,704	2,706	2,695	2,660	2,586	2,566	2,581	2,585	2,616	2,631
Al	1,373	1,223	1,433	1,473	1,346	1,416	1,279	1,290	1,287	1,305	1,336	1,419	1,433	1,419	1,423	1,400	1,369
Fe	0,000	0,000	0,000	0,000	0,000	0,000	0,011	0,000	0,000	0,000	0,000	0,000	0,000	0,000	0,000	0,000	0,000
Ca	0,325	0,127	0,394	0,413	0,335	0,369	0,248	0,267	0,258	0,267	0,311	0,379	0,399	0,388	0,374	0,340	0,321
Na	0,684	0,819	0,652	0,582	0,692	0,632	0,742	0,768	0,787	0,759	0,718	0,642	0,626	0,642	0,642	0,658	0,728
K	0,011	0,000	0,000	0,000	0,000	0,000	0,017	0,011	0,011	0,011	0,011	0,000	0,011	0,000	0,000	0,000	0,000
Ba	0,000	0,000	0,000	0,000	0,000	0,000	0,000	0,000	0,000	0,000	0,000	0,000	0,000	0,000	0,000	0,000	0,000
Total	5,027	4,983	5,044	5,011	5,023	5,013	5,018	5,040	5,049	5,037	5,037	5,026	5,036	5,030	5,024	5,013	5,048
Or	1,1	0,0	0,0	0,0	0,0	0,0	1,7	1,1	1,1	1,1	1,1	0,0	1,1	0,0	0,0	0,0	0,0
Ab	67,0	86,5	62,3	58,5	67,4	63,2	73,7	73,4	74,5	73,2	69,0	62,9	60,4	62,3	63,2	66,0	69,4
An	31,9	13,5	37,7	41,5	32,6	36,8	24,6	25,5	24,4	25,7	29,9	37,1	38,5	37,7	36,8	34,0	30,6

Apêndice C.1. Análises químicas pontuais em plagioclásio (continuação).

Amostra	SOS 873B	SOS 873B	SOS 873B	SOS 873B	SOS 873B	SOS 873B	SOS 873B	SOS 873B	SOS 873B	SOS 876A	SOS 876A	SOS 876A	SOS 876A	SOS 876A	SOS 876A	SOS 876A	SOS 876A
Espectro	89	90	91	92	93	99	100	103	104	1	2	3	4	5	6	7	8
UTM	629288	629288	629288	629288	629288	629288	629288	629288	629288	636358	636358	636358	636358	636358	636358	636358	636358
	8909896	8909896	8909896	8909896	8909896	8909896	8909896	8909896	8909896	8909699	8909699	8909699	8909699	8909699	8909699	8909699	8909699
SiO_2	59,9	58,1	57,2	56,7	57,2	57,3	57,4	58,1	56,8	64,2	64,2	63,7	64,0	64,1	64,2	63,8	64,0
Al_2O_3	25,6	26,7	27,5	27,2	26,9	28,5	28,2	27,7	28,6	22,6	22,5	23,1	22,6	22,4	22,6	22,7	22,6
FeO	0,0	0,0	0,0	0,0	0,3	0,0	0,0	0,0	0,0	0,0	0,0	0,0	0,0	0,0	0,0	0,0	0,0
CaO	6,4	7,8	8,4	8,2	7,9	7,3	7,2	6,5	7,7	3,2	3,1	3,0	3,1	3,1	3,0	2,8	3,1
Na_2O	8,2	7,3	6,9	7,7	7,6	6,9	7,2	7,7	6,9	9,9	10,0	9,9	10,1	10,1	9,9	10,4	9,9
K_2O	0,0	0,2	0,0	0,1	0,1	0,0	0,0	0,0	0,0	0,2	0,2	0,4	0,2	0,2	0,2	0,3	0,3
BaO	0,0	0,0	0,0	0,0	0,0	0,0	0,0	0,0	0,0	0,0	0,0	0,0	0,0	0,0	0,0	0,0	0,0
Total	100,1	100,1	100,0	99,9	100,0	100,0	100,0	100,0	100,0	100,1	100,0	100,1	100,0	99,9	99,9	100,0	99,9
Si	2,664	2,597	2,561	2,551	2,569	2,554	2,560	2,588	2,537	2,830	2,832	2,811	2,826	2,832	2,833	2,820	2,828
Al	1,342	1,407	1,451	1,442	1,424	1,497	1,483	1,454	1,506	1,174	1,170	1,201	1,176	1,167	1,175	1,183	1,177
Fe	0,000	0,000	0,000	0,000	0,011	0,000	0,000	0,000	0,000	0,000	0,000	0,000	0,000	0,000	0,000	0,000	0,000
Ca	0,305	0,374	0,403	0,395	0,380	0,349	0,344	0,310	0,369	0,151	0,147	0,142	0,147	0,147	0,142	0,133	0,147
Na	0,707	0,633	0,599	0,672	0,662	0,596	0,623	0,665	0,598	0,846	0,855	0,847	0,865	0,865	0,847	0,891	0,848
K	0,000	0,011	0,000	0,006	0,006	0,000	0,000	0,000	0,000	0,011	0,011	0,023	0,011	0,011	0,011	0,017	0,017
Ba	0,000	0,000	0,000	0,000	0,000	0,000	0,000	0,000	0,000	0,000	0,000	0,000	0,000	0,000	0,000	0,000	0,000
Total	5,018	5,022	5,013	5,066	5,053	4,996	5,010	5,017	5,009	5,012	5,016	5,023	5,024	5,023	5,009	5,043	5,016
Or	0,0	1,1	0,0	0,5	0,5	0,0	0,0	0,0	0,0	1,1	1,1	2,2	1,1	1,1	1,1	1,6	1,7
Ab	69,9	62,2	59,8	62,6	63,2	63,1	64,4	68,2	61,9	83,9	84,4	83,7	84,6	84,6	84,7	85,6	83,8
An	30,1	36,7	40,2	36,8	36,3	36,9	35,6	31,8	38,1	15,0	14,5	14,0	14,3	14,3	14,2	12,7	14,5

Apêndice C.1. Análises químicas pontuais em plagioclásio (continuação).

Amostra	SOS 876A	SOS 876A	SOS 876A	SOS 876A	SOS 876A	SOS 876A	SOS 876A	SOS 876A	SOS 876A	SOS 876A	SOS 876A	SOS 876A	SOS 876A	SOS 876A	SOS 876A	SOS 876A	SOS 876B
Espectro	9	10	11	12	13	14	15	16	17	26	27	28	29	30	31	32	1
UTM	636358	636358	636358	636358	636358	636358	636358	636358	636358	636358	636358	636358	636358	636358	636358	636358	636358
	8909699	8909699	8909699	8909699	8909699	8909699	8909699	8909699	8909699	8909699	8909699	8909699	8909699	8909699	8909699	8909699	8909699
SiO_2	63,9	64,0	64,1	63,4	63,4	63,6	64,4	64,7	66,2	64,0	64,0	63,6	65,0	64,5	64,5	65,9	60,7
Al_2O_3	22,6	22,7	22,7	23,2	23,3	22,9	22,7	22,3	21,0	22,7	22,9	23,0	22,1	22,3	22,4	21,5	25,7
FeO	0,0	0,0	0,0	0,0	0,0	0,0	0,0	0,0	0,0	0,0	0,0	0,0	0,0	0,0	0,0	0,0	0,0
CaO	3,4	3,2	3,2	3,6	3,5	3,5	2,4	2,7	1,5	3,3	3,5	3,4	2,7	3,0	3,1	2,1	4,8
Na_2O	9,8	9,8	9,7	9,5	9,6	9,8	10,2	10,3	11,3	9,7	9,5	9,6	10,2	10,0	10,0	10,5	8,8
K_2O	0,3	0,3	0,2	0,3	0,3	0,1	0,4	0,0	0,0	0,2	0,2	0,2	0,0	0,2	0,0	0,0	0,0
BaO	0,0	0,0	0,0	0,0	0,0	0,0	0,0	0,0	0,0	0,0	0,0	0,0	0,0	0,0	0,0	0,0	0,0
Total	100,0	100,0	99,9	100,0	100,1	99,9	100,1	100,0	100,0	99,9	100,1	99,8	100,0	100,0	100,0	100,0	100,0
Si	2,823	2,825	2,829	2,801	2,798	2,811	2,836	2,849	2,908	2,826	2,820	2,812	2,859	2,844	2,841	2,893	2,690
Al	1,177	1,181	1,181	1,208	1,212	1,193	1,178	1,157	1,087	1,181	1,189	1,199	1,146	1,159	1,163	1,112	1,342
Fe	0,000	0,000	0,000	0,000	0,000	0,000	0,000	0,000	0,000	0,000	0,000	0,000	0,000	0,000	0,000	0,000	0,000
Ca	0,161	0,151	0,151	0,170	0,166	0,166	0,113	0,127	0,071	0,156	0,165	0,161	0,127	0,142	0,146	0,099	0,228
Na	0,839	0,839	0,830	0,814	0,822	0,840	0,871	0,879	0,963	0,830	0,812	0,823	0,870	0,855	0,854	0,894	0,756
K	0,017	0,017	0,011	0,017	0,017	0,006	0,022	0,000	0,000	0,011	0,011	0,011	0,000	0,011	0,000	0,000	0,000
Ba	0,000	0,000	0,000	0,000	0,000	0,000	0,000	0,000	0,000	0,000	0,000	0,000	0,000	0,000	0,000	0,000	0,000
Total	5,017	5,013	5,002	5,010	5,015	5,015	5,021	5,012	5,029	5,005	4,997	5,006	5,003	5,010	5,004	4,998	5,017
Or	1,7	1,7	1,1	1,7	1,7	0,6	2,2	0,0	0,0	1,1	1,1	1,1	0,0	1,1	0,0	0,0	0,0
Ab	82,5	83,3	83,6	81,3	81,8	83,1	86,5	87,3	93,2	83,2	82,1	82,7	87,2	84,8	85,4	90,0	76,8
An	15,8	15,0	15,2	17,0	16,5	16,4	11,2	12,7	6,8	15,6	16,7	16,2	12,8	14,1	14,6	10,0	23,2

Apêndice C.1. Análises químicas pontuais em plagioclásio (continuação).

Amostra	SOS 876B	SOS 876B	SOS 876B	SOS 876B	SOS 876B	SOS 876B	SOS 876B	SOS 876B	SOS 876B	SOS 876B	SOS 876B	SOS 876B	SOS 876B	SOS 876B	SOS 876B	SOS 876B	SOS 876B
Espectro	4	5	18[a]	18[b]	19[a]	19[b]	20[a]	20[b]	21[a]	21[b]	22[a]	22[b]	23[a]	23[b]	24[a]	24[b]	25[a]
UTM	636358	636358	636358	636358	636358	636358	636358	636358	636358	636358	636358	636358	636358	636358	636358	636358	636358
	8909699	8909699	8909699	8909699	8909699	8909699	8909699	8909699	8909699	8909699	8909699	8909699	8909699	8909699	8909699	8909699	8909699
SiO_2	60,5	61,5	63,3	61,2	63,1	60,7	66,4	60,7	63,2	59,5	62,8	59,7	62,3	59,6	64,0	60,1	63,5
Al_2O_3	25,8	25,1	23,0	25,1	23,1	25,5	21,2	25,9	23,0	26,8	23,4	26,9	23,8	26,5	22,7	26,1	22,9
FeO	0,0	0,0	0,0	0,0	0,0	0,0	0,0	0,0	0,0	0,0	0,0	0,0	0,0	0,0	0,0	0,0	0,0
CaO	4,9	4,2	4,0	4,5	4,2	4,8	1,6	4,8	3,9	5,4	4,0	5,3	4,0	5,5	3,1	5,3	3,6
Na_2O	8,8	9,2	9,6	9,2	9,5	9,0	10,1	8,6	9,8	8,3	9,5	8,1	9,8	8,4	9,9	8,5	9,9
K_2O	0,0	0,0	0,0	0,0	0,1	0,0	0,7	0,0	0,2	0,0	0,2	0,0	0,2	0,0	0,3	0,0	0,2
BaO	0,0	0,0	0,0	0,0	0,0	0,0	0,0	0,0	0,0	0,0	0,0	0,0	0,0	0,0	0,0	0,0	0,0
Total	100,0	100,0	99,9	100,0	100,0	100,0	100,0	100,0	100,1	100,0	99,9	100,0	100,1	100,0	100,0	100,0	100,1
Si	2,683	2,721	2,800	2,712	2,792	2,692	2,915	2,688	2,795	2,641	2,782	2,646	2,760	2,648	2,825	2,667	2,806
Al	1,349	1,309	1,199	1,311	1,205	1,333	1,097	1,352	1,199	1,402	1,222	1,405	1,243	1,388	1,181	1,365	1,193
Fe	0,000	0,000	0,000	0,000	0,000	0,000	0,000	0,000	0,000	0,000	0,000	0,000	0,000	0,000	0,000	0,000	0,000
Ca	0,233	0,199	0,190	0,214	0,199	0,228	0,075	0,228	0,185	0,257	0,190	0,252	0,190	0,262	0,147	0,252	0,170
Na	0,757	0,789	0,823	0,791	0,815	0,774	0,860	0,738	0,840	0,714	0,816	0,696	0,842	0,724	0,847	0,731	0,848
K	0,000	0,000	0,000	0,000	0,006	0,000	0,039	0,000	0,011	0,000	0,011	0,000	0,011	0,000	0,017	0,000	0,011
Ba	0,000	0,000	0,000	0,000	0,000	0,000	0,000	0,000	0,000	0,000	0,000	0,000	0,000	0,000	0,000	0,000	0,000
Total	5,021	5,019	5,012	5,028	5,016	5,028	4,986	5,006	5,031	5,015	5,021	4,999	5,045	5,020	5,017	5,016	5,028
Or	0,0	0,0	0,0	0,0	0,6	0,0	4,0	0,0	1,1	0,0	1,1	0,0	1,1	0,0	1,7	0,0	1,1
Ab	76,5	79,9	81,3	78,7	79,9	77,2	88,3	76,4	81,1	73,6	80,2	73,4	80,7	73,4	83,8	74,4	82,4
An	23,5	20,1	18,7	21,3	19,5	22,8	7,7	23,6	17,8	26,4	18,7	26,6	18,2	26,6	14,5	25,6	16,5

Apêndice C.1. Análises químicas pontuais em plagioclásio (continuação).

Amostra	SOS 876B	SOS 876B	SOS 876B	SOS 876B	SOS 876B	SOS 876B	SOS 876B	SOS 876B	SOS 876B	SOS 876B	SOS 876B	SOS 876B	SOS 876B	SOS 876B	SOS 876B	SOS 876B	SOS 876B
Espectro	25[b]	26[a]	26[b]	27	28	29	30	31	32	33[a]	33[b]	34[a]	34[b]	35[a]	35[b]	36[a]	36[b]
UTM	636358 8909699	636358 8909699	636358 8909699	636358 8909699	636358 8909699	636358 8909699	636358 8909699	636358 8909699	636358 8909699	636358 8909699	636358 8909699	636358 8909699	636358 8909699	636358 8909699	636358 8909699	636358 8909699	636358 8909699
SiO_2	60,5	63,7	60,3	59,6	60,0	60,0	60,0	59,1	59,5	62,7	58,8	62,5	59,1	62,4	58,2	60,2	59,5
Al_2O_3	26,0	22,7	25,9	26,4	26,2	26,4	26,2	26,7	26,9	23,4	27,2	23,5	26,9	23,8	27,5	25,5	26,6
FeO	0,0	0,0	0,0	0,0	0,0	0,0	0,0	0,0	0,0	0,0	0,0	0,0	0,0	0,0	0,0	0,0	0,0
CaO	5,1	3,6	5,0	5,6	5,6	5,9	5,3	6,4	5,6	4,5	6,4	4,6	6,3	4,5	6,7	6,1	6,3
Na_2O	8,4	9,6	8,9	8,4	8,3	7,7	8,5	7,9	8,1	9,2	7,6	9,2	7,6	9,0	7,6	7,9	7,7
K_2O	0,0	0,4	0,0	0,0	0,0	0,0	0,0	0,0	0,0	0,2	0,0	0,2	0,0	0,2	0,0	0,2	0,0
BaO	0,0	0,0	0,0	0,0	0,0	0,0	0,0	0,0	0,0	0,0	0,0	0,0	0,0	0,0	0,0	0,0	0,0
Total	100,0	100,0	100,1	100,0	100,1	100,0	100,0	100,1	100,1	100,0	100,0	100,0	99,9	99,9	100,0	99,9	100,1
Si	2,680	2,816	2,674	2,649	2,661	2,660	2,663	2,628	2,638	2,777	2,615	2,770	2,628	2,765	2,593	2,678	2,641
Al	1,358	1,183	1,354	1,383	1,370	1,379	1,371	1,399	1,406	1,221	1,426	1,227	1,410	1,243	1,444	1,337	1,392
Fe	0,000	0,000	0,000	0,000	0,000	0,000	0,000	0,000	0,000	0,000	0,000	0,000	0,000	0,000	0,000	0,000	0,000
Ca	0,242	0,171	0,238	0,267	0,266	0,280	0,252	0,305	0,266	0,214	0,305	0,218	0,300	0,214	0,320	0,291	0,300
Na	0,722	0,823	0,765	0,724	0,714	0,662	0,732	0,681	0,696	0,790	0,655	0,791	0,655	0,773	0,657	0,682	0,663
K	0,000	0,023	0,000	0,000	0,000	0,000	0,000	0,000	0,000	0,011	0,000	0,011	0,000	0,011	0,000	0,011	0,000
Ba	0,000	0,000	0,000	0,000	0,000	0,000	0,000	0,000	0,000	0,000	0,000	0,000	0,000	0,000	0,000	0,000	0,000
Total	5,002	5,015	5,031	5,022	5,011	4,981	5,017	5,013	5,007	5,013	5,000	5,017	4,994	5,006	5,013	4,999	4,995
Or	0,0	2,2	0,0	0,0	0,0	0,0	0,0	0,0	0,0	1,1	0,0	1,1	0,0	1,1	0,0	1,2	0,0
Ab	74,9	81,0	76,3	73,1	72,8	70,3	74,4	69,1	72,4	77,8	68,2	77,5	68,6	77,5	67,2	69,3	68,9
An	25,1	16,8	23,7	26,9	27,2	29,7	25,6	30,9	27,6	21,0	31,8	21,4	31,4	21,4	32,8	29,6	31,1

Apêndice C.1. Análises químicas pontuais em plagioclásio (continuação).

Amostra	SOS 876B	SOS 876B	SOS 876B	SOS 876B	SOS 876B	SOS 876B	SOS 876B	SOS 876B	SOS 876B	SOS 876B	SOS 876B
Espectro	37	38[a]	38[b]	39[a]	39[b]	40	41	42	43	46	56
UTM	636358	636358	636358	636358	636358	636358	636358	636358	636358	636358	636358
	8909699	8909699	8909699	8909699	8909699	8909699	8909699	8909699	8909699	8909699	8909699
SiO_2	64,3	63,3	58,3	63,8	60,2	59,7	65,0	60,6	63,4	61,5	63,1
Al_2O_3	23,0	23,1	27,5	22,8	26,2	26,5	24,8	26,0	24,8	25,1	23,3
FeO	0,0	0,0	0,0	0,0	0,0	0,0	0,0	0,0	0,0	0,0	0,0
CaO	2,0	4,0	6,7	3,8	5,4	5,4	2,3	5,1	2,0	4,3	4,4
Na_2O	10,7	9,3	7,5	9,5	8,2	8,4	7,9	8,3	9,8	9,1	9,1
K_2O	0,0	0,2	0,0	0,0	0,0	0,0	0,0	0,0	0,0	0,0	0,1
BaO	0,0	0,0	0,0	0,0	0,0	0,0	0,0	0,0	0,0	0,0	0,0
Total	100,0	99,9	100,0	99,9	100,0	100,0	100,0	100,0	100,0	100,0	100,0
Si	2,830	2,800	2,596	2,817	2,669	2,651	2,827	2,683	2,782	2,721	2,789
Al	1,193	1,204	1,443	1,187	1,369	1,387	1,271	1,357	1,283	1,309	1,214
Fe	0,000	0,000	0,000	0,000	0,000	0,000	0,000	0,000	0,000	0,000	0,000
Ca	0,094	0,190	0,320	0,180	0,257	0,257	0,107	0,242	0,094	0,204	0,208
Na	0,913	0,798	0,648	0,813	0,705	0,723	0,666	0,713	0,834	0,781	0,780
K	0,000	0,011	0,000	0,000	0,000	0,000	0,000	0,000	0,000	0,000	0,006
Ba	0,000	0,000	0,000	0,000	0,000	0,000	0,000	0,000	0,000	0,000	0,000
Total	5,030	5,003	5,006	4,996	4,999	5,018	4,871	4,995	4,993	5,015	4,997
Or	0,0	1,1	0,0	0,0	0,0	0,0	0,0	0,0	0,0	0,0	0,6
Ab	90,6	79,9	66,9	81,9	73,3	73,8	86,1	74,7	89,9	79,3	78,5
An	9,4	19,0	33,1	18,1	26,7	26,2	13,9	25,3	10,1	20,7	21,0

Apêndice C.2. Análises químicas pontuais de cristais de biotita do Batólito Rio Jacaré. Cálculo da fórmula estrutural com base em 22 oxigênios. H_2O^* obtido por estequiometria.

Rocha	FDS 495	FDS 495	FDS 495	FDS 495	FDS 495	FDS 495	FDS 495	FDS 495	FDS 495	FDS 495	FDS 495	FDS 495	FDS 495
Espectro	10	11	12	13	26	27	35	68	80	81	150	157	168
SiO_2	37,7	37,9	38,1	37,3	38,0	37,8	37,7	38,3	38,1	38,1	38,7	38,4	37,6
TiO_2	1,5	1,8	2,0	2,0	1,5	1,4	1,9	1,5	1,9	1,4	1,7	1,4	2,9
Al_2O_3	15,5	15,6	15,7	15,0	15,8	15,8	15,0	15,6	15,1	14,9	16,2	15,0	15,5
FeO	19,6	18,9	18,6	19,3	18,3	18,7	19,8	17,9	18,1	18,8	17,2	18,0	18,0
MnO				0,5	0,4				0,4			0,4	0,4
MgO	12,2	11,9	11,8	11,8	12,6	12,4	11,6	12,8	12,5	13,0	12,4	13,2	11,6
Na_2O													
K_2O	9,2	9,8	9,7	9,6	9,2	9,8	9,6	9,7	9,5	9,4	9,8	9,4	9,8
F	0,2	0,1	0,1	0,5	0,2	0,0	0,3	0,2	0,4	0,4			
Cl				0,1			0,1						
H_2O^*	3,9	3,9	3,9	3,7	3,9	4,0	3,8	3,9	3,8	3,8	4,0	4,0	4,0
Subtotal	99,8	99,9	100,0	99,8	100,0	100,0	99,8	99,9	99,8	99,8	100,0	99,7	99,8
O=F,Cl	0,084	0,042	0,042	0,233	0,084		0,149	0,084	0,168	0,168			
Total	99,7	99,9	100,0	99,6	99,9	100,0	99,6	99,8	99,6	99,6	100,0	99,7	99,8
Si	5,704	5,718	5,725	5,687	5,704	5,692	5,732	5,743	5,746	5,753	5,761	5,771	5,674
Al^{iv}	2,296	2,282	2,275	2,313	2,296	2,308	2,268	2,257	2,254	2,247	2,239	2,229	2,326
	8,000	8,000	8,000	8,000	8,000	8,000	8,000	8,000	8,000	8,000	8,000	8,000	8,000
Al^{vi}	0,458	0,483	0,513	0,375	0,505	0,502	0,414	0,508	0,424	0,400	0,609	0,424	0,421
Ti	0,175	0,207	0,228	0,231	0,173	0,163	0,219	0,173	0,218	0,163	0,194	0,163	0,327
Fe^{3+}	0,301	0,187	0,130	0,266	0,269	0,265	0,219	0,211	0,212	0,320	0,077	0,290	0,076
Fe^{2+}	2,162	2,191	2,201	2,183	2,019	2,085	2,285	2,020	2,066	2,044	2,055	1,956	2,193
Mn				0,062	0,049				0,049			0,049	0,049
Mg	2,748	2,676	2,644	2,681	2,813	2,778	2,631	2,854	2,805	2,916	2,749	2,946	2,611
	5,843	5,744	5,716	5,798	5,827	5,793	5,769	5,766	5,774	5,844	5,684	5,827	5,677
Na													
K	1,777	1,884	1,858	1,865	1,764	1,880	1,860	1,854	1,828	1,811	1,860	1,803	1,883
	1,777	1,884	1,858	1,865	1,764	1,880	1,860	1,854	1,828	1,811	1,860	1,803	1,883
OH*	3,904	3,952	3,952	3,733	3,905	4,000	3,830	3,905	3,809	3,809	4,000	4,000	4,000
F	0,096	0,048	0,048	0,241	0,095		0,144	0,095	0,191	0,191			
Cl				0,026			0,026						
	4,000	4,000	4,000	4,000	4,000	4,000	4,000	4,000	4,000	4,000	4,000	4,000	4,000
TOTAL	19,620	19,627	19,574	19,662	19,591	19,672	19,629	19,620	19,601	19,655	19,544	19,631	19,561

Apêndice C.2. Análises químicas pontuais de cristais de biotita do Batólito Rio Jacaré (continuação).

Rocha	FDS 495	FDS 495	FDS 495	FDS 495	FDS 495	FDS 495	FDS 496A	FDS 496A	FDS 496A	FDS 496A	FDS 496A	FDS 496A	FDS 496A
Espectro	169	211	212	215	220	232	48	49	50	51	52	53	55
SiO_2	38,4	37,4	37,7	37,2	38,4	37,7	37,6	37,9	37,8	38,0	37,3	37,6	38,1
TiO_2	1,8	1,6	1,4	1,7	1,5	1,4	2,2	2,5	2,6	2,3	2,8	2,8	2,3
Al_2O_3	15,8	15,4	15,4	15,1	16,7	16,6	15,4	15,0	15,1	14,8	15,1	15,0	15,0
FeO	17,0	19,0	18,9	19,6	16,4	18,0	19,0	18,9	18,6	19,0	19,0	18,9	18,9
MnO			0,4	0,5		0,6	0,5						
MgO	12,9	12,6	12,6	12,1	13,5	11,9	11,2	11,8	11,7	11,9	11,8	11,9	11,8
Na_2O													
K_2O	9,8	9,4	9,3	9,4	9,4	9,8	9,8	9,9	9,8	9,9	9,8	9,7	9,9
F		0,5	0,3	0,4			0,2		0,3		0,2		
Cl							0,1		0,1				
H_2O*	4,0	3,7	3,8	3,7	4,0	4,0	3,8	4,0	3,8	4,0	3,9	4,0	4,0
Subtotal	99,7	99,6	99,8	99,7	100,0	100,1	99,8	100,0	99,8	99,9	99,9	99,9	100,0
O=F,Cl		0,211	0,126	0,168			0,107		0,149		0,084		
Total	99,7	99,4	99,7	99,5	100,0	100,1	99,7	100,0	99,7	99,9	99,8	99,9	100,0
Si	5,740	5,675	5,700	5,662	5,687	5,663	5,708	5,722	5,720	5,745	5,656	5,683	5,747
Al ^{iv}	2,260	2,325	2,300	2,338	2,313	2,337	2,292	2,278	2,280	2,255	2,344	2,317	2,253
	8,000	8,000	8,000	8,000	8,000	8,000	8,000	8,000	8,000	8,000	8,000	8,000	8,000
Al ^{vi}	0,531	0,420	0,436	0,369	0,603	0,602	0,455	0,386	0,407	0,378	0,346	0,349	0,409
Ti	0,205	0,186	0,164	0,198	0,171	0,163	0,252	0,283	0,295	0,262	0,317	0,316	0,261
Fe^{3+}	0,139	0,324	0,334	0,353	0,202	0,208	0,141	0,133	0,102	0,156	0,166	0,150	0,130
Fe^{2+}	1,979	2,075	2,044	2,133	1,820	2,051	2,264	2,248	2,247	2,241	2,235	2,231	2,249
Mn			0,049	0,062		0,073	0,062						
Mg	2,866	2,842	2,833	2,748	2,988	2,664	2,540	2,656	2,640	2,682	2,666	2,680	2,654
	5,719	5,846	5,859	5,862	5,784	5,760	5,713	5,706	5,691	5,718	5,730	5,726	5,704
Na													
K	1,867	1,819	1,795	1,829	1,777	1,875	1,895	1,903	1,889	1,906	1,892	1,868	1,902
	1,867	1,819	1,795	1,829	1,777	1,875	1,895	1,903	1,889	1,906	1,892	1,868	1,902
OH*	4,000	3,760	3,857	3,807	4,000	4,000	3,878	4,000	3,831	4,000	3,904	4,000	4,000
F		0,240	0,143	0,193			0,096		0,143		0,096		
Cl							0,026		0,026				
	4,000	4,000	4,000	4,000	4,000	4,000	4,000	4,000	4,000	4,000	4,000	4,000	4,000
TOTAL	19,586	19,665	19,654	19,691	19,562	19,635	19,608	19,609	19,580	19,624	19,621	19,594	19,606

Apêndice C.2. Análises químicas pontuais de cristais de biotita do Batólito Rio Jacaré (continuação).

Rocha	FDS 496A	FDS 496A	FDS 496B	FDS 496B	FDS 496B	FDS 496B	FDS 496B	FDS 496B	FDS 496B	FDS 496B	FDS 496B	FDS 496B	FDS 496B
Espectro	57	60	3	4	5	8	33	60	61	65	78	89	90
SiO_2	37,8	37,6	38,5	39,2	38,8	38,8	38,0	38,7	38,4	37,4	38,2	38,3	37,7
TiO_2	2,2	2,2	1,3	1,4	1,2	1,5	1,3	1,5	1,6	1,5	1,6	1,7	1,5
Al_2O_3	15,4	15,0	15,6	15,6	15,3	15,2	15,5	15,3	15,2	15,5	15,6	15,3	15,4
FeO	18,6	19,3	19,2	18,9	18,7	18,4	18,0	18,8	18,3	19,1	18,3	18,7	20,1
MnO	0,6	0,4			0,7								
MgO	11,8	11,4	12,4	12,5	12,7	13,1	13,2	12,6	12,8	12,0	13,0	12,1	11,6
Na_2O													
K_2O	9,5	10,0	8,7	8,4	8,4	8,7	9,6	9,1	9,6	9,5	8,6	9,7	9,6
F	0,1			0,1	0,3	0,3	0,2			0,2	0,6	0,2	
Cl		0,1	0,1						0,1		0,1	0,1	
H_2O*	3,9	3,9	4,0	4,0	3,9	3,9	3,9	4,0	4,0	3,8	3,7	3,9	4,0
Subtotal	99,9	99,9	99,8	100,0	99,9	99,9	99,8	100,0	100,0	99,1	99,7	100,0	99,9
O=F,Cl	0,042	0,023	0,023	0,042	0,126	0,126	0,084		0,023	0,084	0,275	0,107	
Total	99,9	99,9	99,8	99,9	99,7	99,8	99,7	100,0	100,0	99,0	99,4	99,9	99,9
Si	5,705	5,713	5,777	5,832	5,813	5,799	5,715	5,791	5,764	5,702	5,736	5,769	5,719
Al^{iv}	2,295	2,287	2,223	2,168	2,187	2,201	2,285	2,209	2,236	2,298	2,264	2,231	2,281
	8,000	8,000	8,000	8,000	8,000	8,000	8,000	8,000	8,000	8,000	8,000	8,000	8,000
Al^{vi}	0,436	0,392	0,528	0,562	0,509	0,472	0,454	0,484	0,448	0,477	0,489	0,479	0,463
Ti	0,250	0,252	0,152	0,161	0,130	0,173	0,152	0,173	0,184	0,176	0,184	0,196	0,175
Fe^{3+}	0,180	0,178	0,254	0,191	0,293	0,251	0,316	0,225	0,230	0,265	0,269	0,174	0,263
Fe^{2+}	2,160	2,268	2,137	2,141	2,031	2,036	1,945	2,116	2,062	2,159	2,014	2,176	2,271
Mn	0,074	0,049			0,085								
Mg	2,655	2,585	2,770	2,770	2,831	2,910	2,969	2,806	2,857	2,725	2,901	2,716	2,625
	5,755	5,725	5,841	5,825	5,880	5,841	5,835	5,804	5,782	5,802	5,857	5,741	5,797
Na													
K	1,829	1,933	1,672	1,586	1,615	1,666	1,841	1,741	1,838	1,846	1,655	1,863	1,856
	1,829	1,933	1,672	1,586	1,615	1,666	1,841	1,741	1,838	1,846	1,655	1,863	1,856
OH*	3,952	3,974	3,975	3,953	3,858	3,858	3,905	4,000	3,975	3,904	3,690	3,879	4,000
F	0,048			0,047	0,142	0,142	0,095			0,096	0,285	0,095	
Cl		0,026	0,025						0,025		0,025	0,026	
	4,000	4,000	4,000	4,000	4,000	4,000	4,000	4,000	4,000	4,000	4,000	4,000	4,000
TOTAL	19,583	19,658	19,513	19,412	19,495	19,507	19,675	19,545	19,620	19,648	19,511	19,604	19,653

Apêndice C.2. Análises químicas pontuais de cristais de biotita do Batólito Rio Jacaré (continuação).

Rocha	FDS 497	FDS 497	FDS 497	FDS 497	FDS 497	FDS 497	FDS 497	FDS 497	SOS 836	SOS 836	SOS 836	SOS 836	SOS 836
Espectro	15	19	20	21	29	43	63	64	6	7	45	46	67
SiO2	38,5	38,3	37,8	37,1	38,1	37,6	37,8	37,8	39,6	40,0	39,5	40,0	39,4
TiO2	1,6	1,5	1,7	2,8	1,9	3,5	1,4	1,4	1,9	2,0	1,7	1,7	3,1
Al2O3	16,5	15,8	15,7	15,7	15,7	14,4	15,4	15,5	16,6	17,4	16,5	17,0	17,4
FeO	17,1	18,0	18,9	19,4	18,3	19,6	19,0	18,5	15,6	15,2	16,0	14,4	15,7
MnO									0,2	0,1	0,2		0,1
MgO	12,1	12,5	12,7	10,9	12,3	11,8	12,7	12,7	13,1	13,1	13,1	13,3	10,9
Na2O													
K2O	9,9	9,7	9,0	10,0	9,6	9,2	9,6	9,5	8,6	8,3	8,8	9,2	9,2
F	0,2		0,2		0,1		0,1	0,6	0,3		0,2	0,1	0,2
Cl		0,1								0,1		0,1	
H2O*	3,9	4,0	3,9	4,0	4,0	4,0	3,9	3,7	3,9	4,1	4,0	4,0	4,0
Subtotal	99,8	100,0	100,0	99,9	100,1	100,1	99,9	99,7	100,0	100,2	100,0	99,9	100,0
O=F,Cl	0,084	0,023	0,084	0,000	0,042		0,042	0,253	0,126	0,023	0,084	0,065	0,084
Total	99,7	100,0	99,9	99,9	100,0	100,1	99,9	99,5	99,8	100,2	99,9	99,9	99,9
Si	5,751	5,740	5,678	5,621	5,715	5,679	5,704	5,716	5,824	5,820	5,811	5,851	5,792
Al ^{iv}	2,249	2,260	2,322	2,379	2,285	2,321	2,296	2,284	2,176	2,180	2,189	2,149	2,208
	8,000	8,000	8,000	8,000	8,000	8,000	8,000	8,000	8,000	8,000	8,000	8,000	8,000
Al ^{vi}	0,658	0,538	0,464	0,436	0,497	0,241	0,435	0,469	0,700	0,798	0,678	0,779	0,806
Ti	0,183	0,173	0,195	0,318	0,217	0,392	0,163	0,164	0,212	0,220	0,191	0,190	0,340
Fe^{3+}	0,055	0,189	0,295	0,108	0,176	0,144	0,319	0,286	0,000	0,000	0,040	0,000	0,000
Fe^{2+}	2,074	2,065	2,064	2,348	2,114	2,314	2,069	2,046	1,904	1,820	1,918	1,744	1,910
Mn									0,024	0,012	0,024		0,012
Mg	2,694	2,788	2,836	2,475	2,747	2,656	2,849	2,855	2,859	2,830	2,867	2,907	2,401
	5,664	5,753	5,854	5,684	5,750	5,747	5,835	5,819	5,699	5,681	5,718	5,620	5,469
Na													
K	1,884	1,853	1,728	1,932	1,836	1,774	1,847	1,832	1,619	1,531	1,659	1,718	1,730
	1,884	1,853	1,728	1,932	1,836	1,774	1,847	1,832	1,619	1,531	1,659	1,718	1,730
OH*	3,906	3,975	3,905	4,000	3,953	4,000	3,952	3,713	3,861	3,975	3,907	3,929	3,907
F	0,094		0,095		0,047		0,048	0,287	0,139		0,093	0,046	0,093
Cl		0,025								0,025		0,025	
	4,000	4,000	4,000	4,000	4,000	4,000	4,000	4,000	4,000	4,000	4,000	4,000	4,000
TOTAL	19,548	19,606	19,582	19,616	19,586	19,521	19,682	19,651	19,318	19,212	19,378	19,338	19,199

Apêndice C.2. Análises químicas pontuais de cristais de biotita do Batólito Rio Jacaré (continuação).

Rocha	SOS 836	SOS 836	SOS 836	SOS 836	SOS 836	SOS 836	SOS 836	SOS 836	SOS 836	SOS 836	SOS 836	SOS 837	SOS 837
Espectro	68	69	34	1	3	26	27	29	30	31	32	1	2
SiO_2	39,7	39,8	40,3	37,1	37,3	36,4	35,9	35,7	36,7	35,3	36,5	40,6	40,1
TiO_2	2,5	3,0	2,4	3,7	3,7	3,3	3,4	3,1	3,2	2,4	2,3	1,2	1,3
Al_2O_3	17,8	18,0	17,7	15,1	15,3	16,3	16,0	16,8	16,3	17,1	17,3	16,0	16,1
FeO	16,7	15,5	16,9	19,5	19,6	21,7	22,1	22,7	20,0	22,8	20,0	15,3	15,2
MnO		0,1	0,2	0,4	0,2	0,3	0,2	0,2	0,1	0,4	0,3	0,2	0,4
MgO	10,4	10,4	12,5	10,7	10,7	8,4	8,7	7,6	9,8	10,4	9,6	13,5	13,5
Na_2O													
K_2O	8,8	9,2	9,8	9,5	9,5	9,7	9,5	9,9	9,8	7,8	10,0	9,1	9,4
F			0,3				0,1					1,1	1,1
Cl		0,1	0,1			0,1	0,1						
H_2O*	4,1	4,1	3,9	4,0	4,0	3,9	3,8	3,9	3,9	3,9	3,9	3,6	3,6
Subtotal	100,0	100,1	100,1	99,9	100,3	100,0	99,8	99,8	99,7	100,0	99,8	100,7	100,8
O=F,Cl		0,023	0,149			0,023	0,065					0,463	0,463
Total	100,0	100,1	99,9	99,9	100,3	100,0	99,8	99,8	99,7	100,0	99,8	100,2	100,3
Si	5,841	5,834	5,731	5,624	5,635	5,576	5,527	5,515	5,580	5,388	5,550	5,942	5,886
Al^{iv}	2,159	2,166	2,269	2,376	2,365	2,424	2,473	2,485	2,420	2,612	2,450	2,058	2,114
	8,000	8,000	8,000	8,000	8,000	8,000	8,000	8,000	8,000	8,000	8,000	8,000	8,000
Al^{vi}	0,917	0,933	0,699	0,320	0,350	0,524	0,436	0,572	0,507	0,460	0,649	0,706	0,675
Ti	0,276	0,328	0,257	0,427	0,425	0,376	0,389	0,357	0,363	0,275	0,264	0,137	0,148
Fe^{3+}				0,047	0,021		0,086	0,014	0,019	0,434	0,077		0,023
Fe^{2+}	2,020	1,860	2,010	2,416	2,441	2,773	2,747	2,908	2,516	2,434	2,460	1,854	1,827
Mn	0,000	0,012	0,024	0,049	0,025	0,037	0,025	0,025	0,012	0,050	0,037	0,024	0,048
Mg	2,271	2,263	2,650	2,411	2,397	1,908	2,005	1,746	2,221	2,357	2,177	2,952	2,960
	5,484	5,396	5,639	5,671	5,658	5,618	5,687	5,622	5,638	6,011	5,664	5,674	5,680
Na													
K	1,656	1,721	1,778	1,840	1,829	1,895	1,866	1,948	1,900	1,513	1,938	1,702	1,760
	1,656	1,721	1,778	1,840	1,829	1,895	1,866	1,948	1,900	1,513	1,938	1,702	1,760
OH*	4,000	3,975	3,834	4,000	4,000	3,974	3,925	4,000	4,000	4,000	4,000	3,491	3,490
F			0,141				0,049					0,509	0,510
Cl		0,025	0,025			0,026	0,026						
	4,000	4,000	4,000	4,000	4,000	4,000	4,000	4,000	4,000	4,000	4,000	4,000	4,000
TOTAL	19,140	19,117	19,417	19,511	19,487	19,513	19,553	19,570	19,538	19,523	19,601	19,376	19,441

Apêndice C.2. Análises químicas pontuais de cristais de biotita do Batólito Rio Jacaré (continuação).

Rocha	SOS 837	SOS 837	SOS 837	SOS 837	SOS 837	SOS 837	SOS 837	SOS 837	SOS 837	SOS 837	SOS 837	SOS 837	SOS 837
Espectro	4	5	6	8	9	10	11	12	13	14	15	16	17
SiO_2	40,5	40,5	40,5	40,3	39,9	40,5	40,2	40,1	41,1	40,4	40,6	40,4	39,6
TiO_2	1,3	1,4	1,6	1,3	1,2	1,2	1,5	1,2	1,2	1,4	1,6	1,2	1,3
Al_2O_3	16,0	16,0	16,0	16,0	15,9	16,5	16,2	16,4	16,3	16,8	16,6	16,6	16,4
FeO	15,5	15,5	15,2	15,8	15,9	15,0	15,3	15,4	15,6	14,8	14,4	15,1	15,9
MnO	0,3	0,2	0,3	0,3	0,4	0,4	0,3	0,3	0,2	0,3	0,3	0,3	0,4
MgO	13,2	13,2	12,9	13,0	13,2	13,3	13,2	13,2	12,8	13,1	13,1	13,2	12,7
Na_2O													
K_2O	9,1	9,1	9,5	9,2	9,4	9,0	9,3	9,3	8,9	9,2	9,3	9,2	9,6
F	1,0	0,7	0,5	0,9	0,9	1,2	1,0	1,3	1,2	0,6	0,7	1,1	0,9
Cl					0,1		0,1					0,1	0,1
H_2O*	3,6	3,8	3,9	3,7	3,6	3,5	3,6	3,5	3,5	3,8	3,8	3,6	3,6
Subtotal	100,6	100,5	100,4	100,6	100,7	100,6	100,7	100,8	100,7	100,4	100,4	100,8	100,5
O=F,Cl	0,421	0,295	0,211	0,379	0,401	0,505	0,444	0,547	0,505	0,253	0,295	0,486	0,401
Total	100,2	100,2	100,1	100,2	100,3	100,1	100,2	100,2	100,2	100,2	100,1	100,3	100,1
Si	5,937	5,934	5,942	5,926	5,884	5,924	5,900	5,888	6,000	5,902	5,927	5,912	5,847
Al^{iv}	2,063	2,066	2,058	2,074	2,116	2,076	2,100	2,112	2,000	2,098	2,073	2,088	2,153
	8,000	8,000	8,000	8,000	8,000	8,000	8,000	8,000	8,000	8,000	8,000	8,000	8,000
Al^{vi}	0,706	0,702	0,714	0,703	0,651	0,770	0,704	0,727	0,809	0,794	0,785	0,775	0,708
Ti	0,148	0,159	0,180	0,149	0,138	0,127	0,169	0,138	0,127	0,158	0,179	0,137	0,149
Fe^{3+}													0,011
Fe^{2+}	1,879	1,878	1,845	1,933	1,892	1,816	1,859	1,873	1,878	1,789	1,740	1,829	1,950
Mn	0,036	0,024	0,036	0,036	0,048	0,048	0,036	0,036	0,024	0,036	0,036	0,036	0,048
Mg	2,894	2,893	2,813	2,839	2,910	2,909	2,876	2,898	2,779	2,842	2,841	2,868	2,793
	5,663	5,656	5,588	5,659	5,699	5,669	5,644	5,672	5,617	5,619	5,580	5,645	5,659
Na													
K	1,705	1,704	1,778	1,728	1,768	1,683	1,742	1,743	1,663	1,717	1,734	1,719	1,810
	1,705	1,704	1,778	1,728	1,768	1,683	1,742	1,743	1,663	1,717	1,734	1,719	1,810
OH*	3,537	3,676	3,768	3,582	3,556	3,445	3,511	3,397	3,446	3,723	3,677	3,466	3,554
F	0,463	0,324	0,232	0,418	0,419	0,555	0,464	0,603	0,554	0,277	0,323	0,509	0,421
Cl					0,025		0,025					0,025	0,025
	4,000	4,000	4,000	4,000	4,000	4,000	4,000	4,000	4,000	4,000	4,000	4,000	4,000
TOTAL	19,368	19,360	19,366	19,387	19,467	19,353	19,386	19,414	19,280	19,336	19,314	19,364	19,469

Apêndice C.2. Análises químicas pontuais de cristais de biotita do Batólito Rio Jacaré (continuação).

Rocha	SOS 837	SOS 837	SOS 840A	SOS 840A	SOS 840A	SOS 840A	SOS 840A	SOS 840A	SOS 840A	SOS 840A	SOS 840A	SOS 840A	SOS 840A
Espectro	18	26	1	2	3	4	5	7	8	19	20	21	22
SiO_2	39,7	40,9	38,5	37,9	38,9	38,2	39,0	39,0	38,5	38,5	38,0	38,9	37,7
TiO_2	1,2	1,2	1,8	1,9	1,8	2,0	2,0	2,0	2,2	1,8	1,9	1,6	1,8
Al_2O_3	15,8	16,9	16,3	15,7	16,0	15,9	15,7	16,2	15,7	15,7	15,9	16,2	15,7
FeO	15,4	14,2	17,1	17,4	17,2	17,4	17,8	16,3	16,4	17,4	17,9	17,1	17,6
MnO	0,2	0,4	0,4	0,5	0,5	0,4	0,4	0,5	0,3	0,4	0,3	0	0,5
MgO	12,8	13,1	11,8	11,9	12,2	11,8	11,1	12,1	11,6	12,3	11,8	12,5	11,9
Na_2O									0,7				
K_2O	9,3	9,3	10,0	9,4	9,5	10,3	9,9	9,8	9,7	9,9	10,2	9,7	10,0
F	1,5	0,7	1,1	1,3	0,9	1,3	0,7	0,7	0,9	1,2	1,0	1,0	0,8
Cl													
H_2O*	3,3	3,8	3,5	3,3	3,6	3,4	3,7	3,7	3,6	3,4	3,5	3,6	3,6
Subtotal	99,3	100,5	100,5	99,4	100,6	100,7	100,3	100,3	99,6	100,6	100,5	100,6	99,6
O=F,Cl	0,632	0,295	0,463	0,547	0,379	0,547	0,295	0,295	0,379	0,505	0,421	0,421	0,337
Total	98,6	100,2	100,0	98,8	100,2	100,1	100,0	100,0	99,2	100,1	100,1	100,1	99,3
Si	5,934	5,952	5,754	5,744	5,785	5,732	5,837	5,794	5,790	5,759	5,714	5,780	5,714
Al^{iv}	2,066	2,048	2,246	2,256	2,215	2,268	2,163	2,206	2,210	2,241	2,286	2,220	2,286
	8,000	8,000	8,000	8,000	8,000	8,000	8,000	8,000	8,000	8,000	8,000	8,000	8,000
Al^{vi}	0,721	0,851	0,630	0,554	0,596	0,551	0,616	0,636	0,581	0,536	0,538	0,623	0,525
Ti	0,140	0,137	0,205	0,219	0,204	0,227	0,227	0,225	0,250	0,205	0,217	0,182	0,208
Fe^{3+}			0,033	0,107	0,067	0,062				0,113	0,110	0,074	0,141
Fe^{2+}	1,905	1,712	2,098	2,084	2,061	2,116	2,215	2,020	2,064	2,055	2,132	2,042	2,080
Mn	0,024	0,047	0,049	0,062	0,060	0,049	0,049	0,060	0,037	0,049	0,037	0,000	0,062
Mg	2,842	2,833	2,631	2,688	2,704	2,641	2,486	2,680	2,604	2,740	2,646	2,766	2,688
	5,633	5,580	5,646	5,714	5,693	5,646	5,593	5,623	5,535	5,698	5,679	5,688	5,704
Na									0,196				
K	1,773	1,729	1,904	1,818	1,804	1,966	1,889	1,857	1,860	1,887	1,951	1,839	1,929
	1,773	1,729	1,904	1,818	1,804	1,966	1,889	1,857	2,056	1,887	1,951	1,839	1,929
OH*	3,292	3,678	3,480	3,377	3,576	3,383	3,668	3,671	3,572	3,432	3,525	3,530	3,617
F	0,708	0,322	0,520	0,623	0,424	0,617	0,332	0,329	0,428	0,568	0,475	0,470	0,383
Cl													
	4,000	4,000	4,000	4,000	4,000	4,000	4,000	4,000	4,000	4,000	4,000	4,000	4,000
TOTAL	19,406	19,308	19,549	19,531	19,497	19,612	19,482	19,480	19,592	19,585	19,630	19,527	19,633

Apêndice C.2. Análises químicas pontuais de cristais de biotita do Batólito Rio Jacaré (continuação).

Rocha	SOS 840A	SOS 840A	SOS 840A	SOS 840A	SOS 840A	SOS 840A	SOS 841	SOS 841	SOS 841	SOS 841	SOS 841	SOS 841	SOS 841
Espectro	23	25	26	44	45	49	1	2	3	4	5	6	8
SiO_2	38,5	38,7	38,6	38,3	38,3	37,9	37,5	38,1	37,7	37,4	37,9	37,8	37,9
TiO_2	1,9	1,5	1,4	1,8	1,6	1,6	1,7	1,5	2,0	1,9	2,3	2,2	2,2
Al_2O_3	17,0	16,1	16,4	15,6	15,5	15,4	15,6	15,9	15,7	15,2	15,7	15,5	15,5
FeO	17,3	17,1	17,0	18,0	17,7	18,4	19,6	18,9	19,4	19,6	19,0	19,4	19,3
MnO		0,5	0,4	0,4	0,4	0,4	0,3	0,3	0,3	0,4	0,3	0,3	0,5
MgO	11,4	12,4	12,3	11,9	12,5	11,9	11,2	11,2	10,8	10,6	10,9	10,8	10,9
Na_2O													
K_2O	9,9	9,7	9,9	10,0	10,0	10,3	10,0	10,0	10,1	9,9	9,8	10,0	9,8
F	0,6	0,9	1,2	0,8	0,9	0,7	0,8	1,0	1,0	1,1	0,7	0,7	1,2
Cl					0,1								
H_2O*	3,7	3,6	3,5	3,6	3,5	3,6	3,6	3,5	3,5	3,4	3,6	3,6	3,4
Subtotal	100,3	100,5	100,7	100,4	100,4	100,2	100,4	100,5	100,5	99,4	100,3	100,3	100,7
O=F,Cl	0,253	0,379	0,505	0,337	0,401	0,295	0,337	0,421	0,421	0,463	0,295	0,295	0,505
Total	100,1	100,1	100,1	100,1	100,0	99,9	100,0	100,1	100,1	99,0	100,0	100,0	100,2
Si	5,734	5,769	5,755	5,757	5,754	5,734	5,692	5,748	5,715	5,746	5,720	5,727	5,730
Al^{iv}	2,266	2,231	2,245	2,243	2,246	2,266	2,308	2,252	2,285	2,254	2,280	2,273	2,270
	8,000	8,000	8,000	8,000	8,000	8,000	8,000	8,000	8,000	8,000	8,000	8,000	8,000
Al^{vi}	0,717	0,603	0,640	0,512	0,490	0,472	0,489	0,580	0,526	0,490	0,520	0,486	0,483
Ti	0,215	0,172	0,161	0,206	0,184	0,186	0,197	0,174	0,230	0,222	0,261	0,251	0,251
Fe^{3+}		0,116	0,104	0,125	0,182	0,192	0,205	0,127	0,099	0,119	0,065	0,092	0,104
Fe^{2+}	2,144	2,007	2,009	2,139	2,032	2,138	2,274	2,254	2,354	2,390	2,326	2,360	2,328
Mn		0,061	0,049	0,049	0,049	0,049	0,037	0,037	0,037	0,050	0,037	0,037	0,061
Mg	2,536	2,753	2,731	2,667	2,795	2,683	2,539	2,525	2,428	2,416	2,461	2,449	2,465
	5,612	5,712	5,694	5,698	5,732	5,720	5,742	5,697	5,673	5,688	5,670	5,674	5,692
Na													
K	1,878	1,844	1,881	1,914	1,913	1,981	1,931	1,921	1,947	1,936	1,884	1,928	1,887
	1,878	1,844	1,881	1,914	1,913	1,981	1,931	1,921	1,947	1,936	1,884	1,928	1,887
OH*	3,717	3,576	3,434	3,620	3,547	3,665	3,616	3,523	3,521	3,466	3,666	3,665	3,427
F	0,283	0,424	0,566	0,380	0,428	0,335	0,384	0,477	0,479	0,534	0,334	0,335	0,573
Cl					0,025								
	4,000	4,000	4,000	4,000	4,000	4,000	4,000	4,000	4,000	4,000	4,000	4,000	4,000
TOTAL	19,491	19,556	19,575	19,612	19,645	19,701	19,673	19,617	19,621	19,624	19,554	19,602	19,579

Apêndice C.2. Análises químicas pontuais de cristais de biotita do Batólito Rio Jacaré (continuação).

Rocha	SOS 841	SOS 841	SOS 841	SOS 841	SOS 841	SOS 841	SOS 841	SOS 841	SOS 843A	SOS 843A	SOS 843A	SOS 843A	SOS 843A
Espectro	9	10	17	18	19	20	21	22	2	3	4	5	6
SiO_2	37,3	38,1	38,5	38,8	37,9	37,9	37,5	37,5	39,2	38,9	39,5	39,0	39,3
TiO_2	1,6	1,2	2,4	2,1	1,3	1,6	1,6	2,2	1,9	2,2	2,0	2,0	1,6
Al_2O_3	15,5	15,6	15,4	16,0	15,6	15,7	15,7	15,3	16,6	16,4	16,3	16,5	16,9
FeO	19,2	19,4	18,0	18,0	19,0	19,1	19,6	18,9	17,0	17,0	17,0	17,0	16,8
MnO	0,4	0,3	0,4	0,3	0,3	0,3	0,5	0,4	0,3	0,3	0,2	0,3	0,3
MgO	11,0	11,7	11,1	11,3	11,2	11,4	11,2	10,9	11,6	11,6	11,4	11,5	11,6
Na_2O													
K_2O	9,8	9,6	9,5	9,6	9,8	9,9	9,8	9,9	9,5	9,5	9,6	9,7	9,5
F	1,2	1,0	0,7	1,2	0,8	1,0	1,1	0,9	0,4		0,5	0,1	0,2
Cl						0,1			0,1				
H_2O*	3,3	3,5	3,6	3,4	3,6	3,5	3,4	3,5	3,8	4,0	3,8	4,0	4,0
Subtotal	99,4	100,4	99,7	100,7	99,6	100,6	100,5	99,5	100,4	99,9	100,3	100,1	100,2
O=F,Cl	0,505	0,421	0,295	0,505	0,337	0,444	0,463	0,379	0,191	0,000	0,211	0,042	0,084
Total	98,9	100,0	99,4	100,2	99,3	100,1	100,1	99,2	100,2	99,9	100,1	100,0	100,1
Si	5,723	5,757	5,807	5,790	5,767	5,726	5,690	5,729	5,806	5,782	5,852	5,794	5,816
Al^{iv}	2,277	2,243	2,193	2,210	2,233	2,274	2,310	2,271	2,194	2,218	2,148	2,206	2,184
	8,000	8,000	8,000	8,000	8,000	8,000	8,000	8,000	8,000	8,000	8,000	8,000	8,000
Al^{vi}	0,515	0,526	0,538	0,612	0,572	0,529	0,503	0,475	0,707	0,659	0,705	0,687	0,766
Ti	0,188	0,142	0,272	0,237	0,154	0,185	0,186	0,253	0,214	0,247	0,225	0,225	0,182
Fe^{3+}	0,180	0,238			0,158	0,173	0,225	0,096					
Fe^{2+}	2,276	2,203	2,266	2,231	2,253	2,234	2,251	2,313	2,093	2,100	2,092	2,101	2,068
Mn	0,050	0,037	0,049	0,036	0,037	0,037	0,062	0,050	0,036	0,036	0,024	0,036	0,036
Mg	2,522	2,637	2,504	2,521	2,546	2,572	2,538	2,490	2,567	2,575	2,526	2,553	2,565
	5,731	5,783	5,630	5,638	5,721	5,729	5,764	5,677	5,617	5,618	5,573	5,603	5,616
Na													
K	1,914	1,850	1,829	1,828	1,900	1,905	1,893	1,925	1,797	1,803	1,816	1,839	1,796
	1,914	1,850	1,829	1,828	1,900	1,905	1,893	1,925	1,797	1,803	1,816	1,839	1,796
OH*	3,418	3,522	3,666	3,433	3,615	3,497	3,473	3,566	3,787	4,000	3,765	3,953	3,906
F	0,582	0,478	0,334	0,567	0,385	0,478	0,527	0,434	0,188		0,235	0,047	0,094
Cl						0,026			0,025				
	4,000	4,000	4,000	4,000	4,000	4,000	4,000	4,000	4,000	4,000	4,000	4,000	4,000
TOTAL	19,645	19,632	19,458	19,466	19,620	19,634	19,658	19,602	19,414	19,421	19,389	19,442	19,412

Apêndice C.2. Análises químicas pontuais de cristais de biotita do Batólito Rio Jacaré (continuação).

Rocha	SOS 843A	SOS 843A	SOS 843A	SOS 843A	SOS 843A	SOS 843A	SOS 844	SOS 844	SOS 844	SOS 844	SOS 844	SOS 844	SOS 844B
Espectro	24	25	26	27	28	29	1	3	4	5	6	7	12
SiO_2	38,6	38,4	38,7	38,7	38,9	39,5	38,2	38,2	39,1	38,3	37,8	38,1	39,6
TiO_2	1,7	1,7	1,7	1,5	1,8	1,1	2,0	1,9	1,7	1,8	2,3	1,8	2,1
Al_2O_3	15,8	15,8	15,9	16,5	16,1	15,8	16,1	16,0	16,4	16,2	16,1	16,1	16,0
FeO	18,0	17,8	17,9	17,3	16,4	16,0	17,3	17,5	16,7	17,3	17,8	17,9	15,8
MnO	0,3	0,4	0,4	0,3	0,4	0,3	0,3	0,3	0,3	0,2	0,4	0,4	0,3
MgO	11,9	11,8	11,9	12,0	12,6	13,6	12,1	12,1	12,1	12,1	11,7	11,7	12,6
Na_2O													
K_2O	9,7	9,6	9,5	9,7	9,7	9,4	10,0	9,9	9,8	9,9	9,9	10,0	9,0
F	0,5	0,5		0,2	0,2	0,2		0,4	0,5	0,1	0,1	0,6	0,6
Cl									0,1	0,1			
H_2O*	3,8	3,8	4,0	3,9	3,9	4,0	4,0	3,8	3,8	3,9	3,9	3,7	3,8
Subtotal	100,3	99,8	100,0	100,1	100,0	99,9	100,0	100,1	100,5	99,9	100,0	100,3	99,8
O=F,Cl	0,211	0,211	0,000	0,084	0,084	0,084	0,000	0,168	0,233	0,065	0,042	0,253	0,253
Total	100,1	99,6	100,0	100,0	100,0	99,8	100,0	99,9	100,2	99,9	100,0	100,1	99,5
Si	5,777	5,774	5,782	5,765	5,779	5,846	5,716	5,724	5,798	5,733	5,677	5,721	5,855
Al^{iv}	2,223	2,226	2,218	2,235	2,221	2,154	2,284	2,276	2,202	2,267	2,323	2,279	2,145
	8,000	8,000	8,000	8,000	8,000	8,000	8,000	8,000	8,000	8,000	8,000	8,000	8,000
Al^{vi}	0,571	0,582	0,589	0,665	0,605	0,613	0,560	0,555	0,669	0,595	0,531	0,574	0,652
Ti	0,195	0,195	0,194	0,172	0,204	0,118	0,227	0,216	0,193	0,205	0,260	0,206	0,235
Fe^{3+}	0,097	0,092	0,090	0,069	0,054	0,156	0,087	0,105		0,084	0,091	0,104	
Fe^{2+}	2,142	2,133	2,131	2,076	1,978	1,820	2,070	2,078	2,065	2,073	2,133	2,133	1,944
Mn	0,037	0,049	0,049	0,036	0,048	0,036	0,036	0,037	0,036	0,024	0,049	0,049	0,036
Mg	2,656	2,647	2,652	2,665	2,787	3,011	2,698	2,701	2,676	2,699	2,621	2,621	2,775
	5,698	5,697	5,705	5,684	5,677	5,753	5,678	5,693	5,639	5,681	5,684	5,686	5,643
Na													
K	1,851	1,841	1,812	1,843	1,838	1,778	1,905	1,890	1,853	1,888	1,893	1,912	1,704
	1,851	1,841	1,812	1,843	1,838	1,778	1,905	1,890	1,853	1,888	1,893	1,912	1,704
OH*	3,763	3,762	4,000	3,906	3,906	3,906	4,000	3,810	3,740	3,927	3,953	3,715	3,719
F	0,237	0,238	0,000	0,094	0,094	0,094		0,190	0,235	0,047	0,047	0,285	0,281
Cl									0,025	0,025			
	4,000	4,000	4,000	4,000	4,000	4,000	4,000	4,000	4,000	4,000	4,000	4,000	4,000
TOTAL	19,549	19,539	19,516	19,526	19,515	19,531	19,583	19,583	19,493	19,568	19,577	19,597	19,346

Apêndice C.2. Análises químicas pontuais de cristais de biotita do Batólito Rio Jacaré (continuação).

Rocha	SOS 844B	SOS 844B	SOS 844B	SOS 844B	SOS 844B	SOS 844B	SOS 844B	SOS 844B	SOS 847	SOS 847	SOS 847	SOS 847	SOS 847
Espectro	13	17	18	19	20	21	22	46	28	30	31	33	34
SiO_2	39,9	39,9	39,9	40,0	39,1	39,6	39,6	39,5	39,6	40,2	40,3	40,5	40,5
TiO_2	2,0	1,2	1,3	1,3	1,3	1,2	1,2	1,2	1,3	1,2	1,2	1,4	1,6
Al_2O_3	16,1	17,5	17,3	16,2	16,7	17,0	16,7	16,5	16,7	17,1	17,1	17,6	17,3
FeO	15,4	15,1	15,2	15,9	16,6	15,6	15,6	16,5	15,3	15,2	14,8	15,0	15,0
MnO	0,2	0,1		0,1	0,1	0,1		0,1	0,1	0,3	0,1	0,3	0,2
MgO	12,9	12,6	12,8	12,8	13,1	12,7	12,9	13,0	12,9	12,9	13,2	12,5	12,4
Na_2O													
K_2O	9,0	9,6	9,4	9,2	8,5	8,9	8,9	9,1	8,8	8,6	8,8	8,6	8,8
F	0,3	0,1		0,3	0,6	0,9	1,2	0,2	0,5	0,4	0,4	0,1	0,2
Cl	0,2			0,1	0,1	0,1	0,2			0,1			0,1
H_2O*	3,9	4,0	4,1	3,9	3,7	3,6	3,4	4,0	3,8	3,9	3,9	4,1	4,0
Subtotal	99,9	100,1	100,0	99,9	99,9	99,7	99,6	100,0	99,9	99,9	99,8	100,1	100,1
O=F,Cl	0,171	0,042	0,000	0,149	0,275	0,401	0,550	0,084	0,211	0,191	0,168	0,042	0,107
Total	99,7	100,1	100,0	99,8	99,6	99,3	99,0	99,9	99,6	99,7	99,7	100,0	100,0
Si	5,882	5,850	5,851	5,907	5,785	5,858	5,870	5,831	5,841	5,893	5,897	5,897	5,910
Al^{iv}	2,118	2,150	2,149	2,093	2,215	2,142	2,130	2,169	2,159	2,107	2,103	2,103	2,090
	8,000	8,000	8,000	8,000	8,000	8,000	8,000	8,000	8,000	8,000	8,000	8,000	8,000
Al^{vi}	0,682	0,866	0,835	0,729	0,701	0,818	0,791	0,707	0,742	0,845	0,843	0,911	0,881
Ti	0,223	0,137	0,148	0,149	0,150	0,139	0,129	0,128	0,149	0,138	0,127	0,158	0,179
Fe^{3+}					0,125			0,088					
Fe^{2+}	1,874	1,833	1,844	1,952	1,912	1,906	1,915	1,939	1,874	1,839	1,791	1,799	1,803
Mn	0,024	0,012		0,012	0,012	0,012		0,012	0,012	0,036	0,012	0,036	0,024
Mg	2,825	2,746	2,788	2,809	2,882	2,791	2,846	2,855	2,825	2,810	2,889	2,708	2,693
	5,629	5,594	5,615	5,651	5,782	5,665	5,681	5,729	5,602	5,666	5,661	5,612	5,580
Na													
K	1,695	1,794	1,758	1,735	1,614	1,683	1,690	1,719	1,660	1,615	1,648	1,604	1,643
	1,695	1,794	1,758	1,735	1,614	1,683	1,690	1,719	1,781	1,615	1,648	1,604	1,643
OH*	3,810	3,954	4,000	3,835	3,694	3,554	3,386	3,907	3,767	3,790	3,815	3,954	3,883
F	0,140	0,046		0,140	0,281	0,421	0,563	0,093	0,233	0,185	0,185	0,046	0,092
Cl	0,050			0,025	0,025	0,025	0,050			0,025			0,025
	4,000	4,000	4,000	4,000	4,000	4,000	4,000	4,000	4,000	4,000	4,000	4,000	4,000
TOTAL	19,324	19,388	19,374	19,386	19,395	19,348	19,371	19,449	19,383	19,281	19,309	19,216	19,223

Apêndice C.2. Análises químicas pontuais de cristais de biotita do Batólito Rio Jacaré (continuação).

Rocha	SOS 847	SOS 847	SOS 847	SOS 847	SOS 847	SOS 847	SOS 847	SOS 847	SOS 847	SOS 849A	SOS 849A	SOS 849A	SOS 849A
Espectro	35	53	54	57	90	99	100	101	102	4	24	25	64
SiO_2	39,6	39,1	39,8	40,2	41,7	41,2	41,4	41,4	41,4	40,0	39,6	39,6	39,0
TiO_2	1,3	1,4	1,5	1,2	1,5	1,2	1,2	1,2	1,1	2,3	1,6	1,6	3,4
Al_2O_3	16,8	16,2	16,6	16,1	17,8	17,5	17,7	17,5	17,6	15,9	17,6	17,3	16,0
FeO	15,9	16,4	15,9	13,3	11,4	13,0	13,0	13,4	12,8	15,6	14,0	14,1	16,5
MnO	0,2	0,3	0,3	0,3	0,3	0,3	0,2	0,1	0,2	0,1	0,2	0,1	0,2
MgO	12,3	12,4	12,7	15,0	14,5	13,3	13,8	13,8	14,3	12,8	13,7	13,4	11,3
Na_2O		0,7				0,4							
K_2O	9,2	9,2	9,1	8,8	8,3	8,8	8,6	8,4	8,2	8,9	9,3	9,5	9,2
F	0,6	0,4		1,0	0,5	0,3	0,5	0,3	0,6	0,5	0,1	0,3	0,4
Cl					0,1						0,1	0,1	
H_2O*	3,8	3,8	4,1	3,6	3,9	4,0	3,9	4,0	3,9	3,8	4,0	3,9	3,8
Subtotal	99,8	100,0	100,1	99,6	100,0	100,0	100,2	100,1	99,9	100,0	100,2	100,0	99,9
O=F,Cl	0,253	0,168	0,000	0,421	0,233	0,126	0,211	0,126	0,253	0,211	0,065	0,149	0,168
Total	99,5	99,8	100,1	99,1	99,7	99,9	100,0	100,0	99,7	99,7	100,2	99,9	99,7
Si	5,866	5,810	5,858	5,897	5,963	5,956	5,956	5,961	5,958	5,890	5,766	5,804	5,790
Al^{iv}	2,134	2,190	2,142	2,103	2,037	2,044	2,044	2,039	2,042	2,110	2,234	2,196	2,210
	8,000	8,000	8,000	8,000	8,000	8,000	8,000	8,000	8,000	8,000	8,000	8,000	8,000
Al^{vi}	0,795	0,653	0,736	0,684	0,959	0,935	0,953	0,929	0,940	0,654	0,785	0,786	0,598
Ti	0,150	0,161	0,170	0,127	0,165	0,136	0,125	0,125	0,114	0,255	0,179	0,180	0,375
Fe^{3+}		0,030		0,074									
Fe^{2+}	1,957	2,008	1,945	1,548	1,344	1,549	1,538	1,596	1,515	1,893	1,697	1,716	2,029
Mn	0,024	0,036	0,036	0,036	0,035	0,035	0,023	0,012	0,023	0,012	0,024	0,012	0,024
Mg	2,710	2,745	2,777	3,273	3,093	2,877	2,966	2,969	3,071	2,800	2,983	2,933	2,509
	5,635	5,634	5,663	5,743	5,596	5,532	5,605	5,631	5,664	5,615	5,668	5,626	5,535
Na		0,194				0,108							
K	1,739	1,748	1,710	1,652	1,507	1,629	1,586	1,553	1,499	1,676	1,732	1,775	1,746
	1,739	1,942	1,710	1,652	1,507	1,737	1,586	1,553	1,499	1,676	1,732	1,775	1,746
OH*	3,719	3,812	4,000	3,536	3,749	3,863	3,772	3,863	3,727	3,767	3,929	3,836	3,812
F	0,281	0,188		0,464	0,226	0,137	0,228	0,137	0,273	0,233	0,046	0,139	0,188
Cl					0,024						0,025	0,025	
	4,000	4,000	4,000	4,000	4,000	4,000	4,000	4,000	4,000	4,000	4,000	4,000	4,000
TOTAL	19,374	19,575	19,374	19,394	19,103	19,269	19,192	19,183	19,163	19,290	19,400	19,401	19,281

Apêndice C.2. Análises químicas pontuais de cristais de biotita do Batólito Rio Jacaré (continuação).

Rocha	SOS 849A	SOS 849A	SOS 849A	SOS 849A	SOS 849A	SOS 849A	SOS 849A	SOS 849A	SOS 849A	SOS 849A	SOS 849A	SOS 849A	SOS 849A
Espectro	65	66	67	74	1	2	3	4	10	11	12	13	14
SiO_2	39,4	39,6	39,5	39,9	39,1	53,7	39,2	39,2	39,0	41,2	39,6	39,9	39,6
TiO_2	2,4	2,6	2,3	1,9	2,3	1,2	2,9	2,9	2,4	2,0	1,6	1,7	1,8
Al_2O_3	16,5	16,7	16,3	17,0	16,2	18,2	16,3	16,6	16,4	17,7	16,7	16,9	16,9
FeO	15,6	15,6	15,3	14,6	16,3	8,7	17,6	16,9	15,6	14,0	14,9	14,6	14,8
MnO	0,2	0,3	0,3	0,2	0,2	0,2		0,2	0,3	0,2	0,3	0,2	0,1
MgO	12,7	12,3	12,8	13,2	12,3	7,0	10,7	11,0	12,7	12,4	13,2	13,3	13,2
Na_2O													
K_2O	9,1	9,1	8,9	9,1	9,6	7,0	9,3	9,0	9,5	8,5	9,4	9,0	9,4
F		0,5	0,5	0,7			0,1	0,2		0,1	0,1	0,1	0,1
Cl	0,1							0,1		0,1			0,1
H_2O*	4,0	3,9	3,8	3,8	4,0	4,5	4,0	3,9	4,1	4,1	4,0	4,1	4,0
Subtotal	100,0	100,5	99,7	100,5	100,0	100,5	100,0	100,0	100,0	100,3	99,8	99,9	100,1
O=F,Cl	0,023	0,211	0,211	0,295	0,000	0,000	0,042	0,107	0,000	0,065	0,042	0,042	0,065
Total	99,9	100,3	99,4	100,2	100,0	100,5	99,9	99,9	100,0	100,2	99,8	99,8	100,1
Si	5,796	5,811	5,827	5,829	5,787	7,212	5,821	5,801	5,760	5,944	5,819	5,843	5,811
Al^{iv}	2,204	2,189	2,173	2,171	2,213	0,788	2,179	2,199	2,240	2,056	2,181	2,157	2,189
	8,000	8,000	8,000	8,000	8,000	8,000	8,000	8,000	8,000	8,000	8,000	8,000	8,000
Al^{vi}	0,662	0,696	0,668	0,752	0,619	2,102	0,679	0,701	0,619	0,949	0,716	0,757	0,730
Ti	0,266	0,286	0,256	0,211	0,257	0,116	0,322	0,321	0,267	0,219	0,181	0,190	0,201
Fe^{3+}													
Fe^{2+}	1,899	1,886	1,867	1,765	2,010	0,904	2,160	2,068	1,923	1,662	1,820	1,770	1,799
Mn	0,024	0,036	0,036	0,024	0,024	0,022		0,024	0,036	0,023	0,036	0,024	0,012
Mg	2,782	2,685	2,811	2,882	2,713	1,404	2,361	2,438	2,792	2,664	2,906	2,911	2,894
	5,632	5,588	5,638	5,634	5,623	4,548	5,522	5,551	5,637	5,518	5,658	5,651	5,637
Na													
K	1,713	1,705	1,682	1,698	1,814	1,201	1,765	1,705	1,791	1,573	1,766	1,684	1,759
	1,713	1,705	1,682	1,698	1,814	1,201	1,765	1,705	1,791	1,573	1,766	1,684	1,759
OH*	3,975	3,768	3,766	3,677	4,000	4,000	3,953	3,881	4,000	3,930	3,953	3,954	3,929
F		0,232	0,234	0,323			0,047	0,094		0,046	0,047	0,046	0,046
Cl	0,025							0,025		0,024			0,025
	4,000	4,000	4,000	4,000	4,000	4,000	4,000	4,000	4,000	4,000	4,000	4,000	4,000
TOTAL	19,345	19,293	19,320	19,331	19,436	17,749	19,287	19,256	19,428	19,091	19,424	19,336	19,395

Apêndice C.2. Análises químicas pontuais de cristais de biotita do Batólito Rio Jacaré (continuação).

Rocha	SOS 849A	SOS 849A	SOS 849A	SOS 849B	SOS 849B	SOS 849B	SOS 849B	SOS 849B	SOS 849B	SOS 849B	SOS 849B	SOS 849B	SOS 849B
Espectro	15	18	19	14	15	16	17	19	26	36	37	55	56
SiO_2	39,8	41,3	40,3	39,2	38,7	38,5	37,0	39,2	38,3	39,6	40,1	38,4	38,3
TiO_2	2,0	1,5	1,4	1,6	1,7	3,3	3,5	2,8	2,5	2,0	1,6	3,5	3,3
Al_2O_3	17,0	20,6	16,7	18,9	19,0	17,8	17,4	18,4	19,8	16,7	17,3	17,5	17,9
FeO	14,7	12,6	14,5	13,5	13,6	15,8	18,2	13,8	15,0	14,5	13,5	15,8	15,7
MnO	0,2	0,1	0,2	0,1	0,2	0,1	0,2	0,2		0,1	0,1	0,2	0,1
MgO	13,2	11,5	13,7	13,2	13,1	11,1	9,9	12,4	12,1	13,7	14,1	11,2	10,9
Na_2O													
K_2O	9,1	8,3	9,0	9,4	9,2	9,3	9,8	8,8	8,4	9,2	8,9	9,2	9,5
F	0,3		0,2	0,1	0,5			0,3			0,3	0,3	0,1
Cl	0,1		0,1	0,1	0,1	0,1	0,1	0,1	0,2			0,0	0,1
H_2O*	3,9	4,2	4,0	4,0	3,8	4,0	4,0	3,9	4,1	4,1	4,0	3,9	4,0
Subtotal	100,3	100,1	100,2	100,2	100,0	100,0	100,0	100,0	100,3	100,0	100,0	100,0	99,9
O=F,Cl	0,149	0,000	0,107	0,065	0,233	0,023	0,023	0,149	0,045	0,000	0,126	0,126	0,065
Total	100,2	100,1	100,1	100,1	99,7	100,0	99,9	99,8	100,2	100,0	99,9	99,9	99,8
Si	5,819	5,882	5,880	5,698	5,656	5,677	5,560	5,709	5,573	5,799	5,831	5,673	5,667
Al^{iv}	2,181	2,118	2,120	2,302	2,344	2,323	2,440	2,291	2,427	2,201	2,169	2,327	2,333
	8,000	8,000	8,000	8,000	8,000	8,000	8,000	8,000	8,000	8,000	8,000	8,000	8,000
Al^{vi}	0,744	1,348	0,752	0,940	0,931	0,765	0,641	0,876	0,964	0,679	0,791	0,715	0,780
Ti	0,221	0,165	0,158	0,179	0,190	0,362	0,391	0,305	0,273	0,222	0,178	0,384	0,363
Fe^{3+}													
Fe^{2+}	1,778	1,463	1,753	1,633	1,653	1,931	2,282	1,662	1,798	1,760	1,630	1,934	1,927
Mn	0,024	0,012	0,024	0,012	0,024	0,012	0,024	0,024	0,000	0,012	0,012	0,024	0,012
Mg	2,864	2,447	2,985	2,852	2,845	2,448	2,217	2,691	2,623	2,993	3,057	2,474	2,413
	5,631	5,435	5,672	5,616	5,644	5,518	5,556	5,558	5,659	5,667	5,668	5,531	5,495
Na													
K	1,699	1,500	1,679	1,746	1,719	1,752	1,879	1,642	1,550	1,719	1,655	1,737	1,793
	1,699	1,500	1,679	1,746	1,719	1,752	1,879	1,642	1,550	1,719	1,655	1,737	1,793
OH*	3,837	4,000	3,883	3,929	3,744	3,975	3,975	3,837	3,951	4,000	3,862	3,860	3,928
F	0,139		0,092	0,046	0,231			0,138			0,138	0,140	0,047
Cl	0,025		0,025	0,025	0,025	0,025	0,025	0,025	0,049				0,025
	4,000	4,000	4,000	4,000	4,000	4,000	4,000	4,000	4,000	4,000	4,000	4,000	4,000
TOTAL	19,330	18,935	19,350	19,362	19,362	19,270	19,435	19,200	19,209	19,386	19,322	19,268	19,289

Apêndice C.2. Análises químicas pontuais de cristais de biotita do Batólito Rio Jacaré (continuação).

Rocha	SOS 849B	SOS 849B	SOS 849B	SOS 849B	SOS 849B	SOS 849B	SOS 849B	SOS 849B	SOS 849B	SOS 849B	SOS 849B	SOS 849B	SOS 849B
Espectro	57	58	59	60	61	62	63	64	65	66	67	74	84
SiO_2	38,6	38,6	38,6	38,4	38,3	38,5	38,9	38,5	38,9	38,7	38,3	38,8	39,5
TiO_2	3,4	3,4	3,5	3,5	3,3	3,2	3,4	3,3	3,2	3,1	3,2	3,2	1,6
Al_2O_3	17,1	17,3	17,2	17,1	18,0	17,5	17,2	17,6	18,0	17,8	17,6	16,5	17,1
FeO	15,5	15,7	15,4	15,6	15,8	15,5	15,3	15,3	15,0	15,1	15,4	16,5	14,4
MnO	0,2		0,1	0,3	0,1	0,2	0,1	0,1	0,1	0,1	0,1	0,2	
MgO	11,4	11,5	11,6	11,4	10,9	11,8	11,7	11,5	11,9	11,6	11,4	11,1	13,7
Na_2O													
K_2O	9,6	9,5	9,3	9,5	9,4	9,3	9,3	9,5	8,9	9,5	9,6	9,2	9,5
F	0,4		0,2			0,1	0,2	0,2	0,2		0,5	0,3	0,1
Cl	0,1		0,1			0,1		0,1	0,1	0,1			0,1
H_2O*	3,8	4,1	3,9	4,0	4,1	4,0	4,0	3,9	4,0	4,0	3,8	3,9	4,0
Subtotal	100,0	100,1	99,9	99,8	100,0	100,1	100,0	100,0	100,2	100,0	99,8	99,7	100,0
O=F,Cl	0,191		0,107			0,065	0,084	0,107	0,107	0,023	0,211	0,126	0,065
Total	99,9	100,1	99,7	99,8	100,0	100,0	99,9	99,8	100,1	99,9	99,6	99,6	100,0
Si	5,710	5,691	5,700	5,687	5,653	5,673	5,724	5,682	5,691	5,695	5,674	5,766	5,781
Al^{iv}	2,290	2,309	2,300	2,313	2,347	2,327	2,276	2,318	2,309	2,305	2,326	2,234	2,219
	8,000	8,000	8,000	8,000	8,000	8,000	8,000	8,000	8,000	8,000	8,000	8,000	8,000
Al^{vi}	0,690	0,694	0,692	0,670	0,792	0,708	0,706	0,739	0,788	0,776	0,742	0,660	0,732
Ti	0,374	0,373	0,384	0,385	0,362	0,351	0,372	0,362	0,349	0,340	0,353	0,354	0,180
Fe^{3+}													0,005
Fe^{2+}	1,893	1,922	1,876	1,907	1,933	1,886	1,857	1,865	1,809	1,836	1,885	2,031	1,750
Mn	0,024		0,012	0,036	0,012	0,024	0,012	0,012	0,012	0,012	0,012	0,024	
Mg	2,520	2,532	2,558	2,522	2,408	2,594	2,570	2,535	2,597	2,549	2,523	2,468	2,998
	5,501	5,521	5,521	5,520	5,508	5,564	5,517	5,513	5,555	5,513	5,514	5,537	5,666
Na													
K	1,812	1,788	1,754	1,795	1,771	1,750	1,749	1,789	1,667	1,784	1,814	1,748	1,776
	1,812	1,788	1,754	1,795	1,771	1,750	1,749	1,789	1,667	1,784	1,814	1,748	1,776
OH*	3,788	4,000	3,882	4,000	4,000	3,928	3,907	3,882	3,883	3,975	3,766	3,859	3,929
F	0,187		0,093			0,047	0,093	0,093	0,093		0,234	0,141	0,046
Cl	0,025		0,025			0,025		0,025	0,025	0,025			0,025
	4,000	4,000	4,000	4,000	4,000	4,000	4,000	4,000	4,000	4,000	4,000	4,000	4,000
TOTAL	19,313	19,309	19,276	19,315	19,279	19,314	19,266	19,302	19,222	19,297	19,328	19,284	19,442

Apêndice C.2. Análises químicas pontuais de cristais de biotita do Batólito Rio Jacaré (continuação).

Rocha	SOS 849B	SOS 849B	SOS 849B	SOS 849B	SOS 849B	SOS 849B	SOS 849B	SOS 849B	SOS 850A	SOS 850A	SOS 850A	SOS 850B	SOS 850B
Espectro	85	86	87	1	2	3	4	5	20	21	22	44	45
SiO_2	39,3	38,7	39,3	38,7	38,5	38,7	39,1	38,6	39,2	39,1	38,8	39,9	39,8
TiO_2	1,7	2,0	1,9	2,6	2,3	2,2	1,4	2,2	1,6	1,7	1,5	1,3	1,4
Al_2O_3	16,8	16,7	17,0	15,7	16,1	15,9	16,2	15,8	16,2	15,9	16,4	18,3	18,0
FeO	14,7	15,1	14,7	16,3	15,8	16,9	15,4	15,7	15,2	15,6	15,3	14,3	14,2
MnO		0,1		0,2	0,3	0,3	0,3	0,3	0,1	0,1	0,3	0,1	
MgO	13,6	13,7	13,4	13,2	13,3	12,7	14,1	13,7	14,1	14,0	13,7	13,2	13,2
Na_2O													
K_2O	9,7	9,7	9,4	9,3	9,5	9,2	9,5	9,5	9,4	9,5	9,4	8,8	8,9
F	0,2	0,1	0,3		0,1					0,5	0,5		0,3
Cl					0,1					0,1			
H_2O*	4,0	4,0	3,9	4,0	4,0	4,0	4,1	4,0	4,1	3,8	3,8	4,1	4,0
Subtotal	100,0	100,1	100,0	100,0	100,1	99,9	100,1	100,0	99,9	100,3	99,7	100,2	100,0
O=F,Cl	0,084	0,042	0,126		0,065					0,233	0,211		0,126
Total	99,9	100,1	99,8	100,0	100,0	99,9	100,1	100,0	99,9	100,1	99,5	100,2	99,9
Si	5,773	5,702	5,767	5,733	5,706	5,750	5,762	5,719	5,772	5,771	5,751	5,790	5,801
Al^{iv}	2,227	2,298	2,233	2,267	2,294	2,250	2,238	2,281	2,228	2,229	2,249	2,210	2,199
	8,000	8,000	8,000	8,000	8,000	8,000	8,000	8,000	8,000	8,000	8,000	8,000	8,000
Al^{vi}	0,685	0,603	0,709	0,483	0,524	0,542	0,582	0,486	0,591	0,545	0,620	0,924	0,899
Ti	0,191	0,223	0,212	0,289	0,257	0,247	0,160	0,246	0,181	0,192	0,171	0,147	0,158
Fe^{3+}	0,020	0,091	0,000	0,076	0,105	0,086	0,176	0,144	0,131	0,146	0,137	0,000	0,000
Fe^{2+}	1,779	1,758	1,793	1,935	1,849	2,002	1,709	1,798	1,728	1,765	1,745	1,717	1,713
Mn		0,012		0,024	0,036	0,036	0,036	0,036	0,012	0,012	0,036	0,012	
Mg	2,988	3,016	2,943	2,905	2,949	2,808	3,102	3,033	3,100	3,086	3,034	2,863	2,876
	5,662	5,705	5,657	5,712	5,720	5,720	5,765	5,743	5,743	5,745	5,744	5,662	5,645
Na													
K	1,819	1,823	1,763	1,760	1,797	1,747	1,788	1,797	1,769	1,790	1,779	1,633	1,658
	1,819	1,823	1,763	1,760	1,797	1,747	1,788	1,797	1,769	1,790	1,779	1,633	1,658
OH*	3,907	3,953	3,861	4,000	3,928	4,000	4,000	4,000	4,000	3,741	3,766	4,000	3,862
F	0,093	0,047	0,139		0,047					0,234	0,234		0,138
Cl					0,025					0,025			
	4,000	4,000	4,000	4,000	4,000	4,000	4,000	4,000	4,000	4,000	4,000	4,000	4,000
TOTAL	19,481	19,527	19,420	19,472	19,517	19,468	19,552	19,540	19,511	19,536	19,523	19,295	19,304

Apêndice C.2. Análises químicas pontuais de cristais de biotita do Batólito Rio Jacaré (continuação).

Rocha	SOS 850B	SOS 850B	SOS 850B	SOS 850B	SOS 850B	SOS 850B	SOS 853D	SOS 853D	SOS 853D	SOS 853D	SOS 853D	SOS 861C	SOS 861C
Espectro	46	47	48	49	51	52	14	15	20	53	54	1	2
SiO_2	39,9	40,3	40,5	39,4	39,6	39,7	38,5	38,5	37,8	39,3	39,0	38,2	38,8
TiO_2	1,4	1,3	1,5	1,5	1,5	1,4	2,8	2,6	2,5	2,2	1,9	2,1	1,7
Al_2O_3	18,0	17,8	18,0	18,0	18,5	18,5	15,6	15,7	19,2	16,6	16,2	15,0	15,2
FeO	14,4	14,1	14,2	14,2	13,5	13,7	16,4	16,5	14,7	16,1	16,1	18,4	17,2
MnO	0,1	0,1		0,1			0,2	0,2	0,1	0,2	0,3	0,3	0,3
MgO	13,2	13,3	12,9	13,2	13,1	13,2	12,2	12,6	12,3	12,4	12,9	12,6	12,9
Na_2O													
K_2O	8,9	8,6	8,7	8,7	8,9	8,7	9,2	9,2	8,8	9,1	9,0	9,6	9,3
F		0,3	0,2	0,9	0,8	0,6	0,9	0,6	0,6		0,6	0,7	0,8
Cl							0,1	0,1					
H_2O*	4,1	4,0	4,0	3,7	3,7	3,8	3,5	3,7	3,8	4,1	3,8	3,7	3,6
Subtotal	100,1	99,9	100,1	99,6	99,7	99,9	99,5	99,7	99,8	100,0	99,8	100,6	99,7
O=F,Cl		0,126	0,084	0,379	0,337	0,253	0,401	0,275	0,253		0,253	0,295	0,337
Total	100,1	99,8	100,1	99,2	99,3	99,6	99,1	99,5	99,6	100,0	99,5	100,3	99,4
Si	5,804	5,861	5,868	5,776	5,776	5,782	5,770	5,749	5,560	5,792	5,786	5,734	5,816
Al^{iv}	2,196	2,139	2,132	2,224	2,224	2,218	2,230	2,251	2,440	2,208	2,214	2,266	2,184
	8,000	8,000	8,000	8,000	8,000	8,000	8,000	8,000	8,000	8,000	8,000	8,000	8,000
Al^{vi}	0,896	0,904	0,950	0,882	0,965	0,960	0,534	0,520	0,887	0,680	0,625	0,383	0,497
Ti	0,157	0,147	0,167	0,170	0,169	0,158	0,314	0,291	0,276	0,245	0,214	0,238	0,195
Fe^{3+}								0,030			0,052	0,219	0,147
Fe^{2+}	1,733	1,695	1,698	1,726	1,635	1,651	2,044	2,020	1,788	1,974	1,936	2,086	1,996
Mn	0,012	0,012		0,012			0,024	0,024	0,012	0,024	0,036	0,037	0,037
Mg	2,849	2,891	2,778	2,877	2,842	2,873	2,724	2,800	2,693	2,723	2,847	2,813	2,875
	5,647	5,649	5,593	5,666	5,611	5,642	5,640	5,685	5,655	5,645	5,711	5,775	5,747
Na													
K	1,655	1,602	1,614	1,635	1,663	1,621	1,762	1,755	1,656	1,716	1,709	1,838	1,781
	1,655	1,602	1,614	1,635	1,663	1,621	1,762	1,755	1,656	1,716	1,709	1,838	1,781
OH*	4,000	3,862	3,908	3,582	3,631	3,724	3,548	3,691	3,721	4,000	3,718	3,668	3,621
F		0,138	0,092	0,418	0,369	0,276	0,427	0,283	0,279		0,282	0,332	0,379
Cl							0,025	0,025					
	4,000	4,000	4,000	4,000	4,000	4,000	4,000	4,000	4,000	4,000	4,000	4,000	4,000
TOTAL	19,302	19,251	19,207	19,302	19,274	19,263	19,402	19,440	19,311	19,361	19,420	19,613	19,528

Apêndice C.2. Análises químicas pontuais de cristais de biotita do Batólito Rio Jacaré (continuação).

Rocha	SOS 861C	SOS 861C	SOS 861C	SOS 861E	SOS 861E	SOS 861E	SOS 861E	SOS 861E	SOS 861E	SOS 861E	SOS 861E	SOS 861E	SOS 861M
Espectro	7	8	19	19	20	21	22	23	24	25	26	27	20
SiO_2	38,9	38,4	38,2	39,1	39,5	38,6	39,7	39,4	39,4	39,3	39,2	39,6	37,4
TiO_2	1,2	1,2	1,5	1,8	2,0	2,0	1,9	1,6	2,0	1,4	1,2	1,4	2,8
Al_2O_3	15,7	15,4	15,7	15,8	16,0	16,8	16,4	16,0	16,2	16,2	16,2	16,2	15,6
FeO	17,0	16,9	17,1	16,7	16,1	16,4	16,3	16,5	16,3	16,2	16,9	16,4	17,7
MnO	0,3		0,3	0,2	0,2	0,1	0,1	0,3	0,1	0,1	0,1	0,2	0,2
MgO	13,2	13,6	13,1	12,3	12,4	11,8	12,3	12,6	12,2	12,7	12,8	12,6	12,9
Na_2O		0,5											
K_2O	9,7	9,4	9,4	9,0	8,8	9,2	9,2	9,0	9,0	9,3	9,2	9,0	9,6
F	0,6	0,5	0,7	1,1	0,9	1,2	0,2	0,5	0,8	0,7	0,5	0,5	0,3
Cl		0,1		0,2	0,1	0,2		0,1	0,1			0,2	
H_2O*	3,7	3,7	3,7	3,4	3,6	3,4	4,0	3,8	3,6	3,7	3,8	3,8	3,9
Subtotal	100,3	99,8	99,7	99,7	99,6	99,7	100,2	99,8	99,8	99,6	99,9	100,0	100,3
O=F,Cl	0,253	0,233	0,295	0,508	0,401	0,550	0,084	0,233	0,359	0,295	0,211	0,256	0,126
Total	100,1	99,5	99,4	99,2	99,2	99,2	100,1	99,6	99,4	99,3	99,7	99,7	100,1
Si	5,791	5,757	5,735	5,844	5,864	5,767	5,855	5,848	5,847	5,842	5,821	5,872	5,611
Al^{iv}	2,209	2,243	2,265	2,156	2,136	2,233	2,145	2,152	2,153	2,158	2,179	2,128	2,389
	8,000	8,000	8,000	8,000	8,000	8,000	8,000	8,000	8,000	8,000	8,000	8,000	8,000
Al^{vi}	0,554	0,471	0,521	0,636	0,672	0,727	0,706	0,655	0,688	0,688	0,664	0,704	0,358
Ti	0,140	0,141	0,173	0,205	0,225	0,227	0,213	0,182	0,225	0,161	0,139	0,160	0,314
Fe^{3+}	0,194	0,261	0,221	0,007				0,029		0,025	0,105	0,006	0,212
Fe^{2+}	1,914	1,854	1,914	2,068	1,986	2,037	1,994	2,008	2,010	1,982	1,982	2,013	1,993
Mn	0,036		0,037	0,024	0,024	0,012	0,012	0,036	0,012	0,012	0,012	0,024	0,024
Mg	2,920	3,046	2,922	2,740	2,744	2,631	2,699	2,785	2,700	2,811	2,829	2,777	2,874
	5,759	5,773	5,787	5,680	5,651	5,633	5,624	5,697	5,635	5,679	5,732	5,684	5,775
Na													
K	1,842	1,799	1,801	1,721	1,674	1,757	1,732	1,710	1,710	1,767	1,747	1,705	1,835
	1,842	1,939	1,801	1,721	1,674	1,757	1,732	1,710	1,710	1,767	1,747	1,705	1,835
OH*	3,717	3,738	3,668	3,429	3,552	3,382	3,907	3,740	3,599	3,671	3,765	3,716	3,858
F	0,283	0,237	0,332	0,520	0,423	0,567	0,093	0,235	0,376	0,329	0,235	0,234	0,142
Cl		0,025		0,051	0,025	0,051		0,025	0,025			0,050	
	4,000	4,000	4,000	4,000	4,000	4,000	4,000	4,000	4,000	4,000	4,000	4,000	4,000
TOTAL	19,601	19,711	19,589	19,402	19,325	19,390	19,356	19,407	19,345	19,446	19,479	19,389	19,610

Apêndice C.2. Análises químicas pontuais de cristais de biotita do Batólito Rio Jacaré (continuação).

Rocha	SOS 861M	SOS 861M	SOS 861M	SOS 861M	SOS 861M	SOS 861M	SOS 861M	SOS 861M	SOS 861M	SOS 861M	SOS 861M	SOS 861M	SOS 861M
Espectro	21	37	42	15	16	17	18	19	20	21	35	36	21
SiO_2	37,3	38,0	37,2	36,8	36,7	37,2	37,6	36,6	37,0	36,3	37,7	37,6	36,5
TiO_2	2,5	3,0	3,8	4,0	3,6	3,7	3,6	3,9	3,7	3,8	2,5	2,6	3,8
Al_2O_3	15,9	15,7	15,7	16,0	16,6	16,4	18,0	16,2	16,5	16,5	15,8	15,8	16,4
FeO	18,3	16,6	18,9	17,8	18,1	17,5	15,7	18,0	18,0	18,2	16,8	16,9	17,9
MnO	0,2	0,2	0,3	0,3	0,2	0,3	0,2	0,3	0,3	0,3	0,1	0,2	0,3
MgO	13,3	12,8	10,2	11,4	11,0	11,4	12,5	11,5	11,2	11,8	13,4	13,0	12,1
Na_2O													
K_2O	8,3	9,6	9,8	9,7	9,6	9,5	8,3	9,5	9,4	9,1	9,6	9,8	9,0
F	0,4				0,1		0,2				0,1		
Cl	0,1		0,1		0,1		0,1				0,1		0,1
H_2O*	3,8	4,0	3,9	4,0	3,9	4,0	4,0	4,0	4,0	4,0	3,9	4,0	4,0
Subtotal	100,2	99,9	100,0	100,0	100,0	100,0	100,2	100,0	100,1	100,1	100,1	99,9	100,1
O=F,Cl	0,191		0,023		0,065		0,107				0,065		0,023
Total	100,0	99,9	100,0	100,0	99,9	100,0	100,1	100,0	100,1	100,1	100,1	99,9	100,1
Si	5,579	5,668	5,629	5,531	5,522	5,564	5,530	5,502	5,541	5,451	5,627	5,631	5,470
Al^{iv}	2,421	2,332	2,371	2,469	2,478	2,436	2,470	2,498	2,459	2,549	2,373	2,369	2,530
	8,000	8,000	8,000	8,000	8,000	8,000	8,000	8,000	8,000	8,000	8,000	8,000	8,000
Al^{vi}	0,385	0,435	0,433	0,373	0,469	0,461	0,656	0,379	0,459	0,374	0,412	0,425	0,371
Ti	0,280	0,334	0,436	0,456	0,413	0,422	0,393	0,445	0,422	0,434	0,280	0,292	0,433
Fe^{3+}	0,338	0,075		0,027	0,030			0,072	0,021	0,154	0,213	0,169	0,149
Fe^{2+}	1,930	1,987	2,379	2,200	2,246	2,178	1,914	2,176	2,218	2,123	1,873	1,939	2,075
Mn	0,024	0,024	0,037	0,037	0,024	0,037	0,024	0,037	0,037	0,037	0,012	0,024	0,037
Mg	2,972	2,838	2,292	2,562	2,478	2,550	2,734	2,583	2,510	2,644	2,988	2,891	2,704
	5,928	5,693	5,578	5,654	5,661	5,648	5,720	5,693	5,667	5,766	5,779	5,739	5,769
Na													
K	1,573	1,826	1,887	1,860	1,844	1,815	1,547	1,824	1,799	1,747	1,826	1,869	1,726
	1,573	1,826	1,887	1,860	1,844	1,815	1,547	1,824	1,799	1,747	1,826	1,869	1,726
OH*	3,786	4,000	3,974	4,000	3,927	4,000	3,882	4,000	4,000	4,000	3,928	4,000	3,975
F	0,189				0,048		0,093				0,047		
Cl	0,025		0,026		0,026		0,025				0,025		0,025
	4,000	4,000	4,000	4,000	4,000	4,000	4,000	4,000	4,000	4,000	4,000	4,000	4,000
TOTAL	19,501	19,519	19,465	19,514	19,505	19,464	19,267	19,516	19,467	19,513	19,605	19,608	19,495

Apêndice C.2. Análises químicas pontuais de cristais de biotita do Batólito Rio Jacaré (continuação).

Rocha	SOS 861M	SOS 861M	SOS 861M	SOS 861M	SOS 861M	SOS 861M	SOS 861M	SOS 861M	SOS 861M	SOS 861M	SOS 861M	SOS 861M	SOS 861P
Espectro	22	23	25	56	57	58	59	60	61	62	63	55	15
SiO_2	37,2	37,1	37,0	37,2	37,3	37,2	37,3	37,1	38,2	36,9	37,3	37,5	38,2
TiO_2	4,3	4,0	4,1	3,3	3,5	3,3	3,2	3,5	3,3	3,5	3,5	3,4	2,1
Al_2O_3	16,0	16,2	16,3	15,5	15,5	15,3	15,8	15,4	15,5	15,5	15,5	15,6	15,3
FeO	17,1	18,0	17,9	18,6	18,8	18,9	19,6	19,2	18,4	18,9	18,7	18,7	18,8
MnO	0,3	0,2	0,3	0,2	0,2	0,2	0,3	0,2	0,2	0,3	0,3	0,2	0,3
MgO	11,6	10,8	10,8	11,1	11,3	11,1	11,3	11,2	11,0	11,3	11,5	11,0	11,8
Na_2O													
K_2O	9,4	9,5	9,5	9,3	9,3	9,3	8,4	9,5	9,3	9,7	9,3	9,4	9,5
F	0,2	0,1			0,2								0,1
Cl	0,1				0,1	0,1							0,0
H_2O*	3,9	3,9	4,0	4,0	3,9	3,9	4,0	4,0	4,0	4,0	4,0	4,0	3,9
Subtotal	100,2	99,8	99,9	100,0	100,1	99,8	100,0	100,0	99,9	100,0	100,1	99,8	100,0
O=F,Cl	0,107	0,042			0,107	0,023							0,042
Total	100,1	99,8	99,9	100,0	100,0	99,8	100,0	100,0	99,9	100,0	100,1	99,8	100,0
Si	5,567	5,573	5,554	5,639	5,630	5,639	5,613	5,603	5,733	5,578	5,619	5,660	5,749
Al^{iv}	2,433	2,427	2,446	2,361	2,370	2,361	2,387	2,397	2,267	2,422	2,381	2,340	2,251
	8,000	8,000	8,000	8,000	8,000	8,000	8,000	8,000	8,000	8,000	8,000	8,000	8,000
Al^{vi}	0,392	0,450	0,445	0,398	0,376	0,370	0,420	0,341	0,466	0,335	0,359	0,424	0,455
Ti	0,486	0,456	0,467	0,372	0,392	0,373	0,358	0,393	0,368	0,393	0,391	0,381	0,239
Fe^{3+}				0,048	0,069	0,075	0,148	0,105		0,118	0,093	0,017	0,150
Fe^{2+}	2,123	2,245	2,231	2,303	2,291	2,318	2,291	2,314	2,298	2,268	2,250	2,333	2,208
Mn	0,036	0,024	0,037	0,025	0,025	0,025	0,037	0,025	0,024	0,037	0,037	0,025	0,037
Mg	2,588	2,432	2,430	2,513	2,546	2,520	2,538	2,532	2,469	2,555	2,584	2,482	2,648
	5,625	5,608	5,610	5,659	5,698	5,680	5,793	5,708	5,626	5,707	5,714	5,661	5,737
Na													
K	1,794	1,823	1,822	1,798	1,791	1,803	1,620	1,833	1,782	1,871	1,787	1,809	1,824
	1,794	1,823	1,822	1,844	1,791	1,837	1,620	1,833	1,782	1,871	1,787	1,809	1,824
OH*	3,880	3,952	4,000	4,000	3,879	3,974	4,000	4,000	4,000	4,000	4,000	4,000	3,952
F	0,095	0,048			0,095								0,048
Cl	0,025				0,026	0,026							
	4,000	4,000	4,000	4,000	4,000	4,000	4,000	4,000	4,000	4,000	4,000	4,000	4,000
TOTAL	19,419	19,431	19,432	19,503	19,489	19,517	19,413	19,542	19,408	19,578	19,501	19,471	19,561

Apêndice C.2. Análises químicas pontuais de cristais de biotita do Batólito Rio Jacaré (continuação).

Rocha	SOS 861P	SOS 861P	SOS 861P	SOS 861P	SOS 861P	SOS 861Q	SOS 861Q	SOS 861Q	SOS 861Q	SOS 861Q	SOS 861Q	SOS 861Q	SOS 861Q
Espectro	16	29	30	39	41	9	10	34	35	36	37	38	39
SiO_2	38,1	38,4	38,0	38,0	37,9	37,9	38,3	38,7	38,3	38,3	38,5	37,9	37,8
TiO_2	2,3	1,8	1,9	2,3	2,0	1,4	1,3	1,5	1,4	2,2	2,2	2,5	2,3
Al_2O_3	15,1	15,2	15,5	14,9	14,9	14,7	15,3	15,8	15,5	15,5	15,4	15,3	15,4
FeO	18,0	18,3	18,7	19,0	18,9	19,1	18,1	17,8	18,0	18,1	18,0	18,1	17,9
MnO	0,4	0,4	0,2	0,4	0,4	0,4	0,3	0,2	0,3	0,4	0,5	0,4	0,4
MgO	11,8	12,5	12,4	11,6	12,1	12,8	13,4	12,4	12,4	11,9	12,0	12,1	12,1
Na_2O													
K_2O	9,5	9,4	9,3	9,8	9,9	9,2	8,5	9,4	10,1	9,6	9,5	9,7	9,7
F	0,7	1,0	0,4	0,6	0,3	0,5	0,7	1,1	0,7	0,4	0,6	0,5	0,4
Cl		0,1		0,1		0,1					0,1	0,1	0,1
H_2O*	3,6	3,5	3,8	3,7	3,8	3,7	3,7	3,5	3,7	3,8	3,7	3,7	3,8
Subtotal	99,6	100,6	100,2	100,4	100,2	99,8	99,7	100,4	100,4	100,2	100,4	100,3	99,8
O=F,Cl	0,295	0,444	0,168	0,275	0,126	0,233	0,295	0,463	0,295	0,168	0,275	0,233	0,191
Total	99,3	100,2	100,0	100,1	100,1	99,6	99,4	99,9	100,1	100,0	100,1	100,1	99,6
Si	5,766	5,762	5,710	5,745	5,727	5,746	5,751	5,783	5,759	5,747	5,768	5,702	5,709
Al^{iv}	2,234	2,238	2,290	2,255	2,273	2,254	2,249	2,217	2,241	2,253	2,232	2,298	2,291
	8,000	8,000	8,000	8,000	8,000	8,000	8,000	8,000	8,000	8,000	8,000	8,000	8,000
Al^{vi}	0,453	0,444	0,447	0,395	0,376	0,369	0,453	0,574	0,498	0,481	0,480	0,408	0,442
Ti	0,262	0,206	0,217	0,262	0,229	0,164	0,152	0,173	0,163	0,249	0,249	0,282	0,262
Fe^{3+}	0,096	0,210	0,235	0,147	0,226	0,357	0,344	0,142	0,202	0,109	0,100	0,144	0,142
Fe^{2+}	2,178	2,080	2,105	2,248	2,158	2,051	1,914	2,068	2,064	2,159	2,139	2,130	2,104
Mn	0,049	0,049	0,024	0,049	0,049	0,049	0,037	0,024	0,037	0,049	0,061	0,049	0,049
Mg	2,663	2,791	2,773	2,617	2,723	2,884	3,008	2,760	2,776	2,663	2,680	2,712	2,722
	5,702	5,780	5,800	5,718	5,761	5,875	5,908	5,740	5,738	5,709	5,709	5,725	5,722
Na													
K	1,834	1,801	1,784	1,887	1,905	1,781	1,636	1,794	1,933	1,837	1,816	1,860	1,867
	1,834	1,801	1,784	1,887	1,905	1,781	1,636	1,794	1,933	1,837	1,816	1,860	1,867
OH*	3,665	3,500	3,810	3,688	3,857	3,735	3,668	3,480	3,667	3,810	3,690	3,737	3,783
F	0,335	0,475	0,190	0,287	0,143	0,240	0,332	0,520	0,333	0,190	0,284	0,238	0,191
Cl		0,025		0,026		0,026					0,025	0,025	0,026
	4,000	4,000	4,000	4,000	4,000	4,000	4,000	4,000	4,000	4,000	4,000	4,000	4,000
TOTAL	19,536	19,580	19,584	19,605	19,666	19,656	19,544	19,534	19,671	19,546	19,525	19,585	19,589

Apêndice C.2. Análises químicas pontuais de cristais de biotita do Batólito Rio Jacaré (continuação).

Rocha	SOS 861T	SOS 861T	SOS 861T	SOS 861T	SOS 861T	SOS 861T	SOS 861T	SOS 861T	SOS 862	SOS 862	SOS 862	SOS 864	SOS 864
Espectro	11	12	44	45	46	47	48	49	10	11	12	10	11
SiO_2	39,8	39,6	38,7	38,9	39,1	39,3	38,9	39,1	40,2	40,0	40,1	38,7	37,8
TiO_2	1,2	1,2	2,4	2,5	2,5	2,3	2,4	2,5	1,6	2,0	1,9	1,7	1,8
Al_2O_3	15,5	15,5	15,8	16,0	16,0	16,1	16,1	16,2	16,9	16,1	16,3	15,2	15,0
FeO	16,4	16,6	18,5	17,2	17,6	17,5	17,6	17,3	13,6	14,9	14,7	16,6	17,6
MnO	0,1	0,1	0,1	0,2	0,2	0,1	0,2	0,2	0,2	0,3	0,3	0,2	0,3
MgO	13,4	13,2	10,9	11,2	11,1	11,2	11,1	11,3	14,0	13,5	13,4	13,9	13,7
Na_2O									0,4				
K_2O	8,7	9,2	9,1	9,3	8,9	9,3	9,2	9,1	9,0	9,2	9,2	9,8	9,7
F	0,7	0,8	0,4	0,7	0,5	0,2	0,5	0,3	1,2	0,9	0,8	0,8	0,3
Cl	0,1	0,2	0,1	0,1	0,1	0,1	0,1	0,1					0,1
H_2O*	3,7	3,6	3,8	3,7	3,8	3,9	3,8	3,9	3,6	3,7	3,7	3,7	3,8
Subtotal	99,6	99,9	99,9	99,8	99,8	100,0	99,9	100,0	100,8	100,7	100,5	100,5	100,1
O=F,Cl	0,317	0,382	0,191	0,317	0,233	0,107	0,233	0,149	0,505	0,379	0,337	0,337	0,149
Total	99,3	99,5	99,7	99,5	99,5	99,9	99,6	99,8	100,3	100,3	100,2	100,2	100,0
Si	5,916	5,889	5,802	5,816	5,832	5,841	5,810	5,812	5,847	5,857	5,868	5,757	5,682
Al ^{iv}	2,084	2,111	2,198	2,184	2,168	2,159	2,190	2,188	2,153	2,143	2,132	2,243	2,318
	8,000	8,000	8,000	8,000	8,000	8,000	8,000	8,000	8,000	8,000	8,000	8,000	8,000
Al ^{vi}	0,621	0,601	0,602	0,642	0,652	0,669	0,651	0,656	0,741	0,639	0,681	0,418	0,333
Ti	0,129	0,140	0,271	0,281	0,280	0,258	0,270	0,279	0,178	0,222	0,211	0,193	0,206
Fe^{3+}	0,108	0,101										0,240	0,345
Fe^{2+}	1,913	1,955	2,307	2,132	2,171	2,155	2,178	2,130	1,646	1,807	1,782	1,820	1,854
Mn	0,012	0,012	0,012	0,024	0,024	0,012	0,024	0,024	0,024	0,036	0,036	0,024	0,037
Mg	2,975	2,919	2,447	2,505	2,478	2,491	2,481	2,512	3,037	2,952	2,930	3,088	3,074
	5,759	5,728	5,638	5,584	5,606	5,585	5,603	5,602	5,626	5,656	5,640	5,783	5,850
Na									0,108				
K	1,655	1,750	1,745	1,777	1,700	1,767	1,757	1,730	1,673	1,720	1,719	1,859	1,858
	1,655	1,750	1,745	1,777	1,700	1,767	1,757	1,730	1,781	1,720	1,719	1,859	1,858
OH*	3,646	3,573	3,785	3,643	3,739	3,881	3,738	3,834	3,448	3,584	3,630	3,623	3,832
F	0,329	0,377	0,190	0,331	0,236	0,094	0,236	0,141	0,552	0,416	0,370	0,377	0,143
Cl	0,025	0,050	0,025	0,025	0,025	0,025	0,025	0,025					0,025
	4,000	4,000	4,000	4,000	4,000	4,000	4,000	4,000	4,000	4,000	4,000	4,000	4,000
TOTAL	19,413	19,478	19,383	19,361	19,306	19,352	19,360	19,332	19,407	19,376	19,359	19,641	19,707

Apêndice C.2. Análises químicas pontuais de cristais de biotita do Batólito Rio Jacaré (continuação).

Rocha	SOS 864	SOS 864	SOS 864	SOS 864	SOS 864	SOS 864	SOS 864	SOS 864	SOS 864	SOS 864	SOS 864	SOS 866	SOS 866
Espectro	33	34	8	9	10	11	12	13	14	19	20	30	31
SiO_2	38,2	38,0	37,8	37,8	37,7	38,2	37,9	37,3	37,8	38,0	37,8	38,2	38,0
TiO_2	3,6	2,7	2,0	2,3	2,4	2,4	2,3	2,8	2,6	2,1	2,0	1,6	1,8
Al_2O_3	15,7	16,2	15,6	15,6	15,3	15,4	15,2	15,2	15,1	15,4	15,2	15,6	15,6
FeO	16,9	18,0	17,9	18,1	18,4	18,1	18,6	18,6	18,3	18,0	18,6	18,0	18,4
MnO	0,2	0,1	0,3	0,3	0,3	0,3	0,3	0,3	0,4	0,4	0,0	0,4	0,4
MgO	11,6	11,0	12,6	12,2	12,2	12,1	12,4	12,0	12,0	12,6	12,1	12,3	11,9
Na_2O													
K_2O	9,7	9,9	9,8	9,6	9,7	9,6	9,3	9,8	9,7	9,5	10,0	9,9	9,9
F	0,2			0,1	0,1						0,2	0,3	0,1
Cl	0,1			0,1	0,1						0,2		
H_2O*	3,9	4,0	4,0	3,9	3,9	4,0	4,0	4,0	4,0	4,0	3,8	3,9	3,9
Subtotal	100,1	99,9	99,9	100,1	100,1	100,1	100,0	100,0	99,9	100,0	100,2	100,2	100,0
O=F,Cl	0,107			0,065	0,065						0,129	0,126	0,042
Total	100,0	99,9	99,9	100,1	100,0	100,1	100,0	100,0	99,9	100,0	100,1	100,0	100,0
Si	5,703	5,704	5,686	5,680	5,682	5,728	5,701	5,641	5,702	5,705	5,716	5,738	5,726
Al^{iv}	2,297	2,296	2,314	2,320	2,318	2,272	2,299	2,359	2,298	2,295	2,284	2,262	2,274
	8,000	8,000	8,000	8,000	8,000	8,000	8,000	8,000	8,000	8,000	8,000	8,000	8,000
Al^{vi}	0,473	0,574	0,442	0,450	0,392	0,442	0,388	0,341	0,381	0,422	0,417	0,508	0,487
Ti	0,399	0,303	0,228	0,260	0,272	0,271	0,260	0,316	0,294	0,238	0,229	0,184	0,207
Fe^{3+}			0,214	0,169	0,190	0,122	0,218	0,184	0,146	0,214	0,186	0,186	0,174
Fe^{2+}	2,096	2,245	2,024	2,100	2,124	2,143	2,111	2,162	2,158	2,042	2,165	2,063	2,142
Mn	0,024	0,012	0,037	0,037	0,037	0,037	0,037	0,037	0,049	0,049		0,049	0,049
Mg	2,585	2,469	2,818	2,729	2,737	2,703	2,775	2,702	2,697	2,813	2,725	2,751	2,673
	5,577	5,603	5,763	5,746	5,752	5,718	5,790	5,743	5,725	5,778	5,722	5,740	5,731
Na													
K	1,846	1,892	1,878	1,839	1,863	1,836	1,786	1,887	1,865	1,819	1,924	1,894	1,900
	1,846	1,892	1,878	1,839	1,863	1,836	1,786	1,887	1,865	1,819	1,941	1,894	1,900
OH*	3,880	4,000	4,000	3,927	3,927	4,000	4,000	4,000	4,000	4,000	3,853	3,858	3,952
F	0,094			0,047	0,048						0,096	0,142	0,048
Cl	0,025			0,025	0,026						0,051		
	4,000	4,000	4,000	4,000	4,000	4,000	4,000	4,000	4,000	4,000	4,000	4,000	4,000
TOTAL	19,423	19,496	19,640	19,585	19,614	19,553	19,576	19,629	19,589	19,597	19,664	19,634	19,631

Apêndice C.2. Análises químicas pontuais de cristais de biotita do Batólito Rio Jacaré (continuação).

Rocha	SOS 866	SOS 866	SOS 866	SOS 866	SOS 866	SOS 866	SOS 866	SOS 866	SOS 866	SOS 866	SOS 867A	SOS 867A	SOS 867A
Espectro	32	34	35	54	55	56	57	62	63	64	27	30	37
SiO_2	38,1	37,7	38,1	38,9	39,3	38,6	38,3	38,0	38,2	38,3	42,1	41,9	41,4
TiO_2	2,7	2,5	1,9	1,4	1,3	1,9	1,7	1,7	1,7	1,6	1,0	1,1	1,2
Al_2O_3	15,2	15,1	15,6	15,6	15,9	15,3	15,6	15,1	14,9	14,7	17,8	19,5	17,1
FeO	18,5	18,4	18,2	16,7	16,0	17,4	17,4	18,4	18,5	18,6	11,3	7,7	11,9
MnO	0,2	0,3	0,3	0,3	0,3	0,2	0,4	0,4	0,3	0,3	0,2	0,1	0,2
MgO	11,6	11,6	12,0	13,4	14,1	12,9	12,8	12,7	12,9	13,2	15,6	18,4	15,3
Na_2O												0,7	
K2O	9,7	10,0	9,6	9,5	9,2	9,8	9,8	9,6	9,6	9,1	8,1	5,8	8,8
F	0,4	0,5	0,3	0,6	0,5	0,5	0,6	0,1	0,1	0,2		1,1	0,2
Cl							0,1		0,1			0,1	
H_2O*	3,8	3,7	3,8	3,7	3,8	3,8	3,7	3,9	3,9	3,9	4,2	3,8	4,1
Subtotal	100,2	99,8	99,9	100,3	100,5	100,3	100,4	99,9	100,2	99,9	100,2	101,0	100,2
O=F,Cl	0,168	0,211	0,126	0,253	0,211	0,211	0,275	0,042	0,065	0,084		0,486	0,084
Total	100,0	99,6	99,7	100,0	100,3	100,1	100,1	99,9	100,1	99,8	100,2	100,5	100,1
Si	5,733	5,716	5,738	5,783	5,786	5,769	5,732	5,727	5,743	5,761	5,978	5,788	5,936
Al^{iv}	2,267	2,284	2,262	2,217	2,214	2,231	2,268	2,273	2,257	2,239	2,022	2,212	2,064
	8,000	8,000	8,000	8,000	8,000	8,000	8,000	8,000	8,000	8,000	8,000	8,000	8,000
Al^{vi}	0,423	0,408	0,498	0,527	0,554	0,458	0,492	0,404	0,379	0,365	0,947	0,965	0,826
Ti	0,304	0,284	0,217	0,161	0,149	0,216	0,194	0,196	0,195	0,185	0,102	0,110	0,135
Fe^{3+}	0,071	0,110	0,153	0,198	0,213	0,157	0,193	0,274	0,284	0,324			
Fe^{2+}	2,253	2,222	2,135	1,870	1,750	2,008	1,975	2,039	2,036	2,004	1,323	0,877	1,412
Mn	0,024	0,037	0,037	0,036	0,036	0,024	0,049	0,049	0,037	0,037	0,023	0,011	0,023
Mg	2,605	2,624	2,693	2,980	3,100	2,867	2,848	2,846	2,882	2,949	3,289	3,800	3,264
	5,679	5,684	5,734	5,772	5,802	5,730	5,752	5,808	5,814	5,863	5,684	5,763	5,660
Na												0,180	
K	1,861	1,930	1,844	1,803	1,732	1,867	1,869	1,845	1,841	1,750	1,459	1,016	1,616
	1,861	1,930	1,844	1,803	1,732	1,867	1,869	1,845	1,841	1,750	1,459	1,338	1,616
OH*	3,810	3,760	3,857	3,718	3,767	3,764	3,691	3,952	3,927	3,905	4,000	3,495	3,909
F	0,190	0,240	0,143	0,282	0,233	0,236	0,284	0,048	0,048	0,095		0,481	0,091
Cl							0,025		0,025			0,023	
	4,000	4,000	4,000	4,000	4,000	4,000	4,000	4,000	4,000	4,000	4,000	4,000	4,000
TOTAL	19,540	19,614	19,577	19,576	19,534	19,597	19,621	19,652	19,655	19,613	19,143	19,101	19,277

Apêndice C.2. Análises químicas pontuais de cristais de biotita do Batólito Rio Jacaré (continuação).

Rocha	SOS 867A	SOS 871A	SOS 871A	SOS 871A	SOS 871A	SOS 871A	SOS 871A	SOS 871A	SOS 871A	SOS 871A	SOS 871A	SOS 871A	SOS 871B
Espectro	38	1	2	3	7	8	9	10	21	22	23	40	7
SiO_2	41,2	39,5	38,6	38,6	38,9	38,8	38,7	38,9	39,4	38,9	39,2	38,9	38,1
TiO_2	1,4	1,6	2,0	2,1	1,6	1,8	1,5	1,6	1,2	1,4	1,9	2,7	2,7
Al_2O_3	17,8	16,2	15,7	15,8	15,6	15,8	15,9	16,1	16,4	16,4	15,7	16,4	16,4
FeO	11,5	15,6	16,7	16,6	16,8	16,4	17,3	16,0	15,8	16,1	15,9	15,6	16,3
MnO	0,3	0,3	0,1	0,2	0,2	0,2	0,2	0,3	0,2	0,3	0,3	0,3	0,2
MgO	14,5	13,7	13,4	13,2	13,2	13,2	13,2	13,2	13,5	13,3	13,7	12,9	12,5
Na_2O													
K_2O	9,3	9,2	9,4	9,4	9,7	9,6	9,2	9,7	9,4	9,5	9,2	9,4	9,9
F		0,1	0,3	0,5	0,6			0,1	0,4		0,8		0,6
Cl	0,1		0,1	0,1	0,1	0,1			0,1	0,1	0,1		
H_2O*	4,2	4,0	3,9	3,8	3,7	4,0	4,0	4,0	3,9	4,0	3,7	4,1	3,7
Subtotal	100,3	100,2	100,3	100,4	100,4	100,0	100,1	100,0	100,4	100,1	100,6	100,2	100,4
O=F,Cl	0,023	0,042	0,149	0,233	0,275	0,023		0,042	0,191	0,023	0,359		0,253
Total	100,2	100,2	100,1	100,1	100,1	100,0	100,1	100,0	100,2	100,1	100,2	100,2	100,2
Si	5,908	5,801	5,731	5,730	5,785	5,762	5,747	5,767	5,803	5,755	5,784	5,731	5,665
Al^{iv}	2,092	2,199	2,269	2,270	2,215	2,238	2,253	2,233	2,197	2,245	2,216	2,269	2,335
	8,000	8,000	8,000	8,000	8,000	8,000	8,000	8,000	8,000	8,000	8,000	8,000	8,000
Al^{vi}	0,911	0,612	0,487	0,502	0,513	0,536	0,537	0,587	0,656	0,619	0,525	0,583	0,541
Ti	0,155	0,180	0,225	0,236	0,183	0,204	0,172	0,182	0,138	0,160	0,213	0,298	0,300
Fe^{3+}		0,102	0,172	0,143	0,162	0,132	0,217	0,117	0,122	0,148	0,132		0,031
Fe^{2+}	1,366	1,797	1,892	1,908	1,920	1,899	1,917	1,864	1,821	1,838	1,824	1,905	1,991
Mn	0,035	0,036	0,012	0,024	0,024	0,024	0,024	0,036	0,024	0,036	0,036	0,036	0,024
Mg	3,100	3,009	2,975	2,932	2,938	2,934	2,934	2,929	2,975	2,944	3,022	2,827	2,765
	5,567	5,737	5,764	5,746	5,740	5,729	5,800	5,715	5,736	5,746	5,752	5,649	5,653
Na													
K	1,704	1,728	1,782	1,782	1,840	1,819	1,746	1,835	1,769	1,794	1,736	1,769	1,875
	1,704	1,728	1,782	1,782	1,840	1,819	1,746	1,835	1,769	1,794	1,736	1,769	1,875
OH*	3,976	3,954	3,834	3,740	3,692	3,975	4,000	3,953	3,788	3,975	3,601	4,000	3,718
F		0,046	0,141	0,235	0,282			0,047	0,187		0,374		0,282
Cl	0,024		0,025	0,025	0,025	0,025			0,025	0,025	0,025		
	4,000	4,000	4,000	4,000	4,000	4,000	4,000	4,000	4,000	4,000	4,000	4,000	4,000
TOTAL	19,271	19,465	19,546	19,528	19,580	19,548	19,546	19,550	19,506	19,540	19,488	19,418	19,528

Apêndice C.2. Análises químicas pontuais de cristais de biotita do Batólito Rio Jacaré (continuação).

Rocha	SOS 871B	SOS 871B	SOS 871B	SOS 871B	SOS 871B	SOS 873B	SOS 873B	SOS 873B	SOS 873B	SOS 873B	SOS 873B	SOS 873B	SOS 873B
Espectro	8	9	14	32	4	75	84	85	86	87	88	31	32
SiO_2	38,2	37,8	38,7	38,1	38,1	38,6	39,0	38,5	38,8	38,5	39,8	38,3	38,2
TiO_2	2,5	3,5	1,8	2,7	2,2	3,0	1,8	1,9	1,9	2,1	2,5	3,9	3,8
Al_2O_3	16,7	14,4	15,9	15,1	15,6	16,2	17,2	16,8	17,2	17,2	17,6	15,3	15,2
FeO	16,1	17,8	16,5	16,3	17,2	14,0	13,3	13,6	13,2	13,4	12,6	14,5	14,7
MnO	0,3	0,2	0,2	0,2	0,3	0,1		0,2		0,1	0,1	0,2	0,1
MgO	12,3	12,2	13,2	14,0	13,2	13,8	14,5	14,6	14,5	14,4	13,8	13,5	14,0
Na_2O													
K_2O	9,8	9,4	9,7	9,6	9,6	9,8	9,5	9,6	9,4	9,7	9,5	9,4	9,1
F	0,4	0,8	0,5	1,0	0,2	0,6	0,7	0,7	1,1	0,6	0,1	0,8	0,9
Cl		0,1		0,1	0,1			0,1		0,1		0,2	
H_2O*	3,8	3,6	3,8	3,5	3,9	3,8	3,8	3,7	3,6	3,8	4,1	3,6	3,6
Subtotal	100,1	99,7	100,3	100,6	100,3	99,9	99,8	99,7	99,6	99,9	100,1	99,7	99,6
O=F,Cl	0,168	0,359	0,211	0,444	0,107	0,253	0,295	0,317	0,463	0,275	0,042	0,382	0,379
Total	100,0	99,3	100,1	100,2	100,2	99,6	99,5	99,4	99,1	99,6	100,1	99,4	99,3
Si	5,680	5,719	5,749	5,675	5,689	5,698	5,720	5,683	5,709	5,664	5,775	5,695	5,676
Al^{iv}	2,320	2,281	2,251	2,325	2,311	2,302	2,280	2,317	2,291	2,336	2,225	2,305	2,324
	8,000	8,000	8,000	8,000	8,000	8,000	8,000	8,000	8,000	8,000	8,000	8,000	8,000
Al^{vi}	0,606	0,286	0,540	0,321	0,425	0,522	0,693	0,607	0,691	0,644	0,777	0,369	0,332
Ti	0,279	0,393	0,204	0,301	0,248	0,330	0,201	0,213	0,213	0,234	0,272	0,440	0,429
Fe^{3+}	0,005	0,062	0,134	0,217	0,206		0,052	0,125	0,047	0,072			0,024
Fe^{2+}	1,993	2,174	1,910	1,807	1,930	1,723	1,577	1,550	1,563	1,574	1,509	1,790	1,789
Mn	0,036	0,025	0,024	0,024	0,036	0,012		0,024		0,012	0,012	0,024	0,012
Mg	2,723	2,748	2,913	3,111	2,927	3,043	3,171	3,211	3,181	3,158	2,987	3,000	3,104
	5,643	5,687	5,725	5,781	5,772	5,630	5,694	5,730	5,695	5,695	5,558	5,624	5,691
Na													
K	1,857	1,814	1,838	1,823	1,828	1,844	1,779	1,808	1,767	1,820	1,757	1,784	1,728
	1,857	1,814	1,838	1,823	1,828	1,844	1,779	1,808	1,767	1,820	1,757	1,784	1,728
OH*	3,812	3,592	3,765	3,504	3,880	3,720	3,675	3,648	3,488	3,696	3,954	3,573	3,577
F	0,188	0,383	0,235	0,471	0,094	0,280	0,325	0,327	0,512	0,279	0,046	0,376	0,423
Cl		0,026		0,025	0,025			0,025		0,025		0,050	
	4,000	4,000	4,000	4,000	4,000	4,000	4,000	4,000	4,000	4,000	4,000	4,000	4,000
TOTAL	19,499	19,502	19,563	19,604	19,600	19,474	19,473	19,538	19,461	19,515	19,315	19,408	19,419

Apêndice C.2. Análises químicas pontuais de cristais de biotita do Batólito Rio Jacaré (continuação).

Rocha	SOS 873B	SOS 873B	SOS 873B	SOS 873B	SOS 873B	SOS 873B	SOS 873B	SOS 873B	SOS 873B	SOS 876A	SOS 876A	SOS 876A	SOS 876A
Espectro	33	40	41	42	43	47	48	29	30	1	2	3	4
SiO_2	38,3	37,7	38,7	38,8	38,5	38,6	38,4	38,2	38,1	37,2	37,6	37,3	37,7
TiO_2	3,9	4,0	3,7	3,7	3,7	2,0	2,2	2,5	2,5	3,2	3,2	3,2	3,1
Al_2O_3	15,5	15,2	15,5	15,5	15,5	17,0	16,6	15,8	15,6	16,2	16,2	16,3	16,3
FeO	14,4	15,7	14,3	14,1	14,2	14,2	14,1	15,7	16,0	19,9	19,6	19,7	19,4
MnO		0,1	0,1	0,1				0,3	0,1	0,3	0,3	0,4	0,3
MgO	13,9	13,5	13,8	14,0	14,2	13,9	14,5	13,6	13,8	9,6	9,4	9,5	9,7
Na_2O													
K_2O	9,3	9,5	9,3	9,2	9,0	9,6	9,3	9,6	9,7	9,7	9,7	9,7	9,5
F	0,6		0,4	0,5	0,9		0,8		0,2				0,7
Cl	0,1			0,1			0,1		0,1				0,0
H_2O*	3,7	4,0	3,9	3,8	3,6	4,1	3,7	4,0	3,9	4,0	4,0	4,0	3,6
Subtotal	99,8	99,8	99,7	99,8	99,7	99,4	99,7	99,8	100,1	100,1	100,0	100,1	100,3
O=F,Cl	0,275		0,168	0,233	0,379		0,359		0,107				0,295
Total	99,5	99,8	99,5	99,6	99,3	99,4	99,3	99,8	100,0	100,1	100,0	100,1	100,1
Si	5,671	5,615	5,715	5,720	5,693	5,698	5,676	5,678	5,668	5,640	5,688	5,649	5,689
Al^{iv}	2,329	2,385	2,285	2,280	2,307	2,302	2,324	2,322	2,332	2,360	2,312	2,351	2,311
	8,000	8,000	8,000	8,000	8,000	8,000	8,000	8,000	8,000	8,000	8,000	8,000	8,000
Al^{vi}	0,369	0,276	0,406	0,406	0,387	0,655	0,570	0,453	0,411	0,535	0,579	0,558	0,589
Ti	0,438	0,451	0,416	0,415	0,416	0,224	0,245	0,279	0,279	0,361	0,360	0,360	0,348
Fe^{3+}		0,062				0,056	0,123	0,143	0,180				
Fe^{2+}	1,772	1,888	1,754	1,727	1,744	1,690	1,612	1,805	1,807	2,506	2,461	2,478	2,430
Mn		0,012	0,012	0,012				0,036	0,012	0,037	0,037	0,049	0,037
Mg	3,072	3,003	3,044	3,081	3,132	3,064	3,194	3,020	3,065	2,167	2,120	2,143	2,179
	5,651	5,692	5,633	5,642	5,680	5,688	5,743	5,737	5,754	5,605	5,557	5,589	5,583
Na													
K	1,759	1,804	1,755	1,734	1,702	1,808	1,756	1,820	1,839	1,873	1,869	1,871	1,828
	1,759	1,804	1,755	1,734	1,702	1,808	1,756	1,820	1,839	1,873	1,869	1,871	1,828
OH*	3,694	4,000	3,813	3,742	3,579	4,000	3,601	4,000	3,881	4,000	4,000	4,000	3,666
F	0,281		0,187	0,233	0,421		0,374		0,094				0,334
Cl	0,025			0,025			0,025		0,025				
	4,000	4,000	4,000	4,000	4,000	4,000	4,000	4,000	4,000	4,000	4,000	4,000	4,000
TOTAL	19,409	19,496	19,388	19,375	19,382	19,496	19,499	19,557	19,593	19,478	19,426	19,459	19,411

Apêndice C.2. Análises químicas pontuais de cristais de biotita do Batólito Rio Jacaré (continuação).

Rocha	SOS 876A	SOS 876A	SOS 876A	SOS 876A	SOS 876A	SOS 876A	SOS 876A	SOS 876A	SOS 876A	SOS 876A	SOS 876A	SOS 876A	SOS 876A
Espectro	5	6	7	9	34	35	36	37	38	39	41	42	22
SiO_2	37,5	37,6	37,7	38,2	37,8	38,0	37,5	38,0	37,6	37,5	37,4	37,5	37,7
TiO_2	2,9	2,8	2,3	2,3	2,7	2,4	2,4	2,4	2,5	2,4	2,7	2,4	2,6
Al_2O_3	16,4	16,2	16,4	16,6	16,5	16,6	16,5	16,5	16,3	16,3	16,5	16,7	15,8
FeO	19,4	19,0	19,5	18,8	19,5	19,0	19,5	19,4	19,8	20,1	19,4	19,6	19,2
MnO	0,5	0,3	0,4	0,3	0,4	0,3	0,4	0,3	0,4	0,4	0,3	0,3	0,3
MgO	9,5	9,8	9,9	10,1	9,7	10,0	10,0	9,8	9,9	9,7	9,6	9,7	10,7
Na_2O													
K_2O	9,8	9,5	9,7	9,5	9,5	9,5	9,6	9,7	9,4	9,7	9,4	9,8	9,6
F		0,8		0,9	0,1	0,2	0,3		0,4	0,4	0,6	0,3	
Cl												0,1	
H_2O*	4,0	3,6	4,0	3,6	3,9	3,9	3,8	4,0	3,8	3,8	3,7	3,8	4,0
Subtotal	100,0	99,6	99,9	100,3	100,1	99,9	100,0	100,1	100,1	100,3	99,6	100,2	99,9
O=F,Cl		0,337		0,379	0,042	0,084	0,126		0,168	0,168	0,253	0,149	
Total	100,0	99,3	99,9	99,9	100,1	99,8	99,9	100,1	99,9	100,1	99,3	100,1	99,9
Si	5,677	5,712	5,705	5,745	5,699	5,725	5,675	5,725	5,691	5,684	5,685	5,674	5,698
Al^{iv}	2,323	2,288	2,295	2,255	2,301	2,275	2,325	2,275	2,309	2,316	2,315	2,326	2,302
	8,000	8,000	8,000	8,000	8,000	8,000	8,000	8,000	8,000	8,000	8,000	8,000	8,000
Al^{vi}	0,603	0,615	0,631	0,689	0,631	0,673	0,618	0,657	0,600	0,597	0,640	0,650	0,518
Ti	0,328	0,318	0,262	0,261	0,305	0,272	0,273	0,272	0,284	0,273	0,307	0,273	0,294
Fe^{3+}							0,011		0,005	0,014			0,040
Fe^{2+}	2,441	2,398	2,456	2,352	2,441	2,380	2,445	2,430	2,485	2,519	2,448	2,467	2,376
Mn	0,061	0,037	0,049	0,037	0,049	0,037	0,049	0,037	0,049	0,049	0,037	0,037	0,037
Mg	2,143	2,216	2,229	2,259	2,178	2,241	2,250	2,198	2,229	2,189	2,173	2,185	2,399
	5,576	5,584	5,627	5,597	5,603	5,603	5,646	5,594	5,652	5,642	5,605	5,612	5,664
Na													
K	1,889	1,840	1,870	1,823	1,826	1,826	1,851	1,863	1,815	1,873	1,822	1,888	1,849
	1,889	1,840	1,870	1,823	1,826	1,826	1,851	1,863	1,815	1,873	1,822	1,888	1,849
OH*	4,000	3,616	4,000	3,572	3,952	3,905	3,857	4,000	3,809	3,808	3,712	3,831	4,000
F		0,384		0,428	0,048	0,095	0,143		0,191	0,192	0,288	0,143	
Cl												0,026	
	4,000	4,000	4,000	4,000	4,000	4,000	4,000	4,000	4,000	4,000	4,000	4,000	4,000
TOTAL	19,465	19,424	19,497	19,419	19,430	19,428	19,497	19,457	19,467	19,514	19,427	19,501	19,513

Apêndice C.2. Análises químicas pontuais de cristais de biotita do Batólito Rio Jacaré (continuação).

Rocha	SOS 876A	SOS 876A	SOS 876A	SOS 876A	SOS 876A	SOS 876A	SOS 876A	SOS 876B	SOS 876B	SOS 876B	SOS 876B	SOS 876B	SOS 876B
Espectro	23	24	25	26	27	28	29	45	46	47	48	49	50
SiO_2	37,6	37,6	38,1	37,3	37,7	35,3	38,0	38,1	38,2	37,7	37,9	38,1	37,5
TiO_2	2,4	2,7	2,7	2,4	2,5	2,0	2,2	2,6	3,0	2,8	2,5	2,5	2,6
Al_2O_3	16,3	16,0	16,4	16,0	16,3	15,9	16,1	15,6	15,7	15,4	15,0	14,9	14,7
FeO	18,6	19,0	18,1	19,1	18,7	24,3	18,8	18,0	17,6	18,5	18,0	18,6	19,0
MnO	0,4	0,5	0,4	0,4	0,4	0,4	0,3		0,5	0,4	0,3	0,4	0,4
MgO	10,6	10,4	10,4	10,8	10,6	10,7	10,6	11,7	11,2	11,8	12,1	11,7	11,5
Na_2O													
K_2O	9,8	9,7	9,8	9,6	9,6	7,5	9,7	9,9	9,9	9,4	9,7	10,0	9,5
F		0,1	0,2	0,4	0,2	0,2		0,5		0,7	0,4	0,6	0,6
Cl		0,1	0,1					0,1			0,1		
H_2O*	4,0	3,9	3,9	3,8	3,9	3,8	4,0	3,7	4,0	3,7	3,8	3,7	3,7
Subtotal	99,9	100,1	100,2	99,9	99,9	100,1	99,7	100,2	100,1	100,4	99,7	100,5	100,2
O=F,Cl		0,065	0,107	0,168	0,084	0,084		0,233		0,295	0,191	0,253	0,253
Total	99,9	100,0	100,1	99,7	99,8	100,0	99,7	100,0	100,1	100,1	99,5	100,2	99,9
Si	5,683	5,685	5,722	5,657	5,689	5,429	5,737	5,724	5,723	5,676	5,732	5,742	5,709
Al^{iv}	2,317	2,315	2,278	2,343	2,311	2,571	2,263	2,276	2,277	2,324	2,268	2,258	2,291
	8,000	8,000	8,000	8,000	8,000	8,000	8,000	8,000	8,000	8,000	8,000	8,000	8,000
Al^{vi}	0,587	0,540	0,627	0,519	0,589	0,315	0,606	0,477	0,503	0,400	0,400	0,385	0,341
Ti	0,273	0,305	0,304	0,273	0,283	0,233	0,251	0,293	0,335	0,315	0,284	0,283	0,296
Fe^{3+}	0,014	0,006		0,106	0,009	0,588	0,002	0,042		0,133	0,122	0,113	0,153
Fe^{2+}	2,333	2,388	2,267	2,306	2,343	2,494	2,365	2,219	2,192	2,187	2,140	2,229	2,260
Mn	0,049	0,061	0,049	0,049	0,049	0,050	0,037		0,061	0,049	0,037	0,049	0,049
Mg	2,377	2,335	2,321	2,450	2,374	2,441	2,376	2,622	2,508	2,648	2,726	2,631	2,612
	5,633	5,635	5,567	5,703	5,646	6,122	5,637	5,653	5,599	5,733	5,708	5,689	5,712
Na													
K	1,886	1,868	1,875	1,855	1,846	1,468	1,866	1,894	1,889	1,805	1,869	1,919	1,844
	1,897	1,874	1,881	1,855	1,846	1,468	1,866	1,894	1,889	1,805	1,869	1,919	1,884
OH*	4,000	3,927	3,880	3,808	3,905	3,903	4,000	3,737	4,000	3,667	3,783	3,714	3,711
F		0,048	0,095	0,192	0,095	0,097		0,238		0,333	0,191	0,286	0,289
Cl		0,026	0,025					0,025			0,026		
	4,000	4,000	4,000	4,000	4,000	4,000	4,000	4,000	4,000	4,000	4,000	4,000	4,000
TOTAL	19,530	19,509	19,448	19,558	19,492	19,589	19,503	19,548	19,488	19,538	19,578	19,608	19,596

Apêndice C.2. Análises químicas pontuais de cristais de biotita do Batólito Rio Jacaré (continuação).

Rocha	SOS 876B	SOS 876B	SOS 876B	SOS 876B	SOS 876B	SOS 876B	SOS 876B	SOS 876B	SOS 876B	SOS 876B	SOS 876B	SOS 876B	SOS 876B
Espectro	51	52	53	47	48	56	58	59	60	61	63	64	65
SiO_2	38,1	38,4	37,5	37,5	38,6	38,5	39,3	38,3	38,1	38,8	37,8	38,3	38,0
TiO_2	2,3	2,1	2,2	3,4	3,9	3,9	0,7	3,5	3,4	3,6	3,4	3,6	4,2
Al_2O_3	14,7	15,2	15,0	16,3	15,6	15,7	15,2	16,7	15,8	15,6	16,1	15,8	15,3
FeO	18,9	18,4	19,1	17,3	15,5	16,1	31,4	15,2	16,0	15,5	16,4	15,3	15,6
MnO	0,3	0,4	0,5	0,2	0,3	0,1		0,2	0,2	0,1	0,1	0,1	0,1
MgO	12,1	11,8	12,3	11,2	12,4	13,0	2,1	12,8	13,2	12,7	12,6	12,8	12,7
Na_2O													
K_2O	9,6	9,7	9,3	9,4	9,3	8,4	7,2	8,9	9,2	9,6	9,6	9,6	9,7
F	0,1	0,8	0,6	0,6	0,2							0,5	0,2
Cl		0,1		0,1								0,1	0,1
H_2O*	3,9	3,6	3,7	3,7	3,9	4,1	3,8	4,1	4,0	4,1	4,0	3,8	3,9
Subtotal	100,0	100,5	100,2	99,7	99,8	99,9	99,6	99,6	99,9	100,0	100,0	99,8	99,8
O=F,Cl	0,042	0,359	0,253	0,275	0,084							0,233	0,107
Total	100,0	100,1	99,9	99,4	99,7	99,9	99,6	99,6	99,9	100,0	100,0	99,6	99,7
Si	5,748	5,774	5,675	5,643	5,723	5,683	6,155	5,659	5,652	5,736	5,626	5,695	5,666
Al^{iv}	2,252	2,226	2,325	2,357	2,277	2,317	1,845	2,341	2,348	2,264	2,374	2,305	2,334
	8,000	8,000	8,000	8,000	8,000	8,000	8,000	8,000	8,000	8,000	8,000	8,000	8,000
Al^{vi}	0,359	0,462	0,344	0,535	0,459	0,423	0,957	0,568	0,421	0,464	0,454	0,472	0,347
Ti	0,261	0,239	0,251	0,380	0,439	0,437	0,079	0,384	0,375	0,406	0,376	0,397	0,473
Fe^{3+}	0,187	0,114	0,286						0,055		0,025		
Fe^{2+}	2,190	2,195	2,117	2,159	1,899	1,970	4,037	1,857	1,921	1,898	2,008	1,886	1,939
Mn	0,037	0,049	0,061	0,024	0,036	0,012		0,024	0,024	0,012	0,012	0,012	0,012
Mg	2,719	2,647	2,769	2,517	2,738	2,852	0,494	2,812	2,908	2,794	2,789	2,830	2,815
	5,753	5,706	5,830	5,616	5,571	5,694	5,567	5,644	5,704	5,574	5,664	5,597	5,587
Na													
K	1,847	1,860	1,796	1,804	1,762	1,591	1,440	1,682	1,743	1,811	1,821	1,821	1,843
	1,847	1,860	1,796	1,804	1,762	1,591	1,440	1,682	1,743	1,811	1,821	1,821	1,843
OH*	3,952	3,594	3,713	3,689	3,906	4,000	4,000	4,000	4,000	4,000	4,000	3,740	3,880
F	0,048	0,380	0,287	0,285	0,094							0,235	0,094
Cl		0,025		0,025								0,025	0,025
	4,000	4,000	4,000	4,000	4,000	4,000	4,000	4,000	4,000	4,000	4,000	4,000	4,000
TOTAL	19,600	19,565	19,625	19,420	19,333	19,285	19,007	19,327	19,448	19,385	19,486	19,418	19,430

Apêndice C.2. Análises químicas pontuais de cristais de biotita do Batólito Rio Jacaré (continuação).

Rocha	SOS 876B	SOS 876B	SOS 876B	SOS 876B	SOS 876B	SOS 876B	SOS 876B	SOS 876B	SOS 876B	SOS 876B	SOS 876B	SOS 876B	SOS 876B
Espectro	67	68	72	73	89	90	91	92	93	108	109	110	111
SiO_2	38,0	38,2	38,1	38,2	38,4	39,0	38,1	38,3	38,4	38,8	38,4	38,4	38,5
TiO_2	3,9	3,5	3,2	3,2	3,6	3,6	3,8	3,6	3,4	3,3	3,3	2,9	2,9
Al_2O_3	15,9	16,3	15,6	15,5	15,9	15,7	15,8	15,5	16,4	17,2	16,7	16,5	16,3
FeO	16,2	16,0	16,6	18,0	15,5	14,7	15,3	16,1	16,5	15,1	15,5	17,1	16,6
MnO	0,1	0,1	0,2	0,2	0,1	0,1	0,1	0,2	0,1	0,1	0,1	0,2	0,1
MgO	11,9	12,0	12,4	10,9	12,4	12,9	13,3	12,7	12,3	12,1	12,6	11,2	11,4
Na_2O													
K_2O	9,7	9,8	9,5	9,4	9,7	9,6	9,1	9,5	8,6	9,3	9,4	9,6	9,5
F	0,2	0,1	0,4	0,6	0,3	0,4	0,4			0,1			0,6
Cl	0,1		0,1	0,2	0,1	0,1	0,1						0,1
H_2O*	3,9	4,0	3,8	3,6	3,9	3,8	3,8	4,0	4,1	4,0	4,1	4,0	3,7
Subtotal	100,0	100,0	99,8	99,9	99,9	99,9	100,0	99,9	99,8	99,9	100,0	99,9	99,7
O=F,Cl	0,107	0,042	0,191	0,298	0,149	0,191	0,191			0,042			0,275
Total	99,9	100,0	99,6	99,6	99,7	99,7	99,8	99,9	99,8	99,9	100,0	99,9	99,5
Si	5,662	5,676	5,702	5,754	5,704	5,763	5,644	5,693	5,685	5,707	5,670	5,722	5,752
Al^{iv}	2,338	2,324	2,298	2,246	2,296	2,237	2,356	2,307	2,315	2,293	2,330	2,278	2,248
	8,000	8,000	8,000	8,000	8,000	8,000	8,000	8,000	8,000	8,000	8,000	8,000	8,000
Al^{vi}	0,460	0,534	0,444	0,498	0,494	0,507	0,409	0,401	0,550	0,687	0,577	0,622	0,626
Ti	0,441	0,386	0,356	0,359	0,408	0,395	0,428	0,408	0,374	0,361	0,362	0,323	0,324
Fe^{3+}			0,006										
Fe^{2+}	2,007	1,980	2,062	2,258	1,906	1,801	1,877	1,993	2,024	1,835	1,895	2,115	2,059
Mn	0,012	0,012	0,024	0,024	0,012	0,012	0,012	0,024	0,012	0,012	0,012	0,024	0,012
Mg	2,643	2,657	2,762	2,457	2,742	2,835	2,946	2,808	2,712	2,653	2,768	2,495	2,545
	5,563	5,569	5,655	5,596	5,562	5,550	5,672	5,633	5,672	5,548	5,614	5,579	5,566
Na													
K	1,842	1,855	1,814	1,807	1,837	1,810	1,723	1,802	1,632	1,748	1,772	1,825	1,811
	1,842	1,855	1,814	1,807	1,837	1,810	1,723	1,802	1,632	1,748	1,772	1,825	1,811
OH*	3,881	3,953	3,785	3,663	3,834	3,788	3,788	4,000	4,000	3,953	4,000	4,000	3,691
F	0,094	0,047	0,189	0,286	0,141	0,187	0,187			0,047			0,284
Cl	0,025		0,025	0,051	0,025	0,025	0,025						0,025
	4,000	4,000	4,000	4,000	4,000	4,000	4,000	4,000	4,000	4,000	4,000	4,000	4,000
TOTAL	19,405	19,424	19,468	19,403	19,399	19,360	19,394	19,435	19,304	19,296	19,386	19,403	19,377

Apêndice C.2. Análises químicas pontuais de cristais de biotita do Batólito Rio Jacaré (continuação).

Rocha	SOS 876B	SOS 876B	SOS 876B	SOS 876B	SOS 876B	SOS 876B	SOS 876B	SOS 876B	SOS 876B	SOS 876B	SOS 876B	SOS 876B	SOS 876B
Espectro	112	113	114	115	116	1	2	3	6	7	8	9	10
SiO_2	37,3	37,9	38,3	38,3	38,0	38,5	38,8	38,6	38,7	38,5	39,0	38,8	39,3
TiO_2	3,5	3,8	3,6	2,9	3,6	2,4	2,4	2,5	1,7	1,7	1,5	1,9	1,8
Al_2O_3	16,3	16,1	16,2	17,3	15,8	16,5	16,4	16,3	16,7	16,6	16,5	16,3	16,7
FeO	15,8	15,9	15,6	16,4	15,6	15,8	15,0	15,7	15,6	15,6	15,3	15,5	15,1
MnO	0,1	0,2		0,1	0,2	0,2	0,3	0,1	0,1	0,1	0,2	0,2	0,0
MgO	12,5	12,1	12,5	11,6	12,9	13,1	13,2	13,2	13,3	13,3	13,6	13,2	13,3
Na_2O													
K_2O	9,8	9,7	9,7	9,2	9,7	9,5	9,6	9,3	9,4	9,5	9,5	9,4	9,7
F	0,6	0,1			0,1		0,3	0,2	0,3	0,5	0,3	0,6	0,1
Cl		0,1			0,1		0,1		0,1	0,1	0,1	0,1	
H_2O*	3,7	4,0	4,0	4,0	4,0	4,1	3,9	4,0	3,9	3,8	3,9	3,7	4,0
Subtotal	99,6	100,0	100,0	99,9	100,0	100,1	100,0	100,0	99,8	99,8	99,9	99,8	100,0
O=F,Cl	0,253	0,065			0,065		0,149	0,084	0,149	0,233	0,149	0,275	0,042
Total	99,4	99,9	100,0	99,9	99,9	100,1	99,9	99,9	99,7	99,6	99,8	99,5	100,0
Si	5,592	5,643	5,672	5,675	5,649	5,694	5,733	5,709	5,732	5,719	5,764	5,759	5,779
Al^{iv}	2,408	2,357	2,328	2,325	2,351	2,306	2,267	2,291	2,268	2,281	2,236	2,241	2,221
	8,000	8,000	8,000	8,000	8,000	8,000	8,000	8,000	8,000	8,000	8,000	8,000	8,000
Al^{vi}	0,473	0,472	0,503	0,692	0,423	0,573	0,593	0,554	0,649	0,628	0,642	0,616	0,676
Ti	0,389	0,430	0,406	0,321	0,408	0,267	0,267	0,278	0,193	0,193	0,171	0,214	0,202
Fe^{3+}	0,002					0,059	0,007	0,056	0,093	0,113	0,105	0,061	0,004
Fe^{2+}	1,975	1,971	1,913	2,017	1,924	1,891	1,836	1,880	1,824	1,822	1,774	1,849	1,843
Mn	0,012	0,024		0,012	0,024	0,024	0,036	0,012	0,012	0,012	0,024	0,024	
Mg	2,786	2,683	2,755	2,565	2,849	2,879	2,919	2,921	2,947	2,955	3,005	2,933	2,928
	5,637	5,580	5,578	5,607	5,628	5,693	5,657	5,701	5,718	5,723	5,720	5,697	5,653
Na													
K	1,870	1,840	1,831	1,742	1,838	1,793	1,810	1,757	1,778	1,801	1,793	1,782	1,820
	1,870	1,840	1,831	1,742	1,838	1,793	1,810	1,757	1,778	1,801	1,793	1,782	1,820
OH*	3,716	3,928	4,000	4,000	3,928	4,000	3,835	3,906	3,834	3,740	3,835	3,693	3,953
F	0,284	0,047			0,047		0,140	0,094	0,141	0,235	0,140	0,282	0,047
Cl		0,025			0,025		0,025		0,025	0,025	0,025	0,025	
	4,000	4,000	4,000	4,000	4,000	4,000	4,000	4,000	4,000	4,000	4,000	4,000	4,000
TOTAL	19,507	19,421	19,409	19,349	19,466	19,486	19,467	19,458	19,495	19,524	19,513	19,479	19,473

Apêndice C.2. Análises químicas pontuais de cristais de biotita do Batólito Rio Jacaré (continuação).

Rocha	SOS 876B	SOS 876B	SOS 876B	SOS 876B	SOS 876B	SOS 876B	SOS 876B	SOS 876B	SOS 876B	SOS 876B	SOS 876B
Espectro	11	12	13	14	15	16	42	43	44	46	47
SiO_2	38,5	38,8	38,8	38,9	38,9	39,2	38,2	38,2	38,4	38,4	38,2
TiO_2	1,9	1,8	2,4	2,4	2,4	2,1	3,4	3,5	2,9	3,5	3,3
Al_2O_3	16,5	16,4	16,2	16,5	16,6	16,5	16,8	16,8	17,2	16,8	16,5
FeO	15,2	15,2	16,2	15,5	15,2	15,2	15,9	16,0	15,7	15,4	14,6
MnO	0,2	0,3	0,1	0,2	0,3	0,2	0,1	0,2	0,2	0,1	0,2
MgO	13,5	13,4	12,8	13,0	13,1	13,1	11,7	11,7	12,6	12,5	13,1
Na_2O											
K_2O	9,6	9,5	9,4	9,5	9,3	9,4	9,6	9,5	9,0	9,4	9,6
F	0,5	0,5		0,1	0,2	0,3	0,3				0,4
Cl	0,1	0,1		0,1	0,1	0,1					0,1
H_2O*	3,8	3,8	4,0	4,0	3,9	3,9	3,9	4,0	4,1	4,1	3,8
Subtotal	99,8	99,8	100,0	100,1	100,0	99,9	99,9	99,9	100,1	100,1	99,8
O=F,Cl	0,233	0,233		0,065	0,107	0,149	0,126				0,191
Total	99,6	99,6	100,0	100,0	99,8	99,8	99,8	99,9	100,1	100,1	99,6
Si	5,714	5,751	5,744	5,739	5,738	5,783	5,673	5,664	5,657	5,661	5,662
Al ^{iv}	2,286	2,249	2,256	2,261	2,262	2,217	2,327	2,336	2,343	2,339	2,338
	8,000	8,000	8,000	8,000	8,000	8,000	8,000	8,000	8,000	8,000	8,000
Al ^{vi}	0,603	0,620	0,576	0,612	0,627	0,656	0,614	0,599	0,640	0,580	0,545
Ti	0,214	0,203	0,267	0,266	0,266	0,234	0,375	0,385	0,319	0,383	0,364
Fe^{3+}	0,099	0,078	0,020								
Fe^{2+}	1,776	1,794	1,979	1,898	1,861	1,861	1,963	1,971	1,924	1,878	1,798
Mn	0,024	0,036	0,012	0,024	0,036	0,024	0,012	0,024	0,024	0,012	0,024
Mg	2,995	2,971	2,819	2,852	2,872	2,873	2,592	2,588	2,762	2,743	2,884
	5,710	5,703	5,673	5,653	5,663	5,649	5,557	5,568	5,669	5,596	5,615
Na											
K	1,817	1,798	1,777	1,790	1,753	1,772	1,818	1,797	1,696	1,769	1,814
	1,817	1,798	1,777	1,790	1,753	1,772	1,818	1,797	1,696	1,769	1,814
OH*	3,740	3,740	4,000	3,928	3,882	3,835	3,859	4,000	4,000	4,000	3,787
F	0,235	0,234		0,047	0,093	0,140	0,141				0,187
Cl	0,025	0,025		0,025	0,025	0,025					0,025
	4,000	4,000	4,000	4,000	4,000	4,000	4,000	4,000	4,000	4,000	4,000
TOTAL	19,528	19,500	19,450	19,442	19,416	19,421	19,375	19,365	19,365	19,366	19,429

Apêndice C.3. Análises químicas de elementos maiores e menores dos enclaves microgranulares do Batólito Rio Jacaré. LOI: perda ao fogo.

%	SOS 850B	SOS 876B	SOS 867B	SOS 860E	SOS 853B	SOS 849B	SOS 861B	SOS 871B	SOS 861S	SOS 844B	SOS 861M	SOS 853D	SOS 861L	SOS 853I	SOS 861O	SOS 853C	SOS 853G	SOS 861Q	SOS 861P	SOS 860D	SOS 860B	SOS 860C	SOS 853M	SOS 861R
SiO_2	48,09	53,99	55,04	55,39	55,52	55,55	55,88	56,56	56,86	57,23	58,19	58,33	58,34	58,49	58,62	58,63	58,65	58,72	58,72	58,74	58,79	58,89	58,93	59,16
TiO_2	1,92	1,29	0,82	0,88	0,56	1,34	0,54	0,61	0,65	0,83	0,72	1,04	0,69	1,35	0,69	0,89	0,92	0,70	0,71	0,73	1,08	0,63	0,56	0,68
Al_2O_3	16,69	15,23	15,08	15,49	14,04	15,13	13,83	13,61	14,19	14,35	15,01	15,16	15,50	16,51	15,22	15,82	16,13	14,85	15,08	15,15	15,26	14,73	14,49	15,14
Fe_2O_3	12,22	9,74	8,61	8,56	8,80	8,99	8,16	9,55	7,00	8,59	6,97	7,27	6,14	5,50	6,92	5,80	5,98	6,77	6,78	6,67	6,92	7,11	7,81	5,90
MnO	0,14	0,12	0,12	0,10	0,14	0,14	0,15	0,13	0,13	0,18	0,10	0,11	0,08	0,08	0,09	0,07	0,06	0,10	0,10	0,08	0,11	0,10	0,13	0,08
MgO	5,22	5,82	4,80	5,05	7,17	4,77	4,50	6,84	4,89	5,83	2,96	4,02	2,64	2,59	3,35	2,53	2,71	3,08	3,06	3,56	3,88	4,05	5,09	2,80
CaO	8,22	7,06	6,04	5,30	6,71	6,17	5,97	5,78	5,50	5,37	5,22	5,25	4,70	3,96	4,76	3,93	3,73	4,99	4,95	4,69	4,91	4,84	5,37	4,53
Na_2O	3,59	3,60	3,79	3,93	3,55	4,57	2,10	2,73	2,74	3,63	3,69	4,05	3,65	4,64	4,03	4,46	4,34	3,65	3,74	3,84	4,06	3,61	4,39	3,43
K_2O	2,99	2,28	4,07	4,38	2,63	2,15	7,54	3,69	6,27	3,03	5,14	3,27	5,88	4,20	4,34	4,92	4,60	5,16	4,85	4,26	3,38	4,30	2,05	6,09
P_2O_5	1,08	0,55	0,70	0,85	0,33	0,37	0,67	0,25	0,72	0,36	0,74	0,62	0,79	1,16	0,67	1,14	1,03	0,71	0,71	0,66	0,71	0,62	0,33	0,66
LOI	0,31	0,77	0,72	0,87	0,86	0,62	0,66	0,93	0,76	0,48	0,71	0,59	0,88	0,84	0,60	0,63	0,83	0,88	0,93	0,73	0,82	0,50	0,65	0,92
Total	100,46	100,45	99,79	99,81	100,32	99,80	100,00	100,69	99,71	99,88	99,45	99,70	99,29	99,32	99,29	98,80	98,97	99,62	99,62	99,3	99,90	99,38	99,80	99,38

Apêndice C.3. Análises químicas de elementos maiores e menores dos enclaves microgranulares do Batólito Rio Jacaré. LOI: perda ao fogo.

%	SOS 861E	SOS 853N	SOS 861J	SOS 861N	SOS 861I	SOS 861F	SOS 861T	SOS 861G	SOS 853J	SOS 853E	SOS 861D	SOS 848B	SOS 860F	SOS 861C	SOS 853F
SiO_2	59,33	59,58	59,64	59,80	60,39	60,62	60,62	60,65	60,89	60,91	60,97	61,70	61,72	61,98	61,98
TiO_2	0,75	0,69	0,68	0,74	0,65	0,65	0,68	0,68	0,70	0,78	0,62	0,83	0,58	0,58	0,52
Al_2O_3	15,00	15,32	15,18	15,39	14,99	14,92	14,91	15,08	14,85	15,14	15,03	15,38	14,97	14,87	14,94
Fe_2O_3	6,73	6,94	6,53	6,36	6,11	6,30	6,03	6,31	6,27	5,80	6,31	6,16	5,67	5,87	6,11
MnO	0,09	0,08	0,09	0,09	0,08	0,09	0,07	0,08	0,09	0,08	0,08	0,08	0,07	0,09	0,09
MgO	3,60	3,61	3,05	3,15	2,86	3,30	2,74	3,19	3,46	2,68	3,37	3,08	2,80	3,07	3,22
CaO	4,35	4,94	4,10	3,91	4,10	4,16	4,08	3,73	4,30	3,59	4,23	4,69	3,70	3,69	4,52
Na_2O	3,65	4,30	3,90	3,80	3,81	3,72	4,10	3,65	4,20	4,11	4,06	4,19	3,86	3,75	4,55
K_2O	4,54	2,72	4,73	4,56	4,94	4,36	4,65	4,54	3,34	4,48	3,45	3,48	4,57	4,26	2,33
P_2O_5	0,66	0,50	0,71	0,71	0,65	0,53	0,70	0,69	0,58	0,89	0,52	0,56	0,55	0,44	0,40
LOI	0,73	0,49	0,67	0,70	0,69	0,75	0,76	0,77	0,58	0,74	0,83	0,45	0,61	0,57	0,75
Total	99,43	99,18	99,28	99,21	99,26	99,40	99,33	99,38	99,25	99,19	99,47	100,59	99,12	99,17	99,41

Apêndice C.4. Análises químicas de elementos traços de enclaves microgranulares do Batólito Rio Jacaré.

	SOS 850B	SOS 876B	SOS 867B	SOS 849B	SOS 844B	SOS 861M	SOS 853D	SOS 861P	SOS 861E	SOS 861T	SOS 848B	SOS 861C
Ba	1162	626	770	564	300	819	655	819	947	896	817	862
Rb	208,4	98,8	158,0	120,0	174,0	234,0	132,5	233,0	233,0	243,0	115,5	213,0
Sr	969	683	540	678	316	463	585	450	491	489	561	521
Zr	271	230	237	228	177	240	196	242	250	242	264	212
Nb	15,35	10,70	9,80	8,74	13,00	11,00	12,36	11,40	10,50	11,30	9,60	11,00
La	50.4	34.5	45.1	33.2	18.8	45.9	35.4	48.2	41.5	42.0	43.5	46.9
Ce	109.3	76.9	80.4	72.3	46.3	98.2	78.4	104.0	95.4	90.9	88.8	84.1
Pr	14.41	9.48	8.28	9.35	5.97	11.45	10.28	12.05	11.35	10.7	10.25	10.2
Nd	64.8	38.6	29.3	41.7	22.9	42.5	44.2	45.6	44.9	40.2	37.0	37.9
Sm	13.1	7.39	5.82	8.80	4.80	7.66	8.40	8.29	8.25	6.90	7.24	6.93
Eu	3.34	2.16	1.32	1.70	1.35	1.29	2.02	1.36	1.39	1.28	1.32	1.69
Gd	10.37	6.74	4.10	6.70	3.79	5.30	6.49	5.60	5.37	4.80	4.67	5.27
Tb	1.23	0.83	0.46	0.83	0.41	0.53	0.84	0.65	0.62	0.50	0.52	0.57
Dy	5.85	4.37	2.62	4.15	2.57	3.14	4.05	2.89	3.17	3.02	2.93	3.3
Ho	0.82	0.85	0.46	0.69	0.47	0.51	0.71	0.51	0.55	0.45	0.53	0.57
Er	2.12	2.16	1.32	2.01	1.35	1.29	1.95	1.36	1.39	1.28	1.32	1.69
Tm	0,24	0,27	0,18	0,28	0,21	0,18	0,27	0,19	0,20	0,16	0,21	0,22
Yb	1,50	1,70	0,99	1,70	1,38	0,92	1,70	1,01	1,11	1,13	1,03	1,32
Lu	0,20	0,29	0,19	0,23	0,23	0,19	0,26	0,18	0,17	0,17	0,19	0,20
Y	24,23	20,30	11,20	19,84	13,20	13,30	21,30	13,40	13,40	12,70	13,00	14,80
Cs	25,00	5,82	7,30	10,36	13,15	13,40	6,71	15,15	17,00	18,65	4,74	14,15
Ta	0,71	0,90	0,70	0,44	0,90	0,90	0,92	0,80	0,70	1,00	0,80	0,90
Hf	7,96	5,80	6,10	6,55	5,50	6,00	5,88	6,40	6,20	6,00	6,70	5,60
Ga	31,9	23,7	23,6	27,1	29,7	24,8	27,1	25	24	25,3	24,2	25,1
Sn	8,4	4,0	6,0	4,1	9,0	5,0	1,1	5,0	4,0	4,0	4,0	4,0
Th	8,40	5,66	9,86	4,60	5,81	10,80	8,80	11,25	9,59	9,84	13,10	10,80
V	227	172	137	133	118	113	110	120	123	102	125	98
W	4,9	276,0	274,0	<0,1	4,0	720,0	<0,1	693,0	529,0	542,0	7,0	428,0
Eu/Eu*	0,88	0,82	0,48	0,68	0,65	0,81	0,84	0,81	0,81	0,87	0,77	0,76
$(La/Yb)_N$	22,40	9,61	30,37	13,02	9,08	33,26	13,88	31,82	24,92	24,78	28,16	23,69
$(La/Sm)_N$	2,37	2,04	4,77	2,32	2,41	3,69	2,59	3,58	3,09	3,74	3,70	4,16

ANEXO A – REGRAS DE FORMATAÇÃO DO "BRAZILIAN JOURNAL OF GEOLOGY"

Instructions to authors

Scope and Policy

Aims and scope

The Brazilian Journal of Geology (BJG) is a quarterly journal published by the Brazilian Geological Society with an electronic open access version that provides an internacional medium for the publication of original scientific work of broad interest concerned with all aspects of the earth sciences in Brazil, South America, and Antarctica, including oceanic regions adjacent to these regions. The BJG publishes papers with a regional appeal and more than local significance in the fields of mineralogy, petrology, geochemistry, paleontology, sedimentology, stratigraphy, structural geology, tectonics, neotectonics, geophysics applied to geology, volcanology, metallogeny and mineral deposits, marine geology, glaciology, paleoclimatology, geochronology, biostratigraphy, engineering geology, hydrogeology, geological hazards and remote sensing, providing a niche for interdisciplinary work on regional geology and Earth history.

The BJG publishes articles (including review articles), rapid communications, articles with accelerated review processes, editorials, and discussions (brief, objective and concise comments on recent papers published in BJG with replies by authors).

Manuscripts must be written in English. Companion papers will not be accepted.

Ethics in publishing

The BJG follows the Code of Good Scientific Practice published by the São Paulo State Research Foundation – FAPESP.

Funding sources

Authors should identify the sources of financial support for the research and/or preparation of the article and briefly describe the role of sponsor(s), if any, in study design; in the collection, analysis and interpretation of data; in the writing of the report; and in the decision to submit the article for publication.

Copyright and open access

Upon acceptance of an article, authors will be asked to complete a "BJG publishing agreement" transferring the copyright to the Brazilian Geological Society.

The BJG is an open access journal which means that all articles will be freely available to the wider public and that reuse will be permitted.

Conflicts of interests

All authors are requested to disclose any actual or potential conflict of interest including any financial, personal or other relationships with other people or organizations that could inappropriately influence, or be perceived to influence, their work.

Submission declaration and verification

Submission of an article implies that the work described has not been published previously (except in the form of an abstract or as part of a published lecture or academic thesis), that it is not under consideration for publication elsewhere, that its publication is approved by all authors as well as tacitly or explicitly by the responsible authorities where the work was carried out, and that, if accepted, it will not be published elsewhere in the same form, in English or in any other language, including electronically, without the written consent of the copyright-holder. Authors should verify the originality of the article by checking for plagiarism with any available software.

In addition, the corresponding author must state that:

- The article has not been partitioned and that its contents are fully and independently understandable;
- The article, edited in Microsoft Word, A4 format, does not exceed 12,000 words;
- Each illustration or table is being sent in a separate file (.tif for figures);
- No text or illustration file exceeds 10 Mb;
- The authors are aware that submissions that do not comply with the “Instructions to authors” for BJG will be returned to the corresponding author;
- The authors are aware that if reviewers indicate the need for major or minor revision, they will have 30 days to make the corrections suggested by the editors;
- The authors are aware that they should carefully check and correct print proofs and return them to publishers within 48 hours to ensure the publication of the article without errors;
- The authors are aware that, should the article be accepted for publication, copyright will be transferred to the Brazilian Geological Society by sending a letter signed by all authors (“BJG publishing agreement”).

Submission

Our online submission system (ScholarOne – SciELO) will guide you stepwise through the process of entering details on your article and uploading your files. The system will convert your article files to a single PDF file for use in the peer-review process. Editable fi- les (e.g., Word, LaTeX) are required to typeset your article for final publication. All correspondence, including notification of the Editor’s decision and requests for re- vision, will be sent by e-mail.

Evaluation

Peer review: Articles will be submitted to critical analysis by least two reviewers.

Type of evaluation: Authors will be identified in the manuscripts received by the Reviewers.

Form and preparation of manuscripts

Use of word processing software

Regardless of the file format of the original submission, at revision you must provide us with an editable file of the entire article. Keep the layout of the text as simple as possible. Most formatting codes will be removed and replaced on processing the article. The electronic text should be prepared in a way very similar to that of conventional manuscripts.

To avoid errors you are strongly advised to use the 'spell-check' and 'grammar-check' functions of your word processor.

Article structure

There are no strict formatting requirements, but all manuscripts must contain the essential elements needed to convey your manuscript, for example, Abstract, Keywords, Introduction, Materials and Methods, Results, Conclusions, References, Artwork and Tables with Captions.

Divide the article into clearly defined and numbered sections. Subsections should be numbered 1.1 (then 1.1.1, 1.1.2, ...), 1.2, etc. (the abstract is not included in section numbering). Use this numbering also for internal cross-referencing: do not just refer to 'the text'. Any subsection may be given a brief heading. Each heading should appear on its own separate line.

Introduction

State the objectives of the work and provide an adequate background, avoiding a detailed literature survey or a summary of the results.

Material and methods

Provide sufficient detail to allow the work to be re- produced. Methods already published should be indicated by a reference. Only relevant modifications should be described.

Theory/calculation

A Theory section should extend, not repeat, the back- ground to the article already dealt with in the Introduction and lay the foundation for further work. In contrast, a Calculation section represents a practical development from a theoretical basis.

Results

Results should be clear and concise.

Discussion

This should explore the significance of the results of the work, not repeat them. A combined Results and Discussion section is often appropriate. Avoid extensive citations and discussion of published literature.

Conclusions

The main conclusions of the study may be presented in a short Conclusions section, which may stand alone or form a subsection of a Discussion or Results and Discussion section.

Appendices

If there is more than one appendix, they should be identified as A, B, etc. Formulae and equations in appendices should be given separate numbering: Eq. (A.1), Eq. (A.2), etc.; in a subsequent appendix, Eq. (B.1) and so on. This also applies to tables and figures: Table A.1; Fig. A.1, etc.

Essential title page information

Title. Concise, informative, and interesting. Titles are often used in information-retrieval systems. Avoid abbreviations and formulae where possible.

Author names and affiliations. Please clearly indicate the given name(s) and family name(s) of each author and check that all names are accurately spelled. Present the authors' affiliation addresses (where the actual work was done) below the names. Indicate all affiliations with a lower-case superscript number immediately after the author's name and in front of the appropriate address. Provide the full postal address of each affiliation, including the country name and, if available, the e-mail address of each author.

Corresponding author. Clearly indicate who will handle correspondence at all stages of refereeing, publication, and post-publication. Ensure that the e-mail address is given and that contact details are kept up to date by the corresponding author.

Present/permanent address. If an author has moved since the work described in the article was done, or was visiting at the time, a 'Present address' (or 'Permanent address') may be indicated as a footnote to that author's name. The address at which the author actually did the work must be retained as the main, affiliation address. Superscript Arabic numerals are used for such footnotes.

Abstract

A concise and factual abstract is required. The abstract should state briefly the purpose of the research, the principal results and major conclusions. An abstract is often presented separately from the article, so it must be able to stand alone. For this reason, References should be avoided, but if essential, then cite the author(s) and year(s). Also, non-standard or uncommon abbreviations should be avoided, but if essential they must be defined at their first mention in the abstract itself.

Keywords

Immediately after the abstract, provide a maximum of 6 keywords, using American spelling and avoiding general and plural terms and multiple concepts (avoid, for example, 'and', 'of '). Be sparing with abbreviations: only abbreviations firmly established in the field may be eligible. These keywords will be used for indexing purposes.

Abbreviations

Define abbreviations that are not standard in this field in a footnote to be placed on the first page of the article. Such abbreviations that are unavoidable in the abstract must be de- fined at their first mention there, as well as in the footnote. Ensure consistency of abbreviations throughout the article.

Acknowledgements

Collate acknowledgements in a separate section at the end of the article before the references and do not, there- fore, include them on the title page, as a footnote to the title or otherwise. List here those individuals who provided help during the research (e.g., providing language help, writing assistance or proof reading the article, etc.), as well as institutions and funding agencies.

Units

Follow internationally accepted rules and conventions: use the international system of units (SI). If other units are mentioned, please give their equivalent in SI.

Math formulae

Please submit math equations as editable text and not as images. Present simple formulae in line with normal text where possible and use the solidus (/) instead of a horizontal line for small fractional terms, e.g., X/Y. In principle, variables are to be presented in italics. Powers of e are often more conveniently denoted by exp. Number consecutively any equations that have to be displayed separately from the text (if referred to explicitly in the text).

Electronic artwork

General points

- Make sure you use uniform lettering and sizing of your original artwork.
- Preferred fonts: Arial (or Helvetica), Times New Roman (or Times), Symbol, Courier.
- Number the illustrations according to their sequence in the text.
- Use a logical naming convention for your artwork files.
- For Word submissions only, you may provide figures, their captions, and tables within a single file at the revision stage.

Formats

Regardless of the application used, when your electronic artwork is finalized, please ‘save as’ or convert the images to one of the following formats (note the resolution requirements for line drawings, halftones, and line/halftone combinations given below):

- EPS (or PDF): Vector drawings. Embed the font or save the text as ‘graphics’.
- TIFF (or JPG): Color or grayscale photographs (half- tones): always use a minimum of 300 dpi.
- TIFF (or JPG): Bitmapped line drawings: use a mini- mum of 1000 dpi.
- TIFF (or JPG): Combined bitmapped line/half-tone (color or grayscale) images: a minimum of 500 dpi is required. Please do not:
- Supply files that are optimized for screen use (e.g., GIF, BMP, PICT, WPG); the resolution is too low.
- Supply files that are too low in resolution.
- Submit graphics that are disproportionately large for the content.

Color artwork

Please make sure that artwork files are in an acceptable format — TIFF (or JPEG), EPS (or PDF), or MS Office files — and with the correct resolution. If, together with your accepted article, you submit usable color figures, the- se will appear in color online.

Figure captions

Ensure that each illustration has a caption. A caption should comprise a brief title (not on the figure itself) and a description of the illustration. Keep text in the illustrations to a minimum, but be sure to explain all symbols and abbreviations used.

Tables

Please submit tables as editable text and not as images. Tables can be placed either next to the relevant text in the article, or on separate page(s) at the end. Number tables consecutively in accordance with their appearance in the text and place any table notes below the table body. Be sparing in the use of tables and ensure that the data presented in them do not duplicate results described elsewhere in the article. Please avoid using vertical rules.

Citation in text

Please ensure that every reference cited in the text is also present in the reference list (and vice versa). Any references cited in the abstract must be given in full. Unpublished results and personal communications are not recommended in the reference list, but may be mentioned in the text. If these references are included in the reference list they should follow the standard reference style of the journal and should include a substitution of the publication date with either 'Unpublished results' or 'Personal communication'. Citation of a reference as 'in press' implies that the item has been accepted for publication.

Web references

As a minimum, the full URL should be given and the date when the reference was last accessed. Any further in- formation, if known (DOI, author names, dates, reference to a source publication, etc.), should also be given. Web references can be listed separately (e.g., after the reference list) under a different heading if desired, or can be included in the reference list.

Reference formatting

There are no strict requirements on reference format- ting at submission. References can be in any style or format as long as the style is consistent. Where applicable, name(s) of author(s), journal title/book title, chapter title/article title, year of publication, volume number/book chapter and the pagination must be present. Use of DOI is highly encouraged. The reference style used by the journal will be applied to the accepted article by SCIELO at the proof stage. Note that missing data will be highlighted at proof stage for the author to correct.

Reference style

All publications cited in the text should be presented in a list of references following the text of the manuscript. In the text refer to the author's name (without initials) and year of publication (e.g. "Since Almeida (1986) has shown that..." or "This is in agreement with results obtained later (Trompette 1994; Heilbron and Machado 2003)."

For three or more authors use the first author followed by “et al.”, in the text. The list of references should be arranged alphabetically by authors’ names. The manuscript should be carefully checked to ensure that the spelling of authors’ names and dates are exactly the same in the text as in the reference list.

References should be given in the following form:

Papers in scientific journals

Almeida F.F.M. 1986. Distribuição regional e relações tectônicas do magmatismo pós-paleozóico no Brasil. Revista Brasileira de Geociências, 16:325-349.

Costa I.P., Bueno G.V., Milhomem P.S., Silva H.S.R.L., Kosin M.D. 2007. Sub-bacia de Tucano Norte e Bacia de Jatobá. Boletim de Geociências da Petrobras, 15:445-453.

Escayola M.P., Pimentel M.M., Armstrong R. 2007. Neoproterozoic backarc basin: sensitive high-resolution ion microprobe U-Pb and Sm-Nd isotopic evidence from the eastern Pampean Ranges, Argentina. Geology, 35:495-498.

Heilbron, M. and Machado, N. 2003, Timing of terrane accretion in the Neoproterozoic-Eopaleozoic Ribeira orogen (SE Brazil). Precambrian Research, 125:87-112.

Books and book chapters

Bedell R., Crósta A.P., Grunsky E. (eds.). 2009. Remote Sensing and Spectral Geology. Littleton, Society of Economic Geologists, 270 p.

Kaufman A.J., Sial A.N., Frimmel H.E., Misi A. 2009. Neoproterozoic to Cambrian palaeoclimatic events in southwestern Gondwana In: Gaucher C., Sial A.N., Frimmel H.E., Helverson G.P. (eds.). Neoproterozoic- Cambrian tectonics, global change and evolution: a focus on southwestern Gondwana. Developments in Precambrian Geology, 16, Amsterdam, Elsevier, p. 369-388.

Pankhurst R.J. & Rapela C.W. (eds.). 1998. The Proto- Andean margin of Gondwana. London, Geological Society of London Special Publication, 142, 382 p.

Trompette R. 1994. Geology of western Gondwana (2000–500 Ma). Rotterdam, Balkema, 350 p.

Papers in scientific meetings

Astini R., Ramos V.A., Benedetto J.L., Vaccari N.E., Cañas F.L. 1996. La Precordillera: un terreno exótico a Gondwana. In: 13°Congreso Geológico Argentino y 3° Congreso Exploración de Hidrocarburos. Buenos Aires, Actas, v. 5, p. 293-324.

Leite-Junior W.B, Bettencourt J.S., Payolla B.L. 2003. Evidence for multiple sources inferred from Sr and Nd isotopic data from felsic rocks in the Santa Clara Intrusive Suite, Rondonia, Brazil. In: SSAGI, South American Symposium on Isotope Geology. Salvador, Short Papers, p. 583-585.

Milani E.J. & Thomaz-Filho A. 2000. Sedimentary basins of South América. In: Cordani U.G., Milani E.J., Thomaz- Filho A., Campos D.A. (eds.). Tectonic evolution of South America. 31st International Geological Congress. Rio de Janeiro, p. 389-452.

Thesis and dissertations

Paes V.J.C. 1999. Geologia da quadrícula Alvarenga, MG, e a geoquímica: implicações geotectônicas e metalogenéticas. MS Dissertation, Instituto de Geociências, Universidade Federal de Minas Gerais, Belo Horizonte, 144 p.

Ávila C.A. 2000. Geologia, petrografia e geocronologia de corpos plutônicos paleoproterozóicos da borda meridional do Cráton São Francisco, região de São João Del Rei, Minas Gerais. PhD Thesis, Universidade Federal do Rio de Janeiro, Rio de Janeiro, 401 p.

Printed maps

Inda H.A.V. & Barbosa J.F. 1978. Mapa geológico do Estado da Bahia, escala 1:1.000.000. Salvador, Secretaria das Minas e Energia, Coordenação da Produção Mineral. Mascarenhas J.F. & Garcia T.M. 1989. Mapa geocronológico do Estado da Bahia, escala 1:1.000.000. Texto explicativo. Salvador, Secretaria das Minas e Energia, Coordenação da Produção Mineral, 186 p.

Schobbenhaus C. (coord.). 1975. Carta Geológica do Brasil ao Milionésimo – Folha Goiás (SD 22). Texto explicativo. Brasília, Departamento Nacional da Produção Mineral, 114 p.

Internal reports

Internal reports will not be accepted, unless of open access for the scientific community and authorized by ad hoc consultants.

Submission checklist

The following list will be useful during the final checking of an article prior to sending it to the journal for review. Please consult this Guide for Authors for further details of any item.

Ensure that the following items are present:

One author has been designated as the corresponding author with contact details:

- E-mail address
- Full postal address

All necessary files have been uploaded, and contain:

- Keywords
- All figure captions
- All tables (including title, description, footnotes)

Further considerations:

- Manuscript has been ‘spell-checked’ and ‘grammar-checked’.
- All references mentioned in the Reference list are cited in the text, and vice versa.
- Permission has been obtained for use of copyrighted material from other sources (including the Internet).

Rapid communications

Rapid communications are limited to 2000 words, including references. Summary and abstract are limited to 100 words. At the discretion of the editors, these communications may be scheduled for the first available edition.

Articles with accelerated review process

An accelerated review process may be requested for complete original studies, for which urgency of publication is adequately justified. At the discretion of the editors, these can be programmed for the first available edition. They must follow the same format described for original articles.

Editorials

Editorials should cover some aspect of the broad spectrum of the Geological Sciences. They will be authored by the editors of BJG, by people linked to the Brazilian Geological Society or by industry personalities. These documents will not be submitted to peer review and will be published at the discretion of the editors.

Review articles

Review articles should cover relevant topics of Geology. These articles may be requested by the editors, but recognized experts may spontaneously submit review articles in their field of expertise. In this case, potential authors should contact the editors to ascertain their interest prior to submitting the article

Manuscript submission

The submission of manuscripts must only be performed online at http://mc04.manuscriptcentral.com/bjgeo-scielo

There are no fees for submission and evaluation of articles.

ANEXO B – REGRAS DE FORMATAÇÃO DO "JOURNAL OF SOUTH AMERICAN EARTH SCIENCES"

GUIDE FOR AUTHORS

Your Paper Your Way

We now differentiate between the requirements for new and revised submissions. You may choose to submit your manuscript as a single Word or PDF file to be used in the refereeing process. Only when your paper is at the revision stage, will you be requested to put your paper in to a 'correct format' for acceptance and provide the items required for the publication of your article.

To find out more, please visit the Preparation section below.

You can use this list to carry out a final check of your submission before you send it to the journal for review. Please check the relevant section in this Guide for Authors for more details.

Ensure that the following items are present:

One author has been designated as the corresponding author with contact details:

• E-mail address

• Full postal address

All necessary files have been uploaded:

Manuscript:

• Include keywords

• All figures (include relevant captions)

• All tables (including titles, description, footnotes)

• Ensure all figure and table citations in the text match the files provided

• Indicate clearly if color should be used for any figures in print

Graphical Abstracts / Highlights files (where applicable)

Supplemental files (where applicable)

Cover Letter:

• How does your paper fit within the scope of the Journal of South American Earth Sciences according to the aims and scope listed on the journal homepage?

• If there are other papers, already published, in review, or in press from any of the authors whose content may overlap with the current submission, the letter must explain how the contents of those other papers and this submission differ.

Further considerations

• Manuscript has been 'spell checked' and 'grammar checked'

• All references mentioned in the Reference List are cited in the text, and vice versa

• Permission has been obtained for use of copyrighted material from other sources (including the Internet)

• A competing interests statement is provided, even if the authors have no competing interests to declare

• Journal policies detailed in this guide have been reviewed

• Referee suggestions and contact details provided, based on journal requirements

For further information, visit our Support Center.

BEFORE YOU BEGIN

Ethics in publishing

Please see our information on Ethics in publishing.

Declaration of competing interest

Corresponding authors, on behalf of all the authors of a submission, must disclose any financial and personal relationships with other people or organizations that could inappropriately influence (bias) their work. Examples of potential conflicts of interest include employment, consultancies, stock ownership, honoraria, paid expert testimony, patent applications/registrations, and grants or other funding. All authors, including those without competing interests to declare, should provide the relevant information to the corresponding author (which, where relevant, may specify they have nothing to declare). Corresponding authors should then use this tool to create a shared statement and upload to the submission system at the Attach Files step. Please do not convert the .docx template to another file type. Author signatures are not required.

Submission declaration and verification

Submission of an article implies that the work described has not been published previously (except in the form of an abstract, a published lecture or academic thesis, see 'Multiple, redundant or concurrent publication' for more information), that it is not under consideration for publication elsewhere, that its publication is approved by all authors and tacitly or explicitly by the responsible authorities where the work was carried out, and that, if accepted, it will not be published elsewhere in the same form, in English or in any other language, including electronically without the written consent of the copyright holder. To verify originality, your article may be checked by the originality detection service Crossref Similarity Check.

Preprints

Please note that preprints can be shared anywhere at any time, in line with Elsevier's sharing policy. Sharing your preprints e.g. on a preprint server will not count as prior publication (see 'Multiple, redundant or concurrent publication' for more information).

Preprint posting on SSRN

In support of Open Science, this journal offers its authors a free preprint posting service. Preprints provide early registration and dissemination of your research, which facilitates early citations and collaboration.

During submission to Editorial Manager, you can choose to release your manuscript publicly as a preprint on the preprint server SSRN once it enters peer-review with the journal. Your choice will have no effect on the editorial process or outcome with the journal. Please note that the corresponding author is expected to seek approval from all co-authors before agreeing to release the manuscript publicly on SSRN.

You will be notified via email when your preprint is posted online and a Digital Object Identifier (DOI) is assigned. Your preprint will remain globally available free to read whether the journal accepts or rejects your manuscript.

For more information about posting to SSRN, please consult the SSRN Terms of Use and FAQs.

Use of inclusive language

Inclusive language acknowledges diversity, conveys respect to all people, is sensitive to differences, and promotes equal opportunities. Content should make no assumptions about the beliefs or commitments of any reader; contain nothing which might imply that one individual is superior to another on the grounds of age, gender, race, ethnicity, culture, sexual orientation, disability or health condition; and use inclusive language throughout. Authors should ensure that writing is free from bias, stereotypes, slang, reference to dominant culture and/or cultural assumptions. We advise to seek gender neutrality by using plural nouns ("clinicians, patients/clients") as default/wherever possible to avoid using "he, she," or "he/she." We recommend avoiding the use of descriptors that refer to personal attributes such as age, gender, race, ethnicity, culture, sexual orientation, disability or health condition unless they are relevant and valid. When coding terminology is used, we recommend to avoid offensive or exclusionary terms such as "master", "slave", "blacklist" and "whitelist". We suggest using alternatives that are more appropriate and (self-) explanatory such as "primary", "secondary", "blocklist" and "allowlist". These guidelines are meant as a point of reference to help identify appropriate language but are by no means exhaustive or definitive.

Author contributions

For transparency, we encourage authors to submit an author statement file outlining their individual contributions to the paper using the relevant CRediT roles: Conceptualization; Data curation; Formal analysis; Funding acquisition; Investigation; Methodology; Project administration; Resources; Software; Supervision; Validation; Visualization; Roles/Writing - original draft; Writing - review & editing. Authorship statements should be formatted with the names of authors first and CRediT role(s) following. More details and an example.

Changes to authorship

Authors are expected to consider carefully the list and order of authors before submitting their manuscript and provide the definitive list of authors at the time of the original submission. Any addition, deletion or rearrangement of author names in the authorship list should be made only before the manuscript has been accepted and only if approved by the journal Editor. To request such a change, the Editor must receive the following from the corresponding author: (a) the reason for the change in author list and (b) written confirmation (e-mail, letter) from all authors that they agree with the addition, removal or rearrangement. In the case of addition or removal of authors, this includes confirmation from the author being added or removed.

Only in exceptional circumstances will the Editor consider the addition, deletion or rearrangement of authors after the manuscript has been accepted. While the Editor considers the request, publication of the manuscript will be suspended. If the manuscript has already been published in an online issue, any requests approved by the Editor will result in a corrigendum.

Article transfer service

This journal is part of our Article Transfer Service. This means that if the Editor feels your article is more suitable in one of our other participating journals, then you may be asked to consider transferring the article to one of those. If you agree, your article will be transferred automatically on your behalf with no need to reformat. Please note that your article will be reviewed again by the new journal. More information.

Copyright

Upon acceptance of an article, authors will be asked to complete a 'Journal Publishing Agreement' (see more information on this). An e-mail will be sent to the corresponding author confirming receipt of the manuscript together with a 'Journal Publishing Agreement' form or a link to the online version of this agreement.

Subscribers may reproduce tables of contents or prepare lists of articles including abstracts for internal circulation within their institutions. Permission of the Publisher is required for resale or distribution outside the institution and for all other derivative works, including compilations and translations. If excerpts from other copyrighted works are included, the author(s) must obtain written permission from the copyright owners and credit the source(s) in the article. Elsevier has preprinted forms for use by authors in these cases.

For gold open access articles: Upon acceptance of an article, authors will be asked to complete a 'License Agreement' (more information). Permitted third party reuse of gold open access articles is determined by the author's choice of user license.

Author rights

As an author you (or your employer or institution) have certain rights to reuse your work. More information.

Elsevier supports responsible sharing

Find out how you can share your research published in Elsevier journals.

Role of the funding source

You are requested to identify who provided financial support for the conduct of the research and/or preparation of the article and to briefly describe the role of the sponsor(s), if any, in study design; in the collection, analysis and interpretation of data; in the writing of the report; and in the decision to submit the article for publication. If the funding source(s) had no such involvement, it is recommended to state this.

Open access

Please visit our Open Access page for more information.

Elsevier Researcher Academy

Researcher Academy is a free e-learning platform designed to support early and mid-career researchers throughout their research journey. The "Learn" environment at Researcher Academy offers several interactive modules, webinars, downloadable guides and resources to guide you through the process of writing for research and going through peer review. Feel free to use these free resources to improve your submission and navigate the publication process with ease.

Language (usage and editing services)

Please write your text in good English (American or British usage is accepted, but not a mixture of these). Authors who feel their English language manuscript may require editing to eliminate possible grammatical or spelling errors and to conform to correct scientific English may wish to use the English Language Editing service available from Elsevier's Author Services.

Submission

Our online submission system guides you stepwise through the process of entering your article details and uploading your files. The system converts your article files to a single PDF file used in the peer-review process. Editable files (e.g., Word, LaTeX) are required to typeset your article for final publication. All correspondence, including notification of the Editor's decision and requests for revision, is sent by e-mail.

Submit your article

Please submit your article via https://www.editorialmanager.com/sames/default.aspx

PREPARATION

Queries

For questions about the editorial process (including the status of manuscripts under review) or for technical support on submissions, please visit our Support Center.

NEW SUBMISSIONS

Submission to this journal proceeds totally online and you will be guided stepwise through the creation and uploading of your files. The system automatically converts your files to a single PDF file, which is used in the peer-review process.

As part of the Your Paper Your Way service, you may choose to submit your manuscript as a single file to be used in the refereeing process. This can be a PDF file or a Word document, in any format or layout that can be used by referees to evaluate your manuscript. It should contain high enough quality figures for refereeing. If you prefer to do so, you may still provide all or some of the source files at the initial submission. Please note that individual figure files larger than 10 MB must be uploaded separately.

References

There are no strict requirements on reference formatting at submission. References can be in any style or format as long as the style is consistent. Where applicable, author(s) name(s), journal title/book title, chapter title/article title, year of publication, volume number/book chapter and the article number or pagination must be present. Use of DOI is highly encouraged. The reference style used by the journal will be applied to the accepted article by Elsevier at the proof stage. Note that missing data will be highlighted at proof stage for the author to correct.

Formatting requirements

There are no strict formatting requirements but all manuscripts must contain the essential elements needed to convey your manuscript, for example Abstract, Keywords, Introduction, Materials and Methods, Results, Conclusions, Artwork and Tables with Captions.

If your article includes any Videos and/or other Supplementary material, this should be included in your initial submission for peer review purposes.

Divide the article into clearly defined sections.

Figures and tables embedded in text

Please ensure the figures and the tables included in the single file are placed next to the relevant text in the manuscript, rather than at the bottom or the top of the file. The corresponding caption should be placed directly below the figure or table.

Peer review

This journal operates a single anonymized review process. All contributions will be initially assessed by the editor for suitability for the journal. Papers deemed suitable are then typically sent to a minimum of two independent expert reviewers to assess the scientific quality of the paper. The Editor is responsible for the final decision regarding acceptance or rejection of articles. The Editor's decision is final. Editors are not involved in decisions about papers which they have written themselves or have been written by family members or colleagues or which relate to products or services in which the editor has an interest. Any such submission is subject to all of the journal's usual procedures, with peer review handled independently of the relevant editor and their research groups. More information on types of peer review.

REVISED SUBMISSIONS

Use of word processing software

Regardless of the file format of the original submission, at revision you must provide us with an editable file of the entire article. Keep the layout of the text as simple as possible. Most formatting codes will be removed and replaced on processing the article. The electronic text should be prepared in a way very similar to that of conventional manuscripts (see also the Guide to Publishing with Elsevier). See also the section on Electronic artwork.

To avoid unnecessary errors you are strongly advised to use the 'spell-check' and 'grammar-check' functions of your word processor.

LaTeX

You are recommended to use the Elsevier article class elsarticle.cls to prepare your manuscript and BibTeX to generate your bibliography.

Our LaTeX site has detailed submission instructions, templates and other information.

Article structure

Subdivision - numbered sections

Divide your article into clearly defined and numbered sections. Subsections should be numbered 1.1 (then 1.1.1, 1.1.2, ...), 1.2, etc. (the abstract is not included in section numbering). Use this numbering also for internal cross-referencing: do not just refer to 'the text'. Any subsection may be given a brief heading. Each heading should appear on its own separate line.

Introduction

State the objectives of the work and provide an adequate background, avoiding a detailed literature survey or a summary of the results.

Material and methods

Provide sufficient details to allow the work to be reproduced by an independent researcher. Methods that are already published should be summarized, and indicated by a reference. If quoting directly from a previously published method, use quotation marks and also cite the source. Any modifications to existing methods should also be described.

Theory/calculation

A Theory section should extend, not repeat, the background to the article already dealt with in the Introduction and lay the foundation for further work. In contrast, a Calculation section represents a practical development from a theoretical basis.

Results

Results should be clear and concise.

Discussion

This should explore the significance of the results of the work, not repeat them. A combined Results and Discussion section is often appropriate. Avoid extensive citations and discussion of published literature.

Conclusions

The main conclusions of the study may be presented in a short Conclusions section, which may stand alone or form a subsection of a Discussion or Results and Discussion section.

Data Availability

Authors are encouraged to include a 'Data Availability' section in their manuscript which is visible in ALL reading formats and may refer to data hosted in ANY repository. It should be placed before the references to provide readers with information about where they can obtain the research data required to reproduce the work reported in the manuscript, and typically consists of a simple sentence giving the URL(s) of and citation(s) to the dataset(s). Full information can be found here.

Appendices

If there is more than one appendix, they should be identified as A, B, etc. Formulae and equations in appendices should be given separate numbering: Eq. (A.1), Eq. (A.2), etc.; in a subsequent appendix, Eq. (B.1) and so on. Similarly for tables and figures: Table A.1; Fig. A.1, etc.

Essential title page information

• Title. Concise and informative. Titles are often used in information-retrieval systems. Avoid abbreviations and formulae where possible.

• Author names and affiliations. Please clearly indicate the given name(s) and family name(s) of each author and check that all names are accurately spelled. You can add your name between parentheses in your own script behind the English transliteration. Present the authors' affiliation addresses (where the actual work was done) below the names. Indicate all affiliations with a lowercase superscript letter immediately after the author's name and in front of the appropriate address. Provide the full postal address of each affiliation, including the country name and, if available, the e-mail address of each author.

• Corresponding author. Clearly indicate who will handle correspondence at all stages of refereeing and publication, also post-publication. This responsibility includes answering any future queries about Methodology and Materials. Ensure that the e-mail address is given and that contact details are kept up to date by the corresponding author.

• Present/permanent address. If an author has moved since the work described in the article was done, or was visiting at the time, a 'Present address' (or 'Permanent address') may be indicated as a footnote to that author's name. The address at which the author actually did the work must be retained as the main, affiliation address. Superscript Arabic numerals are used for such footnotes.

Highlights

Highlights are mandatory for this journal as they help increase the discoverability of your article via search engines. They consist of a short collection of bullet points that capture the novel results of your research as well as new methods that were used during the study (if any). Please have a look at the examples here: example Highlights.

Highlights should be submitted in a separate editable file in the online submission system. Please use 'Highlights' in the file name and include 3 to 5 bullet points (maximum 85 characters, including spaces, per bullet point).

Abstract

A concise and factual abstract is required. The abstract should state briefly the purpose of the research, the principal results and major conclusions. An abstract is often presented separately from the article, so it must be able to stand alone. For this reason, References should be avoided, but if essential, then cite the author(s) and year(s). Also, non-standard or uncommon abbreviations should be avoided, but if essential they must be defined at their first mention in the abstract itself.

Graphical abstract

Although a graphical abstract is optional, its use is encouraged as it draws more attention to the online article. The graphical abstract should summarize the contents of the article in a concise, pictorial form designed to capture the attention of a wide readership. Graphical abstracts should be submitted as a separate file in the online submission system. Image size: Please provide an image with a minimum of 531 × 1328 pixels (h × w) or proportionally more. The image should be readable at a size of 5 × 13 cm using a regular screen resolution of 96 dpi. Preferred file types: TIFF, EPS, PDF or MS Office files. You can view Example Graphical Abstracts on our information site.

Authors can make use of Elsevier's Illustration Services to ensure the best presentation of their images and in accordance with all technical requirements.

Keywords

Immediately after the abstract, provide a maximum of 6 keywords, using American spelling and avoiding general and plural terms and multiple concepts (avoid, for example, 'and', 'of'). Be sparing with abbreviations: only abbreviations firmly established in the field may be eligible. These keywords will be used for indexing purposes.

Abbreviations

Define abbreviations that are not standard in this field in a footnote to be placed on the first page of the article. Such abbreviations that are unavoidable in the abstract must be defined at their first mention there, as well as in the footnote. Ensure consistency of abbreviations throughout the article.

Acknowledgements

Collate acknowledgements in a separate section at the end of the article before the references and do not, therefore, include them on the title page, as a footnote to the title or otherwise. List here those individuals who provided help during the research (e.g., providing language help, writing assistance or proof reading the article, etc.).

Formatting of funding sources

List funding sources in this standard way to facilitate compliance to funder's requirements:

Funding: This work was supported by the National Institutes of Health [grant numbers xxxx, yyyy]; the Bill & Melinda Gates Foundation, Seattle, WA [grant number zzzz]; and the United States Institutes of Peace [grant number aaaa].

It is not necessary to include detailed descriptions on the program or type of grants and awards. When funding is from a block grant or other resources available to a university, college, or other research institution, submit the name of the institute or organization that provided the funding.

If no funding has been provided for the research, it is recommended to include the following sentence:

This research did not receive any specific grant from funding agencies in the public, commercial, or not-for-profit sectors.

Units

Follow internationally accepted rules and conventions: use the international system of units (SI). If other units are mentioned, please give their equivalent in SI.

Math formulae

Please submit math equations as editable text and not as images. Present simple formulae in line with normal text where possible and use the solidus (/) instead of a horizontal line for small fractional terms, e.g., X/Y. In principle, variables are to be presented in italics. Powers of e are often

more conveniently denoted by exp. Number consecutively any equations that have to be displayed separately from the text (if referred to explicitly in the text).

Footnotes

Footnotes should be used sparingly. Number them consecutively throughout the article. Many word processors build footnotes into the text, and this feature may be used. Should this not be the case, indicate the position of footnotes in the text and present the footnotes themselves separately at the end of the article.

Electronic artwork

General points

• Make sure you use uniform lettering and sizing of your original artwork.

• Preferred fonts: Arial (or Helvetica), Times New Roman (or Times), Symbol, Courier.

• Number the illustrations according to their sequence in the text.

• Use a logical naming convention for your artwork files.

• Indicate per figure if it is a single, 1.5 or 2-column fitting image.

• For Word submissions only, you may still provide figures and their captions, and tables within a single file at the revision stage.

• Please note that individual figure files larger than 10 MB must be provided in separate source files.

A detailed guide on electronic artwork is available.

You are urged to visit this site; some excerpts from the detailed information are given here.

Formats

Regardless of the application used, when your electronic artwork is finalized, please 'save as' or convert the images to one of the following formats (note the resolution requirements for line drawings, halftones, and line/halftone combinations given below):

EPS (or PDF): Vector drawings. Embed the font or save the text as 'graphics'.

TIFF (or JPG): Color or grayscale photographs (halftones): always use a minimum of 300 dpi.

TIFF (or JPG): Bitmapped line drawings: use a minimum of 1000 dpi.

TIFF (or JPG): Combinations bitmapped line/half-tone (color or grayscale): a minimum of 500 dpi is required.

Please do not:

• Supply files that are optimized for screen use (e.g., GIF, BMP, PICT, WPG); the resolution is too low.

• Supply files that are too low in resolution.

• Submit graphics that are disproportionately large for the content.

Color artwork

Please make sure that artwork files are in an acceptable format (TIFF (or JPEG), EPS (or PDF) or MS Office files) and with the correct resolution. If, together with your accepted article, you submit usable color figures then Elsevier will ensure, at no additional charge, that these figures will appear in color online (e.g., ScienceDirect and other sites) in addition to color reproduction in print. Further information on the preparation of electronic artwork.

Figure captions

Ensure that each illustration has a caption. A caption should comprise a brief title (not on the figure itself) and a description of the illustration. Keep text in the illustrations themselves to a minimum but explain all symbols and abbreviations used.

Tables

Please submit tables as editable text and not as images. Tables can be placed either next to the relevant text in the article, or on separate page(s) at the end. Number tables consecutively in accordance with their appearance in the text and place any table notes below the table body. Be sparing in the use of tables and ensure that the data presented in them do not duplicate results described elsewhere in the article. Please avoid using vertical rules and shading in table cells.

References

Citation in text

Please ensure that every reference cited in the text is also present in the reference list (and vice versa). Any references cited in the abstract must be given in full. Unpublished results and personal communications are not recommended in the reference list, but may be mentioned in the text. If these references are included in the reference list they should follow the standard reference style of the journal and should include a substitution of the publication date with either 'Unpublished results' or 'Personal communication'. Citation of a reference as 'in press' implies that the item has been accepted for publication.

Web references

As a minimum, the full URL should be given and the date when the reference was last accessed. Any further information, if known (DOI, author names, dates, reference to a source publication, etc.), should also be given. Web references can be listed separately (e.g., after the reference list) under a different heading if desired, or can be included in the reference list.

Data references

This journal encourages you to cite underlying or relevant datasets in your manuscript by citing them in your text and including a data reference in your Reference List. Data references should include the following elements: author name(s), dataset title, data repository, version (where available), year, and global persistent identifier. Add [dataset] immediately before the reference so we can properly identify it as a data reference. The [dataset] identifier will not appear in your published article.

Preprint references

Where a preprint has subsequently become available as a peer-reviewed publication, the formal publication should be used as the reference. If there are preprints that are central to your work or that cover crucial developments in the topic, but are not yet formally published, these may be referenced. Preprints should be clearly marked as such, for example by including the word preprint, or the name of the preprint server, as part of the reference. The preprint DOI should also be provided.

References in a special issue

Please ensure that the words 'this issue' are added to any references in the list (and any citations in the text) to other articles in the same Special Issue.

Reference management software

Most Elsevier journals have their reference template available in many of the most popular reference management software products. These include all products that support Citation Style Language styles, such as Mendeley. Using citation plug-ins from these products, authors only need to select the appropriate journal template when preparing their article, after which citations and bibliographies will be automatically formatted in the journal's style. If no template is yet available for this journal, please follow the format of the sample references and citations as shown in this Guide. If you use reference management software, please ensure that you remove all field codes before submitting the electronic manuscript. More information on how to remove field codes from different reference management software.

Reference Formatting

There are no strict requirements on reference formatting at submission. References can be in any style or format as long as the style is consistent. Where applicable, author(s) name(s), journal title/book title, chapter title/article title, year of publication, volume number/book chapter and the pagination must be present. Use of DOI is highly encouraged. The reference style used by the journal will be applied to the accepted article by Elsevier at the proof stage. Note that missing data will be highlighted at proof stage for the author to correct. If you do wish to format the references yourself they should be arranged according to the following examples:

[dataset] Oguro, M., Imahiro, S., Saito, S., Nakashizuka, T., 2015. Mortality data for Japanese oak wilt disease and surrounding forest compositions. Mendeley Data, v1. http://dx.doi.org/10.17632/xwj98nb39r.1.

Reference style

All publications cited in the text should be presented in a list of references following the text of the manuscript. In the text refer to the author's name (without initials) and year of publication (e.g. "Since Condie (2001) has shown that..." or "This is in agreement with results obtained later (Meert, 2003; Burrett and Berry, 2000)."

For three or more authors use the first author followed by "et al.", in the text. The list of references should be arranged alphabetically by authors' names. The manuscript should be carefully checked to ensure that the spelling of authors' names and dates are exactly the same in the text as in the reference list.

References should be given in the following form:

Kusky, T.M., Stern, R.J., Tucker, R.D., 2003. Evolution of East African and related orogens, and the assembly of Gondwana. Precambrian Research, 123, 81–85.

Pili, E., Sheppard, S.M.F., Lardeaux, J.M.,1999. Fluid–rock interaction in the granulites of Madagascar and lithospheric transfer of fluids. Gondwana Research, 2, 341–350.

Suzuki, K., Adachi, M., 1992. Middle Precambrian detrital monazite and zircon from Hida gneiss in OkiDogo island, Japan: their origin and implications for the correlation of basement gneiss of Southwest Japan and Korea. Tectonophysics, 235, 277–292.

Touret, J.L.R., 1985. Fluid regime in southern Norway, the record of fluid inclusions. In: Tobi, A.C., Touret, J.L.R. (Eds.), The Deep Proterozoic Crust in the North Atlantic Provinces. Reidel, Dordrecht, 517–549.

Kinny, P. D., Collins, A. S., Razakamanana, T., 2004. Provenance hints and age constraints of metasedimentary gneisses of Southern Madagascar from SHRIMP U–Pb zircon data. In: Chetty, T.R.K. and Bhaskar Rao, Y.J. (Eds.), International Field Workshop on the Southern Granulite Terrane. National Geophysical Research Institute, Hyderabad, India, 97–98.

Rogers, J.J.W. and Santosh, M., 2004. Continents and Supercontinents. Oxford University Press, New York. Li, Z.X., Metcalfe, I., Powell, C.M. (Eds.), 1996. Breakup of Rodinia and Gondwanaland and Assembly of Asia. Australian Journal of Earth Sciences 43.

Albee, H.F., Cullins, H.L., 1975. Geologic map of the Alpine Quadrangle, Bonneville County, Idaho, and Lincoln County Wyoming. United States Geological Survey Geologic Quadrangle Map GQ–1259, scale 1:24,000.

Sajeev, K., 2003. Evolution and metamorphic zoning of Highland Complex, Sri Lanka: a comparison with Madurai Block, southern India. Ph.D. thesis, Okayama University.

Video

Elsevier accepts video material and animation sequences to support and enhance your scientific research. Authors who have video or animation files that they wish to submit with their article are strongly encouraged to include links to these within the body of the article. This can be done in the same way as a figure or table by referring to the video or animation content and noting in the body text where it should be placed. All submitted files should be properly labeled so that they directly relate to the video file's content. In order to ensure that your video or animation material is directly usable, please provide the file in one of our recommended file formats with a preferred maximum size of 150 MB per file, 1 GB in total. Video and animation files supplied will be published online in the electronic version of your article in Elsevier Web products, including ScienceDirect. Please supply 'stills' with your files: you can choose any frame from the video or animation or make a separate image. These will be used instead of standard icons and will personalize the link to your video data. For more detailed instructions please visit our video instruction pages. Note: since video and animation cannot be embedded in the print version of the journal, please provide text for both the electronic and the print version for the portions of the article that refer to this content.

Data visualization

Include interactive data visualizations in your publication and let your readers interact and engage more closely with your research. Follow the instructions here to find out about available data visualization options and how to include them with your article.

Supplementary material

Supplementary material such as applications, images and sound clips, can be published with your article to enhance it. Submitted supplementary items are published exactly as they are received (Excel or PowerPoint files will appear as such online). Please submit your material together with the article and supply a concise, descriptive caption for each supplementary file. If you wish to make changes to supplementary material during any stage of the process, please make sure to provide an updated file.

Do not annotate any corrections on a previous version. Please switch off the 'Track Changes' option in Microsoft Office files as these will appear in the published version.

Research data

This journal requires and enables you to share data that supports your research publication where appropriate, and enables you to interlink the data with your published articles. Research data refers to the results of observations or experimentation that validate research findings. To facilitate reproducibility and data reuse, this journal also encourages you to share your software, code, models, algorithms, protocols, methods and other useful materials related to the project.

Below are a number of ways in which you can associate data with your article or make a statement about the availability of your data when submitting your manuscript. When sharing data in one of these ways, you are expected to cite the data in your manuscript and reference list. Please refer to the "References" section for more information about data citation. For more information on depositing, sharing and using research data and other relevant research materials, visit the research data page.

Data linking

If you have made your research data available in a data repository, you can link your article directly to the dataset. Elsevier collaborates with a number of repositories to link articles on ScienceDirect with relevant repositories, giving readers access to underlying data that gives them a better understanding of the research described.

There are different ways to link your datasets to your article. When available, you can directly link your dataset to your article by providing the relevant information in the submission system. For more information, visit the database linking page.

For supported data repositories a repository banner will automatically appear next to your published article on ScienceDirect.

In addition, you can link to relevant data or entities through identifiers within the text of your manuscript, using the following format: Database: xxxx (e.g., TAIR: AT1G01020; CCDC: 734053; PDB: 1XFN).

To maximise the visibility of your data, authors are invited to add a citation to their datasets by including a data reference in their Reference List as per the 'Data References' instructions elsewhere on this page.

Data in Brief

You have the option of converting any or all parts of your supplementary or additional raw data into a data article published in Data in Brief. A data article is a new kind of article that ensures that your data are actively reviewed, curated, formatted, indexed, given a DOI and made publicly available to all upon publication (watch this video describing the benefits of publishing your data in Data in Brief). You are encouraged to submit your data article for Data in Brief as an additional item directly alongside the revised version of your manuscript. If your research article is accepted, your data article will automatically be transferred over to Data in Brief where it will be editorially reviewed, published open access and linked to your research article on ScienceDirect. Please note an open access fee is payable for publication in Data in Brief. Full details can be found on the Data in Brief website. Please use this template to write your Data in Brief data article.

MethodsX

You have the option of converting relevant protocols and methods into one or multiple MethodsX articles, a new kind of article that describes the details of customized research methods. Many researchers spend a significant amount of time on developing methods to fit their specific needs or setting, but often without getting credit for this part of their work. MethodsX, an open access journal, now publishes this information in order to make it searchable, peer reviewed, citable and reproducible.

Authors are encouraged to submit their MethodsX article as an additional item directly alongside the revised version of their manuscript. If your research article is accepted, your methods article will automatically be transferred over to MethodsX where it will be editorially reviewed. Please note an open access fee is payable for publication in MethodsX. Full details can be found on the MethodsX website. Please use the methods template or protocol template to prepare your MethodsX article.

Data statement

To foster transparency, we require you to state the availability of your data in your submission if your data is unavailable to access or unsuitable to post. This may also be a requirement of your funding body or institution. You will have the opportunity to provide a data statement during the submission process. The statement will appear with your published article on ScienceDirect. For more information, visit the Data Statement page..

AFTER ACCEPTANCE

Online proof correction

To ensure a fast publication process of the article, we kindly ask authors to provide us with their proof corrections within two days. Corresponding authors will receive an e-mail with a link to our online proofing system, allowing annotation and correction of proofs online. The environment is similar to MS Word: in addition to editing text, you can also comment on figures/tables and answer questions from the Copy Editor. Web-based proofing provides a faster and less error-prone process by allowing you to directly type your corrections, eliminating the potential introduction of errors.

If preferred, you can still choose to annotate and upload your edits on the PDF version. All instructions for proofing will be given in the e-mail we send to authors, including alternative methods to the online version and PDF.

We will do everything possible to get your article published quickly and accurately. Please use this proof only for checking the typesetting, editing, completeness and correctness of the text, tables and figures. Significant changes to the article as accepted for publication will only be considered at this stage with permission from the Editor. It is important to ensure that all corrections are sent back to us in one communication. Please check carefully before replying, as inclusion of any subsequent corrections cannot be guaranteed. Proofreading is solely your responsibility.

Offprints

The corresponding author will, at no cost, receive a customized Share Link providing 50 days free access to the final published version of the article on ScienceDirect. The Share Link can be used for sharing the article via any communication channel, including email and social media. For an extra charge, paper offprints can be ordered via the offprint order form which is sent once the article is accepted for publication. Both corresponding and co-authors may order offprints at any time via Elsevier's Author Services. Corresponding authors who have published their article gold open access do not receive a Share Link as their final published version of the article is available open access on ScienceDirect and can be shared through the article DOI link.

AUTHOR INQUIRIES

Visit the Elsevier Support Center to find the answers you need. Here you will find everything from Frequently Asked Questions to ways to get in touch.

You can also check the status of your submitted article or find out when your accepted article will be published.

ANEXO C – COMPROVANTE DE ACEITE DO ARTIGO 1

ELSEVIER

Congratulations on your accepted article!

Dear Author,

We recognize you have a choice of where to submit your research and we thank you for choosing to publish with *Journal of South American Earth Sciences*.

As an expert in the field, you are best placed to explain why your article,

MAGMATIC PROCESSES RECORDED IN PLAGIOCLASE CRYSTALS OF

THE RIO JACARÉ BATHOLITH, SERGIPANO OROGENIC SYSTEM,

NORTHEAST BRAZIL, is interesting or impactful to a wider audience. Find out how you can help your article get the visibility it deserves:

Share and Publish your Reseach Data

Researcher Academy

Get Noticed

We look forward to receiving future manuscripts from you!

Sincerely,

Researcher Engagement Team

Can we assist you with something? Visit our help page "

Elsevier supports responsible sharing:
Responsible sharing in line with copyright enables publishers to sustain high quality journals and the services they provide to the research community.
Find out how you can share your manuscript in Elsevier journals.

- Find useful tools and resources: Author Resources.
- For assistance, please visit our Customer Support site, where you can search for solutions on a range of topics and find answers to frequently asked questions.

Would you like to **update your information**? Amend your profile or publication history by visiting the Scopus profile and content corrections Support Center.

If you do not wish to receive any further Service messages, please send us an email.

ELSEVIER

ANEXO D – COMPROVANTE DE ACEITE DO ARTIGO 2

Brazilian Journal of Geology

Decision Letter (BJGEO-2022-0033.R2)

From: guano@usp.br
To: karlcss@hotmail.com
CC:
Subject: Brazilian Journal of Geology - Decision on Manuscript ID BJGEO-2022-0033.R2
Body: 29-Jul-2022

Dear Mr. Sousa:

It is a pleasure to accept your manuscript entitled "Injections of enriched lithospheric mantle magmas explain the formation of microgranular enclaves in the Rio Jacaré Batholith, Borborema Province, Brazil" in its current form for publication in the Brazilian Journal of Geology. The comments of the reviewer(s) who reviewed your manuscript are included at the foot of this letter.

Thank you for your fine contribution. On behalf of the Editors of the Brazilian Journal of Geology, we look forward to your continued contributions to the Journal.

Sincerely,
Dr. Carlos Grohmann
Editor-in-Chief, Brazilian Journal of Geology
guano@usp.br, carlos.grohmann@gmail.com

Associate Editor
Comments to the Author:
(There are no comments.)

Entire Scoresheet:

Date Sent: 29-Jul-2022

Close Window

ANEXO E – COMPROVANTE DE SUBMISSÃO DO ARTIGO 3

Brazilian Journal of Geology - Manuscript ID BJGEO-2022-0023

Tatiana Alonso <onbehalfof@manuscriptcentral.com>
Qua, 27/04/2022 15:36

Para: karlcss@hotmail.com <karlcss@hotmail.com>

Cc: karlcss@ufba.br <karlcss@ufba.br>;karlcss@hotmail.com <karlcss@hotmail.com>;hiakanss@ufba.br <hiakanss@ufba.br>;dmfernandes@ufba.br <dmfernandes@ufba.br>;lrosa@adademico.ufs.br <lrosa@adademico.ufs.br>;herbet@academico.ufs.br <herbet@academico.ufs.br>

27-Apr-2022

Dear Mr. Sousa:

Your manuscript has been screened for possible publication in the Brazilian Journal of Geology and was forwarded to the Associated Editor, who will handle the peer-review process.

Please note that this message constitutes a confirmation of submission for manuscript ID BJGEO2022-0023, entitled "Mineral chemistry of the Rio Jacaré Batholith biotite, Poço Redondo Domain, Sergipano Orogenic System: petrogenetic implications", to the Brazilian Journal of Geology.

Please mention the above manuscript ID in all future correspondence or when calling the office for questions. If there are any changes in your street address or e-mail address, please log in to ScholarOne Manuscripts at https://mc04.manuscriptcentral.com/bjgeo-scielo and edit your user information as appropriate.

You can also view the status of your manuscript at any time by checking your Author Center after logging in to https://mc04.manuscriptcentral.com/bjgeo-scielo.

Thank you for submitting your manuscript to the Brazilian Journal of Geology.

Sincerely,
Brazilian Journal of Geology Editorial Office